THE UNIVERSITY
of EDINBURGH

The power of kinetic growth curve analysis in determining the mechanism of amyloid fibril formation

Jay E. Gillam

A thesis submitted in fulfilment of the requirements
for the degree of Doctor of Philosophy
to the
University of Edinburgh
May 2016

Abstract

Misfolding and accumulation of insoluble protein aggregates in the form of amyloid fibrils is associated with a number of prevalent and debilitating mammalian disorders. In addition, amyloid-like nanostructures exhibit robust material properties, biological compatibility and replicative properties, making them of particular interest in the development of novel nanomaterials. Understanding fibril formation is essential to the development of strategies to control, manipulate or prevent fibril growth.

The amyloid hypothesis is that since amyloid-like fibrils share a common core structure, they also share common formation mechanisms. Utilising a combination of turbidity and extrinsic fluorescence techniques this thesis provides insight into the diagnostic strength of simple, inexpensive kinetic measurements of aggregate growth. These simple techniques are found to be capable of delivering a substantial amount of information about the growth mechanisms controlling aggregation, and the effect of solution and environmental conditions, forming a solid basis for further investigation.

Two competing fibrillar pathways are observed for hen egg white lysozyme at low pH in the presence of salt. These two pathways, leading to the formation of either curvilinear, worm-like fibrils or to the more widely recognised rigid, straight fibrils are not particular to hen egg white lysozyme, and similar competition may affect growth curve analysis in many other protein assays, including α-synuclein.

Many proteins aggregate in the presence of membranes and detergents, and the kinetics of α-synuclein aggregation in the presence of SDS are strongly influenced by SDS concentration. Most descriptions of amyloid fibril growth currently lack heterogeneous nucleation events, and these may be important for predicting aggregation of membrane-active species *in vivo*.

It is clear that simple analytical solutions to growth models are unable in many

cases to capture the complexities of filament growth. Even in relatively simple *in vitro* experiments different growth processes can dominate growth rate over time, competing fibrillar species can result in composite kinetic growth signals and some growth mechanisms have not yet been sufficiently incorporated into an overall description of fibril growth.

Lay Summary

Proteins are the building blocks of life. They perform a vast array of critical functions for living organisms as enzymes, hormones, antibodies, neurotransmitters and carriers of molecules from one location to another. Proteins are made up of amino acids, and can differ in number of amino acids and amino acid sequence, dictated by the sequence of their genes. The amino acid sequence usually results in specific folding of the protein into a well defined 3D structure that has specific biological activity. A subset of proteins, known as intrinsically disordered proteins, do not fold into a defined 3D structure, and are active in a mostly unfolded native state.

If a protein fails to fold into its correct native structure it can become inactive, but in some cases misfolded proteins can also be toxic. Amyloid fibrils are filament-like structures that are formed by misfolded proteins. In the formation of fibrils, many proteins stick together to form a linear structure that has a characteristic 3D structure of amino acids at its core. The formation and accumulation of fibrils has been linked with a number of prevalent and debilitating neurodegenerative disorders, including Alzheimer's and Parkinson's diseases.

Protein fibrils also exhibit robust material properties, are self-replicating and are biologically compatible, making them particularly interesting in the development of novel nanomaterials. Understanding their formation is essential to control, manipulate or prevent fibril growth.

The growth of protein fibrils can be very complex. The growth mechanisms that control protein fibril growth are numerous and can vary over the time it takes fibrils to form, under different environmental conditions and from protein to protein. A number of mathematical models have been developed to describe the formation of protein fibrils driven by particular growth mechanisms. The formation of protein fibrils can be followed experimentally by capturing growth

curves that represent the amount of fibrils over time. These growth curves can then be compared with the models to determine how the fibrils are formed, the driving growth mechanisms, and important growth rates and sizes that are of potential importance in pathology.

This thesis investigates fibril formation in complex systems, to determine how powerful the analysis of growth curves can be. Two different proteins were studied: hen egg white lysozyme, a model protein with a well defined 3D native structure; and α-synuclein, a model intrinsically disordered protein and the major protein implicated in Parkinson's disease. Both proteins were shown to form two different types of protein fibril, forming either straight and rigid fibrils or worm-like, curly filaments along pathways with distinct growth mechanisms.

Despite the complexity of the fibril growth of hen egg white lysozyme and α-synuclein a substantial amount of information was obtained about the growth mechanisms by growth curve analysis. For both proteins and their different fibril types, the dominant growth mechanisms were determined. However, it was also clear that growth models are currently unable to capture the full complexities of fibril growth, and that some important growth mechanisms have not yet been sufficiently incorporated into the available growth models.

In particular, the two fibril types of hen egg white lysozyme were found to be in competition. The two pathways do not appear to be particular to hen egg white lysozyme, and similar competition may affect growth curve analysis in many other protein assays. Heterogeneous nucleation, where new fibrils are formed on surfaces or interfaces, was shown to be very important for α-synuclein. Most descriptions of amyloid fibril growth currently lack heterogeneous nucleation events, and these may be pathologically relevant in the misfolding of proteins that have cellular membrane activity, such as α-synuclein.

Declaration

Except where otherwise stated, the research undertaken in this thesis was the unaided work of the author. Where the work was done in collaboration with others, a significant contribution was made by the author. The contributions of others are acknowledged in the text where relevent.

J. E. Gillam
March 2016

Acknowledgements

Firstly, I would like to express my sincere gratitude to my supervisor Prof. Cait MacPhee for her continuous support, patience (especially while I was writing this thesis...), enthusiasm, and inspiration. I could not have imagined having a better advisor and inspiration. Secondly, I would like to thank the members of our research group and many other connected researchers for their help, support and enthusiasm during the work represented in this thesis. In particular: Kym Eden, Jason Kalapothakis and Ryan Morris, for imparting their experimental and computational knowledge and providing stimulating group discussions; Dr. Tilo Kunath and his group at the MRC Centre for Regenerative Medicine for providing α-synuclein protein and expression plasmid, and new insights and enthusiasm for my research; Prof. Perdita Barran and her group, for lively discussions at our monthly amyloid meetings; and Angela Dawson, for her constant assistance in the laboratory. I would like to say thank you to all the PhD. students that I spent time with, who provided valued input, knowledge, or a welcome distraction. Especially Craig Gregor, Chrissy Wong, Mira Nishimura and Ben Little, with whom I shared an office. I would like to thank all my friends and family, and above all else I wish to thank my fiancé, Robert Dewar, for his never ending support, love, patience and belief in me.

Contents

List of Figures

Chapter 1

Introduction

1.1 Protein aggregation

The ability of a protein to maintain its native, functional state is fundamental for biological activity. Misfolding and the accumulation of misfolded protein aggregates has been intimately linked with a large number of mammalian disorders. Amyloid fibril related disorders are associated with the unwanted filamentous aggregation of a particular protein or peptide. Most prevalent are the neurodegenerative Alzheimer's (associated peptides $A\beta_{1-40}$ and $A\beta_{1-42}$) [5], Parkinson's (α-synuclein) [6], and Huntington's (Huntington) diseases [7], Type II diabetes (islet amyloid polypeptide IAPP) [8] and the prion diseases [9]. Aggregation of misfolded protein is also a concern during the manufacturing, purification, storage and administration of protein products for use in industry, foodstuffs and pharmaceuticals where aggregation can be either desirable or detrimental [10–13].

Due to their correlation with disease, amyloid-like fibrils have historically been linked with pathology. However, functional fibrils are increasingly being discovered in a wide range of organisms from bacteria to humans. They perform a diversity of functions from biofilm formation [14, 15] and the regulation of melanin synthesis [14, 16] to a more speculative long-term memory encryption [14, 17]. Self assembly and replicative properties, and high resistance to proteolysis, also make them of great interest in the production of biomaterials and nanodevices [12, 15, 18, 19].

The study of amyloid-like fibril formation of proteins has been an ever

expanding field since their implication in neurodegenerative disease, and one of the most common methods of analysis is the study of growth kinetics. Fibril forming systems exhibit characteristic sigmoidal-like mass-of-aggregate growth profiles and it is widely accepted that the dominant growth mechanisms include elongation by monomer addition and secondary growth processes such as filament fragmentation. However, an increasing number of proteins and peptides have been shown to form curvilinear or worm-like fibrils that appear to be correlated with shorter or non-existent lag phases (during which no aggregation is observed) prior to aggregation and a 'ball-on-chain' oligomeric growth mechanism (in which oligomers appear to associate and form chains with a beaded appearance), and may represent an alternative and/or competing fibrillar growth pathway.

Numerous growth models have been developed to describe the formation of linear protein aggregates, with the aim of determining the growth mechanisms and important growth parameters such as growth rates and nucleus size that are of potential importance in pathology. However, it is increasingly obvious that while fibrils of different proteins share a similar β-sheet rich core structure, the growth mechanisms controlling their formation can vary. This heterogeneity complicates growth curve analysis, especially where analytical solutions for growth models are only possible under limiting conditions and contain large numbers of parameters.

This thesis investigates the diagnostic strength of growth curve analysis in the formation of protein fibrils using the simple, inexpensive, high-throughput and *in situ* techniques of turbidity and fluorescence measurement by platereader assay. These methods are applied to model globular and intrinsically disordered protein systems known to exhibit some of the complexities that complicate growth curve analysis.

1.2 The characteristics of amyloid fibrils

A wide range of proteins and peptides with no sequence similarity or common native structural motifs have been shown to form amyloid-like fibril structures [20–22]. The so-called 'cross-βstructure' conserved across amyloid fibril species is formed by hydrogen-bond interactions between groups in the polypeptide backbone, and is therefore a motif that is available to any protein or polypeptide chain [23, 24]. It has further been proposed that this structure may be a

universal lowest energy conformation for polypeptides [22]. Indeed, some fibrillar aggregates have been shown to be more thermodynamically stable than their native protein conformations [25].

The diagnostic structural traits and characteristic self-assembly profiles of amyloid-like fibrils have led to the search for a common fibril formation mechanism. Additionally, a wealth of evidence suggests that metastable, soluble oligomers formed early in the aggregation process and small fibril fragments are the predominant toxic species in most protein deposition diseases [5, 26–31]. A number of different toxic prefibrillar oligomers have been shown to exhibit structural similarity [26, 32], and an oligomer of HypF-N, a protein not implicated in any disease, has been shown to exhibit comparable toxicity to oligomers of $A\beta_{1-42}$ and islet amyloid polypeptide (IAPP) in MTT (3-(4,5-dimethylthiazol-2-yl)-2,5-diphenyltetrazolium bromide) assays [33]. Such findings suggest that fibril forming species may share a common mechanism of cellular toxicity as well as a common formation mechanism. A full description of the fibril formation mechanism and the species formed along the pathway are therefore essential to our understanding of the link between fibril formation and disease, for the development of therapeutic strategies and for the control of protein products.

1.2.1 Structure and morphology

Amyloid or amyloid-like fibrils are distinguished from amorphous aggregates by their β-sheet rich structure and characteristic optical properties [20, 21, 34, 35]. Observed by transmission electron microscopy (TEM) or atomic force microscopy (AFM) amyloid fibrils are typically unbranched linear structures composed of filaments that are wrapped or twisted with regular helicity [20, 34–36]. The fibril diameter is typically in the range 2-20 nm and the length can be up to a few microns [34, 35, 37].

In the presence of certain dyes amyloid-like fibrils display characteristic optical activity. In particular, 'apple-green' birefringence is observed from the sulphonated azo dye Congo red upon binding to fibrillar material [20, 38, 39], and the benzothiazole salt dye Thioflavin T (ThT) displays enhanced fluorescence [38, 39]. The conserved cross-β-core structure that gives rise to this specific optical behaviour is the conclusive determinant of amyloid fibril structure and gives rise to a distinctive X-ray diffraction pattern in which meridional spacings of ~ 10

Å and equatorial spacings of ∼ 4.7 Å correspond to the distances between layers of β-sheet orientated parallel to the fibril axis, and between their constituent β-strands, respectively (see Figure 1.1) [20, 21, 34–36].

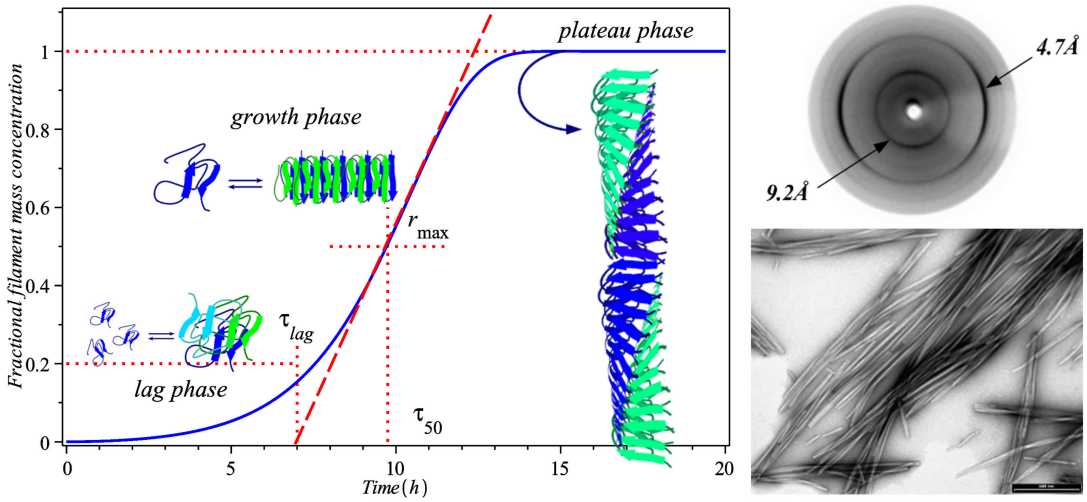

Figure 1.1: Left: Sigmoidal growth profile of fibril mass formation showing typical parameters. Here, τ_{50}, the time for aggregate mass to reach 50% of its final value, is the time at which the maximum growth rate r_{max} occurs. The predominant growth processes occurring in a nucleation-dominated growth scheme are shown. Right, top: X-ray fibre diffraction pattern of $TTR_{105-115}$. Right, bottom: Transmission electron micrograph of $TTR_{105-115}$ fibrils, scale bar 500 nm.

Curvilinear or worm-like fibrils are also commonly observed, and are typically unbranched structures with high flexibility (short persistence length) and diameters in a similar range to the more frequently described straight fibrils, as shown in Figure 1.2. This alternative morphology has been observed for yeast phosphoglycerate kinase (PGK) [40, 41], α-synuclein [42, 43], α_{s2}-casein [44], αB-crystallin [45], human serum albumin (HSA) [46–48], transthyretin (TTR) [49], β-amyloid [50–55], barstar [56–60], bovine serum albumin (BSA) [61], β_2-microglobulin [62–68], β-lactoglobulin [69–76], prion proteins [77–80], apolipoprotein C-II [81–87], hen egg white lysozyme [2, 88, 89], ovalbumin [90, 91], and many other peptides and proteins [92–97]

These curvilinear aggregates have sometimes been described as amorphous or as protofibrils, especially where only very short species are observed. However, in many cases they appear to be the end structure of a growth pathway and exhibit an elongated, linear shape that may have a ball-on-chain or beaded appearance [2, 58, 60, 70, 89, 91, 93, 98], and many exhibit characteristics such as β-rich

content [40, 41, 44, 48, 56, 58, 60, 61, 68, 70, 77, 86, 88, 89, 91, 92, 99, 100], ThT binding [44, 48, 49, 56, 57, 60, 61, 63, 74, 75, 77, 79, 83, 88, 100, 101] and X-ray diffraction patterns [41, 44, 61, 66, 68, 84, 102], similar to the archetypal long, straight fibrillar species.

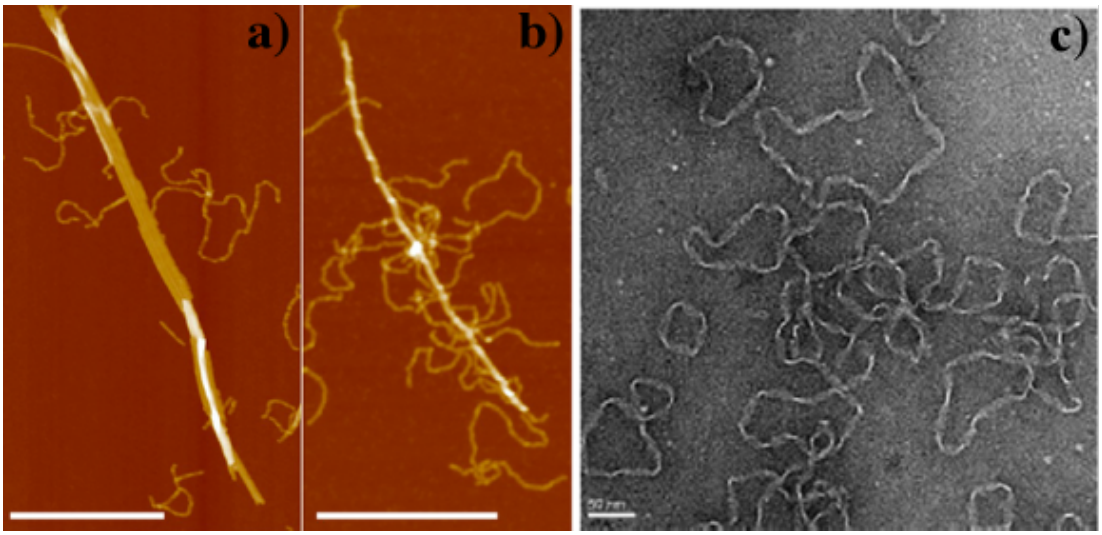

Figure 1.2: AFM height images of *a)* a multistranded flat ribbon and *b)* a left handed twisting fibril, both formed from ovalbumin and alongside thin flexible ovalbumin fibrils (scale bars are 500 nm, selected from Lara *et al.* [91]). Isolated fibril loops of apoC-II are shown in *c)* (scale bar 50 nm, selected from Yang *et al.* [85]).

In contrast to straight, rigid fibrils, weaker ThT fluorescence enhancement appears to be a common feature for curvilinear filaments [63, 86, 88], suggesting a different secondary structure arrangement that may include less β-content. Indeed, a different structure by circular dichroism (CD) [86, 91] and/or Fourier transform infrared spectroscopy (FTIR) [88, 91] has been observed for some of these species when compared to straight filaments formed from the same protein under different conditions, and different protonation states of the carboxyl side chains observed by Raman spectroscopy for species of β_2-microglobulin were thought to be a result of different spatial arrangements of the β-strands and β-sheets [99]. In addition, rigid and curvilinear fibril species have been observed to coexist under certain conditions [70, 75, 91], and have been shown to be competing species in β_2-microglobulin aggregation [70, 103].

Environmental conditions and the properties of the amino acid side chains determine the propensity for fibril formation for a given protein and have been shown to influence the fibrillar structure that is formed: sequences containing

repetitive consecutive hydrophobic and hydrophilic regions have been shown to have higher aggregation propensity [37, 104], and diverse fibril morphologies such as rope-like associations of filaments [20, 36, 105–107], flat assemblies like twisted ribbons [20, 91, 105, 106, 108], the curvilinear filaments described above [2, 40–67, 69–97] and even closed loops [44–46, 73, 83–85, 102, 109–111] have been observed. Examples of some of these fibril morphologies are shown in Figure 1.2.

1.2.2 Analysis of fibril formation

The typical driving force in the aggregation of folded, globular proteins is believed to be destabilisation of the native protein to yield a population of partially folded intermediates with increased aggregation propensity [10, 13, 20, 21, 106, 112–118]. This conformational change is typically described as 'monomer activation' [116]. Small, oligomeric species may then form by association of the partially folded protein units and proceed to assemble into larger, fibrillar aggregates known as protofilaments or filaments which may in turn associate into mature amyloid fibril-like structures [20].

A complete description of this fibril formation process requires identification of the oligomeric species present and the pathway of association, as well as quantification of the kinetic rate constants and reaction orders. Many more techniques than listed here have been implemented to monitor the aggregation process, and in-depth discussion of their advantages and disadvantages may be found elsewhere [38, 119]. Structural information can be obtained by circular dichroism (CD), Fourier transform infrared (FTIR) spectroscopy, size exclusion chromatography (SEC), nuclear magnetic resonance (NMR) imaging [120] or mass spectrometry [121–123], while TEM [38], AFM [38] and X-ray diffraction [20, 21] are typically used to investigate final fibrillar species or intermediates isolated from the aggregation process.

Methods used to measure the kinetics and thermodynamics of fibril growth include light scattering [38, 124, 125], turbidity [8, 38], and fluorescence and absorption spectroscopy of intrinsic fluorophores and extrinsic dyes (Congo red and ThT, as described above, 1-anilinonaphthalene-8-sulphonate (ANS) and their derivatives) [119], and direct approaches such as the use of quartz crystal microbalance (QCM) sensors [126, 127].

More recently, techniques have been developed to enable the elongation of

individual fibrils to be directly monitored with AFM [128] and total internal reflection fluorescence microscopy (TIRFM) [129–131].

In many typical assays, kinetically relevant intermediates may be too short lived or poorly populated to be observed [132]. Moreover, each experimental method typically reports an individual parameter of the aggregating system, such as monomer concentration, mass-of-aggregate, average filament length, or end-point filament length distribution. Analysis of a single parameter is unlikely to be sufficient to distinguish between alternative aggregation models [132], and where possible many different techniques should be compared.

However, mass-of-aggregate (or equivalently monomer depletion) data is likely to be a minimum requirement to differentiate between different combinations of microscopic processes and is the main focus of this investigation.

1.2.3 Kinetics of fibril formation

A characteristic sigmoidal growth profile for the increase in mass-of-aggregate (see Figure 1.1) is observed for a wide range of protein fibrillation phenomena *in vitro*, including the native filament growth of proteins like actin and tubulin [133–135]. Typically an initial lag phase (with associated lag time $\tau_{\text{lag}}(s)$) is observed, during which no measurable aggregation occurs. The effective growth rate then increases as significant numbers of aggregates are produced, until a maximum growth rate $r_{\max}(\text{s}^{-1})$ is reached at the inflection point. We adopt the convention of defining τ_{lag} as the intercept of the $r_{\max}$ tangent with the time axis, as shown in Figure 1.1. Finally, the monomer population is mostly depleted, the reaction rate slows and a plateau phase characterises the end-point of the reaction.

The erratic nature of the protein aggregation process often makes it challenging to obtain quantitative and reproducible measurements of $r_{\max}$ and τ_{lag} [136]. Wildly varying lag times, obtained in apparently identical experiments, have previously and incorrectly been attributed to the inherent stochastic nature of nucleation. Careful experimental control has been shown to drastically reduce scatter of data and provide reliable, reproducible results and a recent review has demonstrated that reproducible rate constants can be obtained across a number of techniques within experimental error [137].

1.3 Modelling amyloid fibril formation kinetics

The growth of amyloid-like fibrils is inherently complex. Possible growth processes include monomer activation, formation of prenuclear species, primary nucleation, secondary growth processes, elongation by monomer addition and coagulation of larger species, conformational rearrangement, lateral association or bundling, and phase separation, and may be further complicated by critical concentration behaviour where rate constants change during growth, or are different above and below a critical initial monomer concentration or filament mass concentration. The growth of fibril mass or number concentration is typically expressed as a differential equation model. It is impossible to obtain an all-encompassing analytical solution to a model of this form for an elaborate growth scheme containing all possible growth processes. Numerical integration is a convenient and versatile method of analysis. However, we typically do not know in advance which growth processes are dominant, and the number of repeated iterations that may be required to determine the best parameter set can make this a slow and computationally expensive process. Additionally, it may be impossible to distinguish between certain mechanisms (in some cases secondary and primary nucleation, or between possible secondary processes).

No current model framework has analysed in detail the different possible contributions to filament growth, and a framework that can incorporate any and all of these possible growth processes should be a general aim in the research of amyloid-like fibril formation. However, essential mechanistic details can be derived by qualitative and quantitative comparison of experimental data with the various individual models that have been proposed.

1.3.1 The classical nucleation-dominated polymerisation model (NDP)

The first key kinetic model for protein filament assembly was proposed by Oosawa *et al.* [133, 134] in the 1960's. Their analytical solution describing the total concentration of monomers participating in helical polymers of F-actin was very successful in describing the native self-assembly of actin and later tubulin [116, 133–135, 138]. This simple model, as described below in a form comparable to more recent analytical solutions, provided a number of valuable insights into the

scaling behaviours that may be experimentally observed in such a system.

As in classical nucleation theory, the formation of a thermodynamically unfavourable nucleus of critical size (n_c) from the monomer in solution is assumed to be necessary for growth to proceed. The change in free energy for the formation of a nucleus is positive, such that primary nucleation occurs only through stochastic fluctuations on microscopic length scales [139]. Nuclei are assumed to be in equilibrium with the monomer population and the addition of monomer to aggregates of size $\geq n_c$ is assumed to be thermodynamically favourable. In nucleation-dominated polymerisation (NDP) models such as this, primary nucleation is the only method of creating new aggregates. The kinetics of aggregation are therefore determined by the population and the growth rate of the nuclei and are nucleation-dependent: nucleation is the slowest and therefore rate limiting process.

Systems where nuclei are formed in accordance with classical nucleation theory are expected to exhibit a critical monomer concentration below which aggregation does not occur [8, 38, 135, 140, 141], defined by the solubility of monomeric protein at equilibrium. The concentration of free monomer is expected to be fixed at this value when the aggregation reaction reaches its equilibrium end point [8, 38].

The simplest NDP system evolving through primary nucleation and reversible elongation of existing filaments by monomer addition is shown in Figure 1.3 and described by the concentration flux equation [142, 143]

$$\frac{\delta f(t,j)}{\delta t} = 2m(t)k_+ f(t,j-1) - 2m(t)k_+ f(t,j) \tag{1.1}$$

$$+ 2k_{\text{off}} f(t,j+1) - 2k_{\text{off}} f(t,j)s \tag{1.2}$$

$$+ k_{\text{n}} m(t)^{n_c} \delta_{j,n_c} \tag{1.3}$$

where $f(t,j)$ is the concentration of filaments of length j at time t, k_+, k_{off}, and k_{n} are the rate constants describing elongation by monomer addition, monomer dissociation (depolymerisation) and nucleation respectively, and $m(t)$ is the concentration of monomeric protein in solution at time t. The first two terms describe the change in the population of filaments of length j due to monomer addition. The third and fourth terms relate to monomer dissociation. In both cases the factor of 2 originates from the assumption of elongation and dissociation

at both filament ends (not typically included in the historical literature [134, 135],) and the rate constants are assumed to be independent of polymer length. The fifth term describes the creation of a critical nucleus of n_c monomers [133–135, 142].

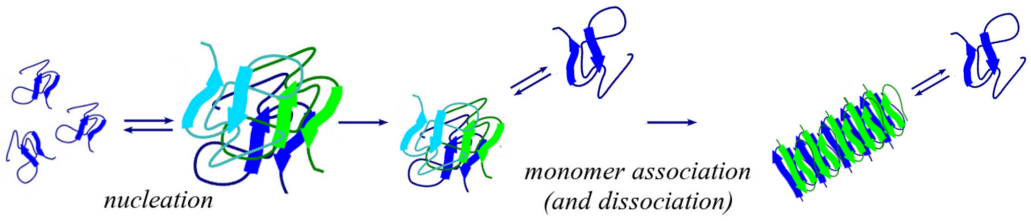

Figure 1.3: Cartoon depicting the growth mechanisms of the simplest nucleation dependent growth model: a primary nucleation step, where a critical thermodynamic nucleus is formed, followed by growth by (reversible) monomer addition.

The concentration flux approach is very powerful since it enables the explicit description of the microscopic processes contributing to filament growth. Summation over both sides of the concentration flux equation provides a differential equation system for the time evolution of the principal moments that relate to the experimental observables of the kinetic process. These basic kinetic equations are well-established; however, their non-linear nature represents a challenge in deriving accurate analytical solutions. As a result, repeated iterations of numerical solutions are typically required in order to obtain the best estimates of model parameters to fit experimental data. To bypass this costly process such equations are integrated in limiting cases to derive approximate equations for the macroscopic, experimentally accessible parameters. The most important are the zeroth and first moments: the filament mass $M(t)$ and number $P(t)$ concentrations respectively [138, 142, 144].

In the classical NDP approach, irreversible filament growth ($k_{\text{off}} \to 0$, as originally applied by Oosawa) [133–135] is invoked to simplify the mathematics and the mass concentration of filaments can be given in closed form as [138, 142, 143]

$$M(t) = m_{\text{tot}} \left[1 - \operatorname{sech}^{2/n_c}\left(\lambda t \sqrt{n_c/2}\right)\right] \tag{1.4}$$

where m_{tot} is the total monomer concentration and $\lambda = (2k_n k_+ m_{\text{tot}}^{n_c})^{1/2}$. This equation describes a sigmoidal curve, dominated by the single parameter λ. As a consequence, NDP processes exhibit characteristic scaling behaviour with λ. The

characteristic lag time can be shown to scale with initial monomer concentration such that $\tau_{\text{lag}} \sim m_{\text{tot}}^{-\gamma}$ where $\gamma = (n_{\text{c}}+1)/2$. Since $n_{\text{c}} \geq 1$ is the size of the critical nucleus, the exponent γ is always greater than, or equal to, unity [8, 142, 145, 146].

The initial ∼10-20% increase of $M(t)$ can be closely approximated to the parabola t^2. In this region, the value of $M(t)$ cannot increase any faster in time than t^2. This early time behaviour is observed whether nuclei are created, or preformed seeds are introduced (and no further nucleation occurs) [142, 145]. Therefore, the observation of an initial $\sim t^2$ time profile is not *a priori* evidence of primary nucleus formation [145].

Numerical integration of equation 1.3 yields an initial Poisson length distribution of filaments. However, the dissociation rate will no longer be negligible compared to monomer addition after the growth stage, when the majority of monomer is incorporated into aggregates, and after including k_{off} the filament length distribution is expected to tend towards an exponential at equilibrium [135, 147], where it takes the form [148]

$$f(j,\infty) = \frac{k_{\text{n}} m(\infty)^{n_{\text{c}}}}{2k_{\text{off}}} \left(\frac{k_{+} m(\infty)}{k_{\text{off}}}\right)^{j-n_{\text{c}}} \tag{1.5}$$

in which $m(\infty)$ is the critical monomer concentration at equilibrium.

Many variations on this simplest NDP model have been proposed [8, 30, 120, 124, 132, 141–143, 146, 149–169]. They are typically similar in construction but differ in mathematical description or the assumptions and approximations used to obtain analytical solutions. In the NDP system described above the rate constant for polymerisation is independent of polymer length, and depolymerisation is assumed to be negligible in order to obtain an analytical solution. These approximations are unlikely to be realistic and may not be good approximations for all experimental data. In many cases authors have considered length-dependent rate constants and/or reversible growth [141, 155, 161], however, due to the complex nature of the mathematics numerical integration is then required.

Inconsistencies with experimental data

Historically, where experimental data have been shown to exhibit features consistent with the NDP mechanism the growth process has been attributed to a pathway of this type. These features may include one or more of the following:

i) a sigmoidal growth profile; *ii)* a lag phase that can be reduced or abolished by the addition of preformed nuclei (seeding); *iii)* concentration dependence; *iv)* a critical concentration below which no observable aggregation occurs; and *v)* a final concentration of monomer in solution after the end-point of the reaction.

However, these observations are not conclusive evidence for a nucleation dependent mechanism [170]: *i)* the mass concentration of fibrils is typically found to exhibit a sigmoidal profile with a more pronounced lag phase and more rapid, exponential-like growth than can be accounted for by the NDP model. [116, 138, 149, 150, 153, 167, 171–174]; *ii)* lag phases are also observed in systems where processes other than primary nucleation dominate (*e.g.* monomer activation) and the addition of seed material also reduces or removes the lag time in a system dominated by other growth processes (for example secondary, filament dependent, growth mechanisms like fragmentation) since seeding acts to increase the number of aggregates earlier in the growth process; *iii)* systems dominated by other growth processes are also expected to exhibit concentration dependence and many have been shown to exhibit weaker concentration dependencies than those predicted by the NDP model [8, 77, 127, 138, 141, 144, 149, 150, 150, 152–154, 166, 169, 169, 175, 176]; *iv)* a critical concentration below which aggregation does not occur is also not exclusive to nucleating systems, micellar dynamics can also give rise to a critical concentration of this type [124, 152] (see section 1.3.3); and, *v)* it is unlikely that true equilibrium is observed in amyloid-like fibril formation, the end-point plateau of the reaction is thought to result from kinetic arrest rather than the system reaching equilibrium [177].

Additionally, proteins with little to no sequence similarity, aggregating under different conditions, have been shown to exhibit a correlation between lag time and maximum growth rate such that the product can be represented by a numerical parameter $\tau_{\text{lag}} r_{\max} = a$. This has been estimated to be in the range $1.6 < a < 7.4$ for a large number of experimental data, despite wide variation in individual values of τ_{lag} and $r_{\max}$ [136, 178–180]. This indicates a kinetic mechanism in which lag time and growth rate are correlated, inconsistent with the classical NDP model where lag time and maximum growth rate are independently related to nucleation and elongation respectively.

Furthermore, current thinking links a narrow region of the aggregate size distribution to cellular toxicity: the domain consisting of small oligomers and

fibril fragments. Xue *et al.* [27] have demonstrated that fibril fragment length correlates with cytotoxicity, and Hall and Edskes [181] postulate that disease initiation and display may correspond to the production of a threshold concentration of toxic species rather than total mass of protein aggregate. In the NDP mechanism a low number concentration of small early aggregates rapidly extends to form amyloid-like fibrils. As a result, the concentration of small, toxic intermediates is always low, inconsistent with predictions [181] and experimental observations of toxicity [27, 182].

1.3.2 Secondary growth processes

Although a primary nucleation process is typically believed to be required for the initiation of filament growth, it is not the only method by which new filaments may be formed. Secondary *de novo* filament formation processes are those in which creation of new filaments is dependent upon the existing filament population.

If a secondary process is active then the rate of aggregation will accelerate as filament number increases in a chain reaction or (auto)catalytic manner, and the aggregate population will increase exponentially. Pronounced lag phases can be observed and are the result of the exponential character of the population increase rather than the result of waiting for a primary nucleation process to occur [138, 145]. Growth profiles of this type are more consistent with typical experimental observations and the postulated autocatalytic processes include fragmentation, secondary nucleation and branching mechanisms.

Using microfluidics experiments Knowles *et al.* [183] recently provided indisputable evidence for aggregate proliferation by secondary growth processes in bovine insulin. Thioflavin T fluorescence intensity was found to spread homogeneously from point sources, suggesting that single nucleation events trigger a cascade of spatially correlated aggregation events in a chain reaction that can only be accounted for by the presence of a secondary growth process [183].

When large quantities of filament are present, secondary processes are expected to dominate over growth by primary nucleation. Knowles *et al.* proposed a critical volume below which primary nucleation becomes the rate limiting process. This volume was determined to be on the order of pL for bovine

insulin, implying that secondary processes will typically dominate in experimental assays that are of the order of µL [183].

Secondary nucleation and branching

In secondary nucleation the lateral surface of existing filaments can facilitate nucleation. This may be further divided into cases where the nucleus remains attached and those where it detaches and diffuses into solution [129]. Branching (or lateral growth) involves the addition of monomer to the lateral surface of an existing filament. While this may seem an identical process to secondary nucleation it is thermodynamically distinct. There is no free energy barrier governing the rate of branching, but a barrier exists to the formation of secondary nuclei [145]. However, this barrier might be orders of magnitude lower than that of primary nucleation and the size of the critical nucleus n_{sec} is not necessarily equal to that of the primary critical nucleus n_{c} [138, 145].

Fragmentation

In fragmentation the breaking of a polymer results in the creation of new ends for filament growth. In 1982 Wegner and Savko [184, 184] proposed that spontaneous fragmentation could account for the differing shapes of actin polymerisation curves in different experimental conditions. They extended their previously applied NDP model of growth by reversible monomer addition to include fragmentation of filaments. Since the mathematics in this case are necessarily complex, numerical integration was employed. The resulting kinetic curves were shown to more accurately represent the experimental data [184, 184], and fragmentation has since been suggested to be the secondary growth process in many other aggregating systems [30, 138, 144, 148–150, 157, 171, 183, 184, 184–190].

An analytical solution to the secondary process dominated polymerisation (SDP) model

Although numerical solutions for secondary nucleation [172, 191] and fragmentation models [30, 149, 157, 171, 184, 184, 189, 190], and the early-time perturbative treatment of Ferrone [145, 159] have had some success, the lack of

an effective analytical solution for the entire time-course of the reaction, and the computational cost associated with numerical integration, has resulted in slow acceptance of secondary-process-dominated polymerisation (SDP) models.

The first successful analytical treatment was presented by Knowles *et al.* in 2009 [144], and treated with a more rigorous mathematical approach in papers that followed [138, 148, 188]. The Knowles model of nucleation-polymerisation in the presence of secondary processes is governed by the concentration flux scheme: [138]

$$\frac{\delta f(t,j)}{\delta t} = 2m(t)k_+ f(t,j-1) - 2m(t)k_+ f(t,j) \tag{1.6a}$$

$$+ 2k_{\text{off}} f(t,j+1) - 2k_{\text{off}} f(t,j) \tag{1.6b}$$

$$- k_-(j-1)f(t,j) + 2k_- \sum_{i=j+1}^{\infty} f(t,i) \tag{1.6c}$$

$$+ k_{\text{sec}} m(t)^{n_{\text{sec}}} \sum_{i=n_{\text{c}}}^{\infty} i f(t,i)\delta_{j,n_{\text{sec}}} + k_{\text{n}} m(t)^{n_{\text{c}}} \delta_{j,n_{\text{c}}} \tag{1.6d}$$

$$\frac{\mathrm{d}m(t)}{\mathrm{d}t} = -\frac{\mathrm{d}}{\mathrm{d}t}\left[\sum_{j=n_{\text{c}}}^{\infty} j \cdot f(t,j)\right] \tag{1.6e}$$

The first four terms, and the final term, in $\delta f(t,j)/\delta t$ are recognisable from the NDP model as the change in population of filaments due to monomer addition, monomer dissociation and nucleus formation respectively [133, 134, 138, 142]. The fifth term accounts for the decrease in concentration of filaments of length j as a result of breakage of a $j-1$ internal bond, and the sixth term describes the creation of smaller filaments by fragmentation, accounting for the doubling in number of fibril ends for polymerisation. Fragmentation proceeds at rate k_- and the fragmentation term contributes to the effective depolymerisation rate as $k_{\text{off}} + k_-$ since it also operates to remove monomer from filament ends [138, 144]. The penultimate term in $\delta f(t,j)/\delta t$ represents a secondary process dependent upon the monomer and filament concentrations, either a secondary nucleation or branching process, governed by rate constant k_{sec} and having critical nucleus size n_{sec}.

The second equation in the scheme ($\mathrm{d}m(t)/\mathrm{dt}$) accounts for the monomer that is consumed by the growth, and the condition $f(t,j) = 0$ is imposed for

all $j < n_c$ to ensure that the critical nucleus (defined as $n_c \geq 2$) is the smallest stable species. As in the NDP model, growth is considered to proceed by monomer addition alone and the rate constants are considered to be independent of filament length [138, 144].

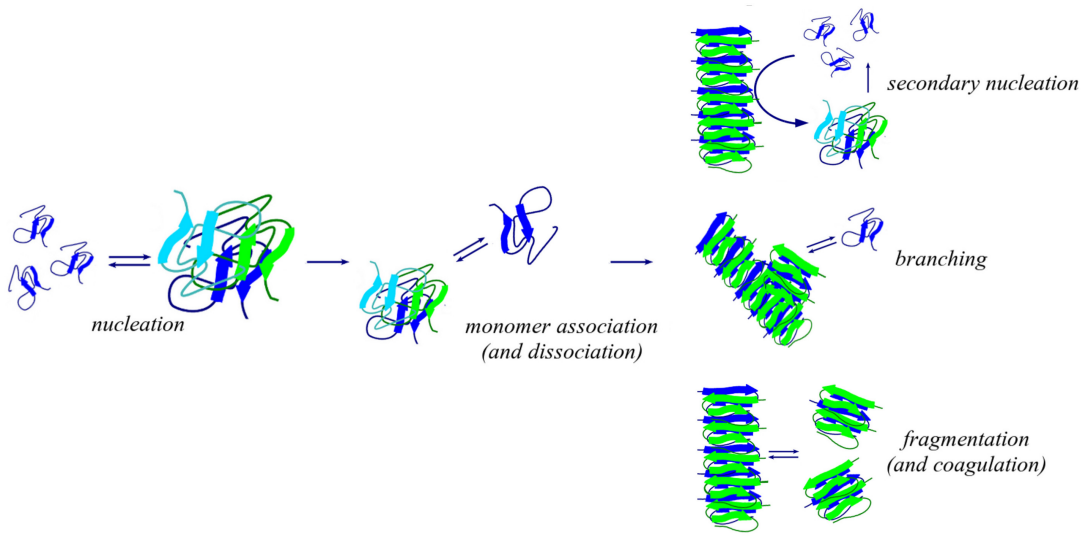

Figure 1.4: Cartoon depicting the growth mechanisms included in the secondary process dependent growth scheme: primary nucleation, (reversible) monomer addition, and either fragmentation, secondary nucleation or branching as the dominant secondary growth process.

The SDP model described above was initially derived for a fragmentation dominated scheme ($k_{sec} = 0$). The framework was extended, in the absence of fragmentation ($k_- = 0$), to describe either secondary nucleation or branching [188], as shown in Figure 1.4. Mechanisms of this type add to the non-linearity of the mathematics. As a result, the first iteration analytical solution, described below, is less accurate for secondary nucleation or branching processes than it is for the fragmentation dominated scheme.

Analytical solutions were derived by fixed-point analysis for $P(t)$ and $M(t)$ in various limiting cases. In the limit of irreversible growth, the closed form, simplified expression for $M(t)$ is given as [138, 144, 188]

$$M(t) = m_{tot}\left[1 - \exp\left(-C_+ \exp^{\kappa t} + C_- \exp^{-\kappa t} + \frac{\lambda^2}{\kappa^2}\right)\right] \tag{1.7}$$

where

$$C_\pm = \frac{k_+ P(0)}{\kappa} \pm \frac{M(0)}{2m_{tot}} \pm \frac{\lambda^2}{2\kappa^2} \tag{1.8}$$

λ is the same as in the NDP model, κ is the analogous parameter for the secondary process of fragmentation $\kappa_- = (2k_+k_-m_{\mathrm{tot}})^{1/2}$ or secondary nucleation $\kappa_{sec} = (2k_+k_{\mathrm{sec}}m_{\mathrm{tot}}^{n_{\mathrm{sec}}+1})^{1/2}$, and $M(0)$ and $P(0)$ are initial filament mass and number concentrations in a system where preformed fibrils or seeds are added [138].

The characteristic scaling laws of this system are as follows [138, 188]

$$r_{\max} \approx \frac{M(\infty)\kappa}{e} \qquad \tau_{\mathrm{lag}} \approx \left[\log\left(\frac{1}{C_+}\right) - \mathrm{e} + 1\right]\kappa^{-1}. \tag{1.9}$$

The (normalised) maximal rate of the reaction is dependent on k_+, k_{sec} or k_-, and the total monomer concentration through κ, and is independent of nucleation rate k_{n}. The lag time scales weakly with C_+ and therefore very weakly with k_{n}. The lag time concentration scaling behaviour obeys the approximate power law $\tau_{\mathrm{lag}} \sim \kappa^{-1} \approx m_{\mathrm{tot}}^{-\gamma}$, where $\gamma = (n_{\mathrm{sec}} + 1)/2$. While this scaling law is analogous to that of the NDP model, it is now the secondary process that dominates the concentration scaling. Moreover, the scaling of $r_{\max}$ with κ and τ_{lag} with κ^{-1} recovers the empirical correlation of lag phase with growth rate [138, 188].

When fragmentation is dominant $n_{\mathrm{sec}} = 0$ and $\gamma = \frac{1}{2}$, a value crucially smaller than the minimum exponent $\gamma = 1$ of the classical NDP model. This scaling factor was first demonstrated by Kunes *et al.* [149] through the assumption that lag time is the time required for aggregates to reach a detectable threshold mass. In the case $n_{\mathrm{sec}} = 1$ the secondary pathway may correspond to secondary nucleation or a branching process [192], and for $n_{\mathrm{sec}} \geq 2$ secondary nucleation is dominant. Importantly, this provides for the first time a method by which the concentration scaling of a system can be used to infer the nature of the dominant *de novo* filament formation mechanism.

In the limits of the classical NDP model ($k_{\mathrm{sec}}, k_- \to 0$) primary nucleation is recovered as the dominant process contributing to the creation of new aggregates and a polynomial form of $M(t)$ is obtained. The model therefore recovers the $\sim t^2$ early time profile of Oosawa-type NDP models where primary nucleation is dominant [138, 144, 188].

The filament length distribution of the fragmentation model, as determined by numerical integration and the first order solution for the integral $f(j,t)$ provided in [188], exhibits an initial skewed-Gaussian shape. At long times this tends towards a very narrow, short-filament biased Gaussian that may be approximated

to an exponential at equilibrium, where

$$\frac{f(j,\infty)}{P(\infty)} = \frac{4j^2 - (1-2n_c)^2}{n_c(1-2n_c)^2} \exp\left(\frac{2(-j^2+n_c^2)}{(1-2n_c)^2}\right) \tag{1.10}$$

holds for large n_c [148]. In the case of secondary nucleation an exponential equilibrium length distribution of the NDP type is recovered [148].

The SDP scaling laws discussed above have been recovered by applying alternative analysis methods to the length-independent SDP model [193, 194]. Ganapol demonstrates an alternative, highly accurate, numerical solution method to the SDP model using a finite difference numerical algorithm, and importantly, recovers the approximate scaling laws of Knowles' analysis by numerical means [194]. Hong and Yong also recover scaling laws of the form $r_{max} \propto m_{tot}^{\nu}$ and $\tau_{lag} \propto m_{tot}^{-\mu}$ [193]. They propose three classifications of growth process: a fragmentation dominated scheme where $\mu = \nu = 1/2$ are independent of nucleus size, a primary (or secondary) nucleation dominated scheme where $\mu = \nu = n_c/2$, both equivalent to the model of Knowles *et al.*, and an intermediate growth process where nucleation dominates in the initial growth stages and in later stages fragmentation becomes important, in which $\mu \approx n_c/2$ and $\nu \approx 1/2$ [193]. Their theoretical predictions have yet to be verified experimentally.

1.3.3 Additional microscopic growth mechanisms

Various additional microscopic processes have been considered in the further development of NDP and NDP-like models and these are described below. Although many of these have not yet been incorporated into a model alongside secondary growth processes, many of the predictions about the resulting growth parameter behaviours will be similar to those made for systems dominated by primary nucleation. Figure 1.5 depicts the many microscopic processes discussed here that may contribute to fibril growth.

Conformational change Since destabilisation of the native state to yield partially folded intermediates is thought to be an important process in the aggregation pathway for many systems [10, 13, 20, 21, 28, 112–118, 163], many authors include a 'monomer activation' term, where monomer in solution transform to monomeric aggregation competent species with a given rate, in

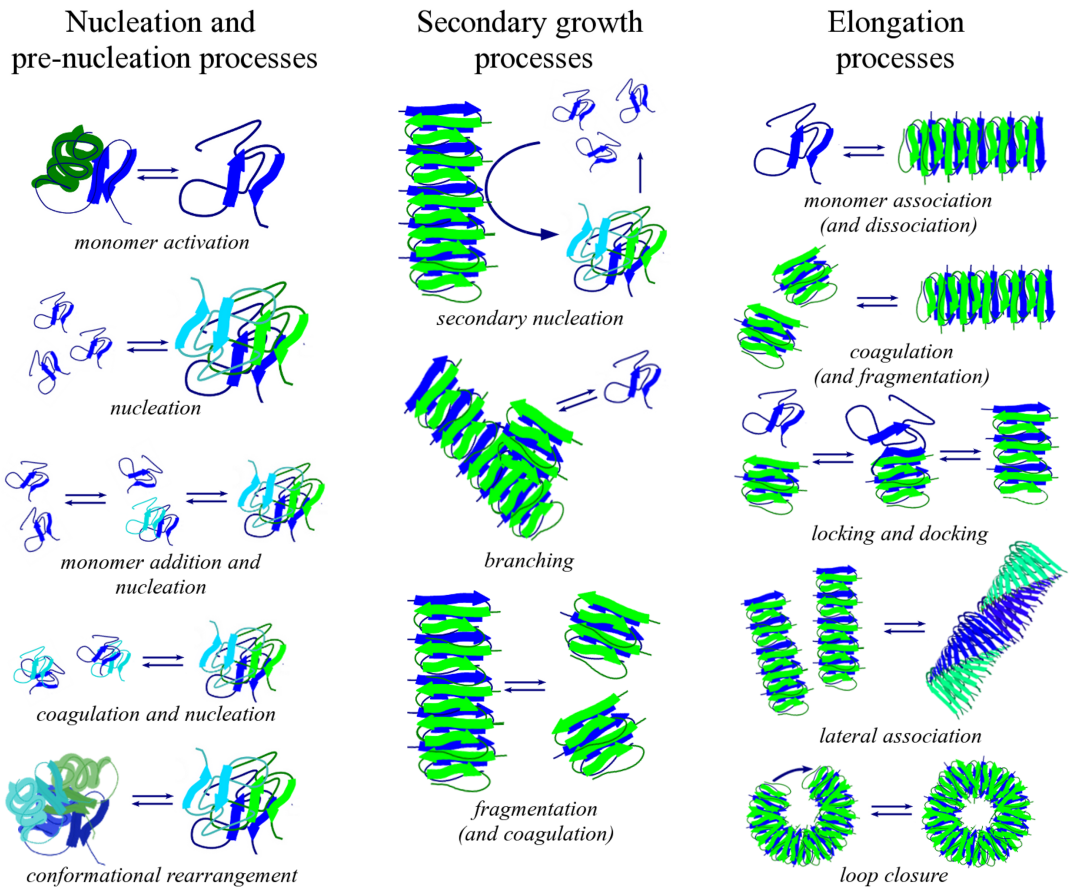

Figure 1.5: A cartoon depicting possible microscopic mechanisms that may contribute to amyloid-like fibril growth. These are separated into three regimes: those that may contribute to the primary nucleation process, secondary *de novo* filament creation processes, and those that may contribute to elongation.

their kinetic description [10, 116, 132, 140, 157, 160, 161]. However, in most cases monomer activation is not assumed to be rate limiting and the system is typically considered to be in 'preequilibrium' with respect to this conformational change [140, 155].

Conformational rearrangement may occur at other stages during the aggregation process, and has recently been experimentally observed [122]. Early native-like aggregates may undergo structural reorganisation into highly β-sheet fibrillar aggregates [28, 120, 122, 166, 169, 195–197]. For example in 'two-step' nucleation and nucleated conformational conversion (NCC) models, oligomers (or micelles) of critical nucleus size are considered to undergo rearrangement into a fibrillar form [120, 132, 166, 169].

Structural reorganisation may also occur at the fibril ends where monomer or other aggregates associate with the fibril (see also the 'lock and dock' mechanism in section 1.3.3) [130, 198]. There may be a number of metastable binding states and a number of possible routes of reorganisation. Even if the individual contributions to growth rate from these states are small it is possible that the total contribution could dominate the kinetics [199].

Micelles Protein micelles have been proposed as nucleation sites in the polymerisation pathway [8, 116, 124, 152, 200]. In such a system very little or no aggregation occurs below the critical micelle concentration (CMC), and nucleation is dependent upon the number of micelles.

In the micellar model proposed by Lomakin *et al.* [152] rapid micelle formation acts to buffer the monomer concentration, with micelles behaving as a monomer source and sink, and as nucleation sites but not themselves aggregation competent. A similar model was recently expanded to include fibril fragmentation [200]. These models are capable of explaining a weak or concentration independent lag time [124, 152, 200]. Other authors have proposed alternative reservoir-like populations, such as off-pathway aggregates, in order to account for apparent concentration-independence [153, 154, 156] or the observation of a critical concentration [155, 156].

Coagulation Coagulation or filament joining terms are frequently included as an alternative or additional method of fibril elongation in NDP models. Interchangeably referred to as end-joining, (random) filament association, diffusion-collision, condensation, stepwise or downhill polymerisation in the literature, we here refer to the reversible association of filaments f_i and f_j to form filament f_{i+j}. Filament coagulation terms have been included in NDP models where the process may be considered irreversible [132, 146, 155], as an alternative growth mechanism with the same rate as monomer addition [85, 146], a different rate to monomer addition, or having length dependent rate constants [132, 155, 201, 202]. In most cases the complexity of the mathematics has typically led to analysis by numerical integration.

For most fibril forming systems monomer addition is assumed to be the dominant elongation process since most of the protein is observed to be monomeric during the filament growth stage [150, 198]. However, this may not

be the case in all filament forming systems. End-to-end joining of filaments has been observed experimentally [44–46, 73, 83–85, 102, 109–111, 189], and in systems where elongation is initially dominated by monomer addition it is possible for coagulation terms to become important at late times when the monomer population is depleted.

The 'lock and dock' mechanism In some systems a significant decrease in the concentration dependence of the maximum growth rate $r_{\max}$ is observed above some initial monomer concentration [77, 127, 141, 150, 169, 203]. This may be the result of a locking and docking process in which monomer initially binds to filament ends with rate proportional to concentration to produce an intermediate species, followed by reorganisation of the intermediate in a concentration-independent manner. At high monomer concentration the rearrangement step will become rate limiting as a result of its sub-diffusive rate constant [127, 203]. A conformational change of this type has been estimated to occur on a timescale equivalent to that required for the native folding of a comparably sized β-sheet rich protein [150].

Lateral filament association Fibrils are often observed to consist of a number of laterally associated filaments [105, 108, 128, 155]. Pallitto and Murphy [155] therefore propose a mechanism by which filaments may be lost by irreversible lateral association to form fibrils at a length independent rate. In their model they assume that fibrils also elongate, but by irreversible coagulation of *fibrils* only, whereas filaments are assumed to grow by both irreversible coagulation of *filaments* and by monomer addition. Their numerical simulations were successful in describing experimental light scattering kinetics of β-amyloid. The model predicts that filaments are predominant at low initial monomer concentrations and that the distribution shifts towards fibrils at higher concentrations [155]. However, the growth patterns of filaments and fibrils are difficult to separate experimentally in order to confirm their predictions.

Supercritical concentration The most important feature commonly associated with NDP pathways is the strong concentration dependence of both τ_{lag} and $r_{\max}$, however, concentration dependence has been observed to weaken as concentration increases in a number of experimental systems [77, 127, 141, 150,

169]. Powers and Powers propose that this transition occurs at the 'supercritical concentration', above which the monomer becomes the least stable species in solution, and the monomer population is quickly sequestered into small off-pathway oligomers [77, 127, 141, 150, 169].

The Powers and Powers [141] reversible aggregation model considers nucleation by sequential monomer addition ($o_{i-1} + m \rightleftharpoons o_i$ for $i \leq n_c$), followed by fibril elongation by monomer addition ($f_i + m \rightleftharpoons f_{i+1}$ for $i \geq n_c$), with the supercritical concentration given by the ratio of the backward and forward rates of polymerisation for species smaller than the nucleus. At concentrations sufficiently below the supercritical concentration they find that numerical solutions for their model agree with the solution for the NDP pathway described above. Above the supercritical concentration monomer dissociation from oligomers becomes rate limiting. Both τ_{lag} and r_{max} may then become concentration independent. However, Powers and Powers note that the assumption of growth by monomer addition may not be physically realistic and that coagulation may also occur [141].

1.3.4 Coagulation models and loop formation

A number of fibrillating systems exhibit kinetic profiles inconsistent with both the NDP and SDP models. Many of these appear to be characterised by the absence of a nucleation process and do not exhibit sigmoidal growth profiles. In most cases the growth rate is maximum at $t = 0$, suggesting that these systems are dominated by elongation processes [28, 138, 142, 192]. The growth slows and eventually plateaus, giving rise to a concave or exponential profile of the form $M(t) \sim 1 - \exp^{-kt}$. In addition, a number of these systems have been shown to be unaffected by seeding, providing further evidence for either the lack of a nucleation process [61] or kinetics that are rate-limited by elongation processes.

Kinetic profiles of this form appear to be correlated with the formation of curvilinear or worm-like fibrils. Ovalbumin [90], yeast phosphoglycerate kinase (PGK) [40], α-synuclein [42, 43], α_{s2}-casein [44], human serum albumin (HSA) [46, 47], transthyretin (TTR) [49], β-amyloid [50–53], barstar [56, 57], bovine serum albumin (BSA) [61], β_2-microglobulin [62–64], prion proteins [77–80] and apolipoprotein C-II [81, 83, 85, 86, 189, 204, 205] have all been shown to exhibit this type of behaviour.

A number of models have been developed specifically to describe these systems. In many cases primary nucleation is not considered to occur. Additionally, for a number of systems exhibiting worm-like fibrillar species and exponential growth profiles an oligomeric growth pathway has been proposed [206], with oligomers rapidly formed from the monomer solution and elongation, the rate limiting step, proceeding via oligomer rather than protein monomer addition [2, 40, 56, 64, 78, 88, 206].

These systems may also exhibit sigmoidal kinetics under alternative experimental conditions. Indeed, some proteins, such as apoC-II [81, 86], β_2-microglobulin [62, 63], mouse prion protein [77] and α-synuclein [42, 43] have been shown to exhibit dramatically variable, environment-dependent, kinetic profiles.

Coagulation models

In coagulation models, also referred to as downhill, random association or condensation polymerisation models, polymerisation proceeds through association of any two species of length i and j on the aggregation pathway with reaction rate $k_{i,j} = k_{j,i}$. These models are distinct from NDP or SDP models that include coagulation as an elongation process, since no classical thermodynamic nucleation process is considered to occur. Traditional Smoluchowski coagulation theory of colloidal association, upon which many fibril coagulation models have been based, considers this growth process to be irreversible and diffusion-limited. As with NDP and SDP models, a single length-independent association rate is often assumed in order to provide analytical solutions [40, 132].

Simple growth proceeding by monomer addition was initially proposed as the self association mechanism for many proteins [207–209]. While this type of model has had little success describing the kinetic profiles of experimental data, the generalisation of this elongation-only model to include coagulation of any two species has been more successful [85, 116, 210–212].

The parameters of coagulating systems are predicted to be (inversely) first order with respect to initial monomer concentration: τ_{lag}, $\tau_{50} \propto m_{\text{tot}}^{-1}$, $r_{\max} \propto m_{\text{tot}}$ [140, 146, 172]. The time to 50% completion, τ_{50}, is typically a more useful parameter in systems dominated by elongation processes, since a lag time may not be observed. However, some models also include a nucleation-like process where initial growth is slow (growth proceeds with rate k_1 until some critical size

is reached after which growth proceeds with rate k_2, where $k_2 > k_1$), or where a species of critical size f_{m_c} is the smallest detectable species. In this case monomer concentration scaling of τ_{lag} is predicted

To refine the simplest coagulation model further, Modler *et al.* [40] included the homogeneity relation $k_{ai,aj} \propto a^{\sigma} k_{i.j}$, where $a > 0$ and σ is a constant ≤ 2, to account for length dependence of the association rate constants. They observed two different regimes of growth along the kinetic profile of PGK fibrillation and associated these with two coagulation regimes. They propose that the early growth is dominated by clustering into 'critical oligomers' with $0 < \sigma < 1$ and that the second period of growth is dominated by slower coagulation of these critical oligomers into filaments with $\sigma = -1$.

Loop formation

Closed-loop fibrils have been observed alongside fibrillar species of ovalbumin [90], HSA [46], FtsZ from *E. coli* [110], α-synuclein [111], β-lactoglobulin [73], α_{s2}-casein [44], crystallin proteins [45, 109] and apoC-II [83–85, 102]. Yang *et al.* [85] developed a simple equilibrium model to account for this observation in apoC-II. Although loop formation is similar in form to coagulation it acts as a sink for growth-competent filaments, and inevitably depends on the persistence length of the fibrillar species and must therefore be length dependent. In Yang's model, closed-loop species were assumed to form with a length-dependent probability of loop closure, while a single equilibrium constant was assumed for all other association processes. A monomer activation term was included as a slow nucleation-like step preceding elongation and elongation was considered to proceed through monomer association and coagulation [85].

Predictions for the length distribution were shown to reproduce the general shape of experimental data but overestimate the width of the distribution: a discrepancy thought to be the result of assuming length independent equilibrium constants. A simplified version of the model was shown to be in reasonable agreement with kinetic data [85]. Although not directly comparable to the kinetic descriptions discussed above, this model makes an important contribution towards including a previously neglected growth process.

A model of fragmentation and end-joining

Recently, a model for growth including coagulation (end-joining) was developed and shown to accurately reproduce the growth kinetics of chicken egg white ovalbumin by computer simulation [90]. This joining model begins as a highly seeded system with an initial fibril mass and number concentration M_0 and N_0. Elongation of fibrillar species then occurs via monomer addition with rate k_+ or the end-to-end joining of two fibrillar species with rate k_j. End-joining may also result in the formation of a closed loop, with rate k_l. Fragmentation, the reverse process of end-joining, occurs with rate k_f. The rate equations for the fibril mass density M(t) and fibril number density N(t) in this system are:

$$\frac{dM}{dt} = 2k_+(m_\mathrm{tot} - M)N - k_\mathrm{f} n_\mathrm{c}(n_\mathrm{c} - 1)N, \quad M(0) = M_0 \tag{1.11a}$$

$$\frac{dN}{dt} = k_\mathrm{f}[M - (2n_\mathrm{c} - 1)N] - k_\mathrm{j}N^2, \quad N(0) = N_0 \tag{1.11b}$$

where m_tot is the total density of protein monomers, n_c is the number of monomers in the smallest stable fibril and to a first approximation terms from loop formation and breaking are omitted, since these are usually small [90].

A number of exact solutions and an approximate analytical solution for this system are obtained in limited conditions where kinetics do not exhibit a sigmoidal shape (no lag phase). In the absence of fragmentation there is an exact analytical solution, but the inclusion of fragmentation was found to be necessary to reproduce growth curves of the form obtained for ovalbumin aggregation [90]. 'Kinked' aggregation kinetics are observed as a result of the competition between fragmentation and end-joining of fibrils: an initial rapid growth, followed by continued but slower growth and then a plateau region. In the absence of fragmentation the intermediate, slower growth region prior to the plateau phase is absent [90].

1.3.5 The limits of analytical solutions

The numerous assumptions and approximations made in order to obtain analytical solutions to concentration flux equations limits their ability to accurately describe realistic growth processes. As a result, many analytical solutions are

approximate rather than exact descriptions, but nonetheless provide valuable insight into molecular mechanisms.

Growth is often assumed to be filament length independent and irreversible ($k_{\text{off}} = 0$) [133, 134, 138, 142, 144, 145, 159, 184, 184]. In most cases length independent growth by monomer addition is thought to be a reasonable approximation, but this is unlikely to be the case for fragmentation/coagulation processes. In the SDP model filaments are assumed to break with equal probability at any position. However, experimental and theoretical analyses have shown that shorter filaments are much harder to break, and that the probability of breakage in the middle of filaments is greater [193, 202]. The assumption of length independent fragmentation is therefore much less likely to be a realistic approximation, and has been improved elsewhere by the introduction of a simple power law dependence $k_{-}(j) = k_{-}^{0} j^{\alpha}$ [150, 164]. The value $\alpha = 3$ was determined to provide the best fit to data by Arosio *et al.* [164] and Collins *et al.* [150] for the fibrillation of β-lactoglobulin and actin respectively.

Monomer dissociation from filaments has been observed experimentally [213], and reversible growth processes are thought to be important in determining accurate equilibrium length distributions [147, 186]. Higher order iterations of the SDP solution described above include depolymerisation [188], but necessarily increase in complexity. Nonetheless, this is a great improvement over previously derived analytical solutions for filament growth.

Depolymerisation has been included in the numerically derived equilibrium filament length distributions of both the NDP and SDP models, and in both cases the predictions of exponential length profiles are inconsistent with most experimental results. Length distributions of the native filament assembly of actin have been observed to be exponential [135, 147], but amyloid-like fibril length distributions are typically observed to peak at some intermediate fibril length and longer fibrils are observed to be stable on much longer timescales than predicted by either model [164, 197, 198, 214].

The inaccuracy of predicted length distributions is thought to result from simplistic assumptions about the growth process. In particular: the omission of filament coagulation (which would be expected to widen the length distribution), the assumption of length independent growth and fragmentation rates, and the assumption that the end-point length distributions obtained experimentally are

steady-state distributions. In addition, lateral filament association or bundling [148], precipitation, or gelation (as discussed in section 1.3.5) processes may occur and affect the length distribution, the time required to reach equilibrium, or cause kinetic arrest.

A critical fibril mass concentration

Current fragmentation-dominated models predict unrealistic end-point filament length distributions [164, 186, 197, 198, 214], based upon the assumption of equilibrium at the end-point of the kinetic process. However, experimental and theoretical results support the existence of a critical fibril mass concentration (CFC), for bovine insulin, above which a structural transition results in suppression of fragmentation. This is attributed to the transition of the filament solution from a viscous fluid to a viscoelastic gel [177].

A qualitatively new SDP model which includes this CFC predicts the formation of distinct fibril length distributions for protein concentrations above and below a critical threshold, observations that were confirmed by experiment [177]. For initial protein concentrations less than a critical threshold concentration c_{T}, filaments continue to fragment and in the long time limit the exponentially decaying length distribution of the SDP model is recovered. However, for initial concentration greater than c_{T} the mass concentration of fibrils exceeds the CFC during the exponential growth phase and fragmentation is arrested. The fibrils continue to extend by monomer addition but the shape of the length distribution is fixed in the long time limit as the log-normal curve with a defined peak that is predicted as an intermediate-time length distribution by the SDP model, in agreement with experimental observations [177].

Importantly, this concept of a structural transition enables successful prediction of the influence of environmental conditions on the fibril assembly pathway, since the CFC and therefore length of fibrils formed depends critically on both protein concentration and environmental conditions [177].

The presence of two distinct length distributions is also consistent with the observation that there is no direct correlation between mass of fibrillar material and the loss of function in disease states [215], and with the proposal that a change in environment within the host may be a trigger for toxicity or infectivity in the case of prions [30]. The existence of a CFC may therefore have dramatic

implications for determining the bias toward high toxic species or benign fibrillar load.

Reversible processes and length dependence

In a recent and noteworthy article, Hong and Yong [186] make an effort to include some of the complex growth terms discussed in Section 1.3.5 that are frequently assumed to be negligible in order to obtain analytical solutions. They demonstrate an alternative general moment-closure method to the fixed-point analysis of Knowles *et al.* [138, 144, 188], for a system proliferating by primary nucleation, monomer association and dissociation, and filament coagulation and fragmentation. Their method, based upon minimisation of the free energy of the system under certain constraints, has allowed for the first time the closure of moment equations in which the reverse processes of both elongation and fragmentation, and length dependence of rate constants are included. Their numerical solutions are shown to successfully replicate the shape of $M(t)$ data [186]. The scaling laws predicted from their solution [186]

$$r_{\max} \propto \left[(k_+ m_{\mathrm{tot}})^{n-1} k_- \right]^{1/n} \qquad \tau_{\mathrm{lag}} \propto \frac{\ln\left[(k_-)^{2/n} / (k_{\mathrm{n}} m_{\mathrm{tot}}^{n_{\mathrm{c}}-1}) \right]}{\left[(k_+ m_{\mathrm{tot}})^{n-1} k_- \right]^{1/n}} \tag{1.12}$$

where n is a constant, recover the result of the SDP fragmentation model in the case $n = 2$ and approximately recover the empirical relation $r_{\max} \propto \tau_{\mathrm{lag}}^{-1}$. Lag time scaling with concentration is determined to be $\tau_{\mathrm{lag}} \sim m_{\mathrm{tot}}^{-(n-1)/n}$. The authors note that monomer dissociation and filament coagulation rates, typically assumed to be negligible, contribute greatly to the equilibrium values of the final aggregate mass $M(\infty)$ and number $P(\infty)$ concentrations predicted by their model and are thus critical for accurate calculation of these values and therefore the equilibrium length distribution. However, $P(t)$ and the length distributions obtained from their model still only partially replicate experimental observations, and to obtain better results higher order moments (of filament length for example) would be required as minimisation constraints and dramatically increase the computational complexity [186].

The native environment

The *in vivo* environment is considerably more complex than the homogeneous environment of a typical *in vitro* experiment. The cellular and extracellular matrix are crowded environments where proteins may come into contact with numerous macromolecules, lipid membranes and other interfaces. System volume and concentration of aggregating protein are typically orders of magnitude lower *in vivo* [183, 216] and macromolecular crowding may be up to 400 g/L [217]. The typical 'physiological' experimental conditions *in vitro* are far from a realistic representation of the native environment.

The critical volume proposed by Knowles *et al.* [183], below which growth kinetics are dominated by primary nucleation, was determined for insulin ($\sim$pL) to be larger than that of typical living cells (pL-fL). Primary nucleation events may therefore play a much more important role in the initiation of aggregation processes *in vivo*.

Crowding has been shown to facilitate fibril formation in many cases [218–222], suggesting that the crowded physiological environment could play an important role in pathogenesis. Excluded volume theory predicts that oligomer formation will be favoured under crowded conditions. Unwanted aggregation can therefore be accelerated under conditions of macromolecular crowding [218, 222].

In addition, crowding has been shown to enhance fragmentation [218], which may also result from mechanical stress, thermal motion, interaction with lipids or the activity of chaperones *in vivo* [27, 100, 223]. Lipids, mica, surfactants and organic solvents have all been shown to affect aggregation [204, 205, 224, 225], and biological membranes and interfaces are likely to play an important part in the formation of aggregates and fibril toxicity *in vivo* [205, 216, 223, 226].

Supersaturation

There are parallels between nucleation of fibrillar species and crystallisation, where thermodynamic supersaturation is the driving force for the formation of nuclei from solution and aggregation is a function of monomer concentration relative to the protein solubility (C_a^*) [103, 227–229]. Recent evidence suggests that many proteins are kinetically, but not thermodynamically, stable in their native states, and at cellular concentrations that are close to or above their critical solubility concentration, suggesting that supersaturation may be a major driving

force of aggregation *in vivo* [230].

When aggregation is a function of monomer concentration relative to solubility, the lag time is expected to scale exponentially with initial supersaturation $\sigma_0 = (C_0 - C_a^*)/C_a^*$ rather than the initial monomer concentration $C_0 = m_{\mathrm{tot}}$. As the initial concentration approaches C_a^* the concentration scaling factor γ ($\tau_{\mathrm{lag}} \sim m_{\mathrm{tot}}^{-\gamma}$) then changes in value, and discontinuities in concentration behaviour may be observed as γ varies with monomer concentration [227]. This may explain some of the 'breaks' in concentration scaling that have been reported in a number of protein systems including bovine insulin [231] and β_2-microglobulin [171]. However, in *in vitro* systems, changes in time scaling behaviours may be further complicated by and difficult to distinguish from competition between secondary processes and primary nucleation.

Similarities between amorphous aggregation (and systems with kinetic profiles of the kind described in Section 1.3.4 that have no lag time) and glass transitions have also been described [103, 229].

Competing aggregate species

A number of recent papers have recognised the complexity that competing off-pathways of aggregation add to our description of fibril forming systems, and a number of models have been developed to describe fibril growth in the presence of competing amorphous aggregation [103, 227, 228, 232]. The presence of a competing pathway was found to be capable of radically changing the shape and characteristic kinetics of fibril growth curves, including the formation of multi-phasic mass-off-fibril growth curves [228] and weak concentration scaling of time parameters [227, 232].

Competing and possibly amorphous aggregates are observed alongside fibrils in a number of aggregating systems [53, 103, 227, 232–236]. Such species decrease the concentration of monomer available for fibril growth and may regulate fibril formation, providing false positives and negatives in the evaluation of anti-aggregation agents [228].

These off-pathway amorphous species are not considered to contribute to the kinetic growth curves obtained for the fibrillar growth (for example where the measurement is of ThT fluorescence enhancement and the amorphous species have no affinity for ThT) [103, 227, 228]. However, the presence of a competing

pathway would be highlighted by a comparison of mass-of-aggregate and monomer depletion kinetics, since these are only equivalent (inversely) if amyloid-like fibrils are the only species produced [103, 227].

However, it is also possible given the range of possible fibrillar polymorphs, some of which have been shown to have a different β-core structure, that alternative fibrillar species may compete for monomer. In this case the analysis of growth kinetics is further complicated since the kinetic growth profiles obtained may contain contributions from both species.

Heterogeneous nucleation

The surface activity of fibrillation-prone proteins complicates investigation *in vitro* where surfaces or interfaces that are not present *in vivo* accelerate aggregation [172, 216, 237]. Surface adsorption of protein at the air-water interface (AWI) [216, 237], the water-container interface and on deliberately introduced impurities [238], surfaces [216] and interfaces have been shown to significantly affect aggregation kinetics. Additionally, molecular simulations have suggested that the same surface may accelerate or retard growth depending on the bulk propensity of fibril formation, resulting in different aggregation attenuation between different species or under different conditions [239].

Observed nucleation processes are almost always heterogeneous, occurring with the nuclei in contact with a surface or interface that is difficult or impossible to eliminate or characterise, for example the walls of the containing vessel [240]. If possible, conditions that minimise unwanted surface interaction should be employed, *e.g.* ensuring that the containing vessel walls do not adsorb protein. Alternatively, since heterogeneous nucleation contributions will become concentration independent once the surface in question is saturated, concentrations above this point should be investigated.

It is relatively straightforward to perform experiments in which the AWI is abolished. Removing the AWI has been shown to dramatically slow, diminish or abolish aggregation behaviour in many systems [216, 237]. This demonstrates the dominant effect of the AWI in driving the aggregation process, but in many cases its removal makes kinetic aggregation data experimentally inaccessible. Interestingly, Jean *et al.* [237] recently demonstrated that in the absence of the AWI the influence of anionic liposomes on the aggregation behaviour of IAPP

was enhanced, suggesting that the effects of membranes on aggregation may be underestimated in typical experiments where the AWI is accessible [237].

Although the importance of membrane, surface and interface nucleation is well documented, efforts to include such processes in a kinetic description of protein fibrillation are limited. In part this is due to the additional complexity of the problem, in which the free energy of nucleation depends not only on the interfacial tension between the nucleus and the bulk phase (as in primary homogeneous nucleation) but also on the topology, size and number of binding sites of the surface and the interfacial tensions between nucleus and surface, and bulk phase and surface. Fuller discussions of heterogeneous nucleation may be found in the literature [240].

Jean *et al.* [237] extended the simple micelle NDP-type model of Lomakin *et al* [152] (see section 1.3.3) to include a second, primary-nucleation-like term describing heterogeneous nuclei formation at the AWI from the proportion of the monomer adsorbed at the interface. Their predictions of the effect of removing the AWI at different stages of the kinetic process, above and close to the CMC of islet amyloid polypeptide (IAPP) (assuming that primary nucleation occurs in protein micelles), were confirmed by their experimental results [237].

Protein aggregation is a highly complex problem. Many of the possible growth mechanisms that have been included in nucleation-dominated growth schemes have not yet been investigated in the framework of a secondary-process-dominated growth scheme. A general aim for research in this area should be to extend the analytical equation system to include these growth processes where possible. Notably, kinetic descriptions of systems dominated by heterogeneous nucleation processes are scarce, and one of the most important outstanding challenges in the understanding of amyloid fibril formation and cytotoxicity is the description of the kinetic interplay between fibril forming proteins and biological membranes.

1.4 The power of growth curve analysis

In Section 1.2.2 the many methods used to analyse fibril growth are listed, and kinetic mass-of-aggregate (or monomer depletion) data are proposed as a minimum requirement to describe the microscopic processes resulting in fibril growth.

Many of the methods used to obtain kinetic data that are approximately proportional to mass-of-aggregate are relatively simple and inexpensive, such as turbidity, intrinsic and extrinsic fluorescence assays and light scattering. Such techniques, combined with the predictions of kinetic behaviour from growth models (as described in Section 1.3) and fitting to analytical solutions have been shown to deliver a substantial amount of information about the growth mechanisms of fibril forming systems, for example in highlighting the importance of secondary growth processes in the majority of fibril forming systems *in vitro* [30, 116, 138, 144, 148–150, 150, 153, 157, 167, 171–174, 183, 184, 184–190].

However, it is clear that many growth curves deviate from the forms of analytical solutions that are obtained under limiting conditions, as a result of the complexity of fibrillar growth governed by any number of the growth processes shown in Figure 1.5. Many growth processes have not yet been adequately described in SDP-like models, and many systems exhibit critical concentrations where the dominant growth processes change, and resemble a different analytical solution above and below the critical concentration. Analytical solutions are less likely to be found where changes in the dominant growth process occur as monomer is depleted, especially if the comparative dominance of multiple growth processes changes gradually over time, or where two or more growth processes have similar contributions to the growth rate.

Alternatively, kinetic data may be complicated by the formation of multiple different aggregate species formed along alternative and possibly competing aggregation pathways [1, 70, 75, 88]. Competing off-pathway species have recently been linked to a number of kinetic signatures including highly variable end-point signals and weak concentration dependence of the characteristic times [227, 232]. In this case, a single analytical solution to the growth is impossible.

How much information can then be obtained from growth curve analysis in the absence of performing computationally expensive fits to growth models, or as a prerequisite to determine the likely growth model, and where are the shortfalls?

This research aims to demonstrate the level of information that can be obtained by applying simple, inexpensive measurement techniques and growth curve analysis to model globular and intrinsically disordered protein systems of interest that are known to exhibit some of the complexities outlined above that might complicate growth curve analysis.

Hen egg white lysozyme (HEWL) and α-synuclein are the model proteins examined in this research. HEWL has been extensively studied because of its importance in food science as one of the main constituents of egg white and its similarity to human lysozyme. It is typically considered a model globular system for studying protein folding and misfolding, and is known to aggregate and form fibrils under particular conditions.

HEWL has been found to form a range of fibrillar polymorphs under different solution conditions, and the growth mechanisms of some of these species have not been analysed in detail. In addition, HEWL has been found to form straight fibrils at low pH, high temperature and low ionic strength, and curvilinear species at low pH, high temperature and high ionic strength, along what appear to be distinct assembly pathways that may be in competition.

Alpha-synuclein (α-syn) is studied here as a model intrinsically disordered protein (IDP). IDP's are a subset of proteins defined by their lack of (or regions lacking) tertiary structure. Alpha-synuclein has been extensively studied because of its implication in neurodenegerative disorders. However, the mechanism by which α-syn converts into fibrils is not well understood.

In addition, while fibrils formed from α-syn at low pH and high temperature are characteristically straight, α-syn has been observed to form curvilinear filaments in the presence of the detergent sodium dodecyl sulphate (SDS), where the behaviour of α-syn is believed to be similar to behaviour in the presence of membranes. Alpha-synuclein is a membrane active protein, and this alternative aggregation behaviour may have pathological relevance. The mechanism by which fibrils are formed under these conditions has not been fully investigated.

This thesis is separated into two sections following the methodology, one for each protein: an introduction and background section describes the current understanding of fibril formation of the model protein; a results section outlines the experimental findings and growth curve analysis; and a discussion section for each protein interprets these results and their implications for growth curve analysis.

Chapter 2

Materials and Methods

2.1 Expression and purification of α-synuclein

2.1.1 Purification 1

Recombinant α-synuclein was kindly provided by Dr Tilo Kunath, MRC Centre for Regenerative Medicine, University of Edinburgh. Recombinant α-synuclein was produced in *E.coli* BL21(DE3) from a pT7-7 expression plasmid and purified as described previously [241]; in 20 mM Tris-HCl at pH 7.5 using a Hitrap QFF 5 column. Purified α-synuclein was concentrated to $\sim$ 5.5 mg mL^{-1} and the buffer solution was adjusted to 10 mM Tris-HCl, pH 7.5, 100 mM NaCl before aliquots were flash frozen and stored at -80°C.

2.1.2 Purification 2

Recombinant production was performed in house and purification was performed at the Edinburgh Protein Production Facility. The recombinant α-synuclein pT7-7 expression plasmid was kindly provided by Dr Tilo Kunath, MRC Centre for Regenerative Medicine, University of Edinburgh. Recombinant α-synuclein was produced in *E.coli* BL21(DE3) from the pT7-7 expression plasmid and purified as described in more detail below; in 20 mM Tris-HCl at pH 8 using a Resource-Q column before desalting into 100 mM ammonium acetate using a HiPrep 26/20 Desalt column and freeze-drying. Samples were then stored at -80°C.

E.coli BL21(DE3) C41 harbouring pT7-7 expression plasmid was induced for α-syn expression by 0.1 mM IPTG and 5 hrs growth at 37°C, 200 rpm in LB media.

Cells were harvested by centrifugation, the pellets washed once in 20 mL of PBS. Pellets were stored at -80°C and resuspended to 30 mL (per 1 L equivalent) in cold 20 mM Tris, pH 7.5, 1 mM EDTA, protease inhibitor cocktail (Roche), 1 mM DTT. Lysis was performed by single passage through cell disruptor at 22,000 psi. The lysate was centrifuged for 45 min at 18,000 g at 4°C and the supernatant decanted. The pH of the supernatant was adjusted to pH 3.5 to precipitate *E.coli* contaminating proteins and left gently stirring at room temperature for 20-30 min followed by 4°C for 1 hour. The solution was centrifuged at 27,000 g for 1 hour at 4°C and the pH of the supernatant altered to pH 7.5. This was then filtered through a 0.22 µm filter and loaded, in 100 mL batches, onto a 6 mL Resource-Q column, pre-equilibrated in the same buffer at 20 mL min^{-1}, at 4°C. Elution of α-synuclein was performed by gradient from 0-1 M NaCl (most α-syn elutes between 300 mM and 400 mM NaCl). Samples containing α-syn were then desalted into 100 mM ammonium acetate in 10 mL batches using a HiPrep 26/20 Desalt column run at 10 mL min^{-1} in the same buffer. Protein was collected and immediately freeze-dried and stored at -80 °C.

2.1.3 Purifications 3 and 4

Recombinant production and purification for samples 3 and 4 was performed by the Edinburgh Protein Production Facility. Recombinant α-synuclein was produced in *E.coli* BL21(DE3) from the same pT7-7 expression plasmid and purified as described in more detail below; in 20 mM Tris-HCl at pH 8 using a Resource-Q column before desalting into PBS, pH 7.5, 1 mM EDTA using a HiPrep 26/20 Desalt column. Purified α-synuclein was concentrated to $\sim$ 5 mg mL^{-1} in PBS before aliquots were flash frozen and stored at -80°C for purification 3 and concentrated to $\sim$ 10 mg mL^{-1} in PBS before aliquots were flash frozen and stored at -80°C for purification 4.

E.coli BL21(DE3) C41 harbouring pT7-7 expression plasmid was induced for α-syn expression by 1 mM IPTG and 16 hrs growth at 30°C, 260 rpm in Enpresso-B media. Cells were harvested by centrifugation at 8,000 g for 30 min, the pellets washed once in 50 mL of 20 mM Tris, pH 8.0, 1 mM EDTA. Pellets were resuspended to 20% *w/v* in cold 20 mM Tris, pH 8.0, 1 mM EDTA, protease inhibitor cocktail (Roche), 1 mM PMSF, 1 mM Benzamidine. Lysis was performed by single passage through cell disruptor at 22,000 psi. The lysate was

centrifuged for 1 hr at 15,000 g at 4°C and the supernatant decanted and $AmSO_4$ added to 30% *w/v* (0.296 g mL^{-1}) and the solution left gently stirring at 4°C for 90 min. The solution was centrifuged at 10,000 g for 30 minsat 4°C and then the pellet resuspended in 50 mL of 20 mM Tris, pH 8.0, 1 mM EDTA, 1 mM PMSF per litre equivalent of original culture. This was then filtered through a 0.22 µm filter and loaded, in 100 mL batches (2 litre equivalents), onto a 6 mL Resource-Q column, pre-equilibrated in the same buffer at 20 mL min^{-1}, at 4°C. After loading and washing (10 column volumes of same buffer), followed by a 5 column volume wash at 250 mM NaCl (in same base buffer), elution of α-synuclein was performed by gradient over 10 column volumes from 250 mM NaCl to 500 mM NaCl (most α-syn elutes between 300 mM and 400 mM NaCl). Samples containing α-syn were then desalted into PBS, pH 7.5, 1 mM EDTA in 10 mL batches using a HiPrep 26/20 Desalt column run at 10 mL min^{-1} in the same buffer. Protein was collected and concentrated to $\sim$ 10 mg mL^{-1} using a 5 kDa cut-off spin concentrator and then flash frozen in 2 mL aliquots in liquid N_2. The PBS solution was created in house: 20×PBS (1L) = 160 g NaCl, 4 g KCl, 12.2 g Na_2HPO_4, 4 g KH_2PO_4, resulting in a 1× solution of ∼5 mM phosphate, 137 mM NaCl.

2.2 Thioflavin T and absorbance assays

Six times recrystallised lysozyme from hen egg white was obtained from Seikagaku Co. Ltd. (lot E00301) and used without further purification. Fresh lysozyme stocks were produced by dilution of lyophilised lysozyme in buffer and filtered at 0.22 µm (Millipore) to remove particulate material immediately prior to use. The concentration of each protein stock was determined by UV spectroscopy, using the extinction coefficients 0.41 mL mg^{-1} cm^{-1} for α-synuclein and 2.65 mL mg^{-1} cm^{-1} for HEWL. Where necessary pH was altered by addition of small volumes of HCl or NaOH.

The number of sample replicates varies between experiments from a minimum of 3 replicates up to 60 (the internal microplate wells of a 96-well microplate). Typically, sample replicates vary from 3-8 for α-syn and 6-60 for HEWL. The number of replicates was increased for low HEWL concentrations where the inherent variability is higher in order to obtain more reliable and reproducible

average growth curves. Where additives were found to dramatically increase the growth rate (for example high salt concentrations and SDS) these were added by multichannel pipette immediately before reading in the platereader.

Thioflavin T (ThT) was obtained from Sigma (T3516, lot O27 K2099). Stocks were prepared at 5.5 mM in Nanopure water, filtered at 0.22 µm (Millipore) and frozen in aliquots at -20°C. A fresh aliquot was used for each experiment conducted. Unless otherwise noted, a final concentration of 55 µM ThT was used in ThT kinetic assays. This concentration was selected to ensure that at high protein concentrations fluorescence saturation was not reached before the end of the protein aggregation growth process. In each case the effect of ThT concentration was determined to ensure that chosen concentrations did not notably interfere with the growth process, and that the maximum fluorescence value was independent of a further increase in ThT concentration.

Unless otherwise noted, microplate well volumes were 100 µL in 96 well microplates. Microplate types varied between experiments and were either 96 well, flat bottomed, non-binding-surface coated, clear, Corning microplates (CLS3650-100EA); 96 well, flat bottomed, uncoated clear polystyrene, Greiner microplates (655101); or polystyrene PolySorp Nunc ThermoFisher StarWell microplate strips (441254) with strip caps. Corning and Greiner standard 96-well microplates were sealed using Greiner microplate sealing strips.

Three platereaders were used, and since the conditions in each reader vary no direct comparisons have been made between data obtained in different instruments and where the readings were performed on different instruments this has been noted. The readers used were a FluoStar Optima, FluoStar Omega and a BioTek Synergy 2 plate reader.

In the Fluostar Optima and Fluostar Omega platereaders, filters at 450 and 485 nm were used for ThT fluorescence excitation and emission respectively, both with a bandwidth of 10 nm. A filter at 600 nm with a bandwidth of 10 nm was used for absorbance measurements. Unless otherwise noted, agitation was by double-orbital plate shaking and to avoid temperature gradients where possible the reader was programmed to position the microplate away from the optics during waiting times between readings and shaking. All fluorescence readings were performed at the bottom of the microplate. In the BioTek Synergy 2, filters at 440 and 485 nm were used for ThT fluorescence excitation and emission

respectively, both with a bandwidth of 20 nm. Absorbance was measured at 600 nm by monochromater with 2.4 nm bandwidth. Agitation was performed by linear microplate shaking. Fluorescence readings were performed at the bottom of the microplate.

2.2.1 Analysis of experimental data

The average of multiple kinetic curves is in each case corrected for background ThT buffer solution and normalised to the point considered to be that of maximum fluorescence. ThT fluorescence intensity is assumed to be proportional to the mass of aggregate present, and these normalised curves are assumed to be proportional to the fraction of aggregate total mass. As such, axes are labelled as 'fraction aggregated'.

It should be noted that the normalisation point is not always the largest fluorescence reading, in many cases higher and fluctuating fluorescence values are observed, and are thought to be due to evaporation and/or phase-change effects and not part of the kinetic growth process. Alternatively, where two distinct kinetic growth regions appear to be present the maximum fluorescence values of each region may separately be considered as points for normalisation for separate analysis (for example where two separate growth pathways appear to be active).

A damped least-squares fitting method, using the Levenberg-Marquardt algorithm was implemented in Python using the lmfit package for fitting in all cases. This is the most tested fitting algorithm for this method, where uncertainties and correlations between fitted variables are automatically estimated from the covariance matrix during the fit. However, since the approach that is used to determine uncertainties is sometimes questioned, a brute force search of confidence intervals and correlations was also performed, to ensure that the global minimum and not a local minimum is obtained for parameter values.

2.2.2 Hen egg white lysozyme

Experiments were performed in a BMG labtech Fluostar Omega platereader, at 65°C with double orbital shaking at 700 rpm for 2.5 of 5 minutes per cycle, unless otherwise noted. Fluorescence filters of 450(10) nm and 490(10) nm were used for excitation and emission respectively, with recording of fluorescence emission from

the bottom of the microplate. Experiments were also performed on a BioTek Synergy 2 platereader with equivalent fluorescence filters. Corning NBS coated, 96 well, flat bottomed, non-sterile microplates were used, with 100 µL per well, unless otherwise noted. Plates were sealed with adhesive Greiner coverfilms. Numbers of replicate wells ranged from 6 to 60, with increasing number of replicates as reproducibility decreased with protein concentration.

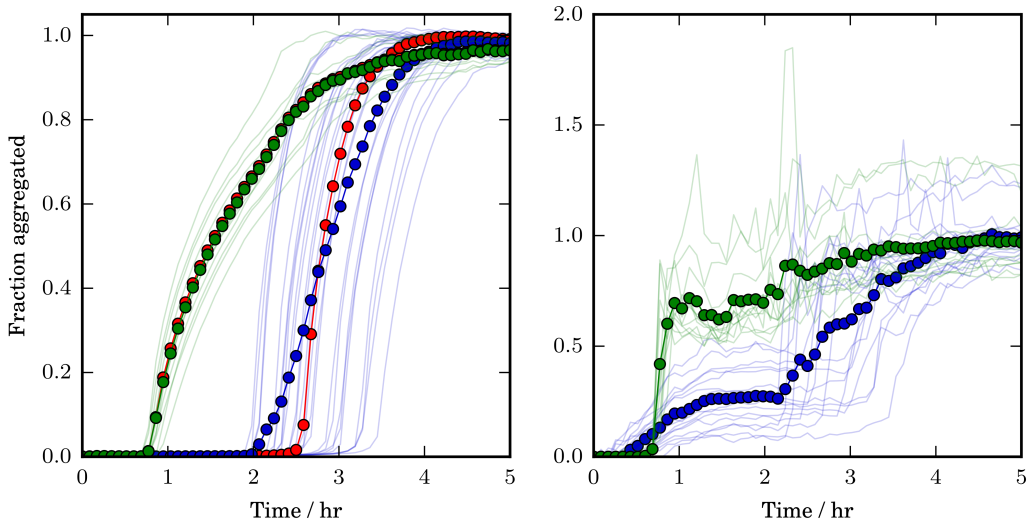

Figure 2.1: ThT fluorescence aggregation data for 1 (blue) and 8mg/ml (green) lysozyme, pH 1.6, 200mM NaCl, 65C, shaking at 700rpm. These data are typical of kinetic traces obtained for lysozyme at concentrations of 5mg/ml and below, and 6mg/ml and above respectively. At lower concentrations a wider range of lag times are observed. Average data are shown with datapoints, those in blue and green are the mean data, those in red are the corrected mean (data corrected for mean x before mean y). Error bars not shown

Shown in Figure 2.1, a wider range of lag times was observed at lower protein concentrations (5 mg mL^{-1} and below) when HEWL is aggregated under the conditions pH 1.6, 200 mM NaCl, 65°C, double orbital shaking at 700 rpm. This is thought to be the result of poor experimental control under the conditions that are achievable with this method (platereader assay) combined with competition between alternative aggregate pathways, with resulting variations exaggerated at lower protein concentrations. The conditions applied were the maximum temperature/agitation achievable for in situ measurements by platereader assay.

Fluorescence results were normalised to both the plateau maximum in y and to $y = 10\%$ completion in x (for concentrations 5 mg mL^{-1} and below) before averaging, due to large variation in final fluorescence/absorbance values and wide

range of lag times that otherwise affect the average curve shape. The effect on average curve shape is evident in the blue trace with circles (the average of y-normalised only data) versus the red trace with circles (the average of x and y-normalised data) in Figure 2.1.

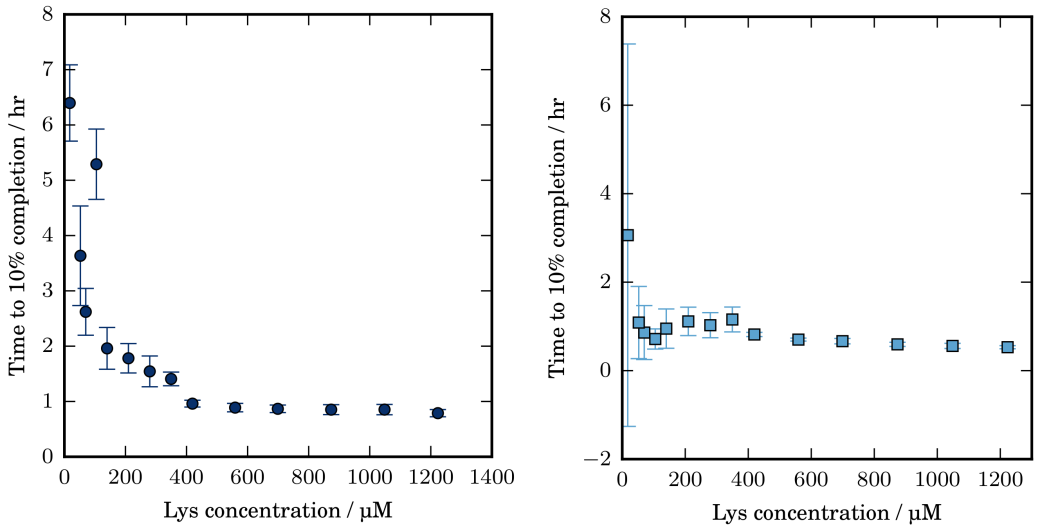

Figure 2.2: Time to 10% completion by ThT fluorescence (left) and absorbance at 600 nm (right) for various concentrations of hen egg white lysozyme incubated at pH 1.6, 200mM NaCl, 65C, shaking at 700rpm. At lower concentrations a wider range of times are observed. Error bars are standard deviation.

Fluorescence data were normalised horizontally along x by shifting data towards the average x value at $y = 10\%$ completion by integer timesteps (a timestep being the time between consequetive data points) since this value (10% completion) was consistently in the linear region of the curve and seemingly less affected by changes in curve shape with HEWL concentration than τ_{lag} or τ_{50}. This 'corrected' mean is indistinguishable from the normal mean of the data when the variation in x of $y = 10\%$ completion is small, for example by absorbance (except at the lowest concentration) and at concentrations above 5 mg mL^{-1} by fluorescence, and the normal mean is used instead. This is clearly seen in the smaller standard deviations shown in Figure 2.2 for absorbance readings and the fluorescence readings for 5 mg mL^{-1} and above.

2.3 Transmission Electron Microscopy and image analysis

Aliquots from aggregate samples were diluted immediately prior to grid preparation to avoid dissociation due to dilution, and the dilution factor varied between samples but was typically in the range 1:10 to 1:20. Aliquots of 4 µL diluted aggregate sample were placed on 400 mesh copper grids (Taab, Aldermaston, UK) coated with formvar and carbon, and allowed to rest for 3-5 minutes depending upon sample type (shorter times were found to produce better results with curvilinear filaments) before removing the excess with filter paper. Grids were then washed with 10 µL MilliQ water and stained by application of 4 µL 1% uranyl acetate for 25-45 s. Excess stain was removed with filter paper and grids were allowed to air dry for at least half an hour prior to imaging. Imaging was performed using a Philips (FEI) CM120 Biotwin Transmission Electron Microscope with an operating voltage of 80 kV.

Image analysis was performed using ImageJ image analysis software. Fibril widths were measured manually over a large number of fibrils identified as individual and across multiple images taken in various regions of the copper grid.

Chapter 3

Fibril formation by Lysozyme

3.1 Introduction

Hen egg white lysozyme (HEWL) is a protein that has been extensively studied and its physiochemical properties examined in detail. It is typically considered a model system for protein folding and misfolding because of its relatively small size, globular nature, structure including both α- and β-domains and because it is inexpensive (most sources are purified from egg white). HEWL forms fibrils *in vitro* [2, 89, 242–261], with structure and kinetic growth profiles that depend on the initial growth conditions [89, 254]. It is therefore ideal for studying the mechanism of protein fibril formation [253, 254, 256].

The study of HEWL is of particular interest because of its importance to food science as one of the main constituents of egg white and its similarity to human lysozyme, an important enzyme in the human body's defense against some bacteria, found abundantly in tears, salica and mucus, whose variants form the amyloid-like fibrils implicated in hereditary systemic amyloidosis [244, 254, 256].

The human and hen egg white forms of lysozyme have a 60% sequence similarity and share a similar 3D structure [262]. The different orthologues of lysozyme have also been found to be capable of cross-seeding fibril formation, with human lysozyme capable of seeding the formation of HEWL fibrils, albeit with lower efficiency than lysozymes with higher sequence similarity including turkey lysozyme [242, 263].

3.2 Structure of hen egg white lysozyme

HEWL is a globular monomeric protein consisting of 129 amino acids, with a molecular weight of 14.307 kDa and pI ∼11 [258, 264]. Its structure has been determined by X-ray diffraction [265]. Two domains bridge an active site cleft: the α- and β-domains. The α-domain consists of the terminal ends and contains four α-helices and two 3_{10}-helices. The β-domain encompasses the central region of the primary sequence and consists of a small, three-stranded β-sheet, a long loop and a 3_{10}-helix [258]. Eight cysteine residues are involved in four disulphide bonds and the overall monomer is roughly ellipsoidal with dimensions $\sim 4.5 \times 3.0 \times 3.0$ nm [265].

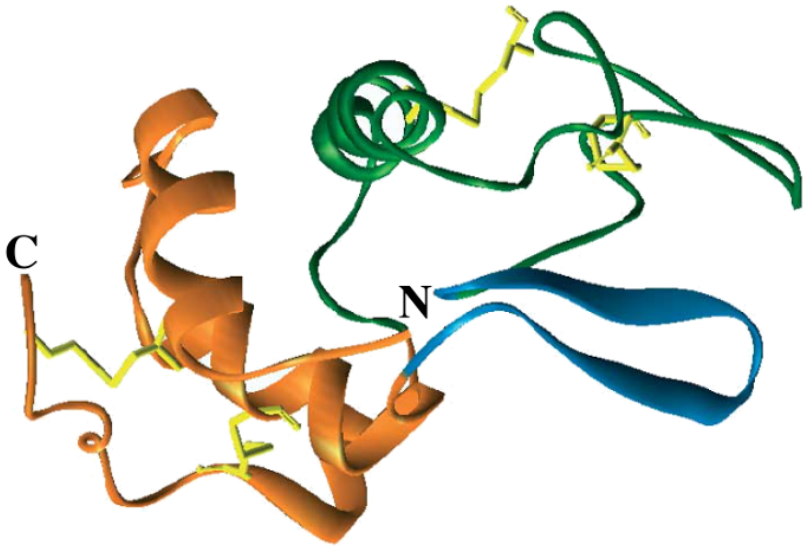

Figure 3.1: Top: A representation of the 3D structure of HEWL (relating to protein fragments obtained by limited proteolysis, edited from Frare *et al.* [252]). The chain segments 1-38 and 108-129 (helices A, B and D) are coloured in orange, segment 57-107 (helix C) in green and 39-56 (β-domain) in blue. The four disulphide bonds are represented by yellow sticks. Bottom: The amino acid sequence of HEWL.

3.3 Aggregation of hen egg white lysozyme

HEWL has been found to form amyloid-like fibrils *in vitro* under a range of environmental conditions: most notably at low pH (pH 1.5-2) and high

temperature ($\geq$ 50°C) [242–244, 247, 251–253, 258]; at high alcohol concentration ($\geq$ 80% EtOH) [254–261]; in the presence of denaturants (urea) or surfactants (SDS) [248–250]; in its reduced form in the presence of DTT; and to be highly sensitive to salt concentration [2, 89, 245–247, 258].

3.3.1 Low pH and high temperature

The structure of HEWL varies weakly with pH, with the formation of molten globule states at low ($\sim$ pH 2.6) and high pH ($\sim$ pH 12.8), while its stability varies more dramatically [258]. Thermal stability of HEWL is maximum between pH 4 and 5, drops off steeply as pH decreases and decreases less drastically with increases in pH [247, 258].

At low pH (pH 1.6-2) on heating, the CD structure of HEWL has been found to coincide with the native structure up to 40-45°C and a major structural change is observed between 50 and 60°C where the ellipticity between 208 and 230 nm increases and the minimum at 208 nm moves to lower wavelengths [244, 251]. Additionally, tryptophan fluorescence analysis has suggested penetration of the tertiary structure by solvent before unfolding of the secondary structure [251]. As pH increases above pH 2 these changes have been found to shift to higher temperatures [244].

Aggregation is observed upon incubation at 50°C and above. Temperature changes between 57 and 65°C were previously found to have no effect as observed by static light scattering, while increasing temperature to 80°C was found to remove the lag time for protein aggregation [244].

The structure of HEWL has also been found to change with incubation time. The melting of α-helix into random coil is reversible for short heating times (up to 30 minutes) in quiescent conditions, but is found to become irreversible as incubation time increases [243]. As time progresses the ellipticity between 208-230 nm has been found to decrease (suggesting an increase in α-content) and a jump in ellipticity was found to coincide with the lag time for aggregation determined by SLS [244]. This is thought to be evidence for a further structural change that occurs in partially destabilised lysozyme after which it is capable of forming amyloid-like fibrils [244].

A gel phase is observed once aggregates are formed and the amount of protein deposited in the gel phase is found to increase with incubation time [243]. CD

spectra of the aggregated solution have been found to be typical of that for largely unfolded proteins. However, when the soluble and fibrillar fractions were separated the soluble fraction was found to show features typical of random coil, with a minimum at 202 nm, while the fibrils had a similar minimum around 200 but also a small minimum at 218 nm that may represent the presence of β-sheet [244]. Although CD spectra do not show significant increases in β-sheet content, the fibril species formed under these conditions are found to exhibit X-ray diffraction patterns characteristic of β-sheet rich amyloid-like fibrils [266] and to bind ThT [247, 252, 253], Congo red and Nile red [251], indicating amyloid-like fibril structure.

In a number of reports of HEWL fibrillation at low pH and high temperature, hydrolysis and the resulting fragmentation of HEWL has been implicated in the aggregation process. HEWL has been found to be completely fragmented after incubation for ten days or more at pH 1.6, 65°C [244] and the main fragments observed are 49-100, 49-101, 53-100, 53-101, 58-101 and the corresponding fragments to either side of this central region [251, 252].

Only the central fragments have been found to form amyloid-like fibrils [251, 252], these encompass part of the β-domain and all the residues of the adjoining α-helix, while the remaining fragments include the rest of the helices and are found to remain largely soluble [252]. The location of the mutations in the amyloidogenic human variants is consistent with these amyloidogenic HEWL fragments: these occur between residues 56 and 112 and are thought to destabilise the interface between the α- and β-domains [252, 263].

The fibril-forming fragments have been proposed as nucleating species required for fibril growth [251, 252]. However, fragmentation of the HEWl monomer population is found to be gradual at pH 2, 57°C, with the fragmented monomer population increasing over time, and the fragments are not found to be preferentially incorporated into fibrils but to be evenly distributed in both fibrils and solute [244]. Additionally, as incubation time increases (incubation for >10 days at pH 1.6, 65°C) the termini are increasingly cleaved from the protein incorporated into fibrils and the population of soluble protein fragments and fibrils composed of 49-101 and 53-101 fragments increases [251]. Finally, fibrils are observed at pH 3 in the absence of any hydrolysis, suggesting that it is not crucial in the aggregation process [244] and the addition of pre-formed fibrils containing

only undamaged HEWL has been found to provide equivalent acceleration of aggregation to the addition of pre-formed HEWL fibrils containing large amounts of fragmented HEWL [242].

At low pH, low ionic strength and high temperature the fibril formation is typified by a long lag period during which no or few oligomeric species are observed. Under these conditions, the lag time is found to be reduced by the addition of pre-formed fibril seeds in a process that is seed-concentration dependent, with lag time decreasing with increasing seed concentration. At pH 2 and 65°C under quiescent conditions the lag time has been shown to be eliminated by addition of 5% *v/v* of seed [242].

The growth rate of HEWL aggregation has been found to be independent of initial HEWL concentration (in the range 0.1 µM to 10 mM HEWL at pH 2, 65°C [243]) and the lag time has been found to be only weakly concentration dependent (in the range 1-3% wt at pH 2, 57°C [244]), leading investigators to suggest an intramolecular transformation as the rate limiting step of the aggregation mechanism [243]. However, in another study, at pH 1.6 and 65°C the growth was found to be highly concentration dependent up to 200 µM, while increasing the protein concentration from 200 to 500 µM was not found to decrease lag time further, indicating a concentration independent rate determining step only at higher concentrations [251]. However, in these studies kinetic data has been obtained by removing and testing a small number of aliquots over time, and as a result too few data points are taken to give a reliable shape of the kinetic curve [251].

3.3.2 Salt sensitivity

The pH sensitivity of HEWL fibril formation could be related to the effect of pH on the charge state, structure, unfolding pathway, rate/specificity of chemical reactions modifying the protein, or a combination of these factors [258]. Since fibril formation increases dramatically from pH 4 to pH 2, it is possible that the protonation state of aspartic or glutamic acid residues is important for fibril formation [258]. The role for charged residues in HEWL formation is supported by the observation that aggregation is dramatically accelerated upon the addition of NaCl, presumably as a result of charge screening [89, 246, 247, 258]. The addition of NaCl at pH 2 and below the melting temperature has also been

shown to change the tertiary structure of the low pH molten globule state to a more native-like, albeit slightly destabilised (melting temperature reduced ∼3°C) conformation [267].

Repulsive charge interactions are thought to be a prerequisite for ordered fibril assembly [89]. It is thought that the charge screening afforded by increasing ionic strength may affect both intra- and intermolecular interactions that are important for fibril formation [258].

Several transitions in behaviour have been observed with changes in salt concentration. Hill *et al.* [89] investigated the aggregation of HEWL at a range of NaCl concentrations, at pH 2 and 50°C. As salt concentration increased they observed a transition from fibril growth by monomer addition to fibril assembly from oligomeric species (around 120-150 mM) followed by precipitation of aggregate species at high salt concentrations (350 mM) [89].

At low salt concentration, below 120 mM NaCl, HEWL aggregation kinetics were found to be characterised by an extended lag period of several days during which only monomeric protein was observed by AFM. After the lag phase, two aggregate populations of stiff, short, rod-like fibrils were observed simultaneously. The fibrils were found to have a bimodal length distribution, with hydrodynamic radii centred around 30 and 300 nm as determined by DLS. The longer length filament population was thought to be the result of growth proceeding through assembly of the shorter filaments [89], although the reverse could equally be the result of fibril fragmentation. As time progressed, thicker fibrils were observed, with width approximately three times that of the monomeric fibrils [89] and a wide range of lengths up to several micrometers were observed by AFM and TEM [2, 89].

At salt concentrations between 150 and 350 mM lag periods were found to reduce to a few hours. During the lag phase, oligomeric intermediates were observed, and based on their ellipsoidal geometry of approximately 3.9×9.5 nm were estimated at 8 monomers. The aggregate size distribution following the end of the lag phase was found to be centred around 20-30 nm and increased in both radius size and distribution-width with time. Short, curvilinear filament-like structures with a beaded structure were observed and found to have cross-sections matching the oligomers observed during the lag phase. At much later times larger, stiffer fibrils were also observed with roughly twice the cross sectional area of

the original filaments [2, 89]. The protofibrils were thought to not yet contain the helical cross-beta-sheet structure of the final fibrils, since their ball-on-string appearance matched the oligomer proportions and not those of the helical fibril twists. The short persistence length of the protofibrils compared with the stiffness of the mature fibrils reinforces this assumption [2].

A critical protein concentration was observed for the formation of curvilinear fibrils from the oligomers, found to be approximately the solubility limit of the curvilinear fibrils below which they decay upon dilution, similar to a critical micelle concentration. This critical concentration was found to be 0.7 mM HEWL, 200 mM NaCl at pH 2 and 52°C [1, 2]. Below this critical concentration the formation of curvilinear fibrils was separated from the onset of oligomer formation by a lag phase and rigid fibrils like those observed at lower salt concentrations were found to form rather than curvilinear filaments [1, 2].

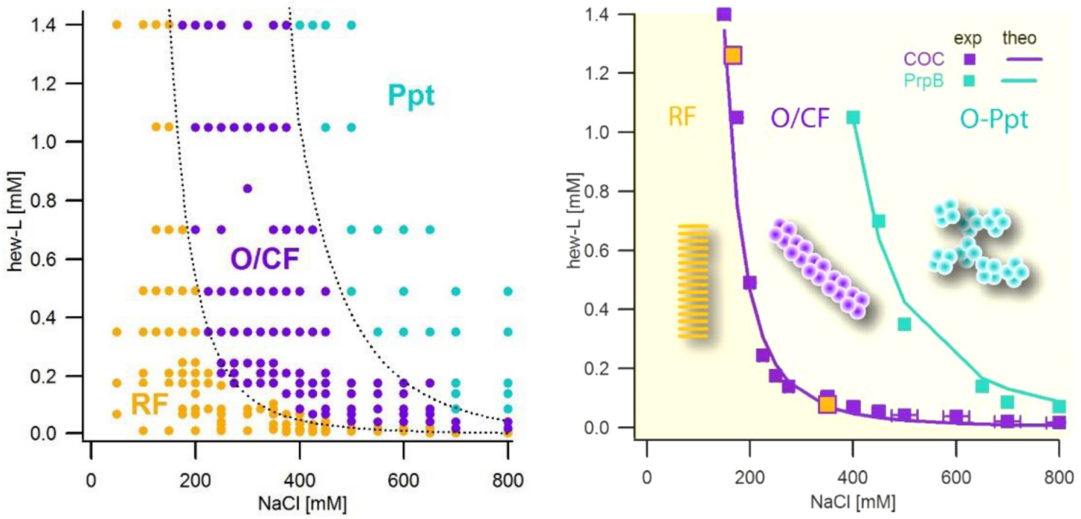

Figure 3.2: Left: Kinetic phase diagram for rigid fibrils (RF), oligomers and curvilinear fibrils (O/CF) and precipitate formation of HEWL undergoing amyloid growth as a function of protein and NaCl concentrations at pH 2, 52°C. The aggregate species obtained at a given combination of protein and salt concentration were determined from a combination of ThT, static light scattering and dynamic light scattering experiments. Right: The experimental observations versus theoretical predictions of oligomer phase boundaries from a colloidal charge repulsion model of oligomeric species. Filled orange squares are the curvilinear fibril solubility determined from relaxation data and the yellow background indicates that the rigid fibrils are the thermodynamically stable phase under all conditions. Taken from Miti *et al.* [1].

The low (<120 mM NaCl) and high-salt (>150 mM NaCl) species were shown by Miti *et al.* [1] to occupy well defined regions of a phase diagram, with both salt and protein concentration boundaries, as shown in Figure 3.2. Increasing

protein and/or salt concentrations was found to favour oligomer/curvilinear fibril formation (O/CF) and at higher concentrations precipitates (Ppt) were formed rapidly by association of oligomeric species and exhibited some similar structural elements to the curvilinear filaments [1].

Additionally, the curvilinear fibrils were shown to be a kinetically stable species, metastable against the growth of the rigid fibril species, while the rigid fibrils are the thermodynamically stable aggregate phase. Rigid fibril seeds were found to grow at the expense of the curvilinear species at protein concentrations above the critical oligomer concentration at salt concentrations up to 250 mM NaCl (above the salt concentration boundary) [1].

Increases in light scattering intensity by SLS were found to coincide with increases in ThT fluorescence for both the low and high ionic strength growth pathways, and in both cases the particle size distribution by DLS was found to be dominated by increases in peak area rather than increase in average hydrodynamic radii at early times during the aggregation (before an inflection point is observed) [2, 89]. This suggests that changes in the particle size distribution may be dominated by the nucleation of new aggregates and/or particle sizes are limited by filament fragmentation in both systems [2, 89].

At both 50 and 200 mM NaCl, the structure of HEWL was found to be marginally disordered at 50°C, however there was no noticeable difference between the two salt concentrations and the midpoint temperature for denaturation was unaffected [89]. Charge screening between aggregation prone species, rather than salt induced denaturation, was therefore proposed as the cause of the transition in aggregation behaviour [89].

Salt-mediated charge screening is thought to overcome the energy cost imposed by charge repulsion, favouring compact oligomeric intermediates over extended disordered monomers [89]. A similar salt transition was found for NaBr and $MgCl_2$, with the transition occurring around 150 mM for both NaCl and NaBr and found to shift to 50-75 mM for Mg, a comparable ionic strength, suggesting a non-specific charge screening effect drives the transition [89].

Additionally, Zhang *et al.* [245] found that the phase behaviour of HEWL solutions at pH 9.4, determined by the cloud point (the point at which the solution becomes turbid) temperature, followed an inverse Hofmeister series (the classification of ions in order of their ability to salt out or salt in proteins)

correlated with the size and hydration thermodynamics of the anions at low salt concentrations (below 200-300 mM) and at higher salt concentrations followed the Hofmeister series, correlated with the polarizability of the anions [245]. They found that the behaviour was only accounted for by modelling both the charge screening and surface tension effects at the protein/water interface (the hydration layer) [245]. Similar behaviour may be occurring at low pH with the changes in salt concentration described above, with a transition driven by both charge screening and surface tension inducing the change between preferred aggregation pathways.

At even higher salt concentrations the lag period was found to be completely abolished and charge screening thought to be such that net attraction between monomers results in both increased amorphous assembly and precipitation of aggregates [89]. Larger bundles of worm-like fibrils have been observed, and large straight fibrils after longer incubation times [247]. The precipitation at high salt and protein concentration was also found to be characterised by well defined phase boundaries [1], as shown in Figure 3.2.

3.3.3 Very high temperatures

At low pH and low ionic strength (11 mM) increasing temperature has been found to have an analogous effect to increasing ionic strength, where hydrophobic attraction is enhanced with respect to repulsion [246]. When temperature was increased to 70°C, the lag phase was found to be extremely reduced and a larger quantity of amorphous-like globular aggregates was observed that appeared to be off-pathway with respect to fibrillation. The apparently off-pathway aggregates were observed at all temperatures 60°C and above [246].

During the lag phase small oligomers with hydrodynamic radius around 10 nm were observed [246, 251] and found to increase in number up to a plateau, suggesting an equilibrium with the monomer population [246]. The oligomers were not found to overlap with the size distribution of the fibrillar species observed at later times, did not bind ThT and had no effect on lysozyme samples when added as a seed population [246]. At 65°C, larger aggregates have also been observed, with diameters in the range 20-40 nm and were found to become smaller and less abundant as the fibril population increased [251].

Additionally, Raccosta *et al.* [246] found a slow and continuous change of

HEWL secondary and tertiary structure at high temperature, starting well before the observation of fibrils or other aggregates. They propose that the spectroscopic changes are due to a shift in the equilibrium between the different denatured conformations, consistent with the results of Buell *et al.* [268] who propose that an equilibrium ensemble of partially denatured states of HEWL with different fibril propensity controls the aggregation propensity of HEWL.

Electrostatic repulsion is thought to operate as a gatekeeper, favouring the association of monomers whose conformations are capable of forming fibrils by shifting the ensemble equilibrium in their favour when the monomeric species is removed following association, until a significant amount of fibrillated protein can be detected [246].

3.3.4 Alcohol

HEWL is known to increase in helical content in the presence of ethanol (EtOH) [254, 256, 257, 260, 261], 2,2,2-trifluoroethanol (TFE) and 1,1,1,3,3,3-hexafluoro-2-propanol (HFIP) [269]. However, as alcohol concentration increases, HEWL molecules associate and form β-rich fibrils [254, 269]. Optimum alcohol concentrations for fibrillation depend on the alcohol species, and HFIP has been found to be the most effective at inducing fibrillation, at 12-16% compared to 40-80% TFE and >60% EtOH (at pH 4.8) [269].

The increase in helical content with increasing EtOH concentration is followed by destruction of the tertiary structure (around 80% EtOH), after which the helical structure is disrupted and β-sheets form (above 85% EtOH), with a rate highly dependent on protein and salt concentration [254]. Fully reduced HEWL has also been shown to form fibrils at pH 4-5 and ≥90% EtOH [270].

On aggregation in 80% EtOH, a gel phase was formed that was found to precipitate upon addition of salt [254, 257]. The precipitate was found to consist of protofilaments with diameters around 7 nm that exhibit Congo red binding and the X-ray diffraction patterns characteristic of amyloid-like fibrils [254]. Dilution of the precipitate resulted in recovery of native structure and enzymatic activity, suggesting that the EtOH-induced transition is reversible, and the fibrils are only stable under high alcohol conditions [254].

Yonezawa *et al.* [256] proposed a mechanism for fibril formation under these conditions in which the structure of the monomers is perturbed and dimers

are formed. Dimers and monomer were observed to coexist under particular conditions and the dimers were estimated to have an elongated shape, with association occurring along the long axes of the dimers. The dimers were thought to be nuclei for further aggregation, with filaments growing by dimer association, and mature fibrils formed by lateral association of filaments [256].

Holley *et al.* [260], investigated the aggregation of HEWL under mild agitation at 22°C in 80% EtOH and found that while as little as 0.05% *v/v* of sonicated fibrils was found to be sufficient seed to abolish the lag time, a 20-fold higher concentration of pre-formed fibrils was required for the same effect [260], suggesting that the number of ends and not lateral surfaces are most important for fibril growth under these conditions.

Additionally, Sassi *et al.* [261] found that the aggregate fraction increased and aggregation rate decreased with incubation at increasing temperature, and proposed that the increase in viscosity connected with the increased gel fraction was responsible for the decrease of aggregation rate due to 'freezing' of conformational motions [261]. The observations of Holley *et al.* [260] and Sassi *et al.* [261] suggest that fibril fragmentation and a critical fibril mass concentration [177] may be important in HEWL aggregation at high alcohol concentration.

3.3.5 Sodium Dodecyl Sulphate

In the presence of low concentrations (less than 0.25 mM) of sodium dodecyl sulphate (SDS) HEWL is known to form fibrils that have a typical straight, unbranched structure by EM after long incubation times and that bind ThT [248–250], while at higher SDS concentrations fibril formation is suppressed [249]. The SDS-HEWL complexes formed at low SDS concentration were found to be in excess at the air-water interface, resulting in a decrease in surface tension. Additionally, in the presence of HEWL the critical micelle concentration of SDS was reduced, suggesting mixed SDS-HEWL micelle formation [271].

Fibrils have been observed following incubation at both pH 9.2 [248, 250] and at low pH and elevated temperature [249] in the presence of SDS. At pH 2 and 55°C, the presence of SDS was found to promote fibrillation and no lag time was observed prior to aggregation, compared to a lag of approximately 10 hours in the absence of SDS [249]. At pH 9.2 at room temperature (24-25°C) HEWL was observed to first undergo a quick conformational change (as observed by

changes in intrinsic and extrinsic fluorescence) upon addition of SDS, the partially unfolded species are then thought to form soluble oligomers, which increase in size over time [250].

3.3.6 Reducing agents

Reduced HEWL has been shown to form fibrils in both the presence [270] and absence of alcohol [272, 273]. At neutral pH, the disruption of the disulphide bonds of HEWL by dithiothreitol (DTT) is found to be a prerequisite for fibril formation on heating [272]. The fibrils formed in the presence of DTT at pH 7 after heating (to 85°C for 10 min before cooling to room temperature) were observed to be around 3 nm in width and to associate to produce thicker, $\sim$ 6 nm wide species and larger bundles on cooling [272].

However, at alkaline pH (pH 12.2 incubated at room temperature) the presence of DTT has been shown to inhibit the formation of HEWL aggregates [273]. This inhibition of fibril formation is thought to be due to the stabilisation of aggregates by the formation of intermolecular disulphide bonds, the formation of these bonds is disrupted when DTT is present at the beginning of the incubation period. The addition of DTT at later times in the aggregation process was found to have a reduced inhibitory effect [273].

3.3.7 Chaotropic agents

HEWL is found to aggregate and form fibrils in the presence of moderate guanidine hydrochloride (GdnHCl, a chaotropic agent that disrupts the hydrogen bonding network, weakening the hydrophobic effect and resulting in protein denaturation) concentrations (2-5 M). At lower GdnHCl concentrations the structure is native and stable and at higher concentrations GdnHCl is capable of dissolving HEWL fibrils [264].

At moderate GdnHCl concentrations (at pH 6.3 in 20 mM potassium phosphate, incubated with agitation by stirring at 50°C) the fibrils formed were typically straight, unbranched and twisted, with diameters around 13 nm, and were found to bind ThT. The lag time under these growth conditions was dramatically reduced by the addition of pre-formed seed. However, seeding was not found to be capable of initiating aggregation in solutions at high or low

GdnHCl, suggesting that the partially unfolded HEWL molecules populated at moderate GdnHCl are the fibril forming species [264].

3.3.8 Modifications

Tango and aggrescan software, designed to predict the aggregation tendencies of different parts of a given protein sequence (based on simple physico-chemical principles of secondary structure formation, and aggregation-propensity scales derived from *in vivo* experiments respectively), suggest an important role for some of the lysine residues in HEWL [274]. Indeed, lysine residues are very reactive, charged aliphatic residues, involved in specific ligand binding and are targets of post-translational modifications that may have consequences for protein stability *in vivo*, including glycation, acetylation, methylation and carboxymethylation [274]. Acetylation of lysine residues has been found to promote fibril formation, resulting in a dramatic decrease in lag time at pH 2.5 and 57°C, while citraconylation produced the opposite effect [274].

3.3.9 Agitation and surface activity

Typically, HEWL aggregation experiments have been performed in quiescent conditions, where lag times are of the order of days [88, 89, 242–244, 251]. Under these conditions large variations in lag time are typically observed between replicate samples [244] and resulting kinetic growth profiles vary.

The combination of agitation and heating has been shown to be an alternative method for effectively inducing the formation of HEWL amyloid-like fibrils up to physiological pH [247], and the enhancement has been shown to be proportional to the power imparted by the agitator [275, 276]. Agitation has also been shown to enhance fibrillation propensity at high alcohol concentration [260], and might therefore afford a method to decrease the time required for aggregation and reduce lag time variation under these conditions.

The reduction of the lag time associated with increased agitation is thought to be the result of *i)* destabilisation of the native structure by adsorption at hydrophobic surfaces, where agitation is thought to increase the probability that monomers encounter a hydrophobic surface by increased mixing and the formation of air bubbles; *ii)* interaction of native HEWL with destabilised HEWL,

where increased mixing increases the probability of collision; or *iii)* because of an increase in fragmentation, where agitation increases the likelihood of breakage [260, 276, 277]. Indeed, HEWL is known to adsorb onto hydrophobic surfaces [278], inactivation of HEWL enzymatic activity has been found to be proportional to the area of glass-liquid, air-liquid and PTFE-liquid interfaces, with PTFE and air found to be the most efficient in promoting inactivation because of their hydrophobicity. Seeding with increasing numbers of inactive HEWL molecules has been found to increasingly enhance enzymatic inactivation [277]. Moreover, the short fibrils observed in sheared and stirred samples suggest an increase in fragmentation [276].

3.4 Polymorphism

The reported characteristics of HEWL fibrils formed under different conditions vary widely and could reflect real differences in fibril structure, differences in imaging or characterisation techniques or differences in the stage of fibril growth, complicating direct comparisons [258].

The amyloid-like fibrils formed at low pH and high temperature are typical of the long, straight, unbranched fibrils observed by EM and AFM for a large number of different, unrelated proteins. Fibrils formed at pH 2, 57°C, in the absence of salt, were found to have a coiled structure with periodicity around 30 nm, thickness of 2.5±0.3 nm and lengths exceeding 5 µm, as shown in Figure 3.3 (left). Thicker fibrils were also observed, with diameter of 4.0±0.7 nm, and as protein concentration was increased the number of fibrils observed by AFM increased in aliquots taken at equivalent time points and bundles were observed [244]. Fibrils observed at pH 2, 65°C have been found to be long, straight and unbranched with diameters ∼10 nm, as shown in Figure 3.3 (centre) [252].

The fibrils formed from reduced HEWL (DTT [272]), and fibrils formed in the presence of GdnHCl [264] appear to share similarities with those formed by HEWL at high temperature, low pH and low ionic strength. In the presence of DTT, fibrils around 3 nm in width were observed and appeared to associate to produce thicker, ∼6 nm wide species and larger bundles on cooling [272]. Straight fibrils, with widths around 13 nm were observed in the presence of 3 M GdnHCl [264].

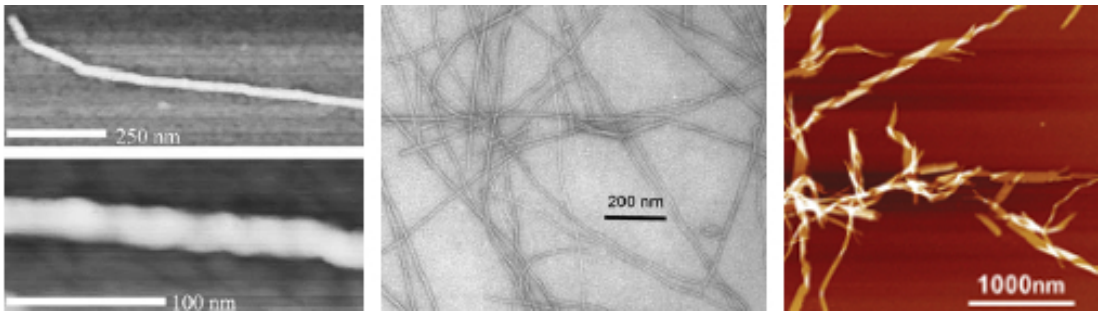

Figure 3.3: Examples of HEWL fibrils formed at high temperature and low pH. Left: consecutive tapping mode AFM images of a fibril from solution of 2.0% *w/v* HEWL at pH 2, heated for 13 days at 57°C [244]. Centre: electron micrograph of HEWL fibrils obtained after 10 days incubation at pH 2 and 65°C [252]. Right: AFM height images of HEWL after 30 hrs incubation at pH 2, 90°C [253].

At low pH, low ionic strength and at higher temperatures (>60°C) small oligomers, 5-10 nm in diameter have been observed during the lag phase and at early times, becoming less abundant as the fibril population increases [246, 251]. The fibrils observed at longer times (pH 2, 11 mM NaCl, 60-70°C) were found to have an average height of 2.3 nm by AFM, while thicker fibrils with widths 30-40 nm were also observed. The fibrils were found to have axial periodicities of at least 20 nm [246]. At even higher temperatures (pH 2, 90°C) multistranded fibrils become more common, containing up to 17 protofilaments, with width increasing over incubation time [253]. Some examples of these ribbons are shown in Figure 3.3 (right). These multistranded ribbons, formed by hydrolysed HEWL fibrils, have also been observed to close into nanotubes [279].

Additionally, the filament chirality of HEWL fibrils formed by incubation at low pH and 65°C has been shown to be sensitive to pH. Left-handed-helical filaments were found to form at pH 2.2 and above, and right-handed-helical filaments were formed at lower pH. The chirality appears to control the mature fibril structure, with left-twisted filaments forming multiple-filament braids while right-twisted fibrils adopt flat, ribbon-like morphologies consisting of parallel side-by-side filaments.

However, for insulin, right-handed ribbon-like fibrils formed at low pH were found to be converted to left-handed rope-like fibrils upon incubation at higher pH, suggesting that a range of morphologies may be the result of environmental conditions rather than changes in internal fibril structure [280]. This may be true for the fibrils formed of other proteins.

HEWL spherulites are also observed after long incubation times at low pH and high temperature, with diameters in the range 50-100 µm. These spherical species have a 3D isotropic assembly of fibrils, extending outwards from the centre of the spherulite, and exhibit a 'Maltese-cross' pattern in a polarizing light microscope. Spherulites have also been observed in insulin and β-lactoglobulin [281] aggregation.

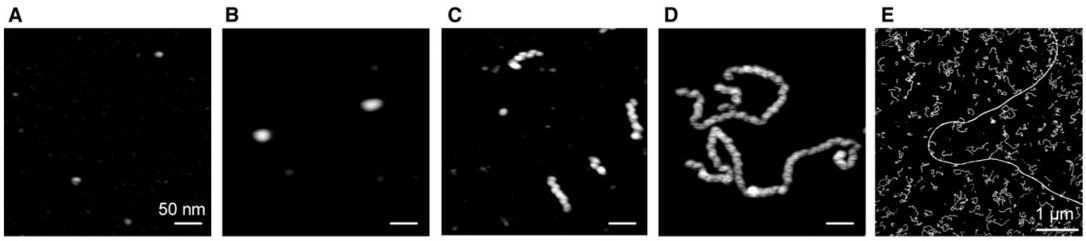

Figure 3.4: AFM images of intermediate fibril aggregates of HEWL at pH 2, 50°C, 175 mM NaCl. *(A)* Before heating (20°C). *(B)* After 3 hours of incubation. *(C)* Protofibrils appearing around 10 hours, shortly after the end of the lag time by DLS. *(D)* After 25 hours of incubation. *(E)* After ∼100 hours of incubation, straight fibrils are observed along with protofibrils. Taken from Hill *et al.* [2].

At high salt concentrations (>150 mM NaCl) at low pH and high temperature, HEWL is found to aggregate into small approximately spherical oligomers with size 3.9 x 9.5 nm, estimated to contain 8 monomers [2]. These appear to assemble by oligomer addition to form worm-like fibrils with a ball-on-chain appearance, as seen in Figure 3.4, where the 'balls' are found to roughly correspond to the oligomer size [2]. In many cases the appearance of worm-like fibrillar species is followed by the appearance of stiffer and longer fibrils at later times, found to be roughly 1.5 times as high and wide as the protofibril species [2, 89, 247].

The fibrils formed at high alcohol concentration (roughly 6-12 nm in diameter and densely tangled) [254, 260], share the worm-like appearance of those formed at high salt, while the structure of the initial fibrils formed in the presence of SDS is unclear. After long incubation times, longer and stiffer fibrils are observed in both cases [249, 260].

The fibrils formed by analogous human lysozyme at high pH (low ionic strength) and low pH (low ionic strength), have also been found to range in morphology, molecular structure, stability, size of the cross-β-core and toxicity. Fibrils formed at pH 7.5, 50 mM Na_2HPO_4, at 60°C under stirring, were rigid, on average 10.7 nm wide and found to associate laterally. Fibrils formed at pH

2, 50°C under stirring were also rigid, on average 6.5 nm wide and found to exhibit a periodic twist. The growth kinetics by ThT binding in both cases were characterised by a lag phase followed by roughly sigmoidal kinetics, however, a much longer lag was observed at pH 2. The fibrils formed at pH 7.5 were found by FTIR to contain considerably less β-content (45% β-sheet, 21% random and α-helix, 34% turns and loops compared to 75%, 15%, 10% in the pH 2 fibrils) and were found to be significantly less toxic to SH-SY5Y neuroblastoma cells in a 3-(4,5-dimethylthiazol-2-yl)-2,5-diphenyltetrazoliumbromide (MTT) assay [282]. The polymorphism for human lysozyme appears to be associated with fundamentally different molecular conformations, and the same might be expected for analogous HEWL. The cytotoxic effects also appear to be related to the amount of β-structure [282], and highlight the importance of investigating the growth mechanisms of different fibril polymorphs.

3.5 Two main HEWL fibril formation mechanisms and polymorphs

Two apparently distinct assembly pathways lead to either thermodynamically stable straight filaments at high temperature, low pH and low ionic strength or globular oligomers and kinetically stable curvilinear/worm-like fibrils at high temperature, low pH and high ionic strength.

The kinetics of the straight, rigid amyloid-like fibril growth are typified by a long lag phase, typically on the order of days in quiescent conditions, followed by a rapid period of growth [88, 89, 242–244, 251] during which the elongation of fibrillar species is observed [89]. Hill *et al.* [88, 89] proposed a mechanism for growth under these conditions in which nucleation occurs from denatured HEWL, nuclei extend by monomer addition of denatured HEWL and these filaments laterally associate at later times to form rope-like fibrils [88, 89]. A cartoon depicting this pathway is shown in Figure 3.5.

At higher salt concentrations an alternative fibrillar pathway that results in curvilinear or worm-like fibrils is thought to progress through the formation of non-ThT-binding oligomers (observed during the short lag phase) that join together to form curvilinear or worm-like filaments that have an initial bead-on-string appearance but increased β-content and exhibit ThT-binding [1, 2, 88, 89].

A cartoon depicting this pathway is shown in Figure 3.6.

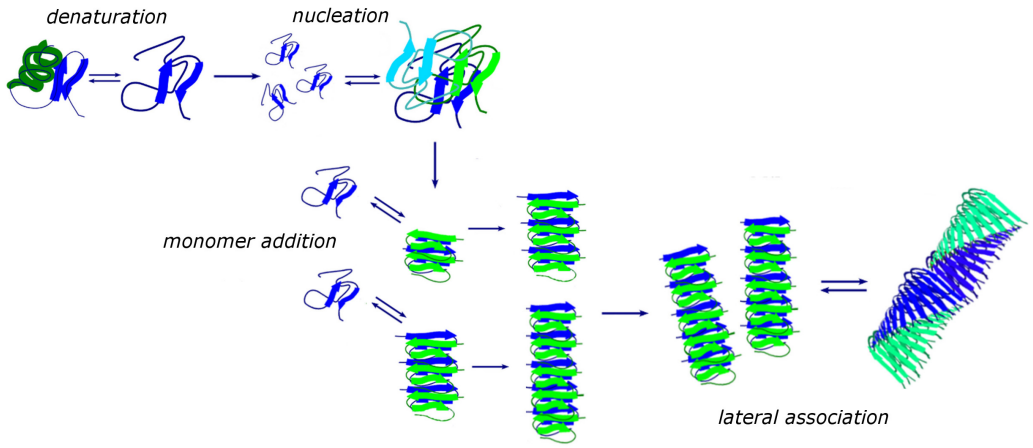

Figure 3.5: A cartoon depicting the proposed growth pathway of straight fibrils of HEWL at low pH, high temperature and low ionic strength. Nucleation is thought to occur from denatured HEWL, nuclei and filaments extend by monomer addition of denatured HEWL, and filaments associate laterally at later times to form rope-like fibrils.

Distinct infrared structural fingerprints and fluorescence enhancement upon ThT binding were found for the two fibrillar species and were found to be independent of the growth conditions, protein hydrolysis and persisted near physiological pH (pH 7) [88]. Both high and low salt induced fibrils exhibited the expected infrared β-sheet peaks but the peaks were found to be shifted to slightly higher wavenumbers at high salt [88]. A marked difference was also apparent in the relative amplitudes of ThT response between the two fibril species, as well as in the shape of the initial growth curves (up to the inflection point, captured by removing aliquots of aggregating sample and not sufficient for comparison with growth models). At high salt, the fluorescence intensity of ThT was found to reach a final value roughly 12 times the background fluorescence, while at low salt the final value reached greater than 90 times the background level [88].

The differences in ThT binding may be the result of a change in the number of available ThT binding sites, differences in the structure or identity of the binding site, the binding affinity or quantum yield of ThT upon binding, these were not investigated further by Foley *et al.* [88]. However, the differences in infrared spectra and ThT binding clearly distinguish the two fibrillar species and hint at differences in the molecular structure of the filaments that may give rise to their competition in solution rather than conversion between structural subtypes.

The fibrillar species observed in the presence of GdnHCl and by reduced

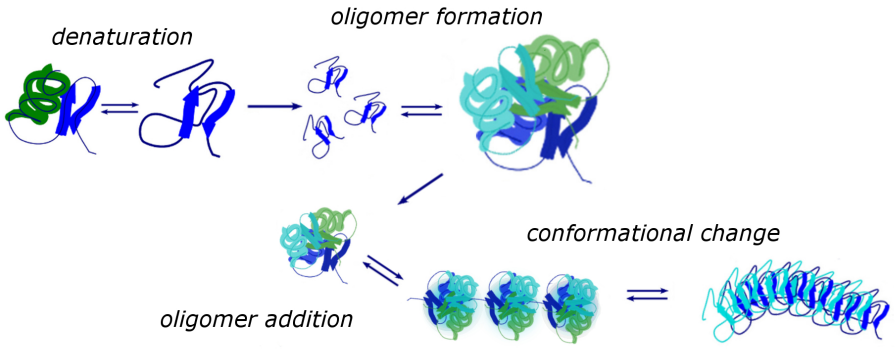

Figure 3.6: A cartoon depicting the proposed growth pathway of curvilinear fibrils of HEWL at low pH, high temperature and low ionic strength. Oligomers are formed from denatured HEWL, filaments extend by oligomer addition and early bead-on-string appearance species undergo conformational conversion, including an increase in β-sheet content, to form the final curvilinear filaments.

HEWL at low ionic strength (in the presence of DTT) share structural similarities with those formed at low ionic strength, and may be formed along a similar aggregation pathway. In particular, the narrower width of these species is more consistent with growth by monomer addition than oligomer formation and addition/coagulation.

In contrast, the fibrillar species observed at high EtOH concentration share similarities with those at high salt, hinting at a similar aggregation mechanism under these conditions. A fibrillar gel is also formed under high alcohol conditions, and both fragmentation and a critical fibril mass concentration have been implicated as important in this system [260, 261].

In the following chapters the aggregation of HEWL at high temperature and high and low salt concentrations is investigated in further mechanistic detail by high-throughput kinetic analysis, adding to the extensive analysis that can be found in the literature [1, 2, 88, 89, 242–247, 251–253, 258]. In addition, the aggregation of HEWL at high alcohol and reduced HEWL at low ionic strength are investigated to determine whether the two highlighted fibril formation pathways are common to the two different polymorphs of HEWL fibrils: straight, rigid fibrils and the curvilinear, worm-like species.

Chapter 4

Results: Fibril formation of HEWL at low pH and high temperature

4.1 Introduction

The aggregation of HEWL has been investigated in great detail here by *in situ* ThT fluorescence and turbidity measurement by microplate-reader assay, allowing for high throughput analysis of many replicate aggregating samples. The morphology of the resulting species was then analysed by EM.

HEWL aggregation was followed under a range of environmental and solution conditions that have previously been shown to induce the formation of amyloid-like fibrils: high temperature and low pH, and in the following chapter, reducing agent DTT and alcohol (HFIP). While these conditions are known to give rise to a range of fibril morphologies and supposed growth mechanisms, only the high and low salt regimes at high temperature and low pH have so far been compared in detail.

The kinetic growth profiles of HEWL assembly are compared with the proposed models of fibril assembly: the traditional nucleation-dependent polymerisation (NDP) model of Oosawa *et al.*, the secondary-process dependent polymerisation (SDP) models of Knowles *et al.*, the end-joining coagulation (JDP) model of Kalapothakis *et al.* and the predictions of growth under these regimes and in the presence of other possible dominant growth mechanisms, as

described in Chapter 1. To my knowledge, such a kinetic analysis, comparing multiple apparently distinct growth regimes of HEWL with the kinetic models proposed for fibril assembly has not yet been performed.

4.2 High temperature and low pH

At low ionic strength a wide variation in lag period was observed and found to be highly sensitive to the environmental conditions. Reproducible lag times were only obtained under strict control of conditions (including temperature, agitation, salt concentration and microplate surface coating).

The system was found to be extremely temperature sensitive, and even with efforts to reduce temperature gradients (positioning of microplates in the far right corner of the platereader, away from the reader door between readings) the positioning of sample within the microplate was found to affect the reproducibility of replicate well kinetics, and suggested a wider temperature gradient between columns than rows of the microplate in this position.

The effects of temperature, agitation and pH were explored briefly, since reproducible results were only obtained under very particular environmental conditions and the effects of these conditions have been described elsewhere [243, 244, 247, 251, 258, 275, 276]. However, similar kinetic growth profiles were observed at 60 and 65°C and higher temperatures could not be obtained within the limits of the experimental method. The lag phase was found to increase with decreasing temperature, but the variation in lag period also increased and was not analysed further. Typically, the aggregation propensity with temperature was found to be consistent with previous reports on the temperature stability of HEWL [244, 251]. The results were similar for increases in pH and decreases in agitation, consistent with previous observations about pH stability [247, 258] and the accelerating effect of agitation [247, 260, 275–277].

Thioflavin T (ThT) fluorescence and turbidity (absorbance at 600 nm) measurements were obtained simultaneously for a range of HEWL concentrations at high temperature (>60°C), low pH (pH 1.5-2, up to 25 mM HCl), and at various NaCl concentrations and surface area (SA) to volume ratios, with agitation by double orbital microplate shaking.

The presence of ThT was determined to have negligible effect on the growth

under these conditions (increasing concentrations of ThT were not found to be strongly correlated with aggregation propensity, see Figure A.1) and a 55 µM concentration of ThT was chosen to ensure an excess of dye at high protein concentration (see Figure A.2).

Various salt (NaCl) concentrations were analysed at pH 1.5-2 and 60-65°C. Decreasing ionic strength was found to increase lag time and decrease reproducibility. Additionally, the concentration of salt was found to affect the growth behaviour as observed in changes in the shape of the kinetic growth curves.

Multiphasic growth curves were observed, as seen in Figure 4.1. At NaCl concentrations of 0.35 M and above an initial increase in fluorescence intensity is followed by a period of meta-stability (region A) and then followed by a more dramatic, rapid increase in fluorescence intensity (region B). A further phase of slower increase in fluorescence intensity is then observed at salt concentrations >0.4 M (region C) before fluorescence increase slows and approaches a final plateau region. These different growth phases are highlighted in Figure 4.2.

The salt concentration dependence of growth at early times (region A) is enlarged on the right in Figure 4.1. As salt concentration decreases it is clear that the initial growth phase decreases in intensity until only the second, more intense growth phase is observed at 0.2 M NaCl and below. Additionally, a change in behaviour is observed at around 2.8 hours in the kinetic curve at 0.1 M NaCl.

The NaCl concentration sensitivity of region A suggests that it is salt-induced; the proportional intensity of this region increases with salt concentration. The slower increase in fluorescence at later times, region C, suggests that a different growth mechanism dominates the kinetics as the monomer population dwindles. The 'kink' between regions B and C becomes sharper and occurs earlier in time as salt concentration increases, and the proportional intensity of region C increases, suggesting that the growth mechanism dominating the kinetics at later times becomes increasingly dominant as the salt concentration increases.

The exact salt concentration of these changes was found to be sensitive to the pH and temperature conditions (data not shown), but roughly coincides with the salt concentration above which Hill *et al.* reported the observation of an alternative aggregate pathway, that of the curvilinear filament species [1, 2, 88, 89].

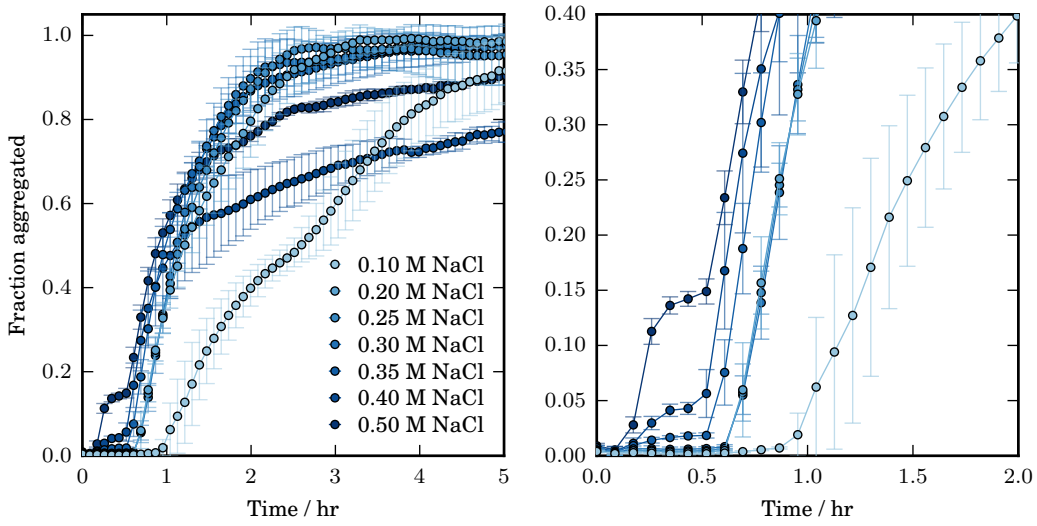

Figure 4.1: Normalised Thioflavin T fluorescence intensity over time for a range of salt concentrations for 10 mg mL^{-1} HEWL at 65°C, pH 1.6 (25 mM HCl), incubated with double orbital shaking at 700 rpm for 2.5 of each 5 minute cycle. On the right, the early time region is shown to highlight the initial growth region that increases in prominence with increasing salt concentration. Legend applies to both graphs.

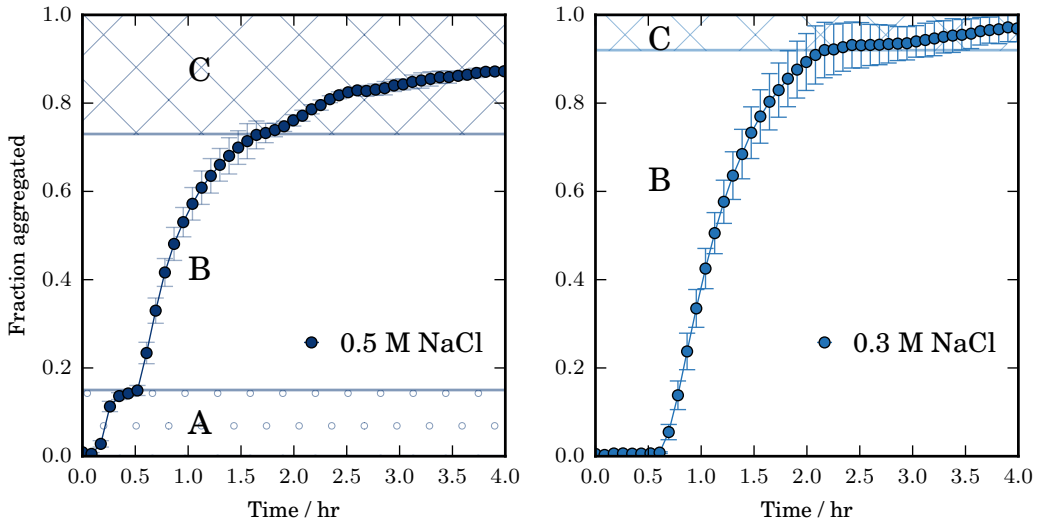

Figure 4.2: Normalised Thioflavin T fluorescence intensity over time for 10 mg mL^{-1} HEWL at 65°C, pH 1.6 (25 mM HCl), incubated with double orbital shaking at 700 rpm for 2.5 of each 5 minute cycle at either 0.3 or 0.5 M NaCl. The three main growth regions are highlighted, the growth at early times, region A, is dotted, the period of rapid growth that follows, region B, has no pattern and the final region of slow increase in fluorescence intensity, region C, is cross-hatched. No region A is observed at 0.3 M NaCl.

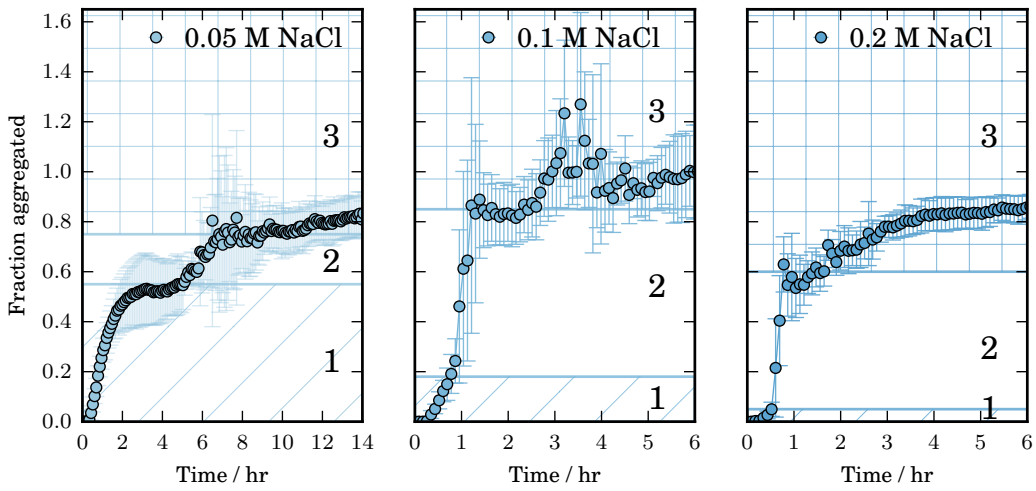

Figure 4.3: Normalised absorbance at 600 nm over time at 0.05, 0.1 and 0.2 M NaCl for 10 mg mL^{-1} HEWL, 65°C, pH 1.6 (25 mM HCl), incubated with double orbital shaking at 700 rpm for 2.5 of each 5 minute cycle. The three main growth regions are highlighted, the growth at early times, region 1, is highlighted by diagonal lines, the period of rapid growth that follows, region 2, has no pattern and the final region of slow increase in fluorescence intensity, region 3, is hatched. A very small region 1 is observed at 0.2 M NaCl.

Corresponding absorbance measurements at 600 nm for the fluorescence results shown in Figure 4.1 are shown in Figure 4.3 for selected salt concentrations. Below 0.1 M NaCl, growth curves observed by absorbance were found to exhibit three clear phases of growth, as seen in Figure 4.3 (left). A short lag is followed by an increase in absorbance, which plateaus at an intermediate value (region 1) before increasing again (region 2, beginning at around 6 hours for 0.05 M NaCl, as shown in Figure 4.3). At a slightly later time there is a notable transition at which the growth rate is decreased, and absorbance increases at a slower rate over time (region 3). At concentrations below 0.1 M NaCl a final plateau was not obtained, and absorbance was normalised to the value at the end of the capture time (30 hours, at which point higher concentrations had been stable for many hours).

As salt concentration increases the intensity of growth region 1 was found to decrease. At 0.1 M NaCl region 1 is still apparent at early times, but is followed by a much more rapid increase in absorbance in region 2. This is followed by a gradual increase to a final plateau region (region 3). At a number of salt concentrations the increase in absorbance in region 2 is followed by a small decrease in intensity, however, at all concentrations excluding 0.5 M, the

absorbance then slowly increases towards a final plateau value (region 3). At 0.5 M NaCl the absorbance was found to decrease to approximately 40% of its maximum value and remain stable at that value over time, as the solubility limit of fibrillar material appears to have been reached (Figure A.3).

Absorbance region 1 is completely diminished at approximately the salt concentration where fluorescence region A is first observed. This suggests that absorbance region 2 corresponds to fluorescence region A. The observation of region 2 at salt concentrations below those where region A is observed then suggests that A is observed at the point when the lag time for A becomes shorter than the lag time for fluorescence region B, and indicates that these may be competing growth processes.

The lag time obtained by absorbance measurements is consistently shorter than the lag time obtained by fluorescence, even where region 2 is the first observable increase in absorbance: a result that does not seem to be dependent upon the salt concentration. This suggests that the fluorescence assay is insensitive to early time aggregates and either that a critical size has to be reached before ThT binding becomes significant, or that these species do not bind ThT.

This insensitivity of the fluorescence assay to the species observed at early times by absorbance is consistent with previous observations about the early curvilinear fibril population observed at >150 mM NaCl, where the initial oligomers and filaments with a bead-on-string appearance were not thought to contain the contain the β-sheet core of the final fibrils [2]. This might suggest that absorbance region 1 is associated with oligomer formation and the formation of early filament species on the curvilinear filament pathway.

Figure 4.4 (left) shows the maximum fluorescence and absorbance values obtained in these experiments. A decrease in final fluorescence intensity coincides with the appearance of fluorescence region C. Additionally, the decrease in total fluorescence is large compared to the fraction of the total fluorescence in region A: a reduction of $\sim 30\%$ from the value before the process is observed, at which point the early process accounts for $\sim 15\%$ of the total fluorescence and appears to be approaching a plateau at that value.

The low fluorescence intensity of region A compared to the final fluorescence, and the corresponding stronger decrease in final fluorescence intensity suggests that this may indeed be the oligomeric growth pathway previously observed at

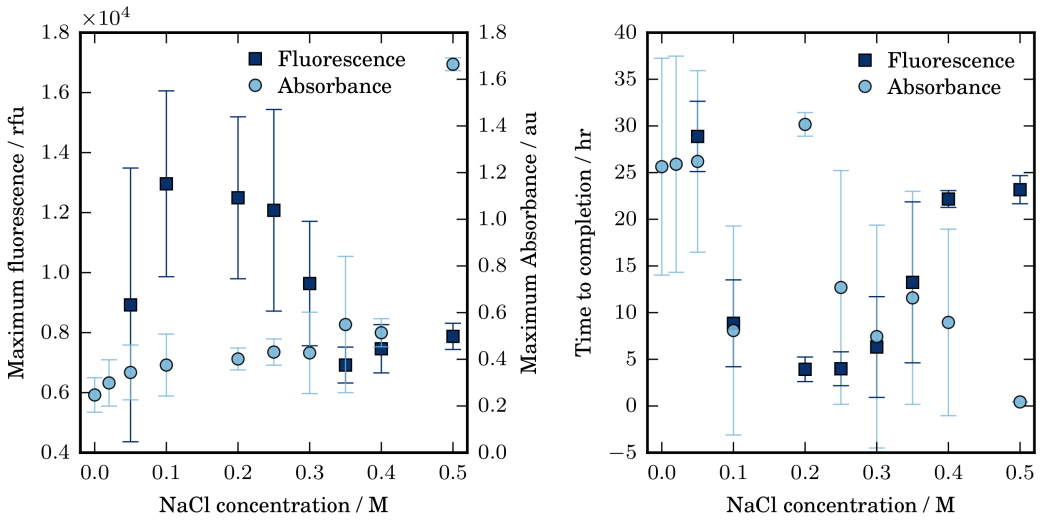

Figure 4.4: Maximum Thioflavin T fluorescence and absorbance at 600 nm obtained for a range of salt concentrations for 10 mg mL^{-1} HEWL at 65°C, pH 1.6 (25 mM HCl), incubated with double orbital shaking at 700 rpm for 2.5 of each 5 minute cycle. Fluorescence data were not included at 0 and 0.02 M NaCl, since reliable final plateau regions were not obtained over the experimental timeframe.

high salt by Foley and Hill *et al.* [2, 88, 89], where curvilinear fibrils were found to exhibit less fluorescence enhancement upon ThT binding [2, 88]. Absorbance region 2 and fluorescence region A are thought to be associated with the formation of these curvilinear species.

The maximum turbidity at 600 nm does not change with the change in maximum fluorescent behaviour, suggesting that no decrease in the aggregate mass or size population occurs. However, as salt concentration increases the solution becomes cloudy upon aggregation as the fibrillar species begin to precipitate, and the absorbance increases significantly, as seen at 0.5 M NaCl, although it should be noted that significant precipitation out of suspension was not observed on the timescale of the kinetic growth curves at lower salt concentrations.

4.3 High temperature, low pH and high salt

At high temperature, low pH and high ionic strength, HEWL has been shown to form fibrils along a pathway where oligomers are formed, assemble into short, curvilinear worm-like filaments or protofibrils, and filaments laterally assemble at

later times to form longer and stiffer fibrils [2, 89]. Indeed, growth matching this description was observed at high salt, as shown in Figure 4.5.

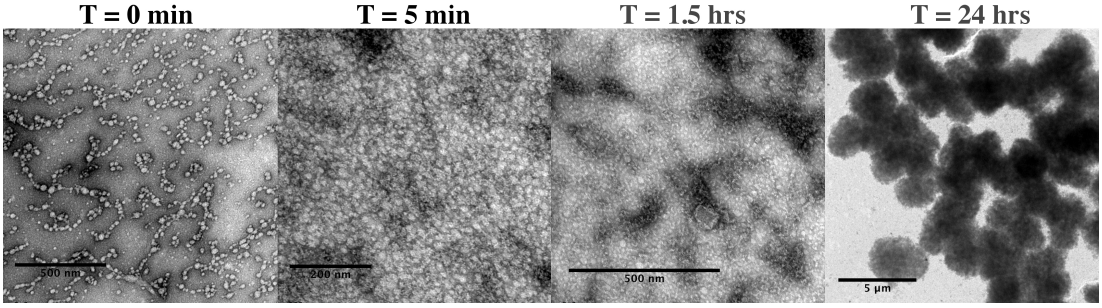

Figure 4.5: Transmission Electron Micrographs of 10 mg mL^{-1} HEWL fibrils formed at 1 M NaCl, pH 2, 60°C over time. From left to right: oligomers immediately observed, after 5 min and after 1.5 hours incubation under quiescent conditions in Eppendorf tubes. Fluorescence readings taken from these time points showed approximately a 3-fold increase in fluorescence at 5 minutes compared to the initial reading, and a similar fluorescence reading was obtained at 1.5 hours. The 24 hr time sample is from a separate sample, incubated in a platereader, but in both experiments spherulites were observed after this time period and coincided with a further increase in fluorescence intensity (approximately 6-fold in the Eppendorf incubation). Samples were diluted 20x immediately prior to grid application and stained with uranyl acetate. Scale bars are (left to right) 500 nm, 200 nm, 500nm and 5µm.

In Section 4.2 the behaviour of HEWL incubated at low pH and high temperature under agitation in the presence of various salt concentrations was shown. As salt concentration increases, a larger proportion of the fluorescence and absorbance increase is attributed to these curvilinear fibril species. The results described in Section 4.2 suggest that this species is in competition with the straight fibrillar species that are thought to give rise to the more intense fluorescence response that was observed.

Agitation was found here to have a large effect on the favoured growth pathway, with increased agitation favouring the formation of straight rather than worm-like fibrils by significantly decreasing the lag time for formation of the straight fibrillar species relative to that of the curvilinear species.

To investigate the salt-induced worm-like fibril growth, experiments were performed in quiescent conditions. At long times, the formation of straight fibrils and spherulites was still observed, but the lag times for this species were typically >15 hours and followed a long plateau period of metastability after growth of the salt-induced species, as shown in Figure 4.6. This plateau-like period is considered the end of the kinetic growth period for the salt-induced curvilinear species and growth curves are normalised to this point. Additionally, no increase in

absorbance is observed at the point that further fluorescence increase is observed, suggesting that this may not be an increase in aggregate mass but the formation of one species at the expense of the other.

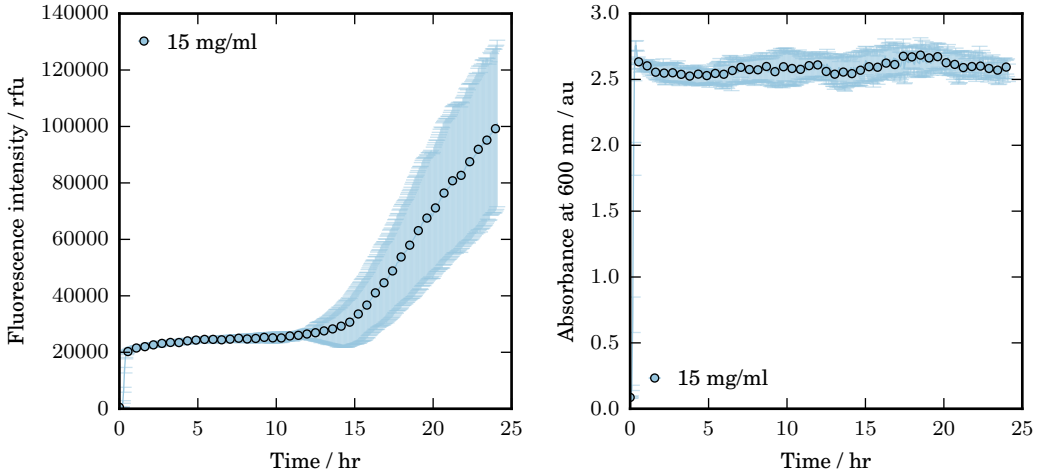

Figure 4.6: Fluorescence (left) and absorbance at 600 nm (right) 15 mg mL^{-1} HEWL, 60°C, pH 2, 1 M NaCl.

The presence of the fluorescent dye ThT was shown to have negligible effect on growth kinetics and the concentration (55 µM) was chosen to be in excess at high HEWL concentration (Figures A.4 and A.5).

The system was found to be highly temperature sensitive. At 40°C and below little aggregation (and no reproducible results) was observed on experimental timescales (up to 72 hours). At 50°C similar growth curves were observed to those in Figure 4.6, consistent with the melting temperature of HEWL [244, 251]. Although the aggregation observed at 50°C was slightly slower (plateauing around 3 hours at 1 M NaCl, 8 mg mL^{-1} HEWL, which would allow for the capture of more data points,) the metastable plateau regions were noisier, and 60°C was chosen as the investigation temperature. The upper limit of the platereader temperature did not give a wide enough range for further temperature analysis.

In addition, increases in pH dramatically reduced aggregation propensity, consistent with literature reports of pH stability [247, 258].

4.3.1 The effect of salt concentration

Figure 4.7 shows growth curves obtained by ThT fluorescence and absorbance at 600 nm for HEWL incubated at pH 2, 60°C in quiescent conditions in the presence of increasing salt concentration. Below 0.5 M NaCl the fluorescence response was much lower and noisier (Figure A.6).

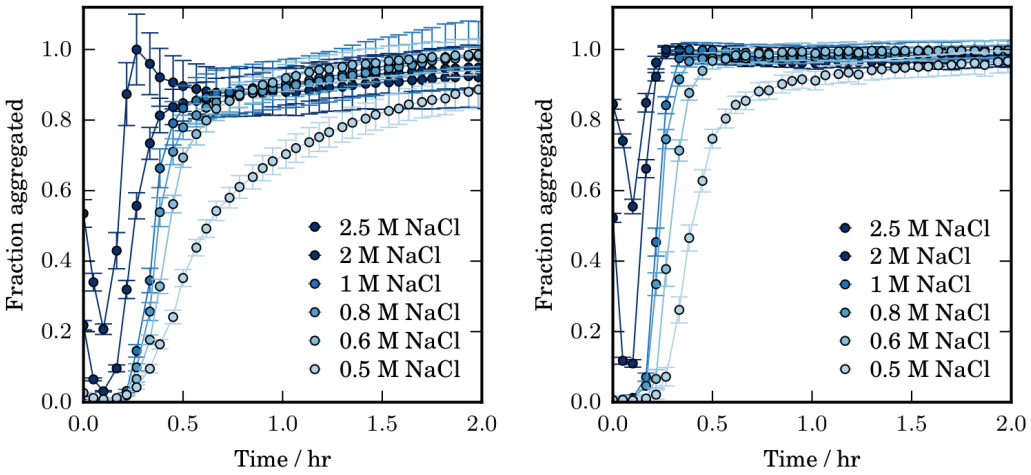

Figure 4.7: Normalised Thioflavin T fluorescence (left) and simultaneous absorbance at 600 nm (right) data for 10 mg mL^{-1} HEWL incubated at pH 2, 60°C, quiescent conditions, in the presence of increasing NaCl concentrations.

The method of sample preparation was different for 0.8 M NaCl and above. Salt solution was added to the microplate in advance and protein was added immediately before the plate was placed in the reader. This is not considered to effect the shape of the growth curves, but this led to a slight discrepancy in the maximum fluorescence and time at which this is reached (Figure A.6). For consistency with the lower salt concentrations and the results observed by absorbance, the growth curves at high salt have been normalised to a value close to the beginning of the decrease in rate of fluorescence increase (closer in time to the points of normalisation for lower concentrations). However, the fluorescence is observed to increase very slowly for a long period of time following this, and there is no true plateau value. The result of taking a later time point as the maximum fluorescence value is shown for 0.8, 0.9 and 1 M NaCl in Figure A.6 (lighter blue squares) but is considered to have little effect on subsequent analysis (because data are normalised).

As shown in Figure 4.7, a lag phase is apparent for all salt concentrations,

and the increase in absorbance occurs earlier than the increase in fluorescence. Additionally, at 2.5 M NaCl there is a large intensity reading at time zero (immediately after the plate enters the reader and before temperature equilibration), which complicates the estimation of a lag time or maximum growth rate.

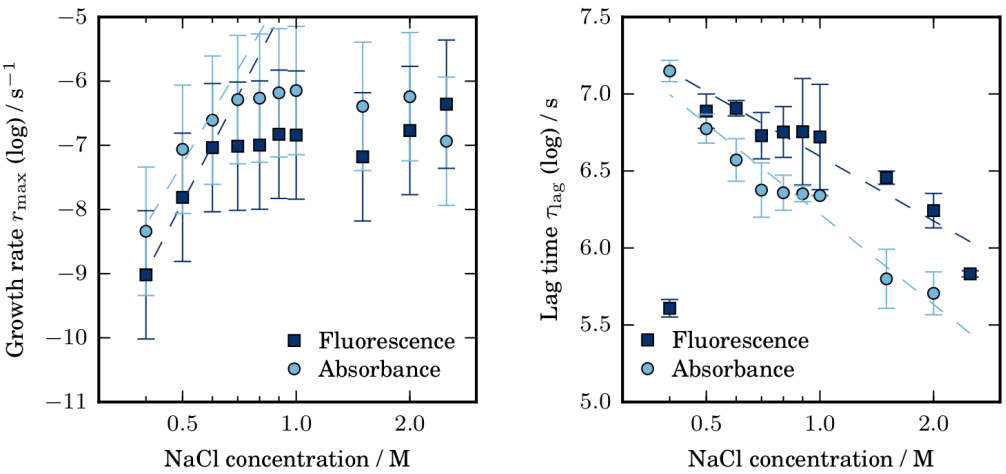

Figure 4.8: Maximum growth rate and associated lag time obtained from the tangent to the maximum growth rate for Thioflavin T fluorescence and absorbance at 600 nm of 10 mg mL^{-1} HEWL incubated at pH 2, 60°C, quiescent conditions, in the presence of increasing NaCl concentrations. Below 0.7 M NaCl growth rate increases with concentration order 4.9(3) and 4.3(9) for fluorescence and absorbance respectively. Excluding the odd fluorescence result at 0.4 M, lag time decreases with increasing salt concentration with order -0.61(8) and -0.85(8) for fluorescence and absorbance respectively.

Estimates of growth rate and lag time were obtained from the best fit tangent to the maximum growth rate. As Figure 4.8 shows, growth rate increases with increasing salt concentration up to 0.7 M and lag time decreases with increasing salt, exhibiting a 'kink' between 0.7 and 1 M NaCl.

Increasing salt therefore increases growth rate and decreases lag time, presumably by increased charge screening between on-pathway species. The growth rate is then limited, and increasing salt concentration acts only to decrease the lag phase. This suggests that the elongation rate of fibrils is limited, perhaps by a structural transition resulting in a 'locking and docking' type growth mechanism as oligomers add to filament ends.

4.3.2 The effect of protein concentration

Figure 4.9 shows the kinetic growth curves obtained for various HEWL concentrations incubated at pH 2, 60°C in the presence of 1 M NaCl. Growth curves are sigmoidal-like at high concentration but as concentration decreases (below 3 mg mL^{-1}) a 'kink' is observed in growth curves around 40% aggregated (clearer by absorbance at 600 nm).

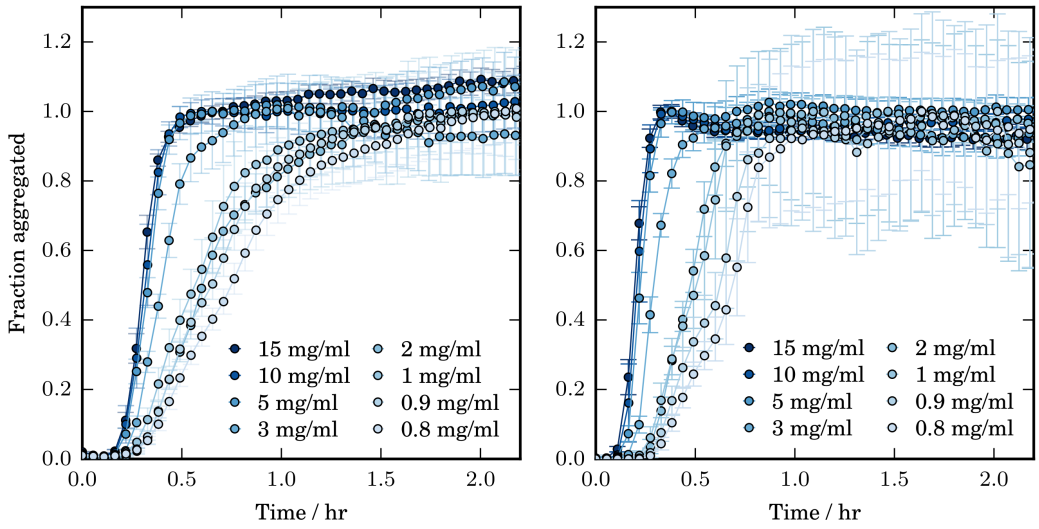

Figure 4.9: Normalised Thioflavin T fluorescence (left) and simultaneous absorbance at 600 nm (right) data for various concentrations of HEWL incubated at pH 2, 60°C in 1 M NaCl, quiescent conditions.

In all cases, intensity increases rapidly and then slows to a plateau-like region. However, in the fluorescence readings the intensity is found to continuously creep upwards. In absorbance readings an initial peak is typically followed by a small dip. For consistency, maximum values were taken following this dip in absorbance, and taken around the same time point for fluorescence. Since absorbance values do not slowly increase in the same way this is thought to be the result of post-growth modifications, for example the formation of thicker, stiffer fibrils by lateral association of filaments.

The maximum fluorescence and absorbance values were found to increase with increasing protein concentration (Figure A.7). However, the increases in intensity were found to be larger than a linear concentration dependence (initially $\sim m_{\mathrm{tot}}^{2.7(2)}$) and this concentration dependence decreased with increasing protein concentration.

The growth at 4 mg mL^{-1} (280 µM) and above has approximately the form of the logistic function, i.e. the inflection point occurs around 50% aggregate total and:

$$M(t) = M(0) + \frac{1 - M(0)}{1 + e^{-k(t-\tau_m)}} \tag{4.1}$$

Where in this case there is a lag phase ($M(0) = 0$) and the parameters of interest are the growth rate k and the time of maximum growth τ_m. The results of the fit to this equation for a selection of data are shown in Figure 4.10.

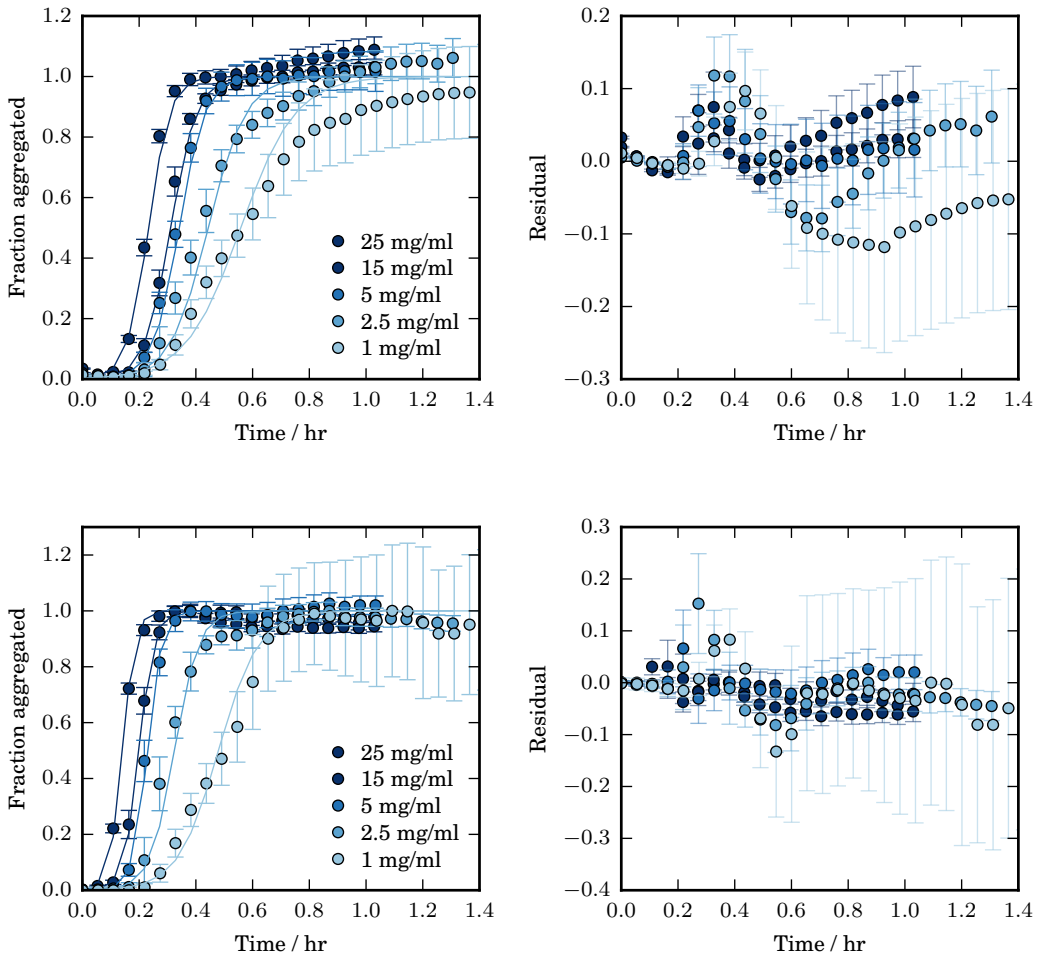

Figure 4.10: Normalised Thioflavin T fluorescence (top charts, circles), normalised absorbance at 600nm (bottom charts, circles) and corresponding fits to the logistic function (solid line in matching shade) for various concentrations of HEWL incubated at pH 2, 60°C in 1 M NaCl, quiescent conditions. Legends apply to all graphs.

At 3mg mL^{-1} and below the growth curves exhibit a kink at around 40% total aggregate. This cannot be accounted for by any of the available model functions, and the growth curves become increasingly less steep than the closest logistic function with decreasing protein concentration. However, the fit results are still considered to give a good approximation for $\tau_{\mathrm{m}} \approx \tau_{50}$. In addition, growth rates and lag times have been estimated from the best fit tangent at the maximum growth rate. In this case it is the maximum growth rate prior to the kink that has been taken for the discontinuous curves (this is not the maximum rate but provides more data points for an estimate).

The growth parameters obtained from the generalised logistic function are shown in Figure 4.11 and the parameters obtained from the tangent to the maximum growth rate are shown in Figure 4.12.

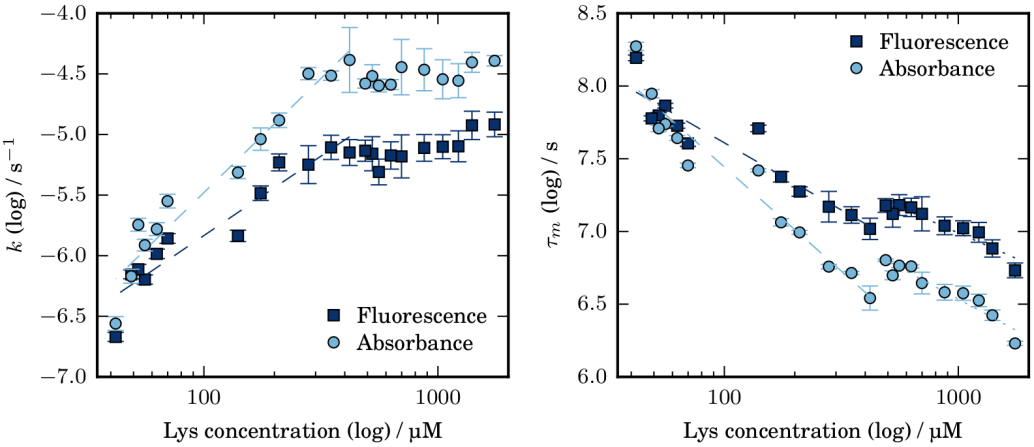

Figure 4.11: Growth rate k and characteristic time τ_m obtained from the closest generalised logistic function to the growth curves of HEWL incubated at pH 2, 60°C in 1 M NaCl, quiescent conditions. Up to 5 mg mL^{-1} (350 µM) k has concentration order 0.57(6), 0.82(6) by fluorescence and absorbance. Up to 6 mg mL^{-1} τ_m decreases with concentration order -0.40(5) and -0.62(5) for fluorescence and absorbance respectively, before continuing to decrease at a slower rate (-0.31(4) and -0.38(4)).

Up to 5 mg mL^{-1} (350 µM) the growth rate k increases with concentration, with concentration order 0.57(6) by fluorescence and 0.82(6) by absorbance. Above this, k becomes essentially concentration independent by absorbance and weakly concentration dependent by fluorescence. The kink at 5mg mL^{-1} is also observed in the characteristic time τ_m. In contrast to the lag time τ_{lag} (Figure 4.12), τ_m (Figure 4.11) is found to decrease faster with respect to concentration at 6 mg mL^{-1} (420 µM) and below.

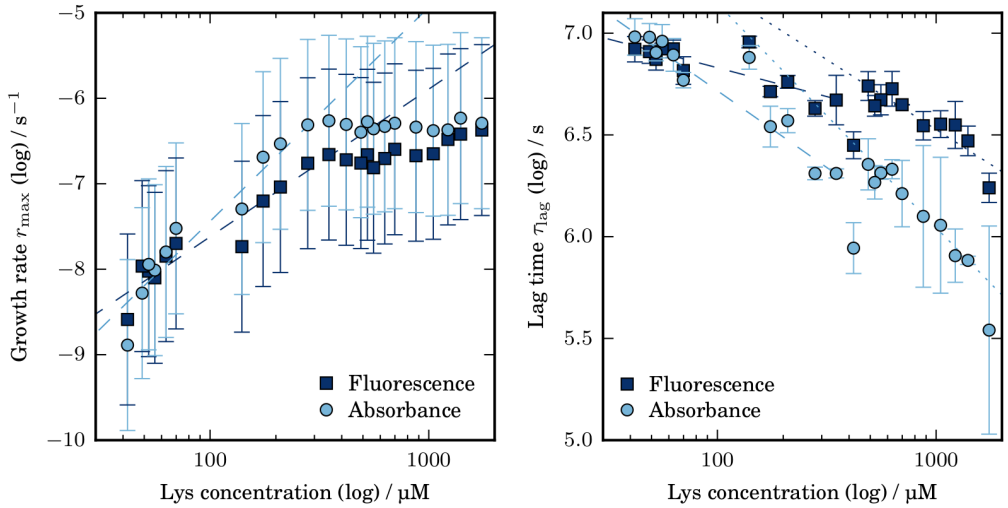

Figure 4.12: The maximum growth rates (left) and associated lag times (right) obtained by fitting a tangent to the linear region of growth about the maximum growth rate for HEWL incubated at pH 2, 60°C in 1 M NaCl, quiescent conditions. Up to 5 mg mL^{-1} (350 µM) growth rate increases with concentration dependence $r_{max} \propto m_{tot}^{\gamma}$ where $\gamma = 0.75(8), 1.1(1)$ for fluorescence and absorbance respectively. Above this absorbance is roughly concentration independent, and fluorescence is weakly concentration dependent with $\gamma = 0.29(5)$. Below 5 mg mL^{-1} lag time has concentration order $\gamma = -0.13(4), -0.33(3)$ by fluorescence and absorbance. Above this the concentration order is $\gamma = -0.31(5), -0.48(2)$ respectively.

The parameters obtained from the tangent at the maximum growth rate (Figure 4.12) show similar behaviour to those obtained from the logistic function (Figure 4.11), with a discontinuity in concentration dependence around 5-6 mg mL^{-1} (350-420 µM). Up to 5 mg mL^{-1} the maximum growth rate r_{max} is found to increase with concentration order 0.75(8) and 1.1(1) for fluorescence and absorbance respectively, higher estimates than obtained by the logistic fit. At higher concentrations the rates are found to be weakly concentration dependent or concentration independent.

The characteristic times obtained by absorbance are shorter than those obtained by fluorescence. As seen in Figure 4.9, the absorbance kinetics typically reach a peak by the time the fluorescence kinetics reach the inflection point around 50%. If this initial increase in absorbance is due to the emergence of an initial, non-ThT-binding oligomer population as proposed in Section 4.4, the contribution of this population to the absorbance cannot be decoupled from the increase in absorbance as the ThT-binding fibrillar species grows from the oligomers. Contributions from both species may be the reason for the kinked

curve shapes observed at low protein concentration.

The decrease in growth rate dependence on concentration at high concentrations may be the result of a conformational change becoming rate limiting, as suggested at high salt concentration in Section 4.3.1. The lower growth rate concentration dependence of fluorescence compared to absorbance may suggest that fragmentation might play a role in the growth of the filaments (related to increases in fluorescence) while either monomer addition or coagulation plays a much larger role in the growth of the initial beaded-string curvilinear species (related to initial increases in absorbance). The weak concentration dependence of the characteristic times (concentration orders in the range -0.62(5) to -0.13(4)) is also suggestive of fragmentation.

Additionally, the parameters obtained from the generalised logistic function are roughly correlated, with $k \propto \tau_m^x$ where $x = -0.75(3), -0.82(3)$ for fluorescence and absorbance. The result is similar for the growth rates and lag times obtained from the linear fit, (Figure A.8). In both cases, there is a high correlation between the two parameters up to 5 mg mL^{-1} and at higher concentrations the correlation decreases dramatically, most clearly in the lag time results. Correlation is predicted between these parameters for the secondary process-dependent model, further suggesting that fragmentation is likely to be an important growth process, particularly at lower protein concentrations where it appears to be more dominant.

Similar results to the logistic fit were obtained by fitting to the simplest version of the secondary process-dependent (SDP) model (Figures A.9 and A.10). The simplest version consists of the two composite parameters κ and λ, associated with the secondary and primary growth processes respectively, where:

$$M(t) = M(\infty)\left[1 - \exp\left(-\frac{2\lambda^2}{\kappa^2}\sinh^2\left(\frac{\kappa t}{2}\right)\right)\right] \tag{4.2}$$

This is the result of the Knowles SDP model in the limit of irreversible growth ($k_{\mathrm{off}} = 0$) and with no aggregate population at time zero ($M(0) = P(0) = 0$). The number of parameters increases very quickly with complexity in the SDP model, and fits to higher numbers of parameters were not pursued in this case as the fit to Equation 4.2 was not of high enough quality.

The parameters obtained are shown in Figure 4.11. As with the generalised

logistic function, absorbance data fit more closely to the SDP model than the fluorescence data, however, since the absorbance data may reflect the growth of two different populations (the initial oligomer population and the worm-like fibrils), this is not conclusive evidence for a secondary growth process. Despite this, the SDP model provides the closest model fit to the growth data obtained for HEWL at high salt, highly suggestive that a secondary growth process is dominant at early and intermediate times, and as discussed above, this is most likely to be fragmentation.

Indeed, the area in which the SDP model deviates most from the data (the plateau approach, see Figures A.9 and A.10) is known to be overestimated in the simplified model applied here. Larger numbers of replicate samples and an increased number of data points over the curve region would be required to obtain fits to the higher number of parameters in the second order solution of the SDP model.

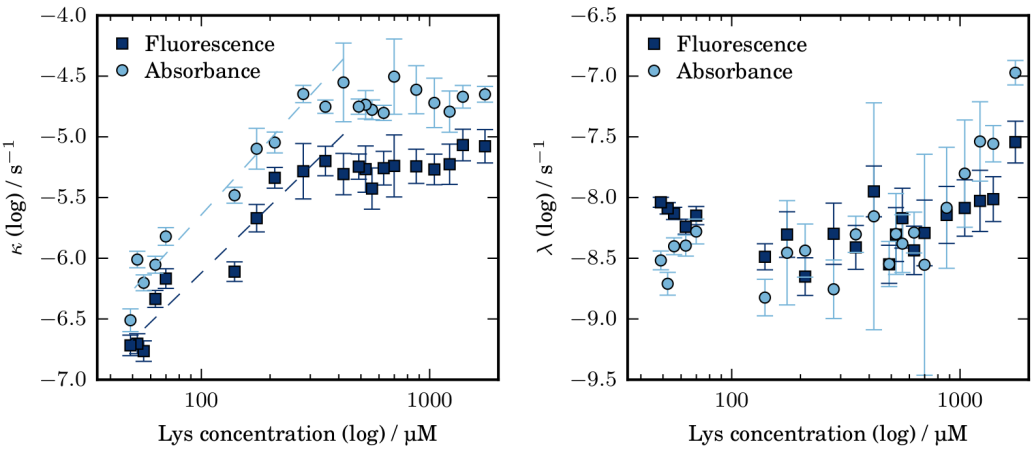

Figure 4.13: Parameters κ and λ (corresponding to secondary and primary growth processes respectively) obtained from the simplest SDP model for the growth curves of HEWL incubated at pH 2, 60°C in 1 M NaCl, quiescent conditions. The initial increase in κ has concentration order 0.80(8) by fluorescence and 0.90(8) by absorbance.

As seen in Figure 4.13, κ is found to have similar behaviour to the maximum growth rate obtained by linear and logistic function fitting, exhibiting roughly concentration independent behaviour above 5 mg mL^{-1} (350 µM). Interestingly, λ is found to be roughly concentration independent below this point and to increase with concentration above around 8 mg mL^{-1} (560 µM). These parameters are composites of the growth rates associated with primary nucleation (k_n where n is

the size of the nucleus) or a secondary growth mechanism (k_{sec} where n_{sec} is the size of the secondary nucleus) with the growth rate for monomer addition (k_+), such that $\kappa = (2k_+k_{\text{sec}}m_{\text{tot}}^{n_{\text{sec}}+1})^{1/2}$ and $\lambda = (2k_nk_+m_{\text{tot}}^n)^{1/2}$, where m_{tot} is the total monomer concentration.

The increase in concentration dependence of λ and the kink observed in the characteristic times suggest that there is a change in the dominant growth process. The correlation of the characteristic time and growth rate only up to 5-6 mg mL^{-1} and the increase in λ at concentrations higher than this both suggest that fragmentation is most dominant below this critical concentration, and above it the importance of fragmentation is diminished.

4.3.3 Surface activity

The experiments described above were performed in Corning Non-Binding Surface coated 96 well, flat bottomed microplates, sealed with microplate film. The surface coating is a nonionic, hydrophilic, polyethylene oxide-like polymer designed to minimise hydrophobic and ionic surface interactions. The effect of surface area to volume ratio (SA:vol) at 5 mg mL^{-1} HEWL at pH 2, 60°C, 1 M NaCl was investigated by varying sample volume in 96-well and 384-well microplates (of the same surface type). Surface area to volume ratios were calculated using average well geometries.

Faster kinetics (faster growth rate and reduced lag time) were observed for the salt-induced growth in 384-well microplates, as seen in Figure 4.14 (and Figure A.11). The 384-well plates have a higher wall:water interface ratio, which might suggest that the walls are more effective in promoting aggregation than the air-water interface or that the air water interface is detrimental.

In contrast to the increasingly slow growth rate the lag time obtained by fluorescence was found to decrease with increasing SA:vol ratio, while the lag time obtained by absorbance was relatively unaffected. Maximum fluorescence and absorbance were also found to decrease with increasing SA:vol ratio (Figure A.12).

Assuming that the initial increase in absorbance is related to the growth of the initial, beaded appearance aggregate population while the fluorescence is a response to the growth of the curvilinear filament population, these results suggest that while the increase in SA:vol ratio appears to have little effect on the oligomer population the curvilinear growth is inhibited in some way, perhaps by

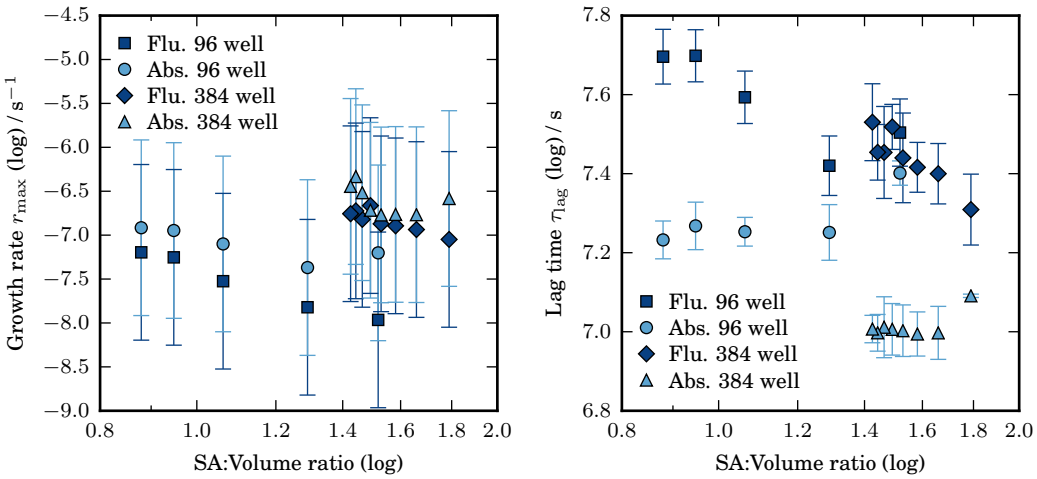

Figure 4.14: Growth rate and lag time obtained from the best fit tangent to the maximum growth rate of 5 mg mL^{-1} HEWL at pH 2, 1M NaCl, 60°C, quiescent conditions at various sample volumes in either a 384-well (the group of 8 data points at higher SA:vol ratio) or 96-well Corning NBS coated microplate. Surface area to volume ratios were calculated using average well geometries.

stabilisation of the oligomeric population and/or adhesion of these species to the surfaces.

Aggregation was found to be more strongly promoted in hydrophobic, uncoated Greiner microplates of roughly equivalent geometry (Figure A.13), suggesting that hydrophobic interactions are important for the aggregation in this system. The trends in lag time and growth rate with increasing SA:vol ratio in the uncoated microplates appeared to be the same as those in the Corning microplates. However, the growth was considerably more rapid and the uncertainty in these results much larger, and they have not been included for analysis purposes. Nevertheless, it would appear that hydrophobic surfaces are important in promoting aggregation, particularly of the oligomers in this system.

4.3.4 The effect of seeding

Seeding with preformed fibrils formed at 1M NaCl (removed prior to increases in fluorescence associated with the formation of straight rigid fibrils at longer times) was found to increase both the initial fluorescence and absorbance value, as shown in Figure 4.15, indicating the higher aggregate population at early times. Indeed, the fluorescence and absorbance response at time zero was found to have

similar exponential concentration dependence to the maximum values obtained by increasing protein concentration (and therefore final aggregate mass) under these conditions and therefore reflects the concentration of the seed population (Figure A.14).

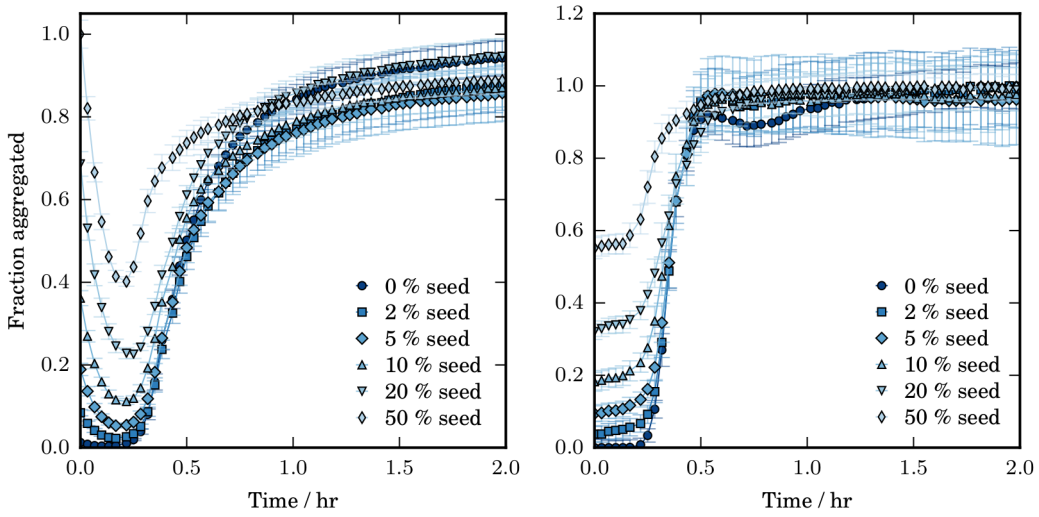

Figure 4.15: Normalised thioflavin T fluorescence (left) and absorbance at 600 nm (right) obtained for samples of 2 mg mL^{-1} total concentration (including seed) HEWL incubated at 1M NaCl, 60°C, pH 2, quiescent conditions in the presence of various seed concentrations. Preformed seeds produced under the same aggregation conditions.

However, a decrease from the initial value was observed by fluorescence while the absorbance response was continuous. This may suggest an initial break-down of curvilinear fibrils into smaller species and oligomers immediately after addition of the seed material and heating, since this indicates a decrease in ThT binding but not of aggregate mass. This hints at the weaker stability of these fibrillar species compared to the straight rigid fibrils.

The growth rates were found to be roughly independent of seed concentration and lag times were found to decrease slightly with increasing seed concentration (Figure A.15). However, the effect of seed on the lag time is much less than expected in systems dependent on some form of nucleation event. This suggests that elongation rather than nucleation processes dominate the observed growth kinetics until seed concentrations become very high. At 50% seed the maximum fluorescence value and lag time are notably higher and lower respectively.

In addition to seeding with preformed fibrils formed by incubation at 1 M NaCl, seeding with fibrils formed under conditions favouring the low ionic

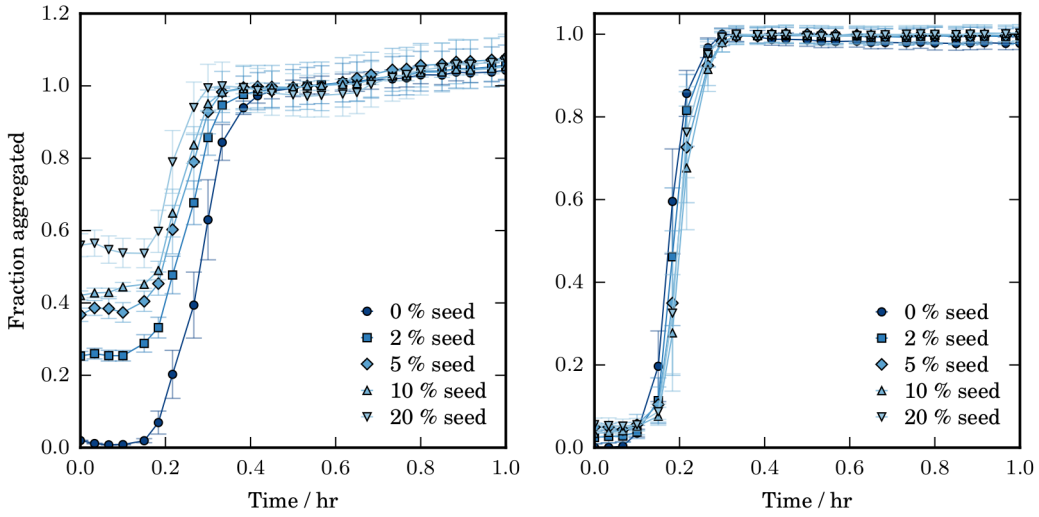

Figure 4.16: Normalised thioflavin T fluorescence (left) and absorbance at 600 nm (right) obtained for samples of 10 mg mL^{-1} total concentration (including seed) HEWL incubated at 1 M NaCl, 60°C, pH 2, quiescent conditions in the presence of various seed concentrations. Preformed seeds produced at pH 1.5, 65°C, 200 mM NaCl with agitation by Eppendorf Thermomixer shaking at 700 rpm for 20 hours.

strength pathway (200 mM NaCl, 65°C, pH 1.5 with agitation by Eppendorf Thermomixer shaking at 700 rpm for 20 hours) was also performed, at both 1 M and 200 mM NaCl, 60°C, pH 2 without agitation. The kinetics obtained are shown in Figures 4.16 and 4.17 for 1 M and 200 mM NaCl respectively. The lower salt concentration was chosen because it matches the salt concentration of the formation of the seeds, incubated at pH 1.5, 65°C, 200 mM NaCl with agitation by Eppendorf Thermomixer shaking at 700 rpm for 20 hours.

In both cases the maximum fluorescence values obtained were similar to those obtained for the aggregation of 10 mg mL^{-1} HEWL in the absence of seeding at 1 M NaCl. At both 1 M and 200 mM NaCl the initial fluorescence response is high, and does not significantly dip. In both cases the initial fluorescence and absorbance values were also similar (Figures A.16 and A.17). However, at 1 M NaCl the initial absorbance is a much smaller fraction of the total absorbance and the final absorbance values are similar to those obtained previously for aggregation at high salt.

The lack of significant absorbance at early times in both cases, and the final absorbance at 200 mM is consistent with a generally lower absorbance result obtained for samples containing predominantly straight rigid fibrils, and

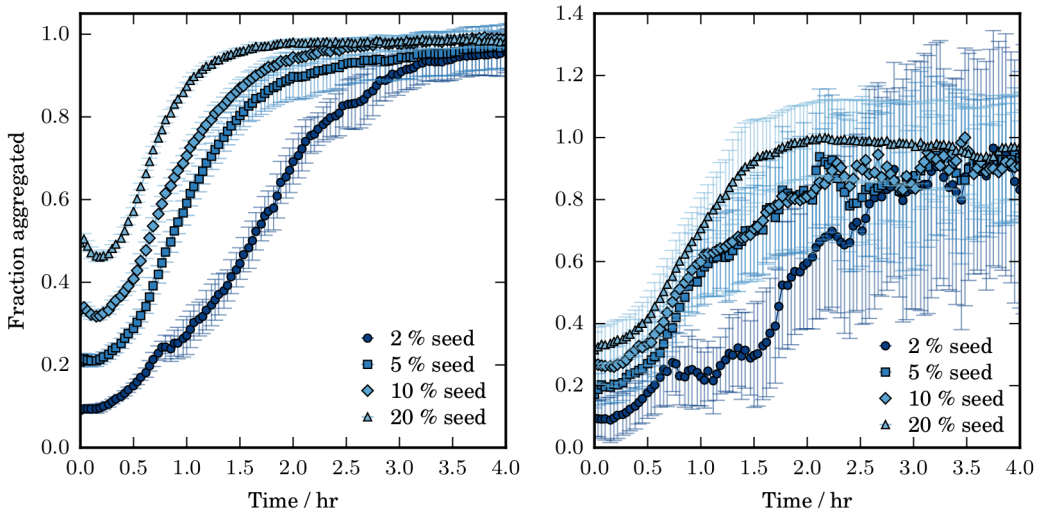

Figure 4.17: Normalised thioflavin T fluorescence (left) and absorbance at 600 nm (right) obtained for samples of 10 mg mL^{-1} total concentration (including seed) HEWL incubated at 200 mM NaCl, 60°C, pH 2, quiescent conditions in the presence of various seed concentrations. Preformed seeds produced at pH 1.5, 65°C, 200 mM NaCl with agitation by Eppendorf Thermomixer shaking at 700 rpm for 20 hours.

confirms that that the straight fibrils persist and grow at 200 mM NaCl while the oligomeric growth dominates at higher salt. The decreasing maximum absorbance and increasing fluorescence with increasing seed concentration in both cases is further evidence for the relative stability and persistence of the straight fibrils, and suggests that the straight fibrils that are added as seed persist and are not converted to curvilinear fibrils under either salt concentration.

At 1 M NaCl the growth curves are very rapid, and consistent with the curve shapes obtained for aggregation at 1 M NaCl in the absence of seed. At 200 mM the curve shape is very different, and more reminiscent of the curve shapes obtained in agitated samples at lower salt, with a slower plateau approach. This is consistent with growth proceeding along the curvilinear pathway at high salt, with none or very little growth of the preformed seed, while it would appear that growth from the seed species is active at the lower salt concentrations from which the seed species originates.

Growth rates and the lag times observed by absorbance at 1 M NaCl were found to be roughly independent of seed concentration, while the lag time observed by fluorescence was found to decrease with seed concentration (Figure A.18). In contrast to previous results at 1M NaCl, the lag times observed

by absorbance were found to be longer than those observed by fluorescence. This suggests that the seed population may be acting as a monomer sink, consistent with the observation that it still contributes to the maximum fluorescence and absorbance values, and that it is a competing species. However, this may be a result of the few data points and the initially high fluorescence value, represented in the large uncertainty of the value at 20% seed (Figure A.18). It is also clear in Figure 4.16 that fluorescence begins to increase at around 0.2 hours, after absorbance has begun to increase from its initial value.

The growth rates obtained at 200 mM NaCl were similarly unaffected by increases in seed concentration (Figure A.19). Under these conditions the characteristic times obtained by both fluorescence and absorbance were found to decrease with increasing seed concentration.

4.4 High temperature, low pH and low ionic strength

Although there is evidence here for the existence of the curvilinear species at concentrations below 0.3 M NaCl, a clear transition in behaviour was found around this point, as seen in Figure 4.4. Reliable and reproducible kinetic curves were not obtained by fluorescence at salt concentrations lower than 0.1 M, and as such the region 0.1-0.25 M NaCl will be referred to as the low ionic strength regime, where the rapid growth profile appears to dominate (i.e. its lag time is shorter than the lag time for the formation of curvilinear species).

4.4.1 The effect of protein concentration

ThT fluorescence and simultaneous turbidity measurements were performed for a range of HEWL concentrations from 0.25 mg mL^{-1} (18 µM) to 17.5 mg mL^{-1} (1.20 mM) at 65°C, pH 1.6 ($\sim$ 25 mM HCl), and 0.2 M NaCl, with agitation at 700 rpm for 2.5 of 5 minutes per cycle, and are shown in Figure 4.18. The kinetic growth curves obtained at all concentrations can be seen in Figures A.20 and A.21. These conditions were found to provide the most reproducible results, determined as variation between replicate wells. However, as concentration of HEWL decreased, the reproducibility decreased, and data have been corrected

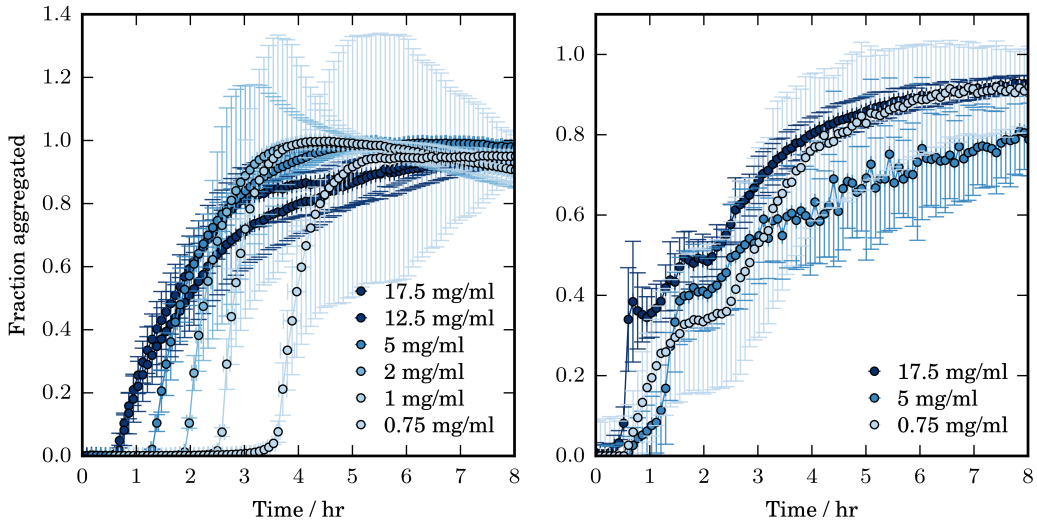

Figure 4.18: Left: Average fluorescence aggregation kinetics. Data are normalised to the maximum fluorescence value for each concentration. Right: Average absorbance 600 nm aggregation kinetics. HEWL was incubated at various concentrations at 65°C, pH 1.6 (∼ 25 mM HCl), and 0.2 M NaCl, with agitation at 700 rpm for 2.5 of 5 minutes per cycle. Error bars are standard deviation.

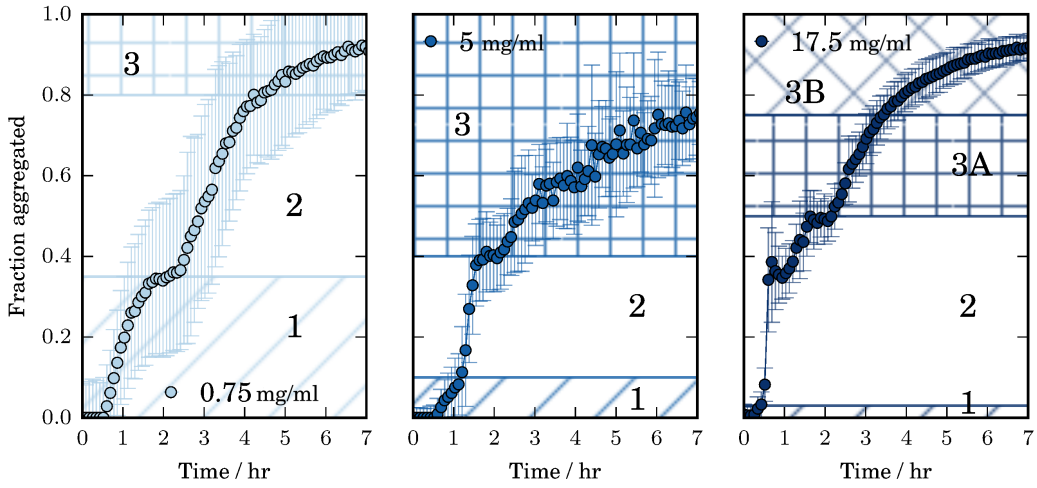

Figure 4.19: Normalised absorbance at 600 nm versus time for HEWL incubated at various concentrations at 65°C, pH 1.6 (∼ 25 mM HCl), and 0.2 M NaCl, with agitation at 700 rpm for 2.5 of 5 minutes per cycle. The main growth regions are highlighted as in Section 4.2. The growth at early times, region 1, is highlighted by diagonal lines, the period of rapid growth that follows, region 2, has no pattern and the final region of slow increase in fluorescence intensity, region 3, is hatched. At very high concentrations ($\geq$12.5 mg mL^{-1}) region 3 is further split into an initial, faster growth region followed by a very slow continuous creep upwards in absorbance that does not reach a plateau over the experimental timeframe.

for the average time to 10% completion obtained, as discussed in Section 2.2.2. Additionally, the maximum fluorescence value obtained increased approximately linearly with protein concentration up to 12.5 mg mL^{-1} (870 µM), and above this the protein concentration dependence was reduced (Figure A.22).

As seen in Figure 4.18, three growth regions are apparent in the kinetic profile of the absorbance data (right). These are highlighted in Figure 4.19. In the growth profile for 5 mg mL^{-1} (centre, Figure 4.19) all three growth regions can be observed: the first growth region (1) is small and consists of a lag phase followed by an increase in absorbance that slows towards $\sim$ 1.2 hours; a very rapid increase in absorbance follows and then plateaus around 2 hours (region 2); after which a third and slower increase in absorbance is observed (region 3) and a plateau is reached at a higher absorbance value. The end points of these regions, associated with the beginning of the next region, are shown in Figure 4.20 along with the lag time obtained from region 2.

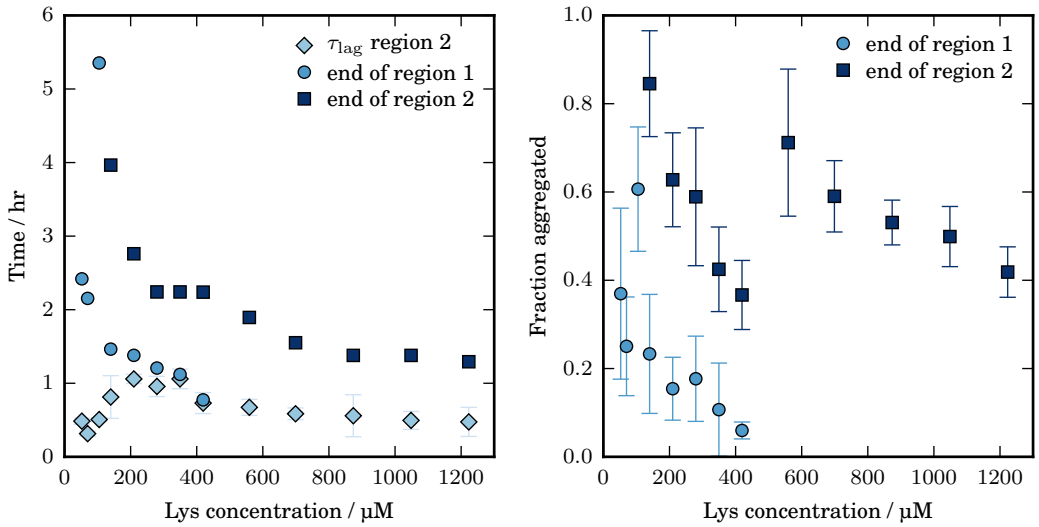

Figure 4.20: Absorbance data. Left: Data points correspond to the beginning of region 2/end of region one (circles), the lag time determined from region 2 (diamonds) and the end of region 2. Right: the fraction aggregated by the end of region 1 or 2. HEWL incubated at various concentrations at 65°C, pH 1.6 ($\sim$ 25 mM HCl), and 0.2 M NaCl, with agitation at 700 rpm for 2.5 of 5 minutes per cycle. Error bars are standard deviation.

At concentrations below 2 mg mL^{-1} (140 µM) region 1 is pronounced, as seen for 0.75 mg mL^{-1} in Figure 4.19, and decreases in intensity as concentration increases until at 6 mg mL^{-1} (420 µM) it is no longer observable, as seen in Figure 4.20. A discontinuity is also seen at this point in the fraction aggregated

(the proportion of total absorbance) by the end of region 2. Both regions 1 and 2 decrease in intensity with increasing monomer concentration, but after region 1 diminishes a larger aggregate fraction is represented by region 2, suggesting either competition between, or a combination of the absorbance profiles for the observed growth processes.

Above 6 mg mL^{-1} HEWL the slower growth curve approaching the final plateau (region 3) is more clearly defined (as seen in Figure A.21). At high concentrations, 12.5 mg mL^{-1} (870 µM) and above, the plateau approach in region 3 becomes a very slow continuous increase in absorbance and the time to completion exceeds the experimental timeframe (plateaus at $\sim$ 65 hours, Figure A.22). At this point region 3 appears to be separated into two further sections: an initial faster growth period (region 3A) followed by a much slower one (region 3B), as highlighted in Figure 4.19.

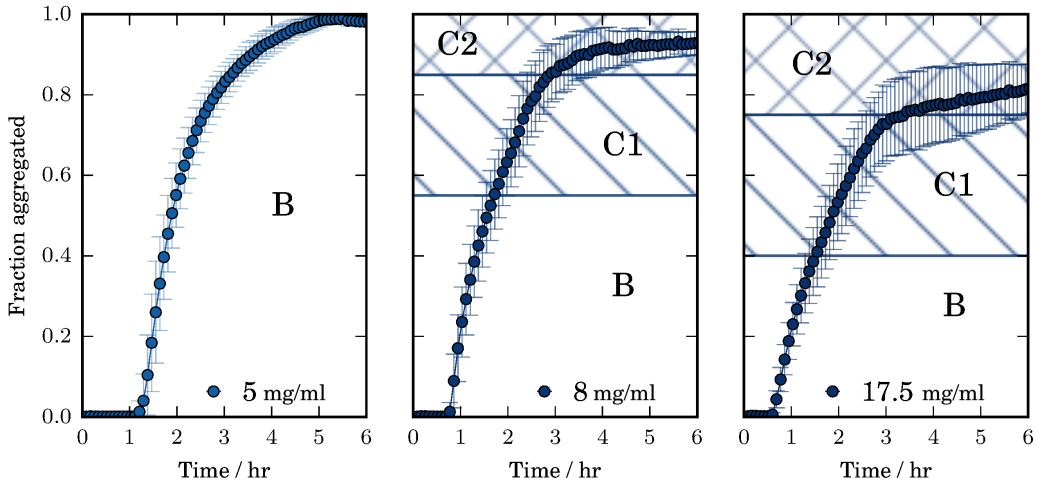

Figure 4.21: Normalised Thioflavin T fluorescence intensity over time for HEWL incubated at various concentrations at 65°C, pH 1.6 ($\sim$ 25 mM HCl), and 0.2 M NaCl, with agitation at 700 rpm for 2.5 of 5 minutes per cycle. The main growth regions are highlighted as in Section 4.2. The period of rapid growth, region B, has no background pattern. Following this a period of slower growth is observed, region C1, and at very high protein concentrations ($\geq$12.5 mg mL^{-1}) a very slow creep in fluorescence is observed rather than a plateau region (C2).

In contrast, the increase in fluorescence intensity over time has the general form of a sigmoidal-like curve, as seen in Figure 4.21: a lag phase is followed by rapid growth, which slows and reaches a final plateau value. Below 2 mg mL^{-1}

(140 µM), the data roughly have the form of the generalised logistic function:

$$M(t) = M(0) + \frac{1 - M(0)}{(1 + Q\mathrm{e}^{-k(t-\tau_\mathrm{m})})^{1/v}} \tag{4.3}$$

Where k is the growth rate, ν is a value dictating the position of the inflection point, Q a value depending upon $M(0)$ (the lower asymptote), τ_m the time of maximum growth when $Q = \nu$ and $M(\infty)$ the upper asymptote.

Above 2 mg mL^{-1} (140 µM) the approach to the plateau is slower than the closest fitting generalised logistic function. At 6mg mL^{-1} (420 µM) and above, a slower linear region in the plateau approach following the inflection point becomes more apparent (region C1) and the inflection point moves to earlier times and smaller aggregate fractions. These regions are highlighted in Figure 4.21, and the point of beginning of each region, along with the lag time obtained from the rapid growth in region B are shown in Figure 4.22.

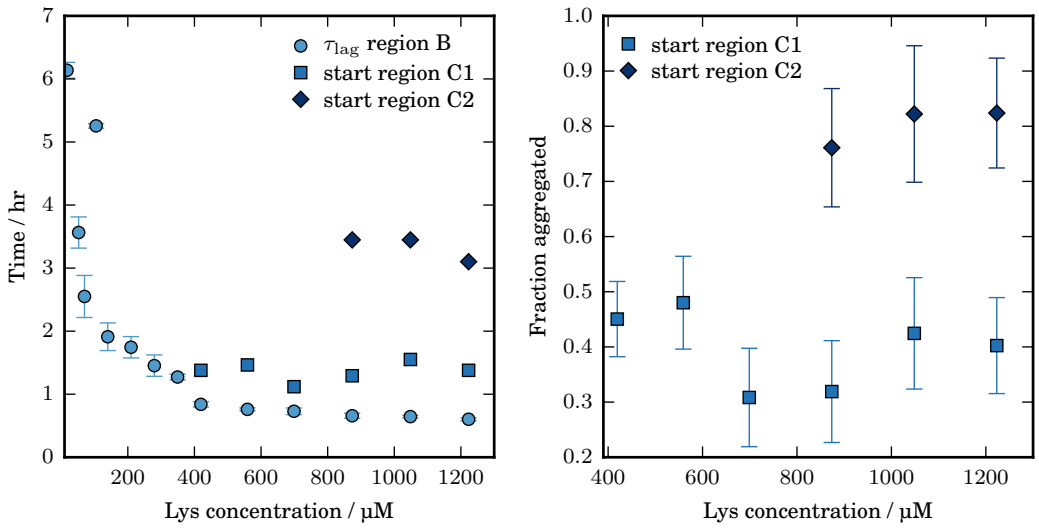

Figure 4.22: Fluorescence data. Data points correspond to the beginning/end of observed regions of kinetic growth. The lag time is associated with the maximum growth rate obtained for HEWL incubated at 65°C, pH 1.6 (∼ 25 mM HCl), and 0.2 M NaCl, with agitation at 700 rpm for 2.5 of 5 minutes per cycle.

At 12.5 mg mL^{-1} (870 µM) and above, as with the absorbance data, the plateau approach becomes a very slow continuous increase in fluorescence (region C2), as shown in Figure 4.21. The similarities between fluorescence regions C, C1 and C2 and absorbance regions 3, 3A and 3B suggest that these correspond to growth of the same species. This is reminiscent of the effect

of coagulation becoming a dominant growth mechanism at long times as the monomer population is diminished, as predicted by the end-joining model (JDP). However, the analytical solution to the joining model only holds for systems where there is no observable lag time. Additionally, the transition between rapid (C1) and slower growth (C2) in the fluorescence plateau approach is much sharper than the transitions that are predicted by the JDP model.

Similar discontinuities in curve shape were observed with increasing salt under these growth conditions, as seen in Section 4.2, but were not observed in the growth pathway at high salt (Section 4.3). As such, this is related to a change in the dominant growth process of the pathway favoured at low ionic strength.

Clearly no current analytical solution is capable of describing the complexities of the growth curves. As such, growth rates and associated lag times were obtained from the best fit tangents to the maximum growth for each observed region.

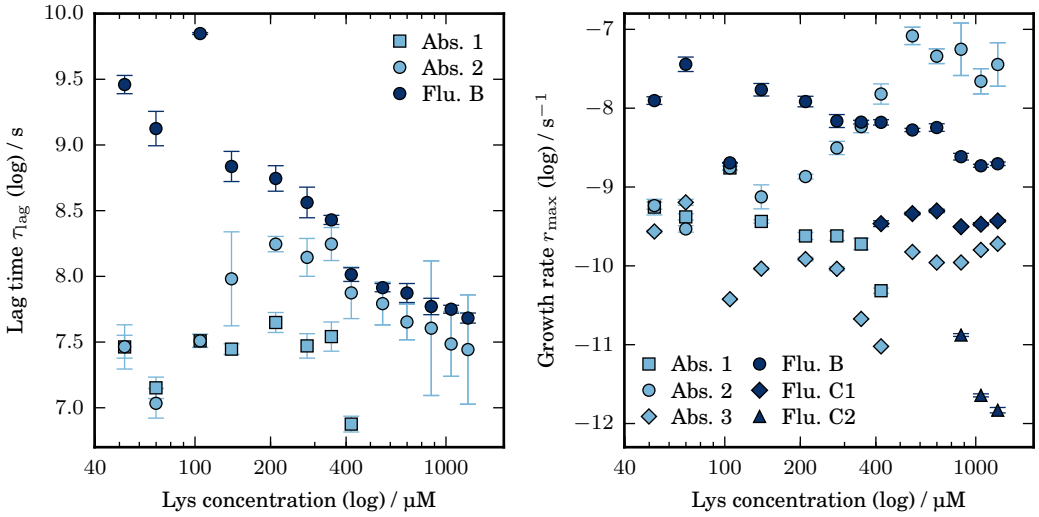

Figure 4.23: The maximum growth rates and associated lag times obtained from the best fit tangent to the maximum growth rate for regions of fluorescence and absorbance at 600 nm increase. Various HEWL concentrations were incubated at 65°C, pH 1.6, 200 mM NaCl with agitation at 700rpm.

As was observed previously (Section 4.2), the lag times obtained by absorbance (regions 1, pale squares, and 2, pale circles, Figure 4.23 left) are consistently shorter than those obtained by fluorescence (region B, dark circles, Figure 4.23 left). Additionally, the lag time obtained in absorbance region 1 (squares) does

not appear to be in any way related to the behaviour of the fluorescence. As previously proposed, this initial increase in absorbance appears to be related to the early, non-ThT-binding, bead-on-string curvilinear or oligomer populations associated with the aggregation favoured at high salt.

The lag time in absorbance region 1 is roughly independent of protein concentration. This is in contrast to the behaviour at high salt. However, this is not incompatible with the oligomeric growth pathway since oligomer formation is less favoured under these lower salt conditions and may be rate-limiting.

The second region of absorbance increase (region 2) is roughly correlated with the increase in fluorescence (Flu. $r_{\max}$) at 6 mg mL^{-1} (420 µM) and above, where the lag time observed by fluorescence appears to have nearly caught up to the lag time observed by absorbance. However, absorbance region 2 is observed below this concentration, where it is less correlated with the fluorescent behaviour. In Section 4.2, absorbance region 2 was associated with fluorescence region A, the formation of curvilinear filaments as observed at high salt, and it was proposed that A is observed only when the lag time for A becomes shorter than the lag time for B. Indeed, the timescale of the observed plateau in absorbance region 2 is similar to those observed at high salt.

The correlation of absorbance region 2 with fluorescence region B at ≥ 6 mg mL^{-1} suggests that absorbance region 2 and fluorescence region B contain contributions from both the oligomeric pathway and the low-ionic strength straight filament pathway that cannot be simply deconvoluted.

The decrease in intensity of both absorbance regions 1 and 2 with increasing HEWL concentration, as seen in Figure 4.20, is then thought to be a result of competition between the oligomeric growth pathway (giving rise to regions 1 and 2) and the straight filament growth (absorbance region 3, part of absorbance region 2 and the majority of the fluorescence response).

Additional evidence for this competitive relationship was seen in an odd result obtained at 1.5 mg mL^{-1}. An unusually pronounced lag time in the fluorescence profile coincided with an extended absorbance region 1 (as seen in Figures A.20 and A.21). This strongly suggests that if conditions favour oligomer formation, this is detrimental to the aggregation observed by fluorescence. However, the reason for the odd result at 1.5 mg mL^{-1} is unknown.

Furthermore, while the difference between the fluorescence and absorbance

lag times is reduced at 6 mg mL^{-1} (420 µM) and above, as seen in Figure 4.23, the two values do not coincide. This suggests that although the lag time for the low-ionic strength pathway catches up to that of the oligomeric pathway, the latter pathway is still active. Along with the result at 1.5 mg mL^{-1} this indicates a strong link between the the lag time observed for the straight filaments (the fluorescent growth) and the population of the early oligomeric species, suggesting that the oligomers and curvilinear filaments may act as a monomer sink.

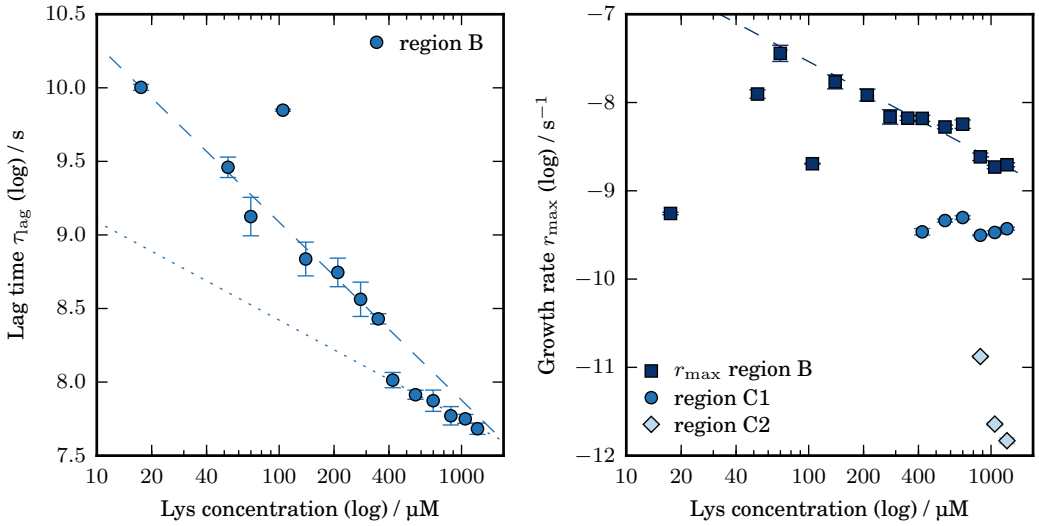

Figure 4.24: Fluorescence data. Left: Lag time vs. concentration for the lower concentration region (below 6 mg mL^{-1}, 420 µM, dashed line) has exponent -0.525(8). At higher concentrations (blue dotted) the exponent is -0.29(2). Right: Excluding the two lowest concentrations the exponent of growth rate v.s concentration is -0.48(4). All fits exclude 1.5 mg mL^{-1} (110 µM) for which the result is anomalous. Results are obtained by linearly fitting about r_{max} for various HEWL concentrations at 65°C, pH 1.6, 200 mM NaCl with agitation at 700rpm for 2.5 of 5 minutes per cycle.

The lag times and growth rates associated with the fluorescence regions are shown again in Figure 4.24. The absorbance data are shown in Figure A.23, but are not included for analysis purposes since the lag times and growth rates are likely to be composites of the behaviour of the two active growth pathways that cannot be deconvoluted.

As seen in Figure 4.24, the fluorescence lag phase decreases as concentration increases. As seen in Figure 4.23, below 6 mg mL^{-1} fluorescence appears to be uncoupled from the oligomeric growth observed by absorbance. The concentration order dependence of the lag time in this region, -0.525(8), suggests fragmentation as a dominant growth process.

Above 6 mg mL^{-1} (420 µM) HEWL there is notable slowing of the decrease in lag time of region B and the concentration order decreases from -0.525(8) to -0.29(2). The growth rate concentration dependence of region B also slows at this point but exhibits a larger discontinuity at 12 mg mL^{-1}, 870 µM). The growth rate in region B is found to initially increase with concentration up to 1 mg mL^{-1} (70 µM) and then to decrease with concentration, at $m_{\mathrm{tot}}^{-0.48(4)}$. In contrast, the growth rate of fluorescence region C1 is roughly concentration independent. The same was found for the appearance of this region in time and in the fraction of the total aggregate intensity, as was shown in Figure 4.22.

The reducing concentration dependence of the lag time coincides with the disappearance of absorbance region 1, the correlation of the fluorescence with absorbance region 2, and the emergence of the slower, discontinuous plateau approach in both absorbance (regions 3A and 3B) and fluorescence (regions C1 and C2). This is also the critical concentration observed at high salt, thought to be the result of a conformational change in the addition of oligomers to the curvilinear species dominating the growth kinetics, as described in Section 4.3.2.

The initial increase in fluorescence intensity and the approach to the plateau region were investigated in more detail. The initial growth observed by fluorescence (up to 10% for 6 mg mL^{-1} and above, up to 30% below 6 mg mL^{-1}) was best approximated as exponential ($M(t) \sim \exp(k_1(t - \tau_1))$), suggesting a secondary growth process is dominant and consistent with the lag time behaviour that suggests fragmentation as a dominant growth process.

In contrast to the maximum growth rate, the apparent growth rate k_1 obtained from the exponential fit to the increase in fluorescence, is roughly concentration independent, as shown in Figure 4.25 (pale circles). This suggests that a concentration independent growth mechanism, like a conformational change during elongation, is rate limiting at early times (before the inflection point) for all concentrations.

The characteristic time τ_1 has weaker concentration dependence than the lag time but exhibits the same trend, as shown in Figure 4.25. Below 6 mg mL^{-1} (420 µM) the concentration order is -0.5(1), consistent with fragmentation, and above this it is found to be concentration independent. This suggests that the lag time concentration dependence shown in Figure 4.24 may be overestimated as a result of the estimation method: which relies on data points that may be

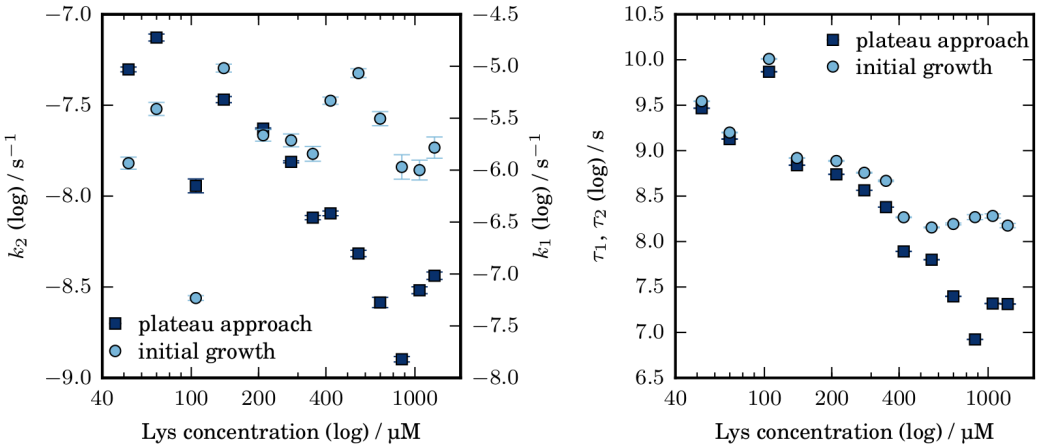

Figure 4.25: Fluorescence data. Apparent growth rates and associated characteristic times obtained from exponential fits to the initial period of growth (k_1, τ_1) and the final plateau approach (k_2, τ_2) for ThT fluorescence kinetics of HEWL incubated at 65°C, pH 1.6 ($\sim$ 25 mM HCl), and 0.2 M NaCl, with agitation at 700 rpm for 2.5 of 5 minutes per cycle.

associated with growth at later times.

The two growth mechanisms that are related to concentration independence of lag time ($\sim \tau_1$) are conformational rearrangement prior to or as part of nucleation and a supercritical concentration above which oligomers are more stable than monomers in solution, as discussed in Section 1.3.3. The latter would be consistent with increased competition from the oligomeric pathway, but would be expected to promote the oligomeric pathway to the detriment of the pathway for straight fibrils as observed for the result at 1.5 mg mL^{-1}.

Since the critical concentration observed (6 mg mL^{-1}) is the same as the critical concentration obtained at high salt in Section 4.3.2, attributed to conformational rearrangement, it is reasonable to assume that a similar or identical process may be occurring under these conditions. Indeed, contributions from the oligomeric pathway are likely to be driving this result. However, the concentration independence of k_1 at concentrations below 6 mg mL^{-1} does suggest that conformational rearrangement may also be rate limiting for the straight filament pathway at early times.

The fluorescence plateau-approach was found to approximately have the form of the exponential $M(t) \sim M(\infty) - \exp(-k_2(t - \tau_2))$ up to 12.5 mg mL^{-1} (870 µM): the point at which the change in curve shape is most obvious and hints at coagulation processes.

As shown in Figure 4.25, the characteristic time τ_2 (dark squares) was found to decrease with concentration, with $m_{\text{tot}}^{-0.51(5)}$ at concentrations below 6 mg mL^{-1} and $m_{\text{tot}}^{-0.6(1)}$ at 6 mg mL^{-1} and above, both most consistent with fragmentation driven growth. Both τ_2 and k_2 exhibit a discontinuity at 6 mg mL^{-1}, but these are notably weaker than the discontinuities observed in the other parameters, suggesting that the growth at later times is less affected by changes in growth mechanisms around 6 mg mL^{-1}. This is consistent with the critical concentration resulting from the competitive oligomeric pathway, and not from the low ionic strength pathway, since growth associated with the oligomeric pathway has typically reached a final plateau state by this time (absorbance region 2, Figure 4.19).

The apparent growth rate k_2 was found to decrease with concentration from 1 mg mL^{-1} (70 µM, excluding the odd results at 1.5 mg mL^{-1}, 110 µM) to 12.5 mg mL^{-1}, at $m_{\text{tot}}^{-0.57(6)}$, in agreement with the results obtained for the maximum growth rate in Figure 4.24. As fragmentation has been shown above to be a dominant growth process in this pathway and a gel phase was observed to form upon aggregation (as previously observed [243, 244]), a growth rate that decreases with increasing concentration suggests a critical gelated fibril concentration (CFC), above which fragmentation is suppressed [177]. According to the results obtained both from maximum growth rate and k_2, this must be around 1 mg mL^{-1} (70 µM) HEWL.

Addition of monomer as it dissociates from the curvilinear species, acting as a monomer sink, may also contribute to a slow final increase in fluorescence. However, this mechanism alone is not consistent with the decrease in growth rate with increasing protein concentration since there is little evidence for an increasing proportion of oligomeric/curvilinear species with increasing protein concentration (for which an increase in absorbance to higher maximum values would be expected, in line with the absorbance responses at high salt) or with the discontinuous nature of the growth curves beyond the inflection point.

Furthermore, it appears that above 12.5 mg mL^{-1}, where the slow plateau approach suggests coagulation processes, the maximum growth rate and k_2 begin to increase. There may be a change in growth mechanism around this point. At this point, the maximum fluorescence is no longer linearly dependent on protein concentration, and other mechanisms may be at play in the supersaturated

environment, for example, precipitation/inhibition of the oligomeric species. This might be an interesting pursuit for further study with techniques better suited to higher protein concentrations.

4.4.2 Surface activity

The effect of surface area to volume ratio at 10 mg mL^{-1} HEWL at pH 1.5, 65°C, 200 mM NaCl was investigated by varying volume in 96-well and 384-well microplates (of the same surface type). Surface area to volume ratios were calculated using average well geometries. The shape of the growth curves obtained in each case were similar, but slower kinetics (smaller growth rates) were observed for experiments performed in 384-well microplates, as seen in Figure 4.26 and in contrast to the results at high salt concentration. This may be the result of altered agitation due to the geometry change or the increased wall:air-water interface ratio (if the air-water interface is important for promoting aggregation).

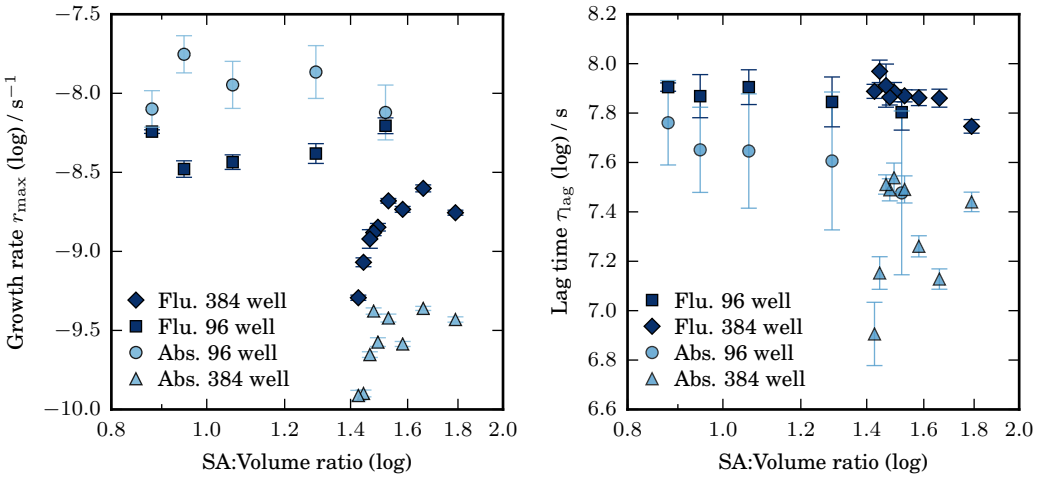

Figure 4.26: Growth rate and associated lag times obtained from the best fit tangent to the maximum growth rate for kinetics obtained by Thioflavin T fluorescence and simultaneous absorbance at 600 nm measurements for 10 mg mL^{-1} HEWL incubated at pH 1.5, 65°C, 200 mM NaCl with agitation (double orbital shaking at 700rpm) at different microplate well volumes in either 384 well (the group of 8 data points at higher SA:vol ratio) or 96 well Corning NBS coated microplates.

The lag times obtained by fluorescence are similar in both plate types. Both characteristic parameters were found to be roughly independent of SA:vol ratio in the 96 well plates and the lag time for fluorescence was found to be roughly independent of SA:vol ratio in the the 384 well plates. The lower lag time obtained

for absorbance in the 384 well plates is consistent with the observation at high salt (Section 4.3.3).

In contrast to the behaviour at high salt, aggregation was found to be clearly promoted (as observed by fluorescence) in Corning NBS coated microplates compared to hydrophobic uncoated polystyrene Greiner microplates of roughly equivalent geometry (Figure A.24). The two surfaces were also found to give rise to different concentration behaviour, with the critical concentration around 6 mg mL^{-1} clearly pushed to higher protein concentrations in the Greiner microplates.

The absorbance data in the Greiner microplates was found to exhibit a larger initial absorbance region, associated above with oligomer formation. The change in behaviour in the Greiner microplates is therefore related to the promotion of the oligomeric pathway by the hydrophobic surface, as previously observed in Section 4.3.3. In the presence of hydrophobic surfaces the rigid fibril pathway is therefore competitively inhibited by the formation of oligomeric species.

4.4.3 The effect of seeding

In contrast to seeding of the pathway at high salt, the addition of preformed seed was found to dramatically promote aggregation, as seen in Figure 4.27. After addition of 2% seed the lag phase was reduced to approximately half its initial value. Maximum absorbance and fluorescence were also higher in seeded samples. The initial fluorescence and absorbance values were non-zero and increased with increasing seed concentration (Figures 4.27 and A.25).

The shape of the curve in the seeded samples is very different, with a rapid approach to the plateau phase rather than the slow smooth curve observed in the absence of seed. At intermediate seed concentrations there is also a notable drop after the initial maximum peak. The slow plateau approach is thought to be the result of a change from fragmentation driven growth to growth by monomer addition and coagulation as a critical fibril mass is created that gels and inhibits fragmentation and to have a contribution from the competing oligomeric pathway with monomer being slowly released by disassociation. The very rapid growth curves observed in the presence of seed are similar to the super-exponential plateau approach predicted for fragmentation driven growth by the SDP model, suggesting that the addition of seed drives the reaction to proceed more rapidly than the process driving the change towards slower growth.

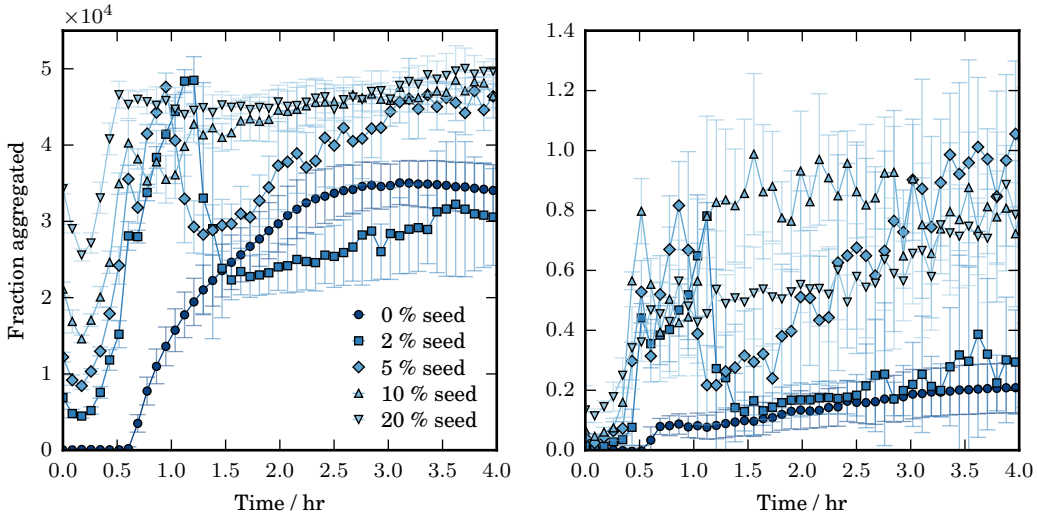

Figure 4.27: Thioflavin T fluorescence (left) and absorbance at 600 nm (right) obtained for 10 mg mL^{-1} HEWL incubated at 65°C, pH 1.5, 200mM NaCl with agitation by double orbital platereader shaking at 700 rpm with various concentrations of added seed. Seeds formed by incubation in the same solution conditions with agitation by Thermomixer shaking at 700rpm at 65°C for 20 hours. Legend applies to both graphs.

The maximum growth rate was found to be relatively unchanged by the addition of or increase in seed concentration, but lag time decreased with increasing seed (Figure A.26). The lack of change in growth rate is consistent with the proposal above that the growth at early times (where the maximum is observed in the absence of seed) is dominated by a rate-limiting conformational change during elongation.

In addition, the effect of seeding with fibrils formed at 1 M NaCl, pH 2, 60°C is shown in Figure 4.28. While there is some variation in curve shape in the plateau region of fluorescence, the growth curves obtained in all cases were very similar, and the addition of preformed seed at 1 M NaCl appears to have negligible effect on the growth curves, maximum intensities or growth parameters under these conditions at 10 mg mL^{-1}. High seed concentrations were not found to have a significant impact on the rate of the plateau approach, suggesting that competition with the oligomeric species does not make a large contribution to the slow growth in this region. This result is consistent with the rigid fibril growth being predominantly favoured in these conditions, and it is possible that the contribution from the curvilinear population may be fixed because only a particular population is stable under these conditions.

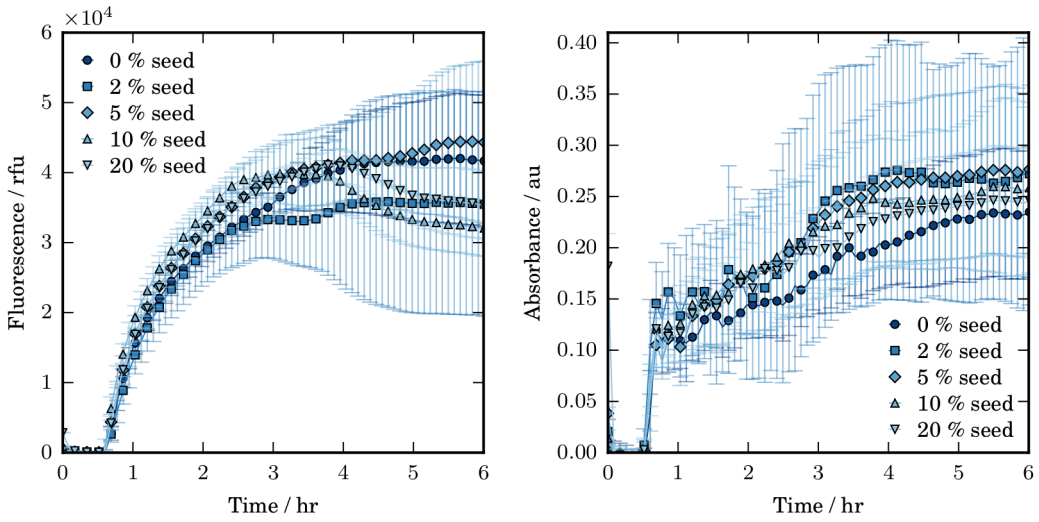

Figure 4.28: Thioflavin T fluorescence (left) and absorbance at 600 nm (right) obtained for 10 mg mL^{-1} HEWL incubated at 65°C, pH 1.5, 200mM NaCl with agitation by double orbital platereader shaking at 700 rpm with various concentrations of added seed. Seeds formed by incubation at 1 M NaCl, pH 2, 60°C in quiescent conditions.

4.5 Aggregation at very high temperature and low pH

At the high temperatures, low pH and low ionic strengths described in the previous section, image analysis by TEM is complicated by the phase separation into sections of viscous gel that are only broken by strong agitation or shear that may also significantly alter the structure. It was found to be easier to obtain EM images of fibrils formed at higher temperatures in the absence of salt. The structure of these fibrils is thought to be identical to those obtained after long incubation times at high temperature and low pH in the earlier experiments, where a large proportion of HEWL will have been subject to hydrolysis. In addition to the single stranded fibrils observed at lower temperatures, at 90°C thick, multistranded ribbons and nanotubes have also been observed [253, 279].

Aggregation at higher temperatures was performed in both a Cary Eclipse Fluorometer with Peltier temperature control and by removing aliquots from samples incubated in an Eppendorf Thermomixer and taking readings in a platereader. Agitation appeared to be a requirement for obtaining reproducible growth kinetics at high temperature however, and sufficient agitation was not possible in situ. An entire kinetic profile was not obtained at high temperatures,

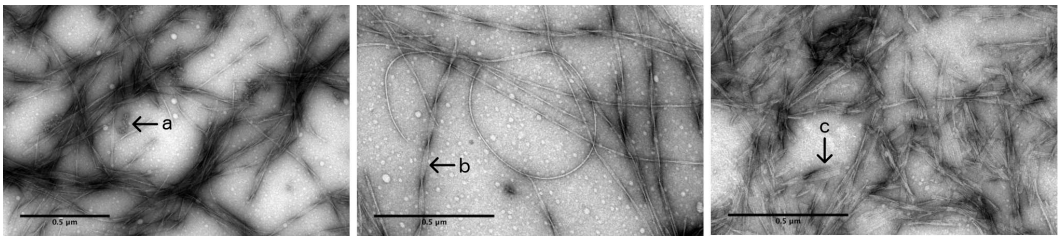

Figure 4.29: Transmission electron micrographs of HEWL after incubation at 90°C under agitation for 24 hours. Samples were diluted 20x immediately prior to grid application and stained with uranyl acetate. Scale bars are 0.5 µm. Left: 10 mg mL^{-1} HEWL aggregated at pH 2 in the absence of salt. Centre: 20 mg mL^{-1} HEWL aggregated at pH 2 in the absence of salt . Right: 10 mg mL^{-1} HEWL aggregated at pH 1.6, 20 mM NaCl. Examples of some of the different species present are highlighted: *a)* small aggregate species, with some elongated appearance, *b)* twisted ribbons consisting of a number of laterally associated filaments and *c)* wide ribbons consisting of a large number of laterally associated filaments.

but fluorescence was found to increase up to around 20 hours for aggregation at 90°C, pH 2 in the absence of salt. After this a sharp decrease in fluorescence was observed, and not found to coincide with a decrease in absorbance (Figure A.27). This might arise from the exclusion of ThT upon formation of multistranded fibrils and nanotubes.

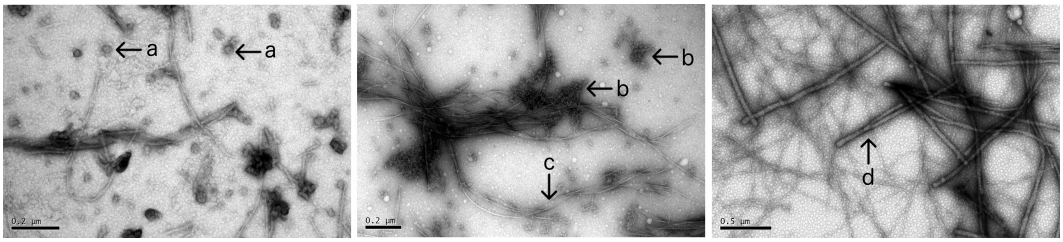

Figure 4.30: Transmission electron micrographs of HEWL after incubation at pH 2 and 90°C under agitation for 24 hours. Samples were diluted 20x immediately prior to grid application and stained with uranyl acetate. Scale bars are 0.2, 0.2 and 0.5 µm from left to right. Left and right: 20 mg mL^{-1} HEWL aggregated in the absence of salt. Centre: 10 mg mL^{-1} HEWL aggregated in the absence of salt. Examples of some of the different species present are highlighted: *a)* small aggregate species, with some elongated appearance, *b)* curvilinear filaments, *c)* twisted ribbons consisting of a number of laterally associated filaments and *d)* larger species that may be nanotubes.

Transmission electron microscopy was used to investigate the effect of salt on the fibrils formed at 90°C and low pH (pH 1.6-2). Imaging revealed small aggregate species (see *a)* in Figures 4.29 and 4.30), some with elongated appearance, alongside individual filaments similar to those observed at low ionic strength elsewhere [89], curvilinear filaments similar to those observed at high salt (for examples at high salt see Figure 4.5, here similar species are shown

at *b)* in Figure 4.30), ribbons of varying widths (see *b)* in Figure 4.29 and *c)* in Figures 4.29 and 4.30) and after prolonged incubation at room temperature following 24 hours at 90°C, what may be nanotubes (see *d)* in Figure 4.29).

A range of filament structures was observed in each case: in the absence of salt, and at 20 and 300 mM NaCl. However, as salt concentration was increased, the ribbons were found to be on average both shorter and wider.

The apparent width of the straight filament species was found to range from 7(1) nm, having the appearance of the lateral association of two individual filaments, to $\sim$ 60 nm, the widest observed ribbons in regions of good staining. Ribbons were found to have periodic twists and a few very wide species appeared helical, consistent with the observations of Lara *et al.* for ribbons on the pathway to closure into nanotubes [253].

Chapter 5

Results: Fibril formation of HEWL in HFIP and fibril formation of reduced HEWL

5.1 Fluorinated alcohol

At high alcohol concentrations HEWL is known to undergo association into amyloid-like fibrils [254–261, 269]. The aggregation of HEWL at high ethanol concentration has been extensively studied [254–261], and fibril formation is thought to progress through dimer formation and association of dimers [256].

Fluorinated alcohols, such as TFE and HFIP, are known to strongly enhance aggregation propensity compared to non-fluorinated alcohols. This is thought to be a result of the tendency of these species to form dynamic clusters over certain concentration ranges that may induce extensive hydrophobic interactions between solvent and solute and further decrease equilibrium solubility [269]. To my knowledge, the growth mechanism of HEWL fibrils in the presence of fluorinated alcohols has not yet been fully investigated.

In the presence of HFIP, HEWL exhibits rapid growth with very little to no apparent lag phase prior to aggregation, as observed by enhanced fluorescence upon binding to ThT in Figure 5.1. Enhancement of fluorescence was on a similar order of magnitude to that observed at high salt. However, no further increase in fluorescence was observed at long times (before this is complicated by evaporation) that might indicate the presence of the pathway giving rise to

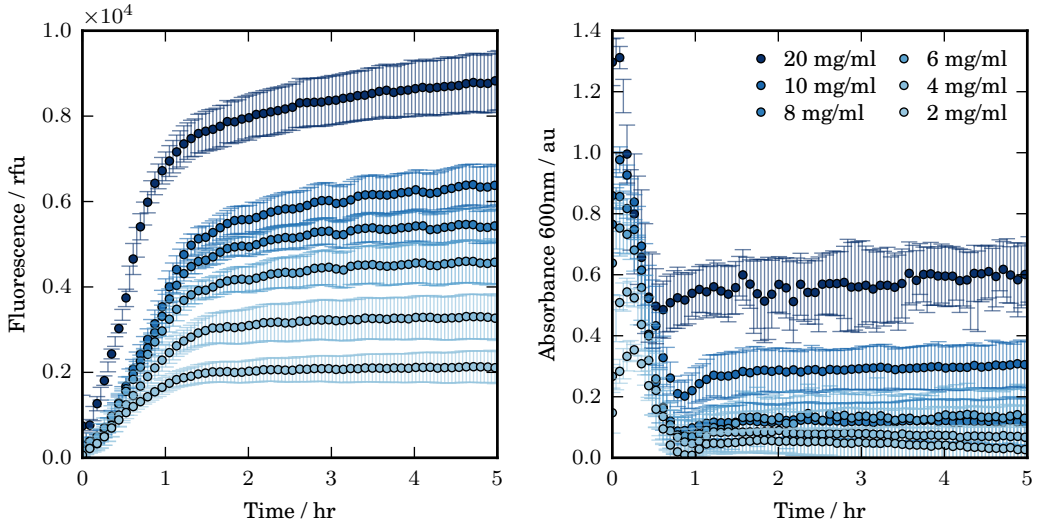

Figure 5.1: Thioflavin T fluorescence and simultaneous absorbance at 600 nm obtained during the aggregation of various HEWL concentrations in the presence of 5% HFIP at 35°C, pH 7.4 (20 mM potassium phosphate buffer) in quiescent conditions. Experiment performed in 96 well, flat bottomed, Corning NBS coated microplates. Legend applies to both graphs.

straight rigid fibrils, and suggesting that the fibril pathway observed at low ionic strength is inhibited by the presence of alcohol.

For 10 mg mL^{-1} HEWL incubated under quiescent conditions at 35°C and pH 7.4 (20 mM potassium phosphate buffer), increasing concentration of HFIP up to 5-7.5% was found to promote aggregate growth, with further increases in HFIP concentration inhibiting aggregation (Figure A.28).

In contrast to the fluorescence kinetics, absorbance readings were initially high and then observed to decrease, reaching a minimum before increasing slightly and finally reaching a plateau at approximately the same time as the fluorescence response, as seen in Figure 5.1. The reason for this result is unknown, although it could be a mixing effect because HFIP was added by multichannel pipette to wells with no mixing of solution prior to reading (due to the rapid nature of the growth), and no growth curve analysis of the absorbance kinetics has been performed.

Aliquots of sample removed immediately after the addition of HFIP to 10 mg mL^{-1} HEWL (at 35°C, pH 7,4) show a significant oligomer/small aggregate population at early times. As shown in Figure 5.2 (two left-most images), a large population of small, roughly spherical oligomer-like species with diameters of roughly 35(4) nm and short, curvilinear filaments with a ball-on-string appearance

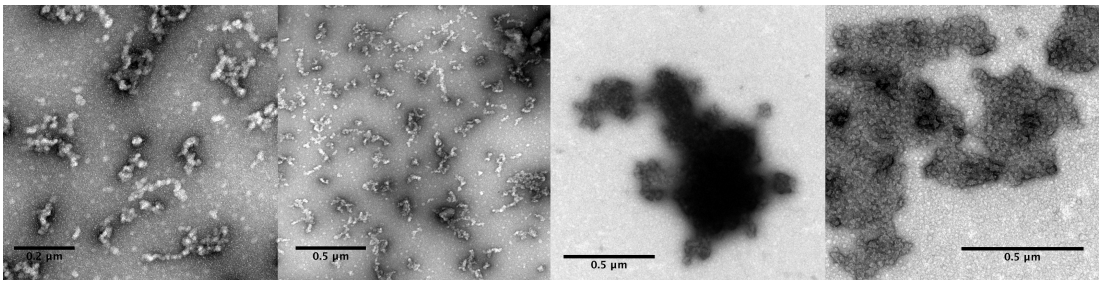

Figure 5.2: Transmission electron micrographs of 10 mg mL^{-1} HEWL aggregated in the presence of 5% HFIP at 35°C under quiescent conditions. Left two images taken from aliquots removed immediately after the addition of HFIP, right two images after 24 hours of incubation. Samples were diluted 20x immediately prior to grid application and stained with uranyl acetate. Scale bars are 0.2 µm (far left) and 0.5 µm.

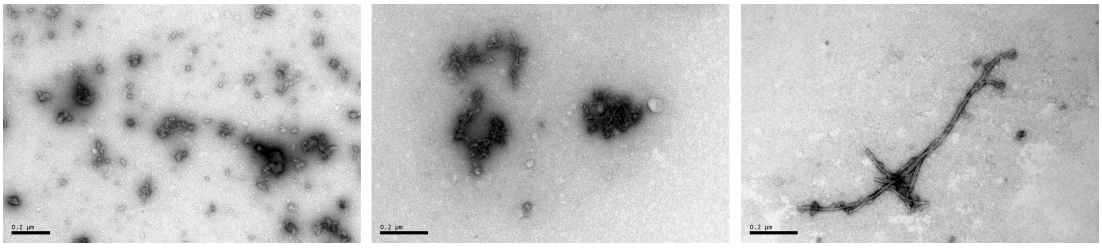

Figure 5.3: Transmission electron micrographs of 10 mg mL^{-1} HEWL aggregated in the presence of 5% HFIP at 35°C under quiescent conditions after 5 days incubation. Samples were diluted 20x immediately prior to grid application and stained with uranyl acetate. Scale bars 0.2 µm.

and width matching the diameters of the spherical species were observed.

At later times, smaller populations of the oligomer-like species are still observed, as shown in Figure 5.3 (left image, after 5 days of incubation). However, over time a larger proportion of these species appear to be converted into curvilinear filaments that tend to associate and become densely tangled, as seen in Figures 5.2 (two right-most images) and 5.3 (centre). These tangles become increasingly dense and hard to image by TEM as they attract more uranyl acetate. In addition, at long times a few straight and rigid fibrils were also observed (Figure 5.3 right).

The observation of curvilinear fibrils, a large oligomer population immediately after addition of HFIP and the correlation in width between this species and the initial small fibrillar species is similar to the observations made at high salt, and suggests a similar growth pathway.

5.1.1 The effect of protein concentration

Figure 5.4 shows the normalised growth curves corresponding to the kinetics that were shown in Figure 5.1, and it is clear that protein concentration has a weak effect on the rate or timescale of growth (for HEWL incubated in 5% HFIP at 35°C, pH 7.4 in quiescent conditions in Corning non-binding surface coated microplates).

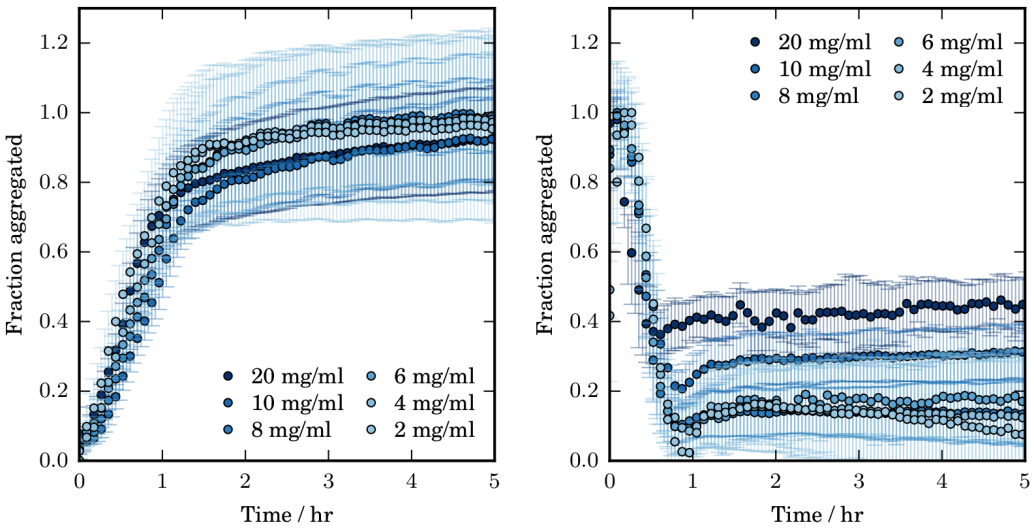

Figure 5.4: Normalised thioflavin T fluorescence and simultaneous absorbance at 600 nm obtained during the aggregation of various HEWL concentrations in the presence of 5% HFIP at 35°C, pH 7.4 (20 mM potassium phosphate buffer) in quiescent conditions. Experiment performed in 96 well, flat bottomed, Corning NBS coated microplates.

The fluorescence plateau approach was found to be slower than exponential, with a very slowly increasing intensity value after the turn-over point, suggesting that coagulation processes may occur at later times during the growth. At 10 mg mL^{-1} and above the turn-over point becomes more clearly a transition between two linear growth regions. While this is characteristic of the transition between monomer addition-dominated elongation and coagulation-dominated elongation in the JDP model, the solution of the JDP model does not account for such a quick change from the rapid initial growth to the very slow creep, and the analytical solution does not apply because a brief lag period is observed at early times.

Maximum fluorescence and maximum absorbance (at both the absorbance peak and after the decrease) were found to increase linearly with increasing

protein concentration, with absorbance having a slightly weaker concentration dependence (Figure A.29).

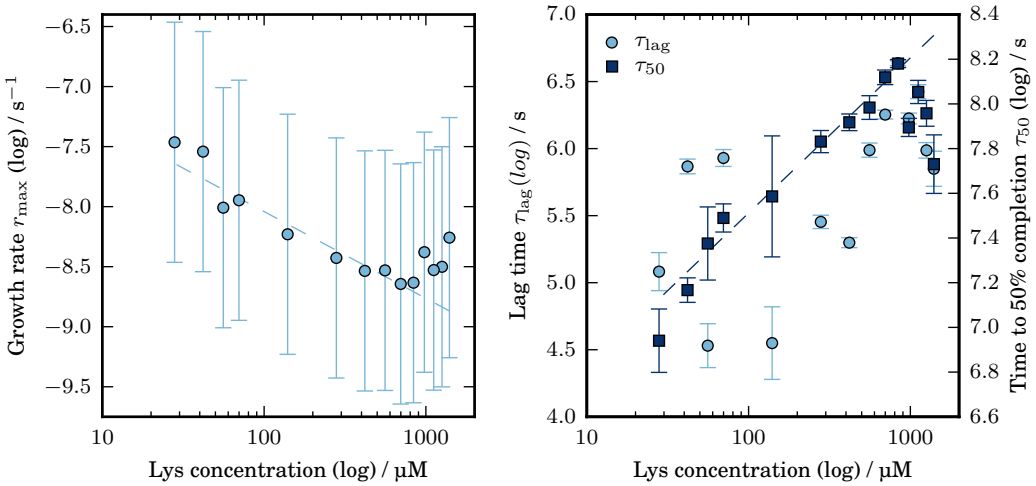

Figure 5.5: Growth rate and associated lag time and time to 50% completion obtained from the best fit tangent about the maximum growth rate for HEWL incubated at 5% HFIP, 35°C, pH 7.4 (20 mM potassium phosphate buffer) in quiescent conditions. 96 well, flat bottomed, NBS coated Corning microplates. Growth rate r_{max} and τ_{50} have concentration order dependence -0.31(4) and 0.30(2) up to 10 mg mL^{-1} and 0.5(3) and -0.6(3) above.

The growth rate and associated characteristic times obtained from the best tangent fit to the maximum growth rate are shown in Figure 5.5. Growth rate was found to initially decrease with increasing concentration while the time to 50% completion, τ_{50}, initially increased with concentration, with order 0.30(2). Above 10 mg mL^{-1} this trend was reversed, growth rate increased with concentration, with order dependence 0.5(3), and τ_{50} decreases with concentration, with order -0.6(3).

It would appear therefore that increasing protein concentration initially inhibits the rate of growth of the aggregate population. This may be the result of selecting a HFIP concentration found to promote aggregation most strongly at 10 mg mL^{-1}, since the HFIP-HEWL interaction may be dependent upon the HFIP:HEWL ratio. Above 10 mg mL^{-1} the concentration dependence suggests fragmentation may be a dominant growth process during the rapid stage of the growth.

The observation of curvilinear and oligomeric species and a similar fluorescence intensity response suggest that growth in the presence of HFIP may progress through a similar pathway to growth at high salt. It would appear that

oligomers are first formed and join together to form bead-on-string like curvilinear filaments that may undergo further conformational change involving an increase in β-sheet content. The evidence for fragmentation at high concentrations and for slow continuous growth, possibly coagulation processes, at later times and with increasing protein concentration is also similar to the growth proposed here for aggregation at high salt.

5.1.2 Surface activity

The effect of the surface area to volume ratio (SA:vol) at 5 mg mL^{-1} HEWL in the presence of 5% HFIP at 35°C, pH 7.4 (20 mM potassium phosphate buffer) was investigated in quiescent conditions by varying well volume in 96-well and 384-well plates of the same surface type. SA:vol ratios were calculated using average well geometries. Similar curve shapes were obtained at each volume. Aggregation was also promoted in the 96-well microplates relative to the 384 well microplates, as seen in Figure 5.6.

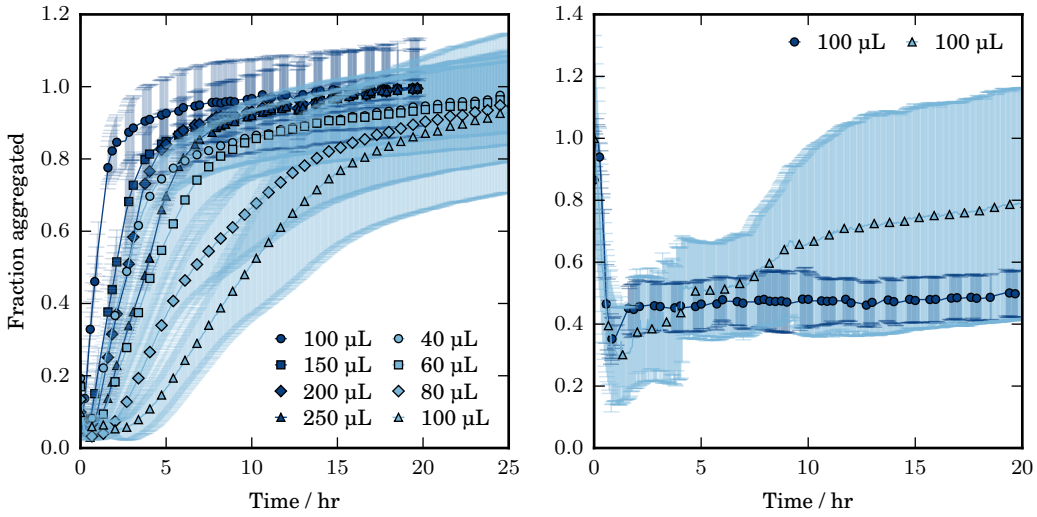

Figure 5.6: Normalised thioflavin T fluorescence and simultaneous absorbance at 600 nm obtained during the aggregation of various volumes of 5 mg mL^{-1} HEWL in the presence of 5% HFIP at 35°C, pH 7.4 (20 mM potassium phosphate buffer) in quiescent conditions. Corning NBS coated microplates, 96 well (dark blue) or 384 well (pale blue).

The maximum fluorescence reading was found to decrease with increasing SA:vol ratio while maximum absorbance was relatively unaffected (Figure A.32) The growth rates and associated lag times obtained are shown in Figure 5.7.

Aggregation was promoted by increasing SA:vol ratio, as seen by the increasing growth rates and decreasing characteristic times. Growth rates were higher in the 96-well plates, suggesting the air-water interface more strongly promotes aggregation than the wall:water interfaces.

The same protein concentration experiments, as described in the previous section, were performed in uncoated, hydrophobic polystyrene Greiner microplates. Similar growth curves were obtained (not shown) and the maximum fluorescence and maximum absorbance (at the absorbance peak) were found to increase with increasing protein concentration with similar concentration dependence. However, in contrast to the results obtained in the Corning microplates, both the growth rate and time to 50% completion were found to be HEWL concentration independent from 2-15 mg mL^{-1} HEWL (no lag time could be estimated, Figure A.30). In addition, the maximum absorbance value obtained after the dip in absorbance was found to be roughly concentration independent at 4 mg mL^{-1} and above (Figure A.31).

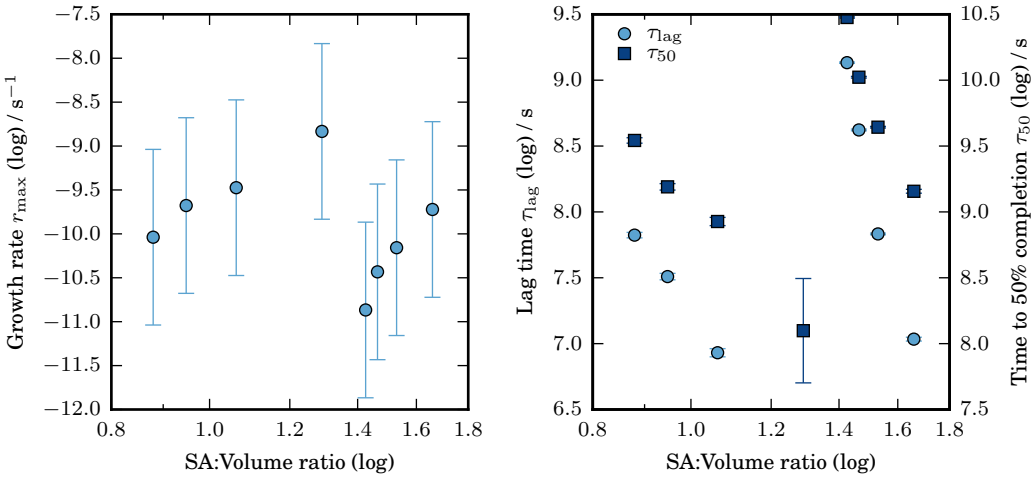

Figure 5.7: Growth rate and associated lag time and time to 50% completion obtained from the best fit tangent about the maximum growth rate for aggregation of 5 mg mL^{-1} HEWL incubated at 5% HFIP, 35°C, pH 7.4 (20 mM potassium phosphate buffer) in quiescent conditions at various volumes in either 96 well or 384 well, flat bottomed, NBS coated Corning microplates.

The SA:vol ratio dependence of the growth parameters obtained in uncoated Greiner microplates (Figure A.33) was equivalent to that found in the NBS coated Corning microplates. However, in the presence of the hydrophobic surface the growth rates were typically faster and characteristic times were shorter.

Hydrophobic surfaces are clearly very important in promoting aggregation in

this system, with increased surface area and increasingly hydrophobic surfaces (air:water interface, uncoated polystyrene) promoting aggregation. A similar result was found for aggregation at high salt, although the effect of SA:vol ratio on growth parameters was different (growth rate decreased with increasing SA:vol ratio) and 384-well plates were found to promote aggregation over the 96-well microplates. This suggests that although the growth mechanism may be similar the driving forces for aggregation are not, and the relative dominance of different mechanisms involved in the growth process may also be expected to differ.

5.1.3 The effect of seeding

The effect of seeding with fibrils formed at 5% HFIP is shown in Figure 5.8. The growth curves obtained match those formed in the absence of seed. Other than the odd result at 20% seed, where the fluorescence intensity is lower, the maximum fluorescence and absorbance values were relatively unaffected by increasing seed concentrations. The maximum growth rate was found to be independent of seed concentration, while the time to 50% completion obtained by fluorescence was found to decrease with increasing seed but with weak seed concentration dependence.

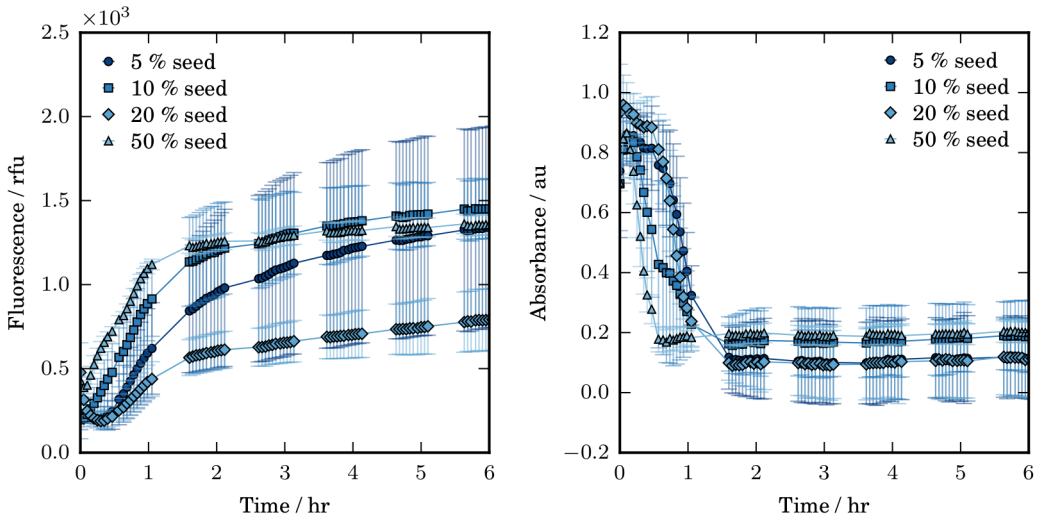

Figure 5.8: Thioflavin T fluorescence (left) and absorbance at 600 nm (right) obtained for 5 mg mL^{-1} HEWL incubated in 5% HFIP at 35°C, pH 7.4 (20 mM potassium phosphate buffer) in quiescent conditions with various seed concentrations. Seed formed under identical growth conditions.

The relatively weak effect of seed addition suggests that elongation processes dominate the growth under these conditions, consistent with the very short apparent lag time. These results are again similar to those made for HEWL aggregation at high salt, high temperature and low pH.

5.2 Reduced HEWL

Reduced HEWL has been shown to form fibrils under approximately the same conditions as the non-reduced form [270, 272, 273], but also at neutral pH where the disruption of the disulphide bonds of HEWL by dithiothreitol (DTT) is thought to be a prerequisite for fibril formation on heating in the absence of other denaturants [272]. Long straight fibrils were observed after heating of reduced HEWL to 85°C and subsequent cooling to room temperature at pH 7, and shared features of the species formed along the low-ionic strength pathway, as described in Section 3.4. If reduced HEWL is capable of forming equivalent aggregates to non-reduced HEWL it may also be possible to obtain curvilinear fibrils under alternative conditions. The aggregation of reduced HEWL at lower temperatures has been subject to examination in this section.

HEWL was incubated at 30°C in the presence of 20 mM DTT at pH 7.4 (20 mM potassium phosphate buffer) and in quiescent conditions. Aggregation was found to be rapid, with a very short lag phase and aggregates were found to bind ThT. Enhancement of fluorescence was a similar order of magnitude to that obtained at high salt and no further increases in fluorescence were observed (that would suggest the formation of rigid fibrils) for aggregation at up to 60°C on the experimental timescales (approximately 24 hours), even with agitation by microplate shaking.

Aggregation was promoted by increasing temperature, with increasing growth rates and decreasing time to 50% completion (approximately 15 minutes at 60°C). In addition, at 60°C fluorescence was found to increase to an initial peak, followed by a small dip before eventually reaching the peak level again at a later time ($\sim$ 5 hours).

The growth kinetics for various HEWL concentrations incubated at 30°C, 20 mM DTT, pH 7.4 in quiescent conditions, are shown in Figures 5.9 and 5.10. The growth curves share a number of similar features with those obtained for varying

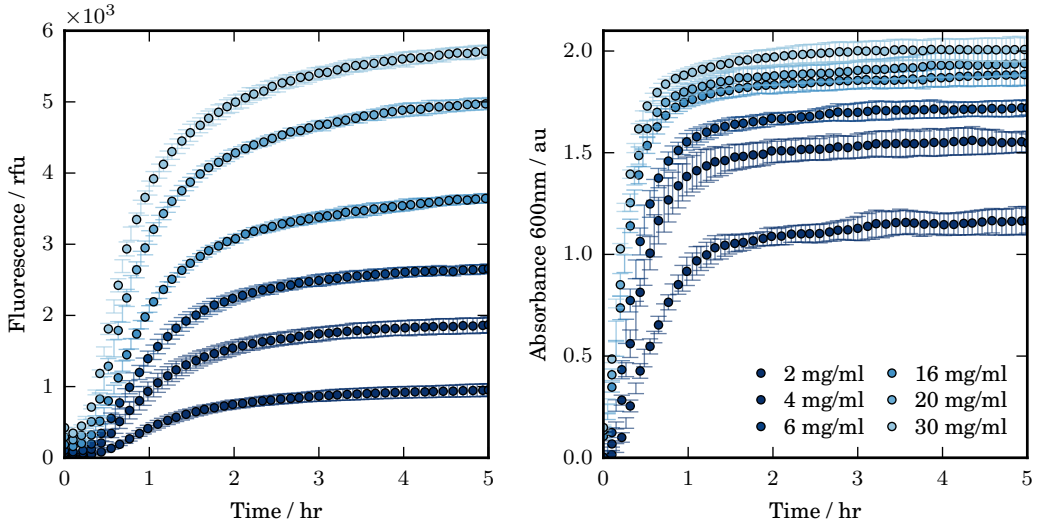

Figure 5.9: Thioflavin T fluorescence and simultaneous absorbance at 600 nm obtained for various HEWL concentrations incubated at 30°C, pH 7.4 (20 mM potassium phosphate buffer), in the presence of 20 mM DTT. Legend applies to both graphs.

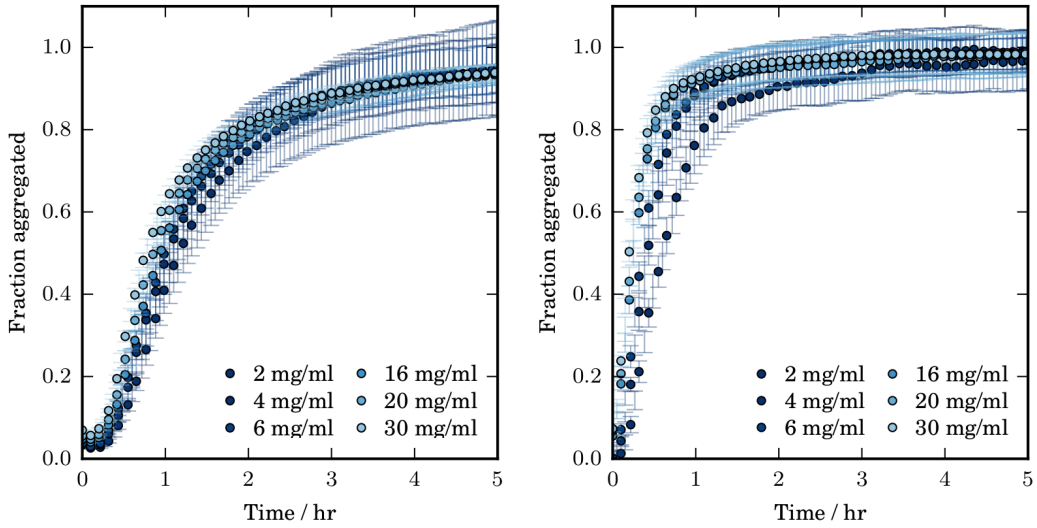

Figure 5.10: Thioflavin T fluorescence and simultaneous absorbance at 600 nm obtained for various HEWL concentrations incubated at 30°C, pH 7.4 (20 mM potassium phosphate buffer), in the presence of 20 mM DTT. Data has been normalised to the maximum value for each growth curve.

protein concentrations in the presence of HFIP, in particular the weak effect of increasing protein concentration on any characteristics apart from total intensity, as is clear in the normalised data shown in Figure 5.10.

It would appear then that the aggregation of reduced HEWL at pH 7.4 and

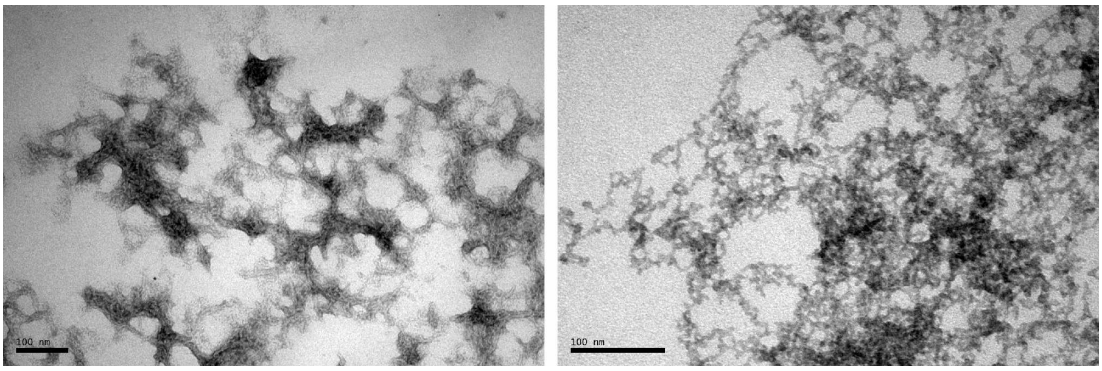

Figure 5.11: Transmission electron micrograph of 10 mg mL^{-1} reduced HEWL incubated in 20 mM DTT at 30°C, pH 7.4 (20 mM potassium phosphate buffer) for 24hrs. Sample diluted 20x immediately before grid application. Stained with uranyl acetate. Scale bars are 100 nm.

temperatures ≤60°C may progress along the same aggregation pathway observed at high salt or in the presence of HFIP. Indeed, TEM images appear to show tangles of curvilinear or worm-like filaments, as seen in Figure 5.11. However, bundling makes obtaining clear images very difficult.

As observed at high ionic strength, absorbance was found to increase and reach a plateau earlier than the growth curves obtained by fluorescence. Maximum fluorescence and absorbance values also had a similar protein concentration dependence, with the maximum intensity exponentially increasing with concentration (initially $\sim m_{\mathrm{tot}}^{1.49(8)}$) but becoming more weakly concentration dependent at higher concentrations (see Figure A.34 and the similar high salt result in Figure A.7).

The initial increase in fluorescence or absorbance (up to $\sim 20\%$) was found to be slightly more rapid than exponential, with a single exponential providing a better fit at 10 mg mL^{-1} and above. This result strongly signifies the importance of secondary processes at early times during the growth. However, analysis of the early absorbance region is complicated by the small number of data points and is less reliable than analysis for the plateau approach.

The plateau approach was found to be roughly exponential below 8 mg mL^{-1} for fluorescence, while the absorbance data were found to be slightly slower but within standard deviation of a single exponential at all concentrations. At 8 mg mL^{-1} and above the fluorescence plateau approach was notably slower than exponential with an increasingly slow and continuous increase in fluorescence rather than a flat plateau at later times.

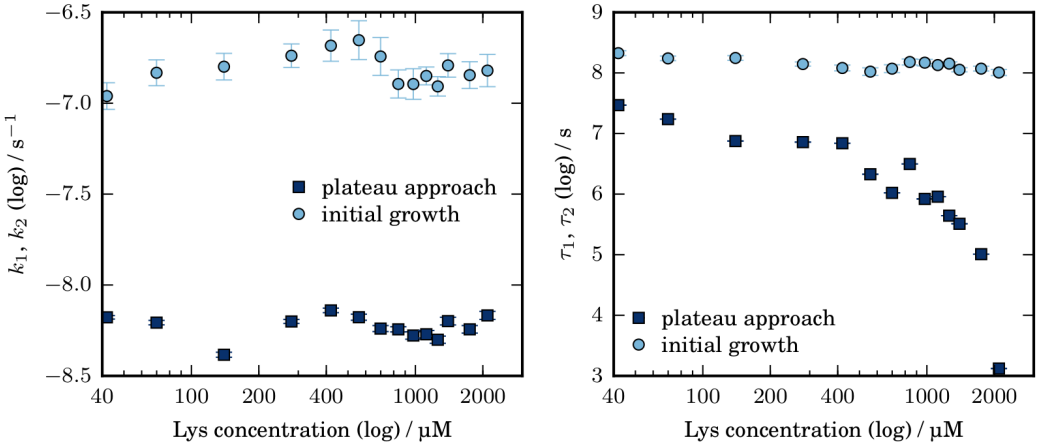

Figure 5.12: Fluorescence data. Apparent growth rates and associated characteristic times obtained from exponential fits to the initial period of growth and the final plateau approach for Thioflavin T fluorescence kinetics of HEWL incubated at 20 mM DTT, 30°C, pH 7.4. Up to 8 mg mL^{-1} (560 µM) the initial growth has growth rate k_1 concentration order 0.11(1) and characteristic time τ_1 concentration order of -0.11(1).

These exponential or slower plateau approaches suggest that the secondary process apparently dominant at early times is replaced by an alternative rate limiting process at later times (after the inflection point). Both monomer (or oligomer) addition and coagulation processes give rise to this behaviour, and the slower-than-exponential plateau approach at higher protein concentration suggests a stronger importance of coagulation processes at high concentrations.

The combination of the very rapid initial increase in intensity and a much slower plateau approach cannot sufficiently be accounted for by any of the available analytical model solutions and is most compatible with the predictions of the JDP model. However, the JDP analytical solution does not apply in this case because a short lag period is observed before fluorescence increases (although the fluorescence at this point is non-zero), as seen in Figure 5.10. As a result, parameters have been estimated using simpler methods.

The parameters obtained from the fits of the initial increase in fluorescence to the exponential $M(t) \sim \exp(k_1(t - \tau_1))$ and the plateau approach to the exponential $M(t) \sim M(\infty) - \exp(-k_2(t - \tau_2))$ are shown in Figures 5.12 and 5.13 for fluorescence and absorbance respectively.

A clear discontinuity in growth rate at early times (initial growth) is seen by both fluorescence and absorbance around 10 mg mL^{-1} (700 µM). Above this the growth rate and characteristic time were found to be roughly

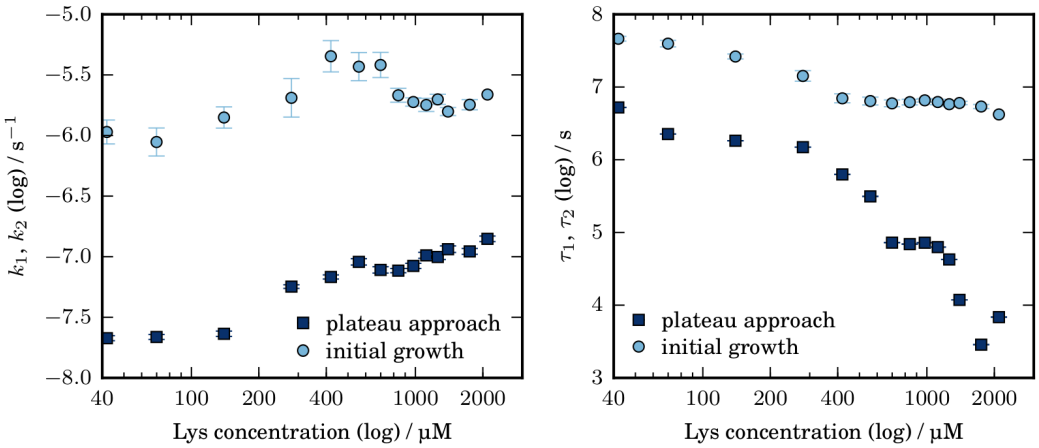

Figure 5.13: Absorbance data. Apparent growth rates and associated characteristic times obtained from exponential fits to the initial period of growth and the final plateau approach for absorbance at 600 nm kinetics of HEWL incubated at 20 mM DTT, 30°C, pH 7.4. At 4 mg mL^{-1} (280 µM) and above the plateau approach has growth rate concentration order dependence 0.17(2). The initial growth rate initially increases with concentration order 0.27(7) and experiences a corresponding decrease in characteristic time τ_1 with order-0.34(5).

independent of protein concentration. Below this, growth rate increases with concentration and the characteristic time decreases, with absorbance data exhibiting higher concentration dependence than the fluorescence response. However, the concentration dependence was weak (less than 0.5 as described in Figures 5.12 and 5.13).

The concentration independence of both parameters (k_1 and τ_1) at high concentrations suggests that a conformational change during nucleation, for example monomer-activation, is rate limiting at early times and high protein concentrations. This concentration independent process may also be contributing to the weak concentration dependence below 10 mg mL^{-1}.

The apparent growth rate k_2 of the plateau approach by fluorescence was found to vary weakly with concentration (Figure 5.12) while the growth rate by absorbance is initially concentration independent (up to 2 mg mL^{-1}, 140 µM) and then increases with increasing concentration (Figure 5.13).

The characteristic time of the plateau approach, τ_2, obtained by both fluorescence and absorbance was found to decrease with increasing concentration. The concentration dependence of τ_2 is initially very weak and increases around 6 mg mL^{-1} (420 µM). Estimates are unreliable because of the discontinuity around 800 µM, however, the concentration order is stronger than $\tau_2 \propto [HEWL]^{-1}$.

Additionally, the relative concentration independence of the growth rate suggests that a conformational change is rate limiting during elongation as well as prior to aggregation.

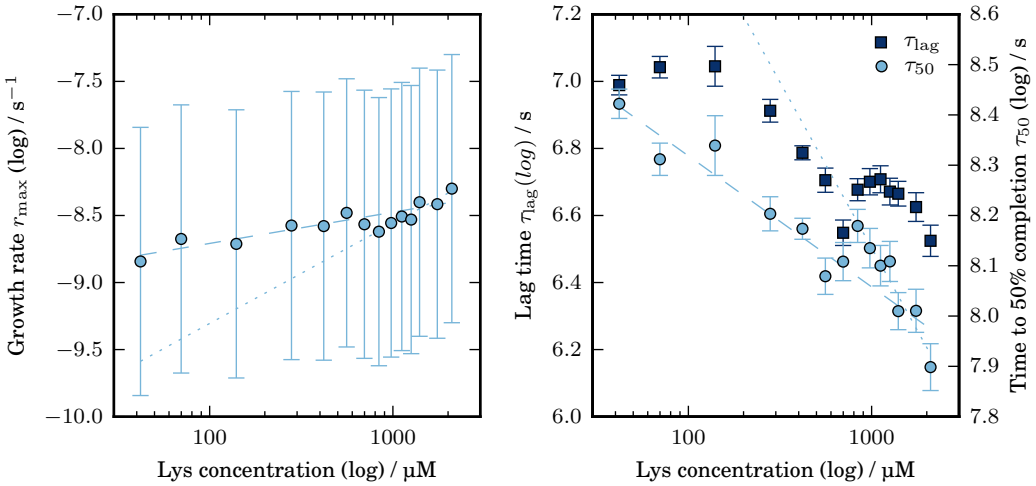

Figure 5.14: Fluorescence data. Maximum growth rates and associated characteristic times obtained from the best fit tangent to the maximum growth rate for thioflavin T fluorescence kinetics of HEWL incubated at 20 mM DTT, 30°C, pH 7.4. Growth rate initially has concentration order dependence 0.10(2) (dashed line) and above 12.5 mg mL^{-1} (870 µM) has order 0.32(5) (dotted line), over the same concentration regions τ_{50} has concentration order -0.11(2) (dashed line) and -0.29(4) (dotted line).

In addition, the growth rates and associated characteristic times obtained from the best fit tangent to the maximum growth rate are shown in Figures 5.14 and 5.15 for fluorescence and absorbance respectively. As with the parameters obtained from the exponential fits for initial growth and plateau approach, all concentration dependencies were weak, with concentration order weaker than ±0.5. As above, absorbance parameters were found to have a stronger concentration dependence. The growth rate, r_{max}, and time to 50% completion, τ_{50}, were also found to have stronger concentration dependence than the apparent growth rate and characteristic times shown above. This is similar to the observation made about the behaviour at high salt, where parameters determined from the maximum growth rate were thought to be a composite of the dominant growth processes on either side of the inflection point.

The growth rates and characteristic times obtained from absorbance measurements are faster and shorter respectively than those obtained by fluorescence at all concentrations. Indeed, the absorbance readings approximately reach a

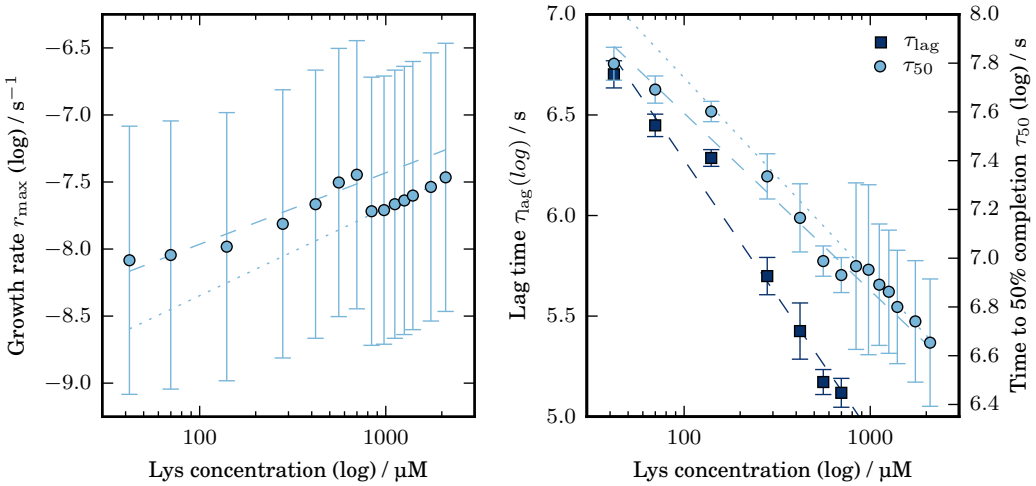

Figure 5.15: Absorbance data. Maximum growth rates and associated characteristic times obtained from the best fit tangent to the maximum growth rate for absorbance (600 nm) kinetics of HEWL incubated at 20 mM DTT, 30°C, pH 7.4. Growth rate initially has concentration order dependence $\sim 0.23(3)$ (dashed line) and above 12.5 mg mL^{-1} (870 µM) has order 0.28(2) (dotted line), over the same concentration regions τ_{50} has concentration order -0.32(3) (dashed line) and -0.35(2) (dotted line). The lag time concentration dependence is stronger, -0.59(4), but lag times were not obtained at all concentrations.

plateau as the fluorescence readings reach the inflection point. This result was previously attributed to the population of a non-ThT-binding small aggregate species at early times, and may also be the case here given the other similarities with the pathway observed at high salt, namely the appearance of the filaments by TEM, the weak ThT fluorescence enhancement and evidence for the importance of a conformational change during elongation. Additionally, there is evidence for increased coagulation at high protein concentrations and long times, and this was also observed in the presence of HFIP where the pathway is also thought to be similar to the oligomeric growth at high ionic strength. A similar aggregation pathway may be active in the aggregation of reduced HEWL under these conditions.

However, under these conditions there is also evidence for a structural change occurring at early times and rate limiting during the formation of new aggregate species. This may be the result of the altered structure of the denatured form of HEWL, such that the reduction process or an additional conformation change is required in the reduced species before it becomes aggregation competent. If the fibrils formed under these conditions form via monomer addition rather

than oligomer addition, the structural change that appears to dominate during elongation may be the same or a very similar monomer-activation process.

5.2.1 The effect of seeding

The effect of seeding with preformed fibrils, formed under the same growth conditions, is shown in Figure 5.16. The addition of seed resulted in a rapid increase in initial fluorescence or absorbance intensity, followed by a short lag in fluorescence and slow growth by absorbance before the growth rate increases again. This final growth phase has the same form as the growth curves obtained in the absence of seed.

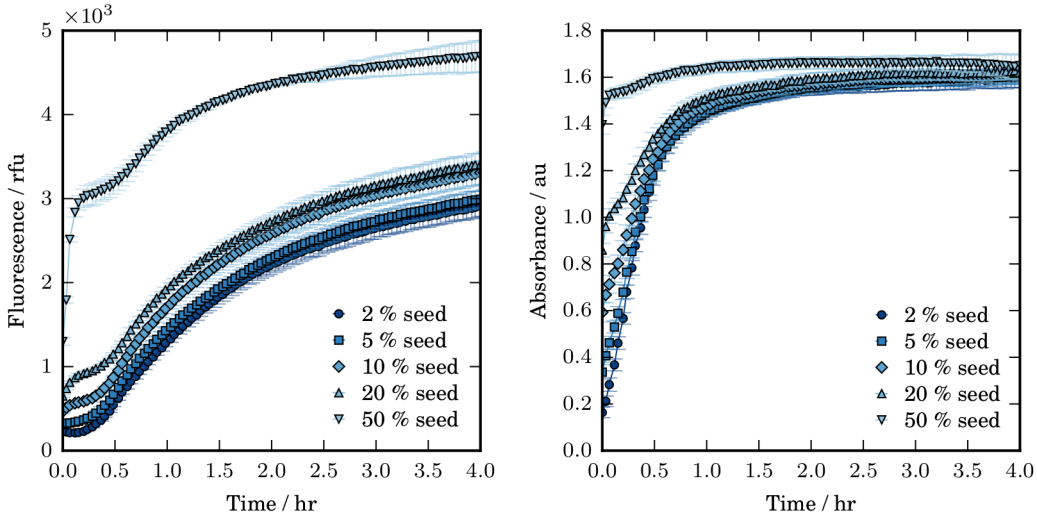

Figure 5.16: Thioflavin T fluorescence (left) and absorbance at 600 nm (right) obtained for the aggregation of 10 mg mL^{-1} HEWL incubated at 20 mM DTT, pH 7.4 (20 mM potassium phosphate buffer), 35°C with various concentrations of preformed seed. Seed formed under the same conditions.

The initial and maximum values of both fluorescence and absorbance were found to increase with seed concentration and were significantly higher for samples of 50% seed (Figure A.35). However, absorbance was found to increase less rapidly than fluorescence intensity. The growth rates and characteristic times obtained for the seeded kinetics are shown in Figure 5.17. These parameters are estimated from the latter growth region that is similar to the growth in the absence of seed, and could not be estimated for 50% seed because this region is too small. The growth rate obtained by fluorescence was found to be roughly

seed concentration independent, while the growth rate by absorbance decreases slightly. The characteristic times were found to decrease with increasing seed concentration but were only weakly seed concentration dependent.

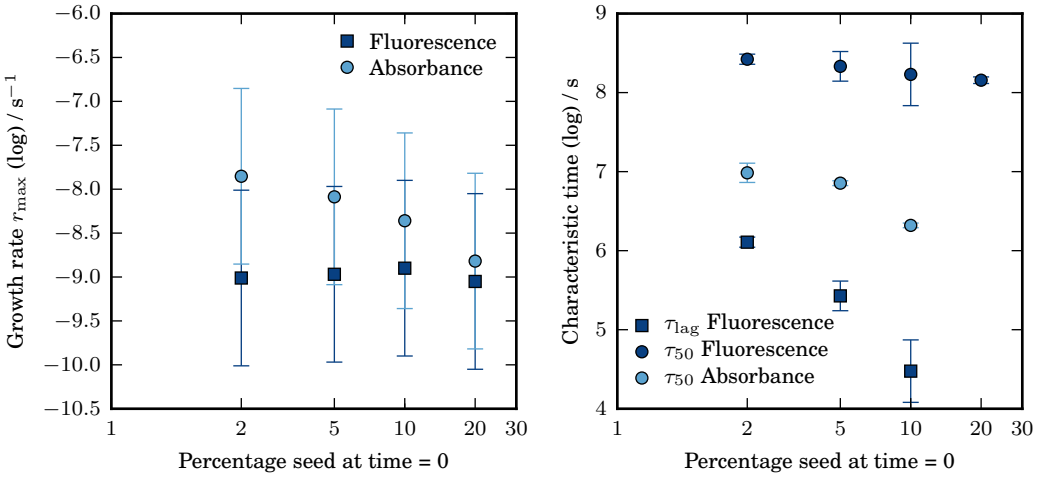

Figure 5.17: Growth rate and associated characteristic times obtained from the best fit tangent to the maximum growth rate for the aggregation of 10 mg mL^{-1} HEWL incubated at 20 mM DTT, pH 7.4 (20 mM potassium phosphate buffer), 35°C with various concentrations of preformed seed. Seed formed under the same conditions.

The weak seed concentration dependence strongly suggests that elongation processes dominate the kinetic growth in this system, consistent with a rate limiting conformational change during elongation as discussed in the previous section. The delay before the increase in fluorescence after the addition of seed is also similar to the observations made during seeding at high salt, high temperature and low pH conditions in Section 4.3.4, and indicates that growth cannot proceed immediately from the seed species. In this case this may be the result of an additional conformational change (which may be the reduction process) rather than a dissociation effect due to heating, and is consistent with a rate limiting monomer-activation process as proposed above.

Chapter 6

Discussion: Fibril formation of HEWL

The aggregation of HEWL, an extensively studied model globular protein, has been investigated here under a range of solution and environmental conditions to determine how much can be inferred about the growth mechanisms that result in the formation of different polymorphs of amyloid-like fibrils by growth curve analysis, whether similar polymorphs result from similar growth mechanisms and whether the possibly competing growth pathways at high temperature and low pH complicate the analysis of growth kinetics under these conditions.

6.1 High temperature and low pH

At high temperature, low pH and low ionic strength conditions HEWL assembles into straight, rigid amyloid-like fibrils [242–244, 247, 251–253, 258]. The kinetics of this growth have previously been observed as sigmoidal-like, with an extended lag phase [88, 89, 242–244, 251] during which only monomeric species are observed [89, 242]. Hill *et al.* [88, 89] proposed a mechanism for growth under these conditions in which nucleation occurs from denatured HEWL, nuclei extend by monomer addition of denatured HEWL and these filaments laterally associate at later times to form rope-like fibrils [88, 89], as shown in Figure 3.5.

At higher salt concentrations an alternative fibrillar pathway that results in curvilinear or worm-like fibrils [1, 2, 88, 89] appears to progress through the formation of non-ThT-binding oligomers, and oligomer coalescence into

linear, bead-on-string filaments that mature into curvilinear fibrils with higher ThT affinity, presumably via conformational rearrangement to a more β-rich arrangement [1, 2, 88, 89], as shown in Figure 3.6.

The curvilinear fibrils were shown to be a kinetically stable species, metastable against the growth of the rigid fibril species, and the two species were found to exhibit distinct structural fingerprints [88]. The two fibrillar species therefore appear to have distinct structures and to be capable of competing for monomer.

The results obtained here confirm the presence of both HEWL polymorphs at high temperature and low pH. Evidence for the coexistence and competition of these species was found in the kinetic growth curves over a range of salt and protein concentration and agitation conditions. In particular, multiple growth phases were observed by *in situ* ThT fluorescence intensity and absorbance at 600 nm for a range of salt and protein concentrations both under agitation (Figures 4.1, 4.2 and 4.3, and Figures 4.19 and 4.21) and in quiescent conditions (Figure 4.6). Additionally, the high variability in end point fluorescence intensity observed for HEWL aggregation hints at the presence of a competing species [227], and high variability was observed at high temperature and low pH even where multiple growth phases were not observable in fluorescence kinetics.

An initial period of fluorescence increase (region A) was observed to plateau at a low fluorescence intensity compared to the following, much more dramatic, period of growth (region B), and is attributed to the growth of curvilinear filaments (region A) prior to the growth of rigid fibrils (region B) under certain growth conditions (>0.35 M NaCl for 10 mg mL^{-1} HEWL incubated at pH 1.6, 65°C with agitation). An additional, earlier, growth phase was observed by absorbance at 600nm (region 1 as seen in Figure 4.3). This is attributed to the growth of oligomer species and early 'bead-on-string' species prior to the formation of curvilinear filaments, since the observation of this growth period by absorbance only is consistent with previous observations about the low β-sheet content and lack of ThT binding affinity of early oligomeric and bead-on-string curvilinear filament species [2, 89].

Despite choosing conditions designed to favour either the rigid fibril growth (low ionic strength and agitation) or the curvilinear growth (high salt and quiescent conditions), the two distinct aggregate pathways were coexistent and in competition for monomer. At high salt (1 M NaCl), in the absence of

agitation, further increases in fluorescence at late times were associated with the formation of rigid fibril species, and were observed after a long period of metastability following the formation of curvilinear filaments (Figure 4.6). Under these conditions, the growth kinetics obtained for the curvilinear fibril growth are not considered to be complicated by competition with the rigid fibril species and the lag times for the formation of the two species were separated by at least 10 hours.

At low ionic strength (0.2 M NaCl) the contribution of the curvilinear species to the fluorescence response is not immediately obvious, since the lag time for the growth of rigid species is shorter than the lag time for the growth of the curvilinear species. However, clear evidence of the curvilinear species was apparent by comparison of fluorescence and absorbance growth curves and parameters (Section 4.4), and highlights the importance of incorporating more than a single experimental technique.

The conditions favouring rigid fibril growth were limited to the region in which reproducible growth kinetics could be obtained by ThT fluorescence microplate assay, and it is not possible to directly compare these with the results of Miti *et al.* that were obtained under quiescent conditions and at different pH and temperature conditions [1, 2, 88, 89]. It is possible that kinetics for the rigid fibrillar species that are not complicated by competition with the curvilinear species might be obtained under different conditions to those used here.

Although the incubation conditions here differ from those of Miti *et al.* [1, 2, 88, 89], the results are roughly consistent with their observations about the two distinct aggregate species, their competition and salt concentration dependence. However, the species were not found to occupy well defined regions of a phase diagram. Instead, a significant overlap of the two species is clear under all incubation conditions. Additionally, since the rigid filament species are eventually found as the thermodynamically stable and major species after long times of incubation even under conditions that initially favour the curvilinear species, calling Figure 3.2 a phase diagram may be misleading.

The apparent phase transition between the oligomers/curvilinear filaments and the rigid fibrils that is demonstrated in Figure 3.2 is described as the critical concentration below which the formation of curvilinear filaments is separated from the onset of oligomer formation by a lag phase, and rigid fibrils are observed to

form rather than curvilinear filaments [1, 2]. This was determined to be at 0.2 M NaCl for 0.7 mM HEWL at pH 2 and 52°C in quiescent conditions [1, 2]. This critical point for curvilinear filament formation (where the lag time for oligomer and curvilinear filaments are approximately equal) does appear to coincide with the critical point where the lag time for the curvilinear species and the lag time for rigid filament growth are approximately equal for the experiments performed under agitation, and occurs here at around 0.3-0.35 M NaCl for 0.7 mM HEWL at pH 1.6 and 65°C under agitation. However, in contrast to the results of Miti *et al.* [1, 2], evidence for both species is found at either side of this critical point, and the rigid fibrils are the major species on both sides of the critical point.

As observed by Miti *et al.* [1, 2, 88, 89], increasing salt concentration was found to favour curvilinear filament growth. However, increasing salt concentration also promotes the rigid fibril growth, reducing the lag period before the observation of the rigid fibril species. At both high and low ionic strength the pH and temperature stability was found to be consistent with previous literature results [244, 247, 251, 258]. However, agitation was found to strongly promote the rigid fibril pathway, dramatically reducing the lag time for the formation of rigid fibrils even at high salt conditions. The effect of agitation has not been previously given much attention, not least because it is difficult to determine whether the enhancement of aggregation is due to increased destabilisation of the native structure by adsorption at hydrophobic surfaces, interaction of native with destabilised HEWL or because of an increase in fragmentation [260, 276, 277].

HEWL is known to adsorb onto hydrophobic surfaces [278], and inactivation of HEWL enzymatic activity has previously been found to be proportional to the area of glass-liquid, air-liquid and PTFE-liquid interfaces, with PTFE and air found to be the most efficient in promoting inactivation because of their hydrophobicity [277]. The microplate surface type was found here to have a notable effect on aggregation propensity. The curvilinear growth at high salt concentration was found to be promoted by hydrophobic surfaces, and the apparent inhibition of the rigid fibril pathway in the presence of hydrophobic surfaces is thought to be a result of the promotion of the competing curvilinear pathway (Section 4.4.2).

6.1.1 Mechanism of formation of curvilinear filaments

In the proposed aggregation pathway at high salt, oligomers are first formed from the monomeric solution and are thought to undergo conformational change [1]. The oligomers then appear to coalesce to form curvilinear filaments with a bead-on-string appearance that are thought to undergo further conformational change, including an increase in β-content, to form the mature species [1, 2, 88, 89].

The particle size distribution by DLS at high salt was previously found to be dominated by increases in peak area rather than increases in hydrodynamic radii at early times during the aggregation, suggesting that changes in the particle size distribution are dominated by the nucleation of new aggregates and/or that particle sizes are limited by fragmentation [2, 89].

Consistent with the observations of Hill *et al.* [1, 2, 88, 89], small spherical oligomeric species were observed at early times followed by curvilinear filaments. The experiments here were performed at pH 2 and at higher temperature and ionic strength than investigated previously (60°C and 1 M NaCl). The aggregates formed under these conditions do not appear to have the form of the precipitates observed by Miti *et al.* [1] at very high salt, but appear to be curvilinear fibril species, as seen in Figure 4.5.

At high salt (1 M NaCl in quiescent conditions), growth of the curvilinear fibril species was very rapid and characterised by a short lag phase of $\sim$ 30 minutes. Growth curves obtained from both ThT fluorescence and absorbance at 600 nm were found to be approximately sigmoidal, with the form of a logistic function.

Growth parameters obtained for the curvilinear species over a range of protein concentrations were found to have concentration order dependence most consistent with fragmentation as a dominant growth mechanism. Parameter correlation was also consistent with the SDP model of secondary process dominated growth ($r_{\max} \propto \tau_{\text{lag}}^{-1}$). A reasonable fit was obtained for the SDP model of fragmentation dominated growth, and the large increases in peak area of the particle size distributions obtained by Hill *et al.* [2, 89] are therefore attributed to particle size being limited by fragmentation at early times.

Aggregation was promoted by increases in protein and salt concentration (increasing growth rate and decreasing lag times). However, growth rate was found to decrease in concentration dependence above 6 mg mL^{-1} HEWL (420 µM) at 1 M NaCl and above 0.7 M NaCl at 10 mg mL^{-1} HEWL. A discontinuity was

also observed in the lag time at this point, as seen in Figures 4.8, 4.11 and 4.12. This is consistent with rate limiting structural change during elongation, and is thought to correspond to conformation change as oligomers add to the curvilinear filaments. This may be related to the increase in β-sheet proposed by Hill *et al.* for the formation of curvilinear filaments from early species with beaded appearance [1, 2, 88, 89]. The proposed growth pathway is shown in Figure 6.1.

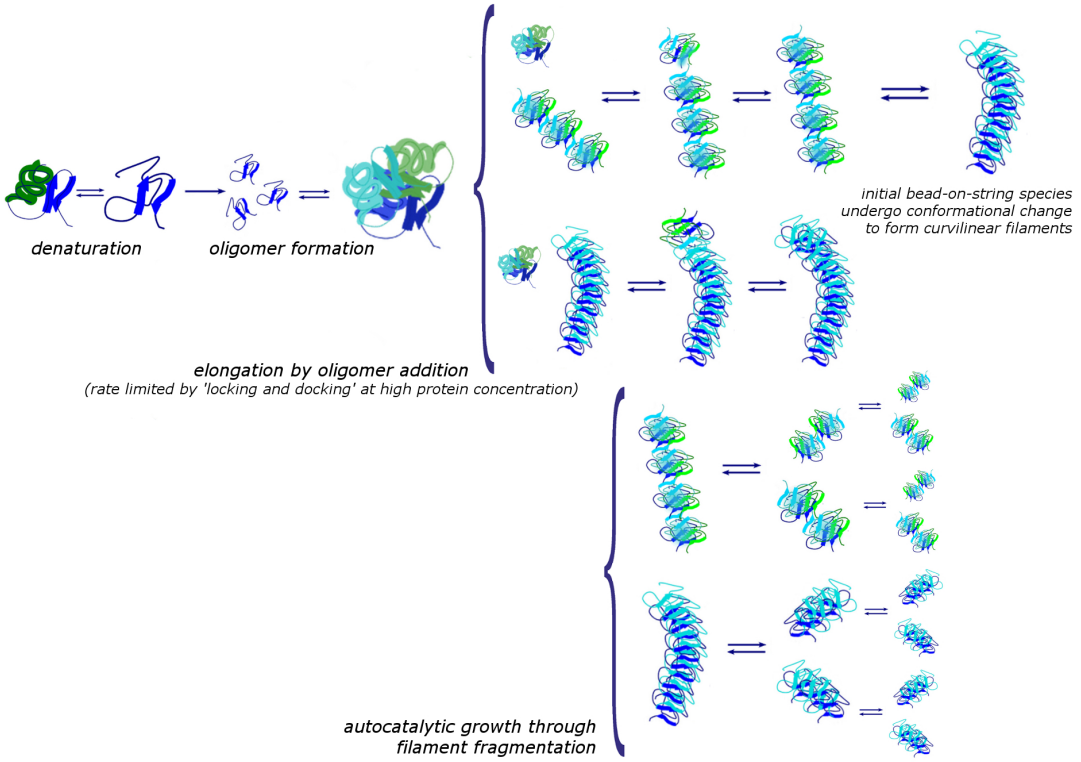

Figure 6.1: A cartoon depicting the proposed growth pathway of curvilinear fibrils of HEWL at low pH, high temperature and high ionic strength. Oligomers are formed from denatured HEWL, filaments are formed and extend by oligomer addition and early bead-on-string species undergo conformational conversion, including an increase in β-sheet content, to form the final curvilinear filaments. Fragmentation is the main dominant growth mechanism. At high concentrations, elongation by oligomer addition is limited by a 'locking and docking' type mechanism thought to involve conformational conversion to include more β-sheet stucture. It is not known whether the locking and docking mechanism and/or fragmentation are related to bead-on-string filaments and/or mature curvilinear filaments.

Seeding experiments were also performed in order to test the relative dominance of elongation and nucleation processes and to compare the growth of preformed curvilinear and rigid fibrils under conditions favouring the curvilinear pathway. Seeding with curvilinear fibrils had little effect on the growth parame-

ters at 10 mg mL^{-1} HEWL, consistent with elongation processes dominating the kinetics at this protein concentration (Figure 4.15).

Seeding with rigid filaments was performed at both 1 M NaCl (Figure 4.16) and 200 mM NaCl (a concentration at which the curvilinear species is not observed, Figure 4.17) in quiescent conditions. In both cases the rigid seed population was found to persist, and at 200 mM NaCl evidence for propagation of the rigid species was clear, confirming that the rigid filaments are the thermodynamically stable species [1]. At high salt concentrations it is therefore apparent that while the growth of the rigid fibrillar species may be inhibited for long times by the much more rapid growth and sequestering of monomer into curvilinear species, rigid fibrillar species are likely to eventually form.

6.1.2 Mechanism of formation of rigid filaments

In the proposed aggregation pathway at low ionic strength the nucleation of fibrillar species is thought to occur from denatured HEWL, which then elongate by addition of denatured HEWL monomers [1, 2, 88, 89]. A bimodal length distribution was observed at early times and dominated by increases in peak area rather than increases in hydrodynamic radii, suggesting that changes in the particle size distribution may be dominated by the nucleation of new aggregates and/or that particle sizes are limited by fragmentation, as in the pathway at high salt [2, 89].

The growth parameters for HEWL aggregation at low ionic strength have previously been found to be weakly protein concentration dependent or concentration independent at pH 2 and 57-65°C [243, 244], while at pH 1.6 and 65°C the growth was found to be concentration independent only above 200 µM ($\sim$ 3 mg mL^{-1}) HEWL, with lag time decreasing with increasing concentration up to 200 µM [251]. Additionally, a jump in structural change was observed by CD to coincide with the lag time observed by SLS, suggesting an additional structural change is required before denatured monomer are capable of forming fibrils [244]. Indeed, a structural change during elongation would be consistent with concentration independence of growth rate, and the soluble denatured monomer population has been shown to exhibit less β-sheet content than the final fibrillar species [244].

As discussed above, the growth curves obtained here for rigid fibril growth at low ionic strength contain contributions from the growth of competing curvilinear

species. A discontinuity was observed in lag time and curve shape around 6 mg mL^{-1} HEWL, as observed for the curvilinear growth at high salt, and is not thought to be coincidental. This is attributed to a change in the behaviour of the curvilinear growth pathway and not thought to be related to changes in the rigid filament growth mechanism. At roughly this concentration the curvilinear growth pathway was found to reach its maximum growth rate, and its contribution to the kinetics obtained at low ionic strength is at a maximum. Above this point the curvilinear population is thought to act as a large monomer sink, reducing the decrease in lag with increasing protein concentration and partially contributing to an increasingly slow creep upwards in final fluorescence (as monomer dissociates from the curvilinear species and adds to the rigid fibril population).

Below 6 mg mL^{-1} the concentration dependence of characteristic times confirmed fragmentation as a dominant growth mechanism in the formation of rigid HEWL fibrils, consistent with the initially exponential increase in fluorescence response, previous observations about the early size distribution [2, 89] and the promotion of this growth pathway by agitation. The apparent growth rate at early times (before the inflection point) was found to be roughly concentration independent, consistent with previous literature reports [243, 244, 251], and suggesting a conformational change during filament elongation dominates the growth rate at all protein concentrations under these conditions. This may be an increase in β-sheet arrangement as denatured monomer join to filament ends.

At low protein concentrations (below 2 mg mL^{-1}) growth curves were found to have the form of the logistic function and as protein concentration increased the plateau approach became increasingly slower than exponential. Above 6 mg mL^{-1} the inflection point was also found to move to earlier times and smaller aggregate fractions, and combined with the decreasing growth rates that were observed for increasing protein concentrations suggests a critical fibril concentration may be reached above which fragmentation is suppressed and elongation of filaments proceeds by coagulation.

The lag phase for HEWL aggregation at low ionic strength was previously found to be dramatically decreased by the addition of preformed fibril seed [242]. A similar result was observed here and is consistent with early growth dominated by fragmentation. Differently shaped growth curves were obtained in the presence

of seed: the slow plateau approach and early inflection point were replaced by a very rapid approach to the plateau region, as expected for growth dominated by fragmentation (Figure 4.27). This suggests that seeding bypasses the formation of the curvilinear species by reducing the lag time for the formation of the rigid species relative to the curvilinear species, and that fragmentation is a dominant growth mechanism throughout the timecourse of aggregation in the absence of the curvilinear fibril sink. However, the maximum growth rate was roughly equivalent at all seed concentrations, consistent with growth rate limited by a conformational change during elongation. Fragmentation and conformational change are therefore relatively equal in importance in this system. The proposed growth pathway is shown in Figure 6.2.

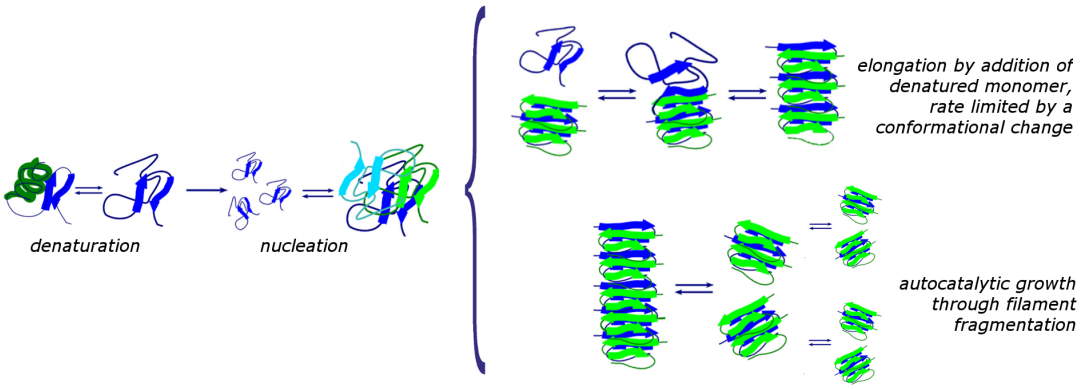

Figure 6.2: A cartoon depicting the proposed growth pathway of straight fibrils of HEWL at low pH, high temperature and low ionic strength. Nucleation is thought to occur from denatured HEWL, nuclei and filaments extend by monomer addition of denatured HEWL at a rate limited by a conformational change that may include an increase in β-sheet content. Fragmentation is an equally dominant growth process, and results in autocatalytic growth. Filaments also associate laterally at later times to form rope-like fibrils, and fragmentation is arrested at high concentrations after a critical fibril mass is obtained (not shown).

The apparently fragmentation dominated growth in seeded samples, at concentrations where slow plateau approaches are observed in the absence of seed, also suggests that the curvilinear species may decrease the CFC by some interaction between the species. It is not possible to determine how much of the slow plateau approach is attributable to the curvilinear species acting as a monomer sink and how much might be due to suppression of fragmentation by gelation.

Furthermore, the addition of curvilinear fibril seed (formed at 1M NaCl in quiescent conditions) had negligible effect on growth of 10 mg mL^{-1} HEWL at pH

1.5, 65°C under agitation, again confirming that the rigid filament species is the thermodynamically stable species. The effect of seeding with curvilinear filaments at lower protein concentrations would be interesting for further study to determine whether the CFC is affected by increasing curvilinear filament populations, but was not pursued as part of this study.

6.2 Fluorinated alcohol

The aggregation of HEWL into amyloid-like fibrils at high EtOH concentrations has been well studied [254–261]. Previous results have suggested that fragmentation [260] and a critical fibril mass concentration [261] may be important in HEWL aggregation at high EtOH concentration. Additionally, Yonezawa *et al.* proposed a mechanism for fibril formation at high ethanol concentration in which dimers are thought to be the nuclei for further aggregation, and filaments grow by dimer association [256].

The aggregation of HEWL in the presence of fluorinated alcohol HFIP was investigated here. HFIP (and TFE) have previously been shown to induce HEWL fibril formation, with strong enhancement of aggregation compared to non-fluorinated alcohols [269], but to my knowledge, the growth mechanisms and kinetics have not previously been analysed.

The aggregation of HEWL in the presence of HFIP was rapid, with little to no lag period prior to increases in ThT fluorescence intensity. Aggregation was promoted by increasing HFIP concentration up to 5-7.5% HFIP (at 10 mg mL^{-1} HEWL), above which increasing HFIP concentrations were found to inhibit aggregation.

As discussed in Sections 3.4 and 3.5, the fibrillar species that have previously been observed at high alcohol concentrations share similarities with the curvilinear fibrils formed under high salt conditions, which may suggest a similar aggregation pathway. Indeed, the aggregation pathway in the presence of HFIP was found to share a number of similarities with the aggregation at high salt.

Clearer TEM images of the filament structure were obtained here than previously reported [254, 260]. At early times spherical oligomers and bead-on-string like filaments were observed by TEM, and at longer times increasing numbers of curvilinear filaments and filament bundles were observed (Figure 5.2).

Growth parameters were consistent with growth dominated by fragmentation, in agreement with previous observations at high EtOH concentrations [260]. Also consistent with growth at high EtOH concentration, a very slow plateau approach suggests a transition into coagulation driven growth at later times that may be the result of a critical fibril mass concentration. Additionally, seeding with preformed fibrils had little effect on the resulting growth parameters and growth rate was found to be independent of seed concentration, suggesting that elongation processes, in this case a conformational change, may be rate limiting.

The dominant growth mechanisms in the presence of HFIP are the same as those at high salt (high temperature and low pH). As a result, I propose that this is the same growth pathway: where oligomers are initially formed from the monomer population, these join to form initial bead-on-string linear species and then undergo a conformational change to form curvilinear fibrils. The growth of curvilinear species is mainly driven by fragmentation, the elongation rate is limited by conformational change, and as the monomer population is diminished and/or at concentrations above the critical filament mass concentration, coagulation becomes the dominant growth mechanism.

6.3 Reduced hen egg white lysozyme

Reduced HEWL has been shown to form similar fibrils to non-reduced HEWL under approximately the same conditions, and also at neutral pH where the disruption of the disulphide bonds of HEWL by dithiothreitol (DTT) is thought to be a prerequisite for fibril formation on heating in the absence of other denaturants [270, 272, 273].

HEWL was incubated in quiescent conditions at 30°C, pH 7.4 (20 mM potassium phosphate buffer), in the presence of 20 mM DTT. Aggregation was rapid, with a very short lag phase, and aggregates were found to induce fluorescence enhancement of ThT to the same order of magnitude as obtained for curvilinear fibrils at high salt and in the presence of HFIP: much lower than the fluorescence enhancement obtained for the rigid fibrils.

In contrast to reports of long, straight fibrils following higher temperature incubations (85°C), no evidence for the formation of rigid fibrils was observed over the experimental timescale ($\sim$ 24 hours) even at temperatures up to 60°C with

agitation. The fibrils observed by TEM appeared to be tangled curvilinear species (Figure 5.11). Further denaturation at lower pH and/or higher temperature may be required to promote rigid fibril growth of reduced HEWL.

The growth kinetics of reduced HEWL were found to share a number of features with those obtained for curvilinear fibrils at high salt and in the presence of HFIP (Figure 5.9). In particular: weak concentration dependence of growth rate and characteristic time, consistent with a rate limiting conformational change (also evident in seeding experiments); changes in the growth curves at high concentrations (above 10 mg mL^{-1}) that suggest a transition into coagulation drive growth; and an exponential increase in intensity at early times indicating growth dominated by a secondary growth mechanism (although it was not possible to determine the exact nature of this process from the growth curves obtained in the presence of DTT). Growth by absorbance was also found to be more rapid (with a shorter lag time) and more concentration dependent than the growth observed by fluorescence, and given the similarities with the growth at high salt and in HFIP, this is attributed to the formation of an early, oligomeric species that has no ThT-affinity.

It appears to be most likely that the growth of reduced HEWL under these conditions progresses along the same curvilinear aggregation pathway observed in the presence of HFIP and at high salt, high temperature and low pH. However, an additional concentration independent process was found to effect both growth rate and characteristic times during reduced HEWL aggregation, and is attributed to a conformational change during nucleation, a monomer-activation process for example. This might be due to a different structure of denatured HEWL in solution compared to non-reduced HEWL at high salt or alcohol concentration, such that an additional conformation change is required prior to aggregation competence.

6.4 Nucleation processes

Surface interactions were also investigated in order to determine the drivers for aggregation. Under most experimental conditions nucleation is known to be heterogeneous in nature, since homogeneous nucleation in bulk solution is typically expected to occur on timescales much longer than those experimentally

observed [283]. The nucleation events that give rise to the aggregation observed here are much more likely to occur through surface activity.

HEWL is known to adsorb onto hydrophobic surfaces [278], inactivation of HEWL (enzymatic activity) has previously been found to be proportional to surface area, with hydrophobic surfaces most efficient in promoting inactivation [277], and the phase behaviour of HEWL at pH 9.4 with increasing ionic strength was found to depend on both charge screening and surface tension effects at the protein/water interface [245], suggesting strong surface activity.

The microplate surface type and size of the air:water interface were found to have a significant effect on aggregation propensity. The growth of the curvilinear species was found to be promoted by hydrophobic surfaces at high ionic strength (high temperature, low pH) and in the presence of HFIP, with the air-water interface having a stronger effect than the wall:solution interfaces. Additionally, increasing surface area appeared to favour the early oligomeric and beaded-string species rather than the final curvilinear fibrils, suggesting that the surfaces do indeed play an important role early in the growth process, perhaps by stabilising oligomers or early filaments. In contrast the rigid fibril pathway was found to be inhibited in the presence of hydrophobic surfaces, presumably as a result of the increased curvilinear population.

6.5 Heating considerations

In order to obtain as much information as possible about the aggregation over time solutions were prepared at room temperature and placed into a temperature equilibrated platereader. Readings were taken before temperature equilibration of the samples is complete and this is estimated to take approximately 20 minutes for a sample from room temperature to 37°C.

However, it was not possible to measure solution temperature during these experiments. The apparent lag phases obtained for HEWL at 1 M NaCl, DTT and HFIP are similar to the time frame required for heating, and the major structural change observed by CD for HEWL incubated at low pH and increasing temperature occurs between 50 and 60°C [244, 251]. The structure of HEWL has also been found to change with incubation time, with a jump in ellipticity previously found to coincide with the lag time for aggregation determined by SLS

[244].

As a result, lag times could be limited by the time taken to heat to a temperature at which a sufficient denatured monomer population is induced. In practice most experiments do not seem to have reached this limit, since lag time is either reduced by increasing concentration in the range analysed or is found to be shorter elsewhere. However, it is likely that this heating effect may have effected seeding experiments, in particular: at high salt, where a decrease in fluorescence was observed during this heating time; and at low ionic strength, where a lag was observed before further growth could occur. It is possible that neither the curvilinear or rigid filaments can propagate under these conditions until a heat induced conformational change results in aggregate competent species.

This limitation, especially where heating is required to induce aggregation should be noted. However, it does not alter any of the conclusions drawn from these experiments.

6.6 Two distinct polymorphs and aggregation pathways

Of the number of polymorphic filaments observed for lysozymes there are two that are most clearly distinct from one another: rigid, straight fibrils whose persistence length is on the order of fibril length; and curvilinear, wormlike fibrils that have considerably shorter persistent lengths, much shorter than the typical fibril length. These two species have been observed to form under differing conditions or to coexist under certain conditions for a wide range of proteins [2, 42, 43, 45–48, 61–91] and while there is a general consensus that the rigid fibril species, more widely recognised as amyloid-like fibrils, are formed along a common aggregation pathway, the formation of curvilinear species along an alternative common aggregation pathway has not yet been widely recognised.

At high temperature and low ionic strength the rigid and curvilinear species were previously shown to form along distinct aggregation pathways and to exhibit distinct structural signatures. They were shown to be in competition, with the more rapid curvilinear aggregate formation metastable against the growth of the rigid filaments that were shown to be the thermodynamically stable species [1, 2, 88, 89]. The results obtained here confirmed these observations (which have

previously all been made by the same laboratory), and provide further insight into the important growth mechanisms in these systems. In addition, curvilinear fibrils were observed to form in the presence of the fluorinated alcohol HFIP and from reduced HEWL in near native conditions (pH 7.4, 30°C).

The formation of curvilinear fibrils of HEWL is clearly not limited to the high temperature, low pH and high ionic strength conditions at which it has been thoroughly investigated and shown to be a clearly distinct aggregation pathway. Rather, it would appear that the aggregation pathway taken by HEWL is influenced by the solution and environmental conditions, and that under certain conditions the kinetically stable curvilinear species persist indefinitely (for example in the presence of alcohol).

The hydrolysis of HEWL was previously proposed as a requirement for fibril formation [251, 252], and while it had been clearly shown that this is not the case [242, 244], the increasing fragmentation of the HEWL monomer over time at low pH may provide added stability to the rigid fibril species compared to the curvilinear species, since the central fragment consisting of the β-core has only been found to have propensity to form rigid fibrils so far [251, 252]. However, the incubation of the central fragments in conditions that favour curvilinear fibrils has not been performed and would be a useful study to determine whether the two fibrillar polymorphs have a different primary sequence in their cross-β-core.

The polymorphism of the analogous human lysozyme has been shown to affect resulting toxicity against neuroblastoma cells [282], and the toxicity of curvilinear species of human lysozyme has not yet been tested. Whether both species are able to form under the conditions native to human lysozyme is also unknown, and might be an interesting avenue of further study.

Additionally, chemical reactions that modify HEWL have been implicated in HEWL enzymatic inactivation [284] and aggregation. Trexler and Nilsson [258] note that the formation of succinimide is a possible chemical modification that may play a role in HEWL fibril formation by neutralising the charge on aspartic acid residues [285], and is often overlooked in analysis of HEWL fibril formation. The formation of succinimide is thought to be particularly relevant for HEWL, because the residue D66 has a pKa around 1.6 and may be partially charged under fibrillation conditions, and the proportion of succinimide is enhanced at low pH where HEWL aggregation propensity increases [258]. Succinimide has been

identified in HEWL fibrils [252], and its formation in HEWL is enhanced by the presence of acetate buffer [284], often found as a residual buffer salt in commercial preparations [258]. The effect of such chemical modifications to HEWL was not investigated here, but is an important consideration for protein aggregation.

Chapter 7

Fibril formation of α-synuclein

7.1 Introduction

Alpha-synuclein (α-syn) is an intrinsically disordered protein (IDP), a member of a subset of proteins defined by their lack of (or regions lacking) tertiary structure [286]. The exact function of α-syn remains unknown, however, it is primarily localised in presynaptic nerve terminals and nuclei and thought to be involved in synaptic function and neurotransmitter release [286–288].

Amyloid-like β-sheet rich α-syn fibrils are the major component of Lewy bodies and Lewy neurites: proteinaceous inclusions associated with a range of diseases including Parkinson's disease and Dementia with Lewy bodies [289–293]. Most cases occur sporadically, but several point mutations of α-syn (e.g. A30P, A53T, E46K, G51D, H50Q) and multiplications of the gene encoding α-syn result in early onset familial Parkinson's disease [288, 292, 294–297], further demonstrating the pathological role of α-syn in neurodegenerative disease [290, 293, 298].

Alpha-synuclein is extensively studied both as a model IDP and because of its implication in neurodegenerative disorders, however, the mechanism by which α-syn converts into the fibrillar form associated with disease states is still elusive. This chapter aims to provide more insight into the aggregation mechanisms of α-syn as both an IDP and as a protein whose aggregation mechanism is of great importance in tackling disease associated with amyloid formation.

7.2 Structure of α-synuclein

Alpha-synuclein is a 140 amino acid protein found to exist as an ensemble of monomeric conformers under native conditions. It is found to be slightly more compact than a fully extended random coil in water at neutral pH and the conformational ensemble is very sensitive to solution and environmental conditions. Reported variations in conformer distribution in the literature make it clear that both sample preparation conditions and measurement techniques can influence the conformation [299, 300].

This ensemble contains both tightly folded and extended forms of the protein, stabilised by transient long-range electrostatic contacts and the burial of hydrophobic residues [289, 301, 302]. Different subcellular locations of α-syn appear to be associated with different α-syn conformations, suggesting that the ability of α-syn to form various native conformations is part of its functionality [303].

A large body of evidence suggests that α-syn exists as an unstructured monomer under a range of biophysical assay conditions *in vitro* [290, 301], and in cells α-syn exists either free (and unstructured) or in plasma membrane or vesicle-bound forms [286, 298, 301, 304]. The N-terminal (residues 1-60) contains lysine-rich, repetitive segments that are critical for membrane interactions [305–307], and residues from 1-25 to 1-97 (including the central hydrophobic region) are found to form either continuous or broken helices depending on membrane curvature [307].

The central region of the protein has the highest hydrophobicity and β-sheet propensity and forms approximately five β-strands which assemble to form a fibril core upon aggregation into amyloid-like filaments [305, 308]. The most aggregation-prone region, residues 61-95, is referred to as the non-amyloid-β component (NAC) region and forms β-strands β3 to β5 of α-syn fibril models [305, 308]. The sequence region 35-59 contains the β-strand segments β1 and β2. This region lies outside of the NAC region but is thought to play a critical role in α-syn aggregation and pathogenesis since it contains most of the disease-related mutations, is part of the core of many highly stable α-syn oligomers (that exhibit high resistance to H/D exchange), regulates the type of filaments formed and seeding efficiency, and when this region is sequestered by binding to specific engineered protein β-wrapin AS69 or by linking in a double-cysteine mutant the

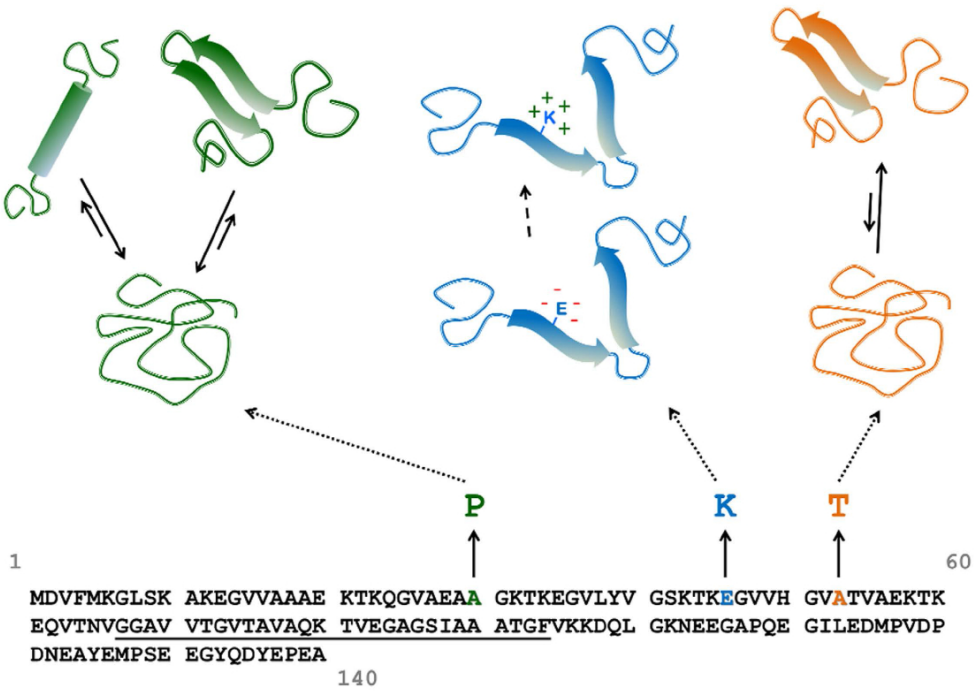

Figure 7.1: Primary structure of wild type α-syn with some of the sites of pathogenic mutations highlighted (A30P, E46K, A53T) along with the structures proposed for the aggregated formed of these mutants. From [3].

.

aggregation and toxicity of α-syn is inhibited [308, 309].

In fibrillar forms both the N-terminus and the C-terminus are less ordered than the central region [305]. The C-terminus (residues 96-140) also remains unfolded in membrane bound forms and is acidic, implicated in interactions with proteins, metals and small molecules [305]. In addition, α-syn has a high net charge at neutral pH (pI 4.7) and the distribution of this charge along the sequence is uneven. The C-terminus contains 8 negative charges at residues 120-140 while the central region (30-100) has a positive net charge of 3 [310].

7.3 Aggregation of wild-type α-synuclein

The natively unfolded character of α-syn arises from its low intrinsic hydrophobicity and high net charge [310]. Its potential energy landscape, as for other IDPs, is characterised by competition between intra- and interchain interactions (collapse and/or folding versus aggregation), where hydrophobicity, electrostatics

and solution conditions play crucial roles. The energy landscape is inherently complex and heterogeneous [311]. Partial folding of IDPs appears to be a crucial step in aggregation.

Factors increasing hydrophobicity or decreasing protein net charge may lead to partial folding and therefore promote aggregation. Decreases in pH and increases in temperature are shown to greatly affect the kinetics of α-syn aggregation [113, 310, 312–314], along with protein concentration [315], molecular crowding [316, 317], agitation [315]. and ionic strength [310, 312–314, 316]. In sporadic cases of synucleinopathy the toxicity and aggregation of α-syn has been linked to further external factors that affect α-syn folding, such as metal ions, small compounds and other biological macromolecules.[299]

In addition, α-syn is capable of forming a variety of different structures: helices upon binding to lipids, micelles and membranes and in the presence of sodium dodecyl sulphate (SDS) or alcohols; both helical and β-rich oligomeric structures and amyloid-like fibrils with rich β-content.

A range of oligomers, fibrils and aggregates formed by α-syn *in vitro* have been found to be toxic to cells and model organisms [305]. The mechanism of toxicity is unclear and may involve both toxicity and a reduction in normal function [318]. However, soluble oligomers with high β-content are widely regarded to be the main culprit while the role fibrils play in toxicity is uncertain [289]. Results comparing the toxicity of oligomers and fibrils in the literature are contradictory, and not all soluble oligomers are found to be toxic [3, 289].

7.3.1 Oligomers

A common conformation is thought to exist between the toxic oligomers of α-syn and other fibril forming proteins, involving a high β-sheet content. However, the structural characterisation of oligomers is challenging due to their often transient nature and their variability in both structure and size.

The soluble oligomers of α-syn are heterogeneous. A variety of oligomeric species differing in structure with different extents and nature of β-sheet content and exposed hydrophobicity, morphology, toxicity and aggregation number (the number of monomers forming an oligomer) have been found, depending upon the aggregation conditions [3, 115, 289, 303, 319–328]. Stabilisation of some of these oligomeric species by lyophilization has allowed for their separation and

investigation, giving insight into their structure, relation to the fibrillar species (whether they are on or off-pathway) and toxicity [115, 326].

Many of the oligomers of α-syn are found to be small, ring-like or toroidal species that are observed in two main orthogonal orientations by cryoEM or TEM: appearing either as small cylinders or ring-like species [303, 322, 326, 328]. However, some of the oligomers generated by lyophilization or isolated by fractionation methods have been found to belong to distinct subgroups that may result from multiple possible misfolding pathways [323, 324, 326]. In particular, two coexisting cytotoxic oligomers obtained by size exclusion chromatography (SEC) by Paslawski *et al.* [323, 324] were found to propagate into distinct higher aggregate structures. The major oligomer ($\sim 80\%$ of the sample) was found not to readily exchange with monomers, have diameter $\sim 13.9 \pm 1.6$ nm with a compact core and flexible chains protruding from the surface and to cluster to form worm-like fibrillar structures after prolonged incubation. The minor oligomer was found to be in equilibrium with the monomer population and to form straight fibrils [323, 324].

Oligomeric species are typically found to contain less β-content than the mature fibrils, and some of the toxic species that have been identified have been found to adopt an antiparallel β-sheet structure, in contrast to the parallel arrangement found in the mature fibrillar species [325, 326], a contrast that has also been noted for other fibril forming proteins [326, 329].

This suggests that internal rearrangement may be required for conversion into fibrillar species, and there is some evidence for such a transition. Single-molecule Förster Resonance Energy Transfer (FRET) investigations highlighted two species of α-syn oligomer on the same aggregation pathway: *1)* an initial amorphous oligomeric species with low FRET efficiency, little to no toxicity, susceptibility to proteinase-K digestion, prone to dissociation when subjected to low ionic strength conditions, presumably due to the reduced charge screening between protein charges, that undergoes structural rearrangement to form *2)* a more compact, proteinase-K resistant, cytotoxic oligomer with higher FRET efficiency and a β-sheet folding core that is stable to decreases in ionic strength [3, 327]. Structural rearrangement might therefore also be an important step in the formation of stable oligomeric species.

In addition to the oligomeric species assumed to contain predominantly β-

stucture, Ghosh *et al.*. [321]. found evidence for an oligomeric helix rich state at early stages during fibril elongation for *wt*, A30P, E46K and A53T by CD and FTIR. For 300 µM α-syn in 20 mM Gly-NaOH, pH 7.4, 0.01% sodium azide, incubated at 37°C an initial transition to a helical conformation ($\sim$ 38% helical, 25% random coil and 15-20% β-sheet) with two distinct minima at 205-208 nm and approximately 222 nm by CD was observed before conversion into a β-rich structure with a single minima at 218-220 nm. The helical intermediate structure was also observed in PBS at pH 7.4, but with shorter duration and less reliable reproducibility. At the point of maximum helical content the solution was found to be heterogeneous, containing oligomers, protofibrils and short filaments by AFM [321]

7.3.2 The effect of pH

The conformation of α-syn is highly sensitive to changes in pH. As pH decreases a shift to a lower charged, more compact species is observed [312, 313], while at basic pH more highly charged and extended conformers are obtained.

At neutral pH (at 20°C) α-syn is typically unordered, found to possesses the CD spectrum typical of an unfolded polypeptide chain, with an intense minimum around 196 nm and the absence of characteristic structure bands in the 210-230 nm region [310]. Little change in structure by CD is observed for changes between pH 9-5.5, but as pH is decreased further pH-induced secondary structure is observed, with corresponding decrease in intensity of the CD minimum at 196 nm and increases in negative intensity around 222 nm indicating an increase in β-sheet content [310, 314].

At pH $\leq$3 the C-terminus is found to undergo substantial collapse, with evidence for restricted chain motion, and to be in close proximity with the NAC region. This collapse is likely driven by the neutralisation of charge in the C-terminus, which is altered from -13.2 at pH 7.4 to +1.0 at pH 3 for residues 101-140, increasing intramolecular contacts within the protein [312, 313].

Additionally, the pH-induced changes at pH 3 are found to be fully reversible upon increasing pH (excluding aggregation) [310, 312], and independent of protein concentration (at least in the range of 0.1-1.5 mg mL^{-1}) indicating that the pH-induced changes are intramolecular [310]. The juxtaposition of hydrophobic residues from the C-terminus and NAC region into a larger hydrophobic cluster

is thought to be capable of driving the aggregation of these partially folded intermediates under these conditions [312].

Under low pH conditions the rate of fibril formation is dramatically accelerated: the lag time is many times shorter and the elongation rate is increased [310, 314]. The turbidity of aggregating samples is also found to increase with decreasing pH, implying an increase in size and/or number of aggregated particles [314]. This pH dependence of the kinetic parameters is found to be correlated with pH-induced structural changes and thought to result from the partial folding of α-syn monomers under low pH conditions [310, 314].

The final fibrillar structure is also found to be pH-dependent, with variations in periodicity, length and diameter. At pH 6 and 7, mature α-syn fibrils are found to have lengths ranging from 100-1000 nm and diameters around 11±2 nm. The fibrils formed at pH 7 were typically found to be untwisted, while the majority at pH 6 displayed periodicity of 40-120 nm. Periodicity of around 45 nm was found to be associated with right-handed twisting, while periodicity around 95 nm was associated with left-handed twists. At pH 4 and 5 large irregularly shaped aggregates composed of short fibrils were observed alongside fewer individual, short fibrils with lengths ~ 50 nm and diameters $\sim 8\pm2$ nm. The different structure of the fibrillar species formed at different pH also affected their seeding efficiency; the fibrils formed at pH 4 were less effective at reducing the lag time of aggregation at pH 7 than seeds formed at pH 7 [314]. Additionally, at pH 5 and below, increased precipitation of aggregate species was observed [314], presumably as a result of the decreased protein charge.

7.3.3 The effect of temperature

Increase in temperature is also found to induce reversible formation of secondary structure in α-syn and promote aggregation [113, 310, 313]. At low temperatures, α-syn is an unfolded polypeptide chain. As temperature is increased, secondary structure is induced [310]. Major CD spectral changes are found to occur between 3 and 50°C [310], and the partially folded species induced by increased temperature are similar to those observed at low pH. The effect of high temperature is attributed to the increased hydrophobic effect as temperature increases [310, 313].

7.3.4 The effect of anions and salts

The addition of various anions is found to promote α-syn aggregation.[312–314]. However, the enhancement of aggregation varies between anions and is found to generally follow the Hofmeister series (the classification of ions in order of their ability to salt out or salt in proteins), suggesting that the major role of anions in fibrillation is their modulation of protein-water interactions [313]. The enhanced fibrillation of α-syn in the presence of anions is attributed to charge screening and an increase in preferential hydration, which strengthens hydrophobic interactions [313].

High concentrations of NaCl enhance α-syn aggregation, and are found to result in charge screening but not to result in the C-terminus collapse observed at low pH. No significant conformational change is observed. The effect on aggregation is thought to result from reduced intermolecular rather than intramolecular electrostatic repulsion [312]

In the presence of salt at neutral pH larger aggregates composed of short fibrillar elements were observed, similar to observations made with decreasing pH [314].

7.3.5 Interfaces

To increase the extent of reproducibility of kinetics α-syn samples are typically subject to constant agitation, which, among other effects also increases the area of the air-water interface (AWI). The removal of the AWI (by capping microplate wells) inhibits the aggregation of α-syn *in vitro*, even at high protein concentration, and the solution is found to be predominantly monomeric, with few rare fibrils and oligomers, suggesting that the interfacial effects are primary triggers for α-syn aggregation [330].

Fibrils formed in the presence of an AWI were found to be surface active and form a dense layer at the interface [330]. PMMA caps (polymethyl methacrylate, a surface thought to be inert) were also scanned by AFM and found to exhibit a higher fibril concentration than in the bulk solution, although much lower than at the AWI, indicating the strong hydrophobic surface activity of α-syn species [330].

In seeded aggregation experiments the AWI was also found to accelerate

aggregation at any seed concentration and reduce the seed concentration required for the complete removal of the lag time. However, aggregation in seeded samples was found to initially proceed faster in the absence of the AWI and to exhibit no lag phase while slower increases in fluorescence were apparent for samples containing the same seed concentration in the presence of the AWI and attributed to the formation of new aggregates at the interface and adsorption of seeds to the AWI [330]

7.3.6 Membranes

The ability of α-syn to bind phospholipid membranes is well documented, and membrane binding is likely important for the protein's function [307, 331]. Upon membrane binding α-syn forms an amphipathic α-helix, ranging from residues 1-25 to 1-97 and including the central hydrophobic region. This helical structure may be continuous or broken depending upon the curvature of the membrane [307].

Membrane binding has typically been shown to be via an α-helical N-terminal anchor that enhances the binding of the central region of the sequence to the membrane surface, while the C-terminus remains largely unstructured and only weakly coupled to the membrane. The central region was further found to have a key role in modulating the affinity of α-syn for cellular membranes [332], while the N-terminal segment (residues 1-25) is found to be critical for membrane binding [307]. However, distinct mechanisms of membrane binding have been observed depending upon the polarity of the membrane surface. In neutral lipid membranes α-syn has been shown to adopt a helical structure through deep penetration of the central membrane region via hydrophobic interactions [333].

In contrast, accelerated aggregation of α-syn is observed in the presence of moderate membrane [307, 321], detergent [334] and phospholipid vesicle [224, 298, 335] concentration and in the presence of supported phospholipid bilayers. Typically at these concentrations detergents and fatty acids are micellar, and α-syn binding decreases the critical micelle concentration of these species [334]. As the relative concentration of membrane or membrane-like species increases the aggregation of α-syn is inhibited. [335, 336].

The surface of the lipid bilayer (or lipid-like bilayer) is thought to increase the probability of molecular interactions needed for oligomerisation [307], and

membrane binding has been shown to cause α-syn to form higher-order multimers with defined orientation that are thought to be the functionally active form of α-syn in promoting SNARE complex assembly [331].

These oligomeric or cluster-like multimers of α-syn might directly transition into β-strand containing aggregates [304], resulting in membrane-induced heterogeneous aggregation that may be physiologically relevant in α-syn function or in the diseased state [298, 298]. Indeed, the presence of small unilamellar vesicles (SUVs) of phospholipid 1,2-dimyristoyl-*sn*-glycero-3-phospho-L-serine (DMPS) has been shown to enhance the rate of heterogeneous primary nucleation by three orders of magnitude or more while under the same conditions other growth processes do not contribute measurably to the aggregation reaction. This was attributed to the locally enhanced concentration of α-syn bound to the SUV surface, which was roughly estimated as up to 36 mM, nearly 10^3 times higher than concentrations in bulk solution [335].

However, it is unclear whether α-syn aggregation *in vivo* originates from the monomeric cytosolic or oligomeric membrane-bound form [304]. In a recent study by Burré *et al.* the introduction of point mutations that block membrane binding and the formation of lipid-bound multimers was found to enhance aggregation *in vitro* and enhance neurotoxicity in mice, suggesting that membrane binding *in vivo* inhibits aggregation. As a result they propose that the toxic aggregation of α-syn *in vivo* is exclusively from the monomeric soluble form [304]. This may not however be the case in early onset forms of Parkinson's disease, where over-expression of α-syn via gene duplication or triplication likely lead to an increase in the protein:synaptic vesicle ratio, since the enhancement of nucleation by membrane binding occurs above a threshold α-syn:lipid ratio [335].

Fibrils formed in the presence of anionic phospholipids have been found to be similar to those observed in the absence of phospholipids: straight and unbranched [224]; and to exhibit ThT binding, albeit with a lower fluorescence enhancement compared to aggregate samples formed in the absence of membranes or membrane-like species [298]. The lower ThT enhancement suggests than these may be an alternative structure however.

7.3.7 Sodium Dodecyl Sulphate (SDS)

The behaviour of α-syn in the presence of the detergent sodium dodecyl sulphate (SDS) has been isolated here as a case in which the aggregation behaviour appears to be similar to that in the presence of membranes and has been well studied in the literature. The effect of SDS on α-syn is concentration dependent. The exact SDS concentration required to induce structural change depends on solution and environmental conditions, but the following is typically observed.

At low SDS concentrations (<0.2-0.3 mM) no significant changes in secondary structure are observed [42, 311]. At concentrations <0.2 mM SDS Basak *et al.* [311] found evidence of a compact monomeric species with decreased hydrodynamic radius, followed by the formation of a second monomeric species at higher SDS concentrations, which they propose is the SDS bound form. This compact monomer was found to be linked to SDS-binding, with the onset concentration for SDS binding increasing when urea was added (to diminish the extent of the early collapsed structure by favouring backbone-solvent over backbone-backbone interactions) and with onset concentration decreasing upon addition of glycerol (as a species favouring backbone-backbone interactions) [311].

In the presence of α-syn the CMC of SDS is reduced, from approximately 2.5 mM to 1.1 mM on addition of 20 µM α-syn under assay conditions [311], and even lower estimates, at around 0.15 mM have been reported [42], compared with a CMC of around 8 mM in water [311]. This is thought to be the result of the formation of mixed α-syn and SDS micelles in which $\sim$ 12 SDS molecules are thought to bind per α-syn monomer, and these complexes are thought to associate to form shared micelles [42]. Similar aggregation of monomeric SDS along the chain of α-syn, followed by formation of collapsed protein-SDS micelle complexes, has been obtained in MD simulations that indicate that both electrostatic and hydrophobic forces contribute to these interactions of α-syn with SDS, as shown in Figure 7.2 [337].

As SDS concentration increases, the α-helical content increases and aggregation is dramatically accelerated [42, 311, 321]. The propensity for fibrillation is optimal at around 0-20% α-helical structure and declines with increasing helical content [42]. Optimal SDS concentrations are typically found around 0.5-0.75 mM SDS and coincide with enhanced accessible hydrophobic surface area [338].

The aggregates formed in the presence of SDS bind ThT, and have been shown

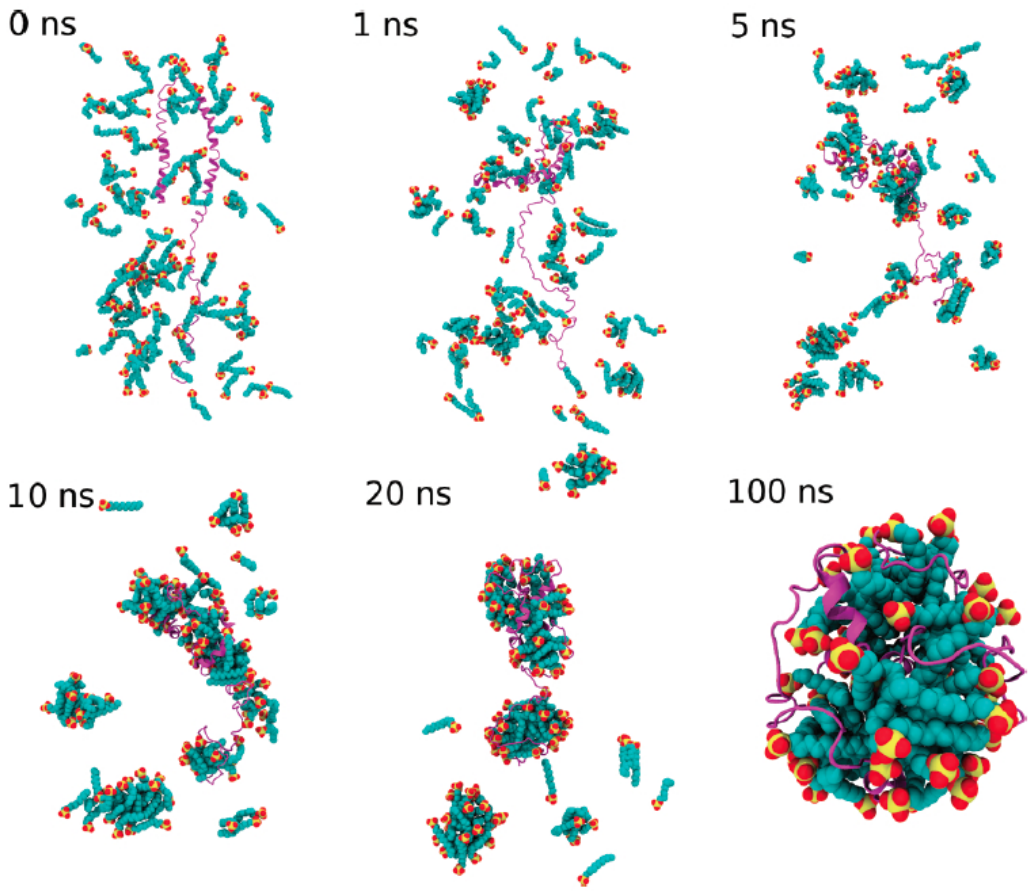

Figure 7.2: VMD Snapshots of SDS micellation at 0, 1, 5, 10, 20, and 100 ns from the self-assembly molecular dynamics simulations of Tian *et al.* [337]. Only the α-syn and SDS in the final complex are shown in the snapshot for clarity. The α-syn is in magenta cartoon presentation. The SDS molecules are in space-filling representation, while the head groups are in red and yellow and the alkyl carbon tails are in cyan. SDS monomers, which are not part of the final complex, are not shown for clarity.

.

to induce approximately a 3-fold increase in fluorescence intensity compared to a 24-fold increase in intensity upon ThT binding with α-syn fibrils formed in the absence of SDS [298], and to contain a mixture of both α-helix and β-sheet content [42]. They have been found to have a flexible, curvilinear worm-like appearance, which upon shaking was found to convert into a more classical, straight fibril morphology with an increased β-sheet content [42, 233].

Based on small angle X-ray scattering results, Giehm *et al.* [42] proposed that these filaments elongate as a beads-on-string structure, in which individual ellipsoidal SDS-α-syn complexes are bridged by strings of the protein and

conversion into β-sheet rich aggregates occurs on the surface of the SDS-protein micelles rather than by primary nucleation [42].

The α-helical content increases up to a maximum at around 0.9 mM SDS [42]. Compared to the native structure in solution, an unfolded CD spectrum which contains approximately 14% helical content, this final SDS-induced structure contains upwards of 50% α-helical structure [298]. Above 2 mM SDS the aggregation of α-syn is inhibited and α-syn exists predominantly in its maximum helical form [338].

7.3.8 The effect of alcohols

The addition of alcohol is found to induce folding of α-syn [339]. At moderate alcohol concentration aggregation propensity is enhanced [289, 321] as a result of increased oligomerisation [289], however, as alcohol concentration increases α-syn aggregation is inhibited [339].

The secondary structure changes as observed by CD are similar to those induced by decreasing pH or increasing temperature and are also found to be reversible and independent of protein concentration (at least in the range $0.1-2.5$ mg mL^{-1}) for low concentrations of alcohol, indicating an intramolecular process enhances aggregation propensity under these conditions [339].

At moderate methanol concentrations (10%) the initial population is partially folded and oligomers were observed, with radii in the range 25-60 nm, which appeared to associate further and precipitate over time [339]. At moderate HFIP or TFE concentrations (2.5% and 5% respectively) a similar transition appears to take place, with the formation of fibrillar species [233, 339]. In all cases, after prolonged incubation (60 hours) with agitation, fibrils were formed that resembled those formed in the absence of alcohol [339].

However, it has been noted that the TFE-induced behaviour is complex [233, 339]. As TFE concentrations were increased further, to around 15%, a further aggregation process was observed where the initial species contained β-structure and appeared to assemble into small amorphous-like aggregates [233, 339]. Indeed, at 10-20% TFE the production of aggregates has been found to correlate with TFE-induced formation of a partly helical intermediate and the small amorphous-like aggregates appeared to extend to form curvilinear filaments with diameters in the range 11-20 nm, compared to 9-23 nm for the longer,

straight fibrils formed under identical conditions but in the absence of TFE. The flexibility of the fibrils obtained in TFE was also such that structures resembling closed, distorted rings were observed by TEM, as shown in Figure 7.3 [4].

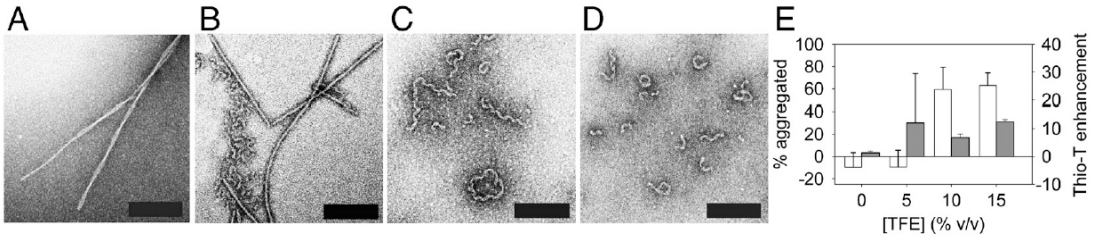

Figure 7.3: Wild-type α-syn aggregates obtained as a function of TFE concentration by Anderson *et al.* [4]. TEM micrographs of structures grown from 50 µM α-syn after 2 weeks of incubation at 37°C with shaking in the presence of (A) 0%, (B) 5%, (C) 10%, and (D) 15% TFE. (Scale bars: 200 nm). (E) For the samples in (A-D), the percentage of total protein incorporated into large aggregates (white bars, left axis) and the ThT enhancement (grey bars, right axis). The error bars reflect the standard deviations for three samples and the uncertainty in volume due to evaporation [4].

.

At high alcohol concentrations the inhibitory effect on aggregation is found to be dependent upon the solvent type. At high concentrations of ethanol and other simple alcohols a transformation into a β-sheet rich oligomeric conformation is observed. The helical propensity of α-syn increases with increasing fluorinated alcohol concentration and at high concentrations of HFIP and TFE an α-helix rich species is formed [333, 339].

7.3.9 Metal binding

A number of metals have been shown to stimulate α-syn aggregation *in vitro*, including Al^{3+}, Fe^{3+}, Co^{3+}, Mn^{2+}, Ca^{2+}, and Cu^{2+} [289, 299, 340, 341], and are implicated as possible causes of sporadic synucleinopathy. Since the effects of metal binding are not considered in the breadth of this study, only a brief overview is included here, and other reviews contain further information [342, 343].

Aluminium is found to have the strongest enhancement effect on α-syn aggregation, and the effectiveness of metal ions was found to correlate with increasing ion charge density and resulting induction of conformational change in α-syn [343]. Copper and Iron have been found to have differential binding towards wild-type α-syn and its disease associated mutants and to induce fibrils with different morphology [342]. The C-terminus is proposed as the major binding

site for α-syn metal interactions [342, 344], although it has also been shown that copper has a further binding site in the N-terminus [342].

7.3.10 Posttranslational modifications

A complete understanding of the α-syn aggregation process *in vivo* is complicated by a number of possible posttranslational modifications that have been identified *in vivo* or in the Lewy bodies isolated from patients [294, 305, 345, 345–347]. Their effects on α-syn aggregation are important in completing the picture of α-syn aggregation and pathology and in identifying potential targets for drug development. A few of the major posttranslational modifications known to affect α-syn are discussed here, but this is not an exhaustive review and more thorough discussions of this topic can be found elsewhere [294, 305, 348]. In addition, the effect of most of these *in vivo* modifications is unclear. Literature results are often contradictory, and it is evident that it is difficult to extrapolate to the effects of these modifications *in vivo*.

Phosphorylated α-syn, in particular on S129, is found to be a major component of aggregates in patients that have succumbed to Parkinson's disease, multiple system atrophy or dementia with Lewy bodies [294, 305]. However, phosphorylation at S129 or at both S129 and S87 has been found to inhibit α-syn aggregation *in vitro* [305, 349] but promote degradation. Certain kinases were found to phosphorylate aggregates of α-syn, perhaps explaining why phosphorylation is associated with aggregates [305].

Ubiquitination has generally been shown to inhibit aggregation, with the position and number of bound ubiquitin proteins influencing the strength of the inhibition or promotion of proteasomal degradation, suggesting a protective role for ubiquitination in disease states. However, ubiquinated protein is found in high concentrations in Lewy bodies, so the potential roles may be more complicated *in vivo* [305].

The small ubiquitin-like modifier sumo belongs to a family of ubiquitin-related proteins and is covalently conjugated to lysine residues in its substrates. The aggregates and inclusions formed as a result of impaired proteasome activity contain sumoylated α-synuclein, suggesting that this process may contribute to the pathogenesis of inclusion formation in synucleinopathies [347]. However, sumoylated α-synuclein has also been found to delay aggregation significantly

in vitro, and replacing lysine is found to increase aggregation propensity and cytotoxicity both *in vitro* and *in vivo*, suggesting that sumoylation promotes protein solubility and that defects in sumoylation may contribute to aggregation-induced diseases [350].

Other posttranslational modifications have been found to have minimal effect on the biophysical properties of α-syn. For example, N-terminal acetylation was found to have little to no effect on α-syn. Importantly, this indicates that the recombinant protein that does not have this modification is appropriate for most studies. However, N^{α}-acetylation has been shown to effect the induction of α-helix formation, interactions between α-syn and membranes, and oligomer and aggregate formation [305]. Various other modifications, including oxidation and nitration have been found to inhibit aggregation, and may have protective effects *in vivo* [294, 305].

Oxidative stress is another important modifier of α-syn aggregation and is characterised by the accumulation of reactive oxygen and nitrogen species that affect biomolecules and lead to posttranslational modification of proteins and lipid peroxidation [346]. Some of the generated aldehyde products are highly reactive to proteins and further trigger posttranslational modifications. For example, 4-hydroxy-2-nonenal (HNE) is found to modify and promote aggregation of α-syn, enhancing neurotoxicity, and residue H50 has been shown to be the main target residue [346].

7.3.11 Mutation

A large portion of α-syn literature compares and contrasts the wild-type protein with the disease associated mutants A53T, A30P, E46K, and the more recently discovered H50Q and G51D [3, 296, 299, 351, 352]. The mutations are located in regions of α-syn that are not thought to be necessary for fibril formation, but strongly influence the the aggregation propensity. Most are found to increase the aggregation rate due to an increased propensity to form β-sheet (A53T) or a decrease in net charge (E46K), while A30P results in an increased lag time for fibril formation, attributed to a decreased ability of the N-terminal to acquire secondary structure, and a reduced propensity to form inclusions *in vivo* [352] but enhanced propensity to form fibril bundles *in vitro* [353].

The mutants A30P, E46K and A53T were all found to have increased dimer

lifetimes compared to wild-type α-syn, suggesting that the mutations promote dimerisation and therefore the formation of higher order structures [354] and consistent with earlier observations that that the differences in aggregation kinetics were due to different nucleation rates [241]. The dimer of A30P was found to have a distinct structural arrangement to those of A46K and A53T and a much longer lifetime [3, 354], and the oligomers formed from A53T and A30P mutants have been found to both have distinct structural signatures compared to those of the wild-type protein [3]. This structural heterogeneity is thought to possibly lead to different aggregation pathways [289, 354].

Under conditions that produce fibrils, the A30P monomer is found to be consumed at a comparable rate or slightly more rapidly than the *wt* monomer, despite an increased fibrillation lag time. This is thought to be the result of the formation of non-fibrillar aggregates, and indeed, spherical aggregates with diameters around 26 nm, chains of spheres resembling protofibrils, and rings resembling circular protofibrils have been obtained alongside fibrils of diameter $\sim$ 8 nm by atomic force microscopy [111].

7.3.12 Molecular crowding

Macromolecular crowding has been shown to dramatically accelerate α-syn fibril formation *in vitro*, with crowding produced by the addition of poly-ethylene glycols (PEG), polysaccharides or proteins [316, 317]. The magnitude of the enhancement is found to depend on the nature of the polymer, its length and concentration [317].

The introduction of these model crowding agents has been shown not to significantly affect the structure of α-syn [316], which remains at least partially disordered even under high concentrations of macromolecules, but to produce differential conformational propensity in different structural regions which may lead to selective stabilisation of certain folds [217].

At low crowding agent concentrations the major effect on protein aggregation is proposed to be the excluded volume effect, which favours self-association and increases the effective protein concentration [316, 317]. However, at higher concentrations of crowding agents, viscosity effects of the polymer solutions may be dominant [316].

7.3.13 Agitation

Agitation of α-synuclein leads to a dramatic increase in the rate of aggregation, shortening the lag phase from weeks to days, and is found to be a major determinant of the fibrillation rate [43, 233, 303, 313, 315, 316]. The exact mechanism by which agitation induces aggregation is unknown. It may increase the air-water interface, leading to increased partial folding of α-syn, or the enhancement of aggregation may be the result of increased fragmentation or collision of monomeric and oligomeric species with one another and with elongating filaments, or a combination of these effects may contribute [316].

Agitation by shaking with glass beads has been shown to significantly decrease the lag time of fibrillation and increase the reproducibility of α-syn aggregation assays, which can typically vary dramatically across sample replicates and between experiments [43].

In addition, agitation has been found to alter fibril morphology. In the presence of SDS, fibrils are found to have a flexible, worm-like appearance. Upon shaking this was found to convert into a more classical, straight fibril morphology with increased β-sheet content [42]. A similar observation has also been made for fibrils induced by the small molecule 2-pyridone compound FN075 in the presence and absence of agitation. This was attributed to increased fragmentation induced by agitation, reducing fibril curvature and making lateral association easier [355].

7.4 Polymorphism

Different fibril polymorphs of α-syn have been obtained as coexisting species or by careful choice of fibrillation conditions, and appear to arise from different production, purification and assembly conditions [4, 42, 310, 314, 355–360].

These range from the typical long (micrometer order) straight, untwisted and unbranched filaments obtained after prolonged incubation at pH 7.4 with diameters around $9-12$ nm [314, 315], to the twisted filaments obtained at pH 6, with left or right-handed twisting associated with different twisting periodicities (around 95 nm and 45 nm respectively) [314], to the much shorter (less than 100 nm in length) and slightly narrower ($\sim$ 8 nm diameter) fibrils obtained at lower pH that are more likely to bundle and precipitate [310, 314], presumably as a result of decreased charge repulsion between the the fibrillar species, and finally

to the worm-like or curvilinear species that have been observed in the presence of SDS [42], TFE [4], and FN075 [355], and in some cases found to convert to a higher β-sheet content, straight fibrillar species upon agitation [42, 355].

The conformation of the initial monomeric distribution and the resulting aggregates are therefore highly sensitive to solution and environmental conditions, and the range of fibril polymorphs likely arise from the range of monomeric [289, 299–302], dimeric [354, 361] and oligomeric [3, 115, 289, 303, 319–328] polymorphs that have been obtained. Indeed, two distinct oligomers obtained by Paslawski *et al.* [323, 324] were found to propagate into distinct higher aggregate structures, forming either worm-like curvilinear species or straight, unbranched filaments [323, 324].

Filaments formed in 5 mM Tris-HCl at pH 7.5, in 50 mM Na phosphate buffer at pH 7.4 (0.1 mM EDTA, 0.02% NaN_3 w/v) and in 50mM Tris-HCL, 150 mM KCl at pH 7.5 have all been shown to exhibit different NMR chemical shifts and differ in the amino-acid stretch that is involved in the β-rich fibril core [356], suggesting that differences in the core filament region may be the cause of the wide range of α-syn fibrils polymorphs. Differences in the β-core region have also been obtained for fibrils formed from the disease-related mutants of α-syn formed under identical conditions to those of the wild-type [360].

The higher β-sheet content in fibrils formed under agitation compared to those formed in quiescent conditions [42, 355] would be consistent with an increased incorporation of amino acids into the β-sheet core, and such filaments would be expected to have higher stability. Indeed, conversion of the straight filaments to curvilinear filaments upon addition of SDS was a slow process, and straight filaments were found to persevere [42], indicating their higher thermodynamic stability.

The central NAC region of the α-syn sequence readily forms cytotoxic fibrils in isolation and the structure of crystals of the NAC core (residues 68-78) has been determined at atomic (1.4 Å) resolution by micro-electron diffraction. The structure of the crystals formed from this region exhibit protofibrils built of pairs of face-to-face β-sheets, with X-ray diffraction patterns similar to the fibrils of full length α-syn [362]. The polymorphs of the NAC region are therefore useful indicators for the possible polymorphic β-sheet core regions in full length α-syn filaments.

A number of different structural models for the NAC region of the aggregated form of α-syn have been proposed [358, 362–365]. The secondary structure models of the groups of Riek [365], Baldus [358], Bockmann [359] and Rienstra [366] for α-syn fibrils formed at pH 7.4-7.5 and 37°C, as compiled by Atsmon-Raz *et al.* [364], are shown in Figure 7.4. Comparing these structures with their own proposed atomic resolution structure for a fibril-like dodecamer by molecular dynamics simulation, Atsmon-Raz *et al.* propose that the self-assembled NAC region presents polymorphic states. The three most populated of these are shown in Figure 7.4. In addition, they propose that the structure shown in H is the structural building block of individual filaments while those shown in I and J are the building blocks of fibrils containing two or more single filaments [364].

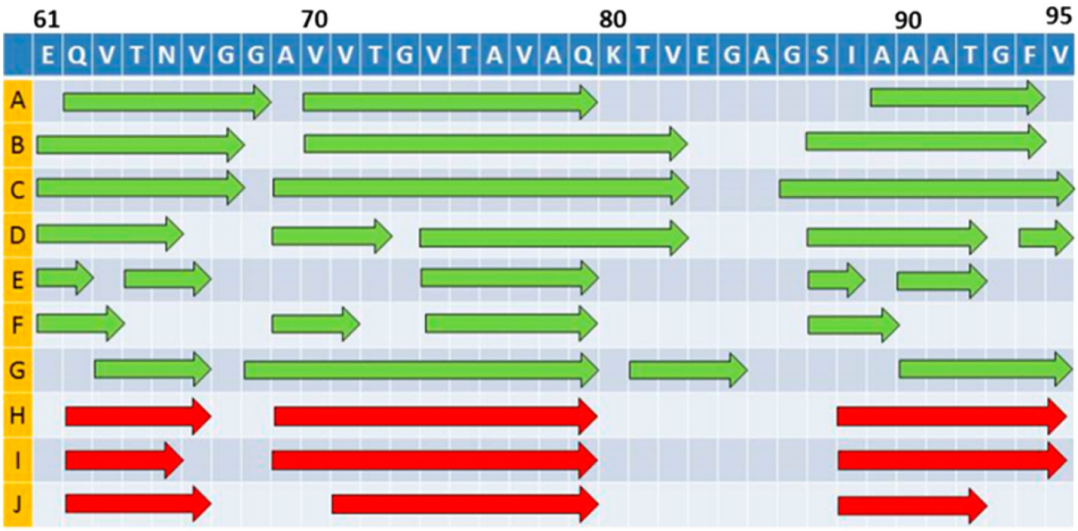

Figure 7.4: Proposed secondary structure of the NAC domain from solid state nuclear magnetic resonance studies. A-C were proposed by Vilar *et al.* [365], D and E by Heise *et al.* [358], F by Gath *et al.* [359] and G by Comellas *et al.* [366]. The secondary structure of simulated dodecamers of the NAC domain by Atsmon-Raz *et al.* [364]. are shown in H-J. The β-strands are illustrated by green (experimental) or red (simulated) arrows [364].

.

7.5 Fibril formation mechanisms

Under physiologically relevant conditions *in vitro* the aggregation of α-syn takes weeks to months and replicate samples are found to exhibit different aggregation behaviour and form a range of amorphous to fibrillar aggregates [233]. Kinetic

growth curves, as obtained by increase in ThT fluorescence intensity, are found to vary depending upon the aggregation type (and presumably therefore mechanism) [233].

In all cases in the absence of seed material or known aggregation inducers, aggregation is typically observed after a long lag phase period. When the final product is fibrillar, the growth curves obtained are sigmoidal-like in form, with an initial increase to a maximum growth rate at an inflection point and then slowing to a plateau region as the monomer population is consumed [43, 233]. The addition of preformed α-syn fibril seeds is found to diminish and eventually remove the lag phase [43, 241, 300, 367], and reproducible growth curves are typically only obtained for seeded experiments or under conditions that reduce the lag phase: usually a combination of high temperature, low pH and agitation with glass or Teflon beads [43].

In the presence of SUVs, Galvagnion *et al.* [335] found that the initial increase in aggregate population (by increased ThT fluorescence intensity) exhibited very weak reaction order with respect to monomer concentration, and they propose that initial growth is driven by heterogeneous nucleation at the lipid-water interface, with little to no contribution from homogenous nucleation on the timescale of most experiments. While their results confirmed that a greatly enhanced nucleation rate due to the heterogeneous nucleation was the origin for the rapid formation of fibrils in the presence of SUVS, they were unable to determine the exact nature of the nucleation step [335].

Given the air-water interface activity of α-syn, heterogeneous nucleation is also proposed as the nucleation event in the absence of lipids *in vitro* [335], and is consistent with the results described in Section 7.3.5, since removal of the air-water interface is found to inhibit aggregation on experimental timescales [330].

Since the oligomeric species obtained from aggregating α-syn solutions are found to contain less β-content than the fibrillar form, or indeed to have a different β-arrangement [325, 326], a conformational conversion step during aggregation is frequently proposed in which nuclei (the oligomers) convert into more compact forms capable of elongating into mature fibrils through monomer addition [3, 321, 327]. In addition, Tosatto *et al.* [3] propose that the initial species may also grow by monomer addition in the absence of the conformational change, resulting in a range of compact nucleus sizes that might allow for parallel aggregation pathways

[3].

While Galvagnion *et al.* [335] found that an approximately protein concentration independent mechanism, attributed to heterogeneous nucleation, was dominant in the very early stages of α-syn fibril growth, the initial growth has been found to be exponential in form [241, 315, 367], typically attributed to autocatalytic growth. Shvadchak *et al.* [367] propose that this process is filament fragmentation, consistent with the sensitivity of α-syn aggregation to agitation, the much higher (>25 fold) seeding efficiency of sonicated fibril material and the concentration order dependence of the maximum aggregation rate, 0.6±0.1: consistent with the predictions of the Knowles SDP model [367]. In addition, they observed that the square of the observed aggregation rate was linearly proportional to the shaking time fraction, and therefore so was the average rate constant for fibril breaking (since $k_{exp} = \sqrt{k_+ k_-([M] - K_d)}$, consistent with the shaking time linearly correlating with the average number of breaking events per second [367].

In contrast to the experiments performed with agitation, in quiescent conditions at neutral pH, Buell *et al.* [300] found no detectable contributions from homogeneous nucleation or secondary processes to fibril growth in seeded solutions [300]. In addition, they observed similar results in experiments with agitation by plate-reader shaking, but on addition of beads aggregation was dramatically accelerated, with seeded reactions increasing in fluorescence intensity several hours before unseeded reactions and growth curves becoming increasingly convex, indicating an increased number of aggregates at earlier times, and consistent with the dominant effect of the addition of beads being to increase the fragmentation rate [300].

As pH decreases the importance of secondary nucleation has been found to increase, and was attributed by Buell *et al.* [300] to a surface-catalysed event on filament surfaces since the experiments were performed in quiescent conditions [300]. The effect was also observed in microcapillary experiments in the absence of any mechanical stress and fewer, larger aggregates were observed at lower seed concentrations, indicating continued growth rather than fragmentation, and that newly formed aggregates may not detach from their origin of nucleation. This result was attributed to the decrease in charge of the C-terminus. The elongation rate constant was found to vary by an order of magnitude between pH 5.2 and

7.4 while the rate of fibril production through secondary processes was found to change by at least four orders of magnitude [300].

These results are consistent with previous observations about the pH behaviour at more acidic pH by Morris *et al.* [368], who observed that while the growth rate after the inflection point increased with decreasing pH, the initial growth rate was also found to have a minimum at the pI, indicating the importance of charge in the nucleation process. The growth rates were found to be maximum around pH 3, and the nucleation-associated rate was found to change by 3 orders of magnitude between pH 3 and pH 4 [368].

Elongation of α-synuclein fibrils under high seeding conditions has been found to be consistent with growth by monomer addition (elongation rate proportional to protein concentration) [300]. This has also been confirmed by total internal reflection fluorescence microscopy using ThT fluorescence, which allows time-resolved imaging on a single fibril level (on a glass surface) [369]. Fibril elongation was observed by TIRFM to proceed by monomer addition through a stop-and-go mechanism where fibrils either extend at a homogenous growth rate or exhibit no growth for variable time intervals. The stop and growing states were approximately isoenergetic (the probability of being in either state was very similar). The pauses are thought to be the result of growth-inhibiting interactions with physical obstacles, surfaces or transitions between templating-competent and templating incompetent conformations at the fibril ends. The dissociation or reconversion rate would need to be sufficiently low to explain the long duration of stop states, and the rates of dissociation of monomers and oligomers from fibrils were found to be on the order of or below the stop-and-go transition rate determined [369]. The rate constant of monomer addition was found to be 8.6×10^3 M^{-1} s^{-1}, with most fibrils growing with a rate of 4-12 nm min^{-1} in 10 mM $MgCl_2$, 20 mM 2-(*N*-morpholino)ethanesulphonic acid MES buffer at pH 6 and 25°C, slow compared to elongation rates reported for other proteins [369].

The rate of fibril elongation has also been found to saturate at monomer concentrations around 100 µM both in the absence [300] and presence of SUVs [335], and was attributed to the diffusive nature of monomer addition [300].

In the presence of 1 mM SDS, sigmoidal and exponential curves were obtained in the presence and absence of seed material by Buell *et al.* [300]. Since the effect of seeding in this case is simply to reduce the time taken to reach the inflection

point of the growth curve and does not appear to affect the elongation process, it would appear that SDS induces α-syn aggregation by enhancing the primary nucleation process, possibly along an alternative nucleation and growth pathway [300].

Additionally, macroscopic, gel-like assemblies of fibrils are observed at high protein, high salt concentrations and at low pH, suggesting further association between filaments following elongation [300]. Under high seed conditions, while the growth rate behaviour was consistent with growth by monomer addition, Buell *et al.* found that the shape of the kinetic curve deviated from the expected single exponential profile (of the form $M(t) \sim 1 - \exp(-kt)$). They propose that this deviation is the result of sedimentation of these aggregate flocs, which might enhance fluorescence relative to a homogeneous sample, and gelation effects, which may affect mobility of soluble species and the accessibility of fibril ends, decreasing the rate of conversion. Indeed, they found that in the absence of salt no macroscopic species were observed and kinetics conformed more closely to a single exponential profile [300].

In the following chapter the aggregation of α-syn at elevated temperatures and low pH and in the presence of SDS are investigated in further mechanistic detail by high-throughput kinetic analysis, adding to the extensive analysis that that has been described above.

Chapter 8

Results: Fibril formation of α-synuclein

8.1 Introduction

The aggregation of α-synuclein has been investigated in detail here by *in situ* ThT fluorescence and turbidity measurement by microplate-reader assay, allowing for high throughput analysis of many replicate aggregating samples. The morphology of the resulting species were then analysed by TEM.

Aggregation was followed under a range of environment and solution conditions that have previously been shown to induce the formation of amyloid-like fibrils: elevated temperature, low pH, under agitation, in the presence of SDS and under increasing salt concentration. These conditions are also known to give rise to a range of fibril morphologies that may be the result of different growth mechanisms.

The kinetic growth profiles of α-synuclein assembly in each case have been compared with the proposed models of fibril assembly: the traditional nucleation-dependent polymerisation (NDP) model of Oosawa *et al.*, the secondary-process dependent polymerisation (SDP) models of Knowles *et al.*, the end-joining coagulation (JDP) model of Kalapothakis *et al.* and the predictions of growth under these regimes that are described in Chapter 1.3 to test the ability of these models and predictions to distinguish between different growth processes.

The difficulty in obtaining reproducible kinetic growth curves during α-syn aggregation is well documented, and reliable and reproducible growth is

typically only obtained by orbital agitation with beads in platereader assays or by eliminating the lag phase with the addition of preformed seeds [43, 233]. The conformers and resulting aggregates of α-syn are highly sensitive to the purification method, storage, sample preparation conditions and measurement techniques, therefore, if any of these conditions is changed the results may vary [299, 300]. All stages from α-syn production to the final measurement must therefore be carefully controlled for reproducible and reliable results, and the exact results may be expected to vary between laboratories. Importantly, ideal assay conditions must be redetermined after the change of any upstream α-syn processing condition.

The conditions that were found to be required here for producing reproducible growth curves were mostly equivalent to those discussed in the literature and included elevated temperature, pH values of around pH 5 and below ($\leq$ pI) and agitation. The exact combination of conditions required was found to vary between different α-syn preparations that followed different purification protocols and had different stock solutions (concentration of buffer and/or salt and type of buffer/salt and the initial α-syn concentration). The differences in aggregation behaviour between these batches are discussed in the Section 8.3.

8.2 Platereader assays

Fluorescence platereader assays for protein aggregation are very convenient, low volume and high throughput methods for obtaining kinetic data. There is also the added advantage of recording simultaneous measurements at different wavelengths.

In order to obtain simultaneous information from both ThT fluorescence and from absorbance measurements (turbidity at 600 nm) and to eliminate the extra surface type introduced by the addition of beads, an alternative microplate type was investigated. Nunc StarWell microplates have been designed for maximising available wall surface area and contain 8 internal fins that increase the surface area by approximately 1.5 times compared to standard flat bottom 96 well microplates. The surface type of the Nunc StarWell microplates chosen was PolySorp, a treated polystyrene surface with high affinity to hydrophobic molecules. The design of these plates is also thought to increase the effect of agitation, although whether

this effect is due to the protruding fins increasing fragmentation of aggregates or due to an increased effective air-water interface is unclear.

These microplates were found to be equivalent or better than introducing glass beads in promoting aggregation and increasing reproducibility, and a comparison is discussed in Section 8.5. Microplate surface type was also found to affect reproducibility, with hydrophobic surface types producing more reproducible results.

8.3 Reproducibility and α-synuclein assays

Four different stocks of α-syn were investigated during this research and varied to differing degrees. The purification methods are described in full in Section 2.1, but briefly are as follows *i)* α-syn 1: liquid stocks of $\sim$ 5.5 mg mL^{-1} wild-type α-syn, 10 mM Tris-HCl, 100 mM NaCl at pH 7.5 and stored at -80°C, *ii)* α-syn 2: lyophilised stock of α-syn stored at -80°C where the solution of α-syn contained 50 mM ammonium acetate (amac) prior to lyophilisation and trace amounts of this salt would remain, *iii)* α-syn 3: a liquid stock of $\sim$ 5 mg mL^{-1} α-syn in 5 mM phosphate buffer, 137 mM NaCl, 1mM EDTA at pH 7.5, stored at -80°C, *iv)* α-syn 4: α-syn was purified and stored using the same method as α-syn 3 but the stock solution was concentrated to $\sim$ 10.4 mg mL^{-1}.

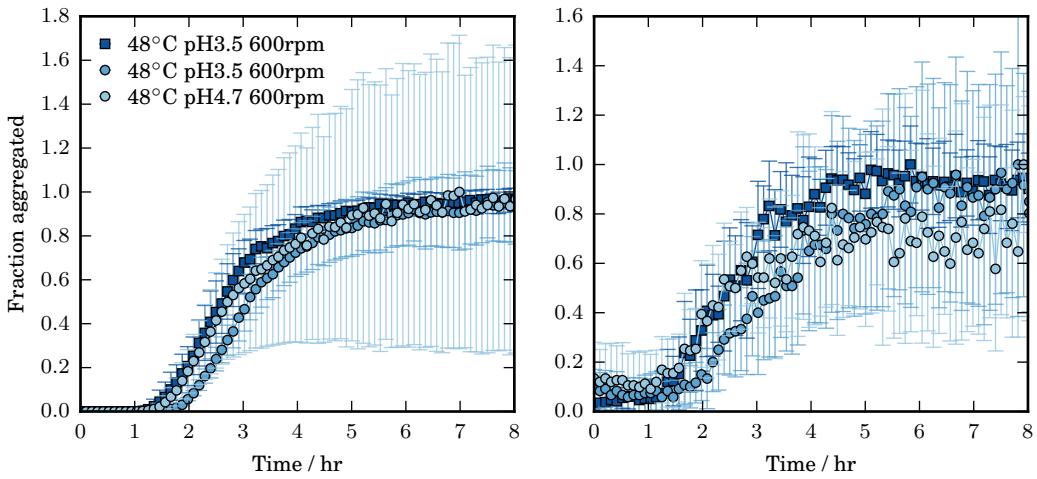

Figure 8.1: Normalised thioflavin T (ThT) fluorescence (left) and absorbance at 600 nm (right) obtained for 1 mg mL^{-1} α-syn 1, 3 mM Tris-HCl, 120 mM NaCl incubated with shaking at 600 rpm for 5 minutes every 6 minute cycle, 48°C and pH 3.5 or pH 4.7. The error bars, reflecting the standard deviation, are much larger for the fluorescence response at pH 4.7.

For α-syn 1 (Tris-buffered), elevated temperature, low pH (≤pH 5) and agitation were sufficient to provide reproducible kinetic growth curves in individual experiments. However, the growth curves obtained at pH 3.5 in Figure 8.1 show the standard deviation for 3 (circles) or 9 (squares) replicate samples performed in different experiments.

A large variability in final fluorescence plateau values was found to be associated with both increased agitation and increasing pH, as seen in the error bars for the standard deviation at pH 4.7 compared to those at pH 3.5 in Figure 8.1. At higher shaking speeds only much lower pH conditions were found to produce growth curves with reproducible final fluorescence values.

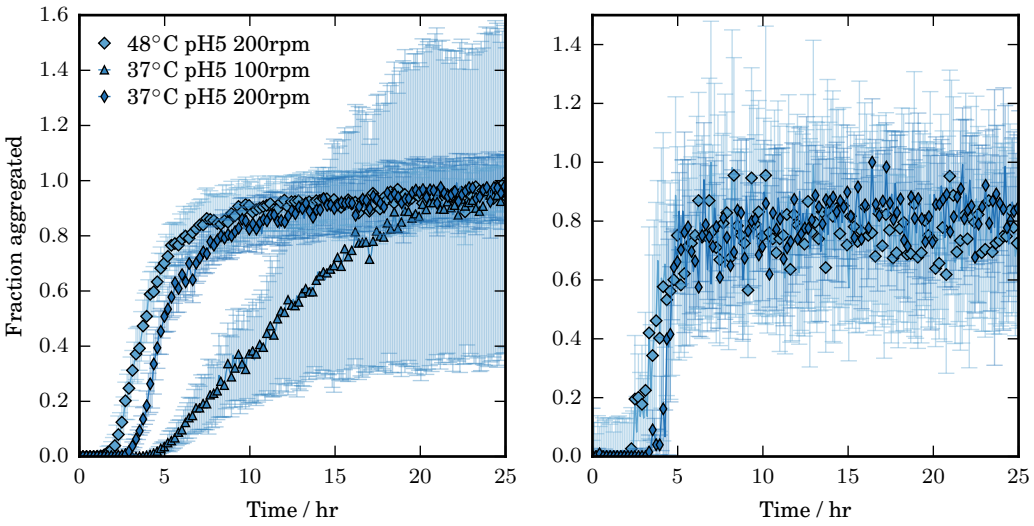

Figure 8.2: Normalised thioflavin T (ThT) fluorescence (left) and absorbance at 600 nm (right) obtained for 1 mg mL^{-1} α-syn 1, 3 mM Tris-HCl, 120 mM NaCl incubated with shaking at 100 or 200 rpm for 5 minutes every 6 minute cycle and 37 or 48°C at pH 5. The error bars, reflecting the standard deviation, are much larger for the fluorescence response at 100 rpm, this is also reflected in absorbance readings which were significantly more noisy and are not shown.

Reproducible results were obtained up to pH 5 with platereader double orbital agitation at 200 rpm for 5 minutes in every 6 minute cycle, as shown in Figure 8.2. At lower shaking speeds growth curves were more erratic, less reproducible and did not display the sigmoidal-like curve associated with fibril formation, although shown here on a comparative scale with results at 200 rpm, no plateau region was reached at 25 hours and fluorescence continued to creep slowly upwards. Non-sigmoidal growth curves like these have previously been associated with the formation of increased non-fibrillar aggregate populations in α-syn assays

[233], and similar observations were made here by TEM of end-point samples, suggesting that filament fragmentation, induced by agitation in these assays, may be an important driver of α-syn fibrillation. No such non-fibrillar aggregates were observed for samples with variable end-point fluorescence at high shaking speeds however, and at high shaking speeds the variation is therefore thought to be associated with the accumulation of aggregate on the well walls, where it can become trapped in corners behind the StarWell plate fins.

In addition, the decrease in lag time with elevated temperature can be seen in Figure 8.2. However, at pH values greater than 5 no reproducible growth curves were obtained by increasing temperature or agitation, or by decreasing pH over reasonable laboratory timescales.

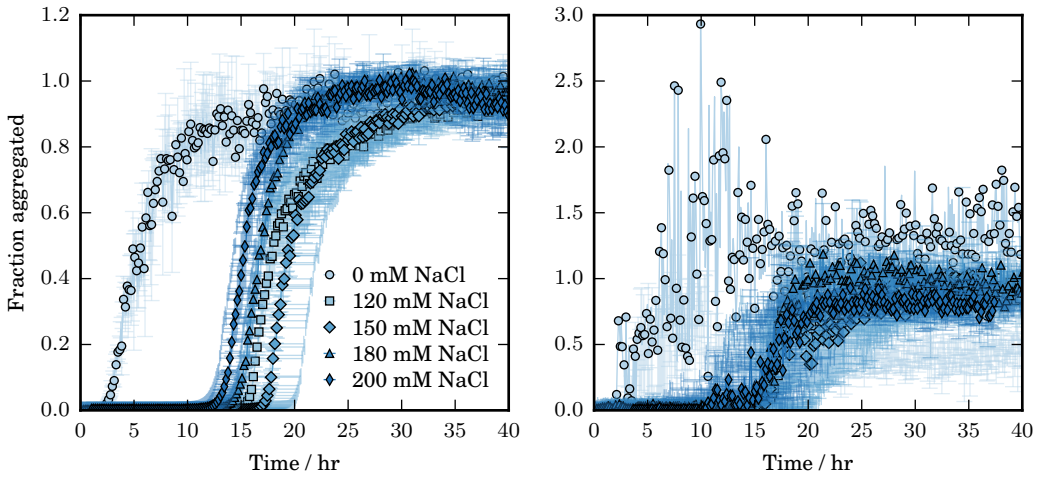

Figure 8.3: Normalised thioflavin T (ThT) fluorescence (left) and absorbance at 600 nm (right) obtained for 1 mg mL^{-1} α-syn 2 in the presence of various salt concentrations, incubated with shaking at 200 rpm for 5 minutes every 6 minute cycle, 37°C at pH 5. Data were normalised before taking an average of triplicate (for 0, 180 and 200 mM NaCl) or quadruple (for 120 and 150 mM NaCl) growth curves corrected for variation in lag time as described in Section 2.2.2, the x error bars represent the variation in time.

In contrast to α-syn 1, where the elevated salt concentration (120 mM NaCl) was found to be necessary for reproducible aggregation on a reasonable time scale (no increase in fluorescence was observed over 40 hours for samples at 1 mg mL^{-1} with $\sim$ 18 mM NaCl, data not shown), aggregation of the α-syn preparation in ammonium acetate (α-syn 2) was inhibited in the presence of NaCl. This is clear in Figure 8.3 where the lag time for aggregation in the absence of NaCl is significantly shorter than those in the presence of salt, and reached maximum

fluorescence before observable increases in fluorescence occur for the salt samples.

The conditions found to produce the most reliable and reproducible growth curves for α-syn 2 involved addition of buffer, increases in agitation and higher temperatures, although it is possible that alternative conditions would produce the same effect and were not investigated. Reintroducing 50 mM amac (the concentration prior to lyophilisation of the sample), higher amac concentrations, Tris-HCl and potassium phosphate buffer in the presence and absence of NaCl were investigated as possible solution conditions. The most reproducible growth curves at pH 5 were obtained in the presence of 10 mM phosphate buffer, 10 mM Tris-HCl and either 50 mM amac or 120 mM NaCl, with increased agitation speed to 700 rpm, reduced agitation time fraction to 3.5 minutes each 5 minute cycle (both changes to agitation were required) and temperature increased to 50°C and above.

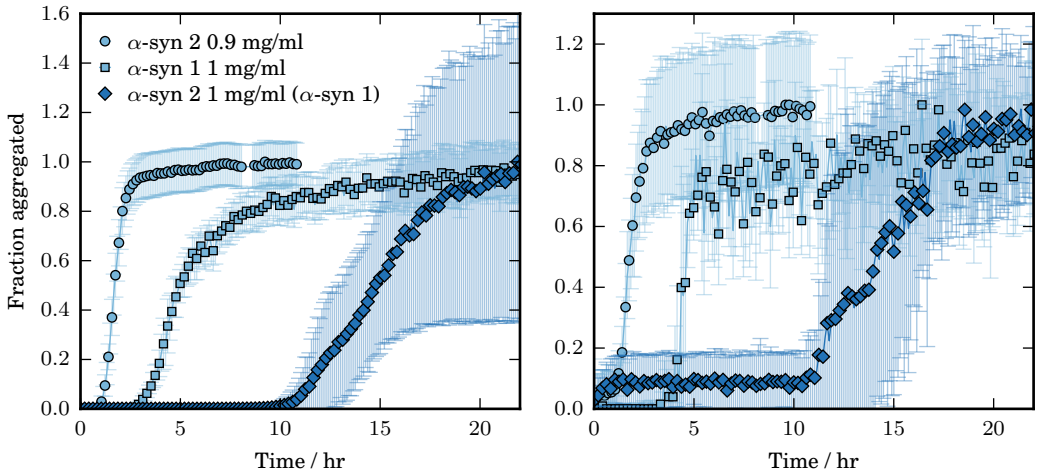

Figure 8.4: Normalised thioflavin T (ThT) fluorescence (left) and absorbance at 600 nm (right) obtained at the optimum conditions for α-syn 2 (shaking at 700 rpm for 3.5 minutes each 5 minute cycle, 60°C, 10 mM K phosphate buffer, 10 mM Tris-HCl, 120 mM NaCl, pH 5, 0.9 mg mL^{-1} α-syn, average of 7 replicates), the optimum conditions for α-syn 1 (shaking at 200 rpm for 5 minutes each 6 minute cycle, 37°C, 3 mM Tris-HCl, 120 mM NaCl, pH 5, triplicate) and α-syn 2 incubated under the same solution and environmental conditions as α-syn 1 (average of 4 replicates).

A comparison of the behaviour of the purifications α-syn 1 (squares) and 2 (diamonds) under identical solution and environmental conditions is shown in Figure 8.4. It is clear that by determining new working conditions (α-syn 2, circles) an equivalently reproducible sample is obtained, but the large change in conditions required clearly complicates comparisons that can be made between

the two purifications.

Further purifications of α-syn: α-syn 3 and 4, were purified in different batches according to the same protocol. The first purification, α-syn 3 with stock concentration $\sim$ 5 mg mL^{-1}, was found to produce reproducible growth curves under the same or similar working conditions to α-syn 2 (results not shown). In contrast, α-syn 4, with stock concentration $\sim$ 10.4 mg mL^{-1} was not found to produce reliable and reproducible growth curves under these conditions or under the same conditions as α-syn 1 (results not shown). This suggests that the storage concentration of α-syn affects the aggregation behaviour, as might be expected for a protein whose aggregation behaviour is concentration dependent, and stock concentrations at such a high concentration would not be recommended.

The optimum conditions obtained for α-syn 4 were found to be 5 mM phosphate buffer, temperatures 50°C and above (although temperature was not explored in detail here), 150 mM NaCl and double orbital shaking at 500 rpm for 2.5 minutes every 5 minute cycle. Purification α-syn 4 is used for the majority of the experiments explored here, and it is clear that this is a non-ideal sample. In addition to the high stock concentration this sample was provided as large sample aliquots of 2 mL. Each large aliquot was defrosted to 4°C and immediately separated into individual aliquots of $\sim$ 200 µL either for immediate use or flash frozen in liquid nitrogen and returned to storage at -80°C. However, even after this single freeze-thaw cycle a reduction in reproducibility was observed in growth curves and affects the majority of the experiments performed in the absence of SDS in this research. Both a lower stock concentration and smaller aliquots would have been preferable.

The most ideal methodology to follow is clearly being followed by other in the literature, and involves size exclusion chromatography (SEC) of α-syn immediately prior to each experiment to ensure an entirely monomeric solution. In particular, researchers should avoid if possible any freeze-thaw cycles of α-syn or be aware of the degradation risk.

8.4 Thioflavin T as a aggregation indicator

The most reproducible growth kinetics for the α-syn stock used for the majority of experiments in this research (α-syn 4 as described in Section 2.1) were obtained at

pH 5 (and below), 5 mM phosphate buffer, 50°C (and above), 150mM NaCl, with agitation by double orbital platereader shaking at 500 rpm for 2.5 min in every 5 min cycle between readings in StarWell microplates. The effect of Thioflavin T addition on the resulting growth kinetics was investigated under these growth conditions at 1 mg mL^{-1} α-syn (Figure B.1).

Increasing ThT concentration was found to weakly affect aggregation behaviour, although most changes to growth rate and lag time were within standard deviation (Figure B.2). With increasing ThT concentration the maximum fluorescence increased up to 20 µM ThT while growth rate and lag time were relatively unaffected. Above this there were no further changes in maximum fluorescence (Figure B.3) or lag time, but the growth rate was found to decrease. In contrast, the growth rate by absorbance was increased at 10 µM ThT and above. However, since changes in behaviour were found to be within standard deviation the addition of ThT was considered to have negligible effect on aggregation by fluorescence or absorbance, and a high concentration of ThT was chosen to ensure excess at higher protein concentrations (55 µM).

8.5 Surface activity and agitation

The microplate surface type was found to have a large effect on aggregation propensity and reproducibility in assays with α-syn. For all α-syn purifications aggregation was enhanced by increasing the hydrophobicity of the surface area: changing from non-binding surface coated Corning microplates to uncoated polystyrene Greiner microplates (increasing surface hydrophobicity) and again to Polysorp Nunc StarWell microplates with increased surface area and increased hydrophobicity.

Changing from NBS coated Corning to polystyrene Greiner or StarWell microplates more than halved the lag time. A significant difference between the variability obtained in the hydrophilic versus hydrophobic microplates is also clear in the time uncertainty (the x-axis error bars show the standard deviation in the time to 50% completion) shown in the NBS Corning results in Figure 8.5. In addition, the growth rate was slower in the NBS Corning microplates (Figure B.5).

Changing from Greiner to StarWell microplates was found to further decrease variability between replicate samples. However, the conditions used for this

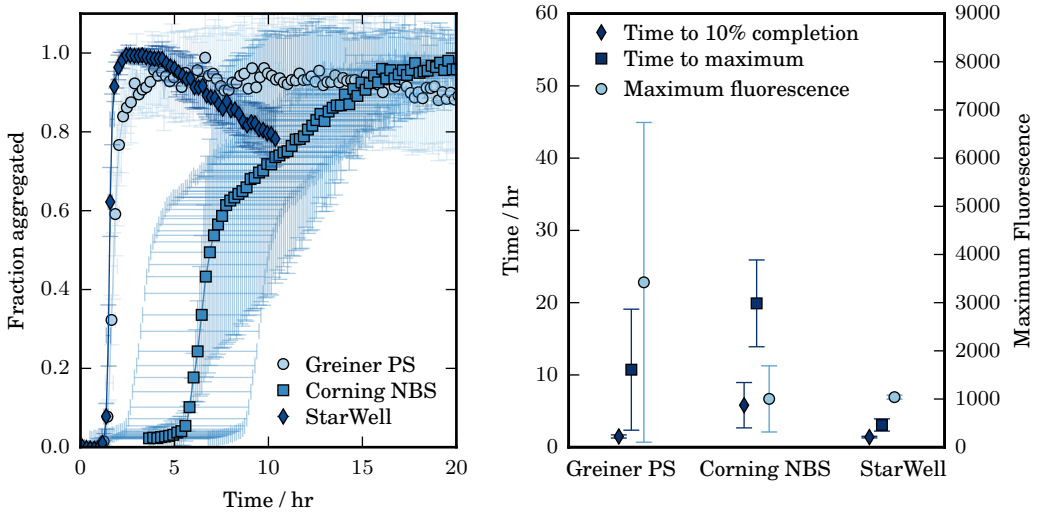

Figure 8.5: Thioflavin T fluorescence and simultaneous absorbance at 600 nm for 1 mg mL^{-1} α-syn 4 at 60°C, pH 3.5, 150 mM NaCl under agitation (double orbital shaking at 600 rpm for 5 min every 6 min) in different microplate types. Average of 8 replicate Greiner samples, 10 replicate Corning samples and 8 replicate StarWell samples. The x-axis error bars show the standard deviation in the time to 50% completion.

comparison were chosen to decrease variability in the samples in the Greiner and NBS Corning microplates, and are less ideal for the StarWell sample, resulting in a loss of material into StarWell corners and a corresponding decrease in fluorescence intensity.

The effect of increasing the surface area to volume ratio was investigated in StarWell microplates (Figure B.4). Increasing the SA:volume ratio (decreasing sample volume) was found to increase aggregation propensity; growth rate was found to increase and lag time to decrease (Figure B.6). This importance of the surfaces for aggregation is consistent with the increased aggregation propensity with the change from hydrophilic to hydrophobic surface type. However, the difference between the results obtained in Greiner versus StarWell microplates are small given the large increase in SA:volume ratio in the StarWell plates. This suggests that the air-water interface and/or increased agitation are more important for driving aggregation than the microplate walls. This is consistent with previous observations about both the air-water interface and agitation in driving α-syn aggregation, as described in Sections 7.3.5 and 7.3.13. The faster plateau approach observed in the StarWell plate results suggests that increased fragmentation, presumably the result of increased agitation, may be the major

difference between the Greiner and StarWell microplates.

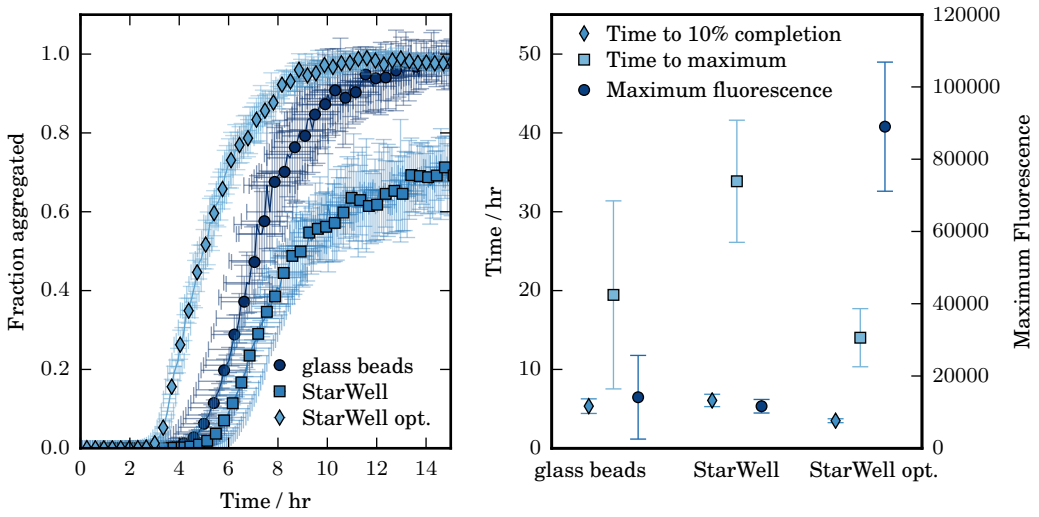

Figure 8.6: Left: Thioflavin T fluorescence for 1 mg mL^{-1} α-syn 4 at 50°C, pH 5, 150 mM NaCl under agitation (double orbital shaking at 300 rpm for 2.5 min every 5 min) in uncoated polystyrene Greiner microplates with a 4 mm glass bead in each well or in Polysorp StarWell Nunc microplates. Also shown are the results for 1 mg mL^{-1} α-syn 4 at 50°C, pH 5, 150 mM NaCl with agitation by double orbital shaking at 600 rpm for 2.5 min every 5 min. Each result is the average of 6 replicates, error bars are standard deviation. Right: The time taken to reach the maximum value, 10% completion and the maximum fluorescence value.

Introducing glass beads to increase agitation is common practice in α-syn aggregation assays, and StarWell plates were used in this investigation as a means to increase agitation and hydrophobic surface area while both reducing the complication of introducing a third surface type and obtaining absorbance measurements.

A comparison of aggregation in uncoated polystyrene Greiner microplates with a 4 mm glass bead in each well and the StarWell microplates in shown in Figure 8.6. Identical conditions in the StarWell plates to those in the Greiner microplates are shown for comparison, along with results from optimal conditions in the StarWell microplates at higher agitation. The results obtained in StarWell plates at optimal conditions have a smaller uncertainty in lag time and similar uncertainty and noise in the plateau region. Even under the less favourable conditions for the StarWell plates shown in Figure 8.6, those identical to the conditions with glass beads, the uncertainty in time is reduced in the StarWell microplates. The reason for the slower plateau approach after around 10 hours in the StarWell sample shown in Figure 8.6 is unknown, but may be the result

of increased precipitation or competition with other aggregate species and is not observed at higher shaking speeds.

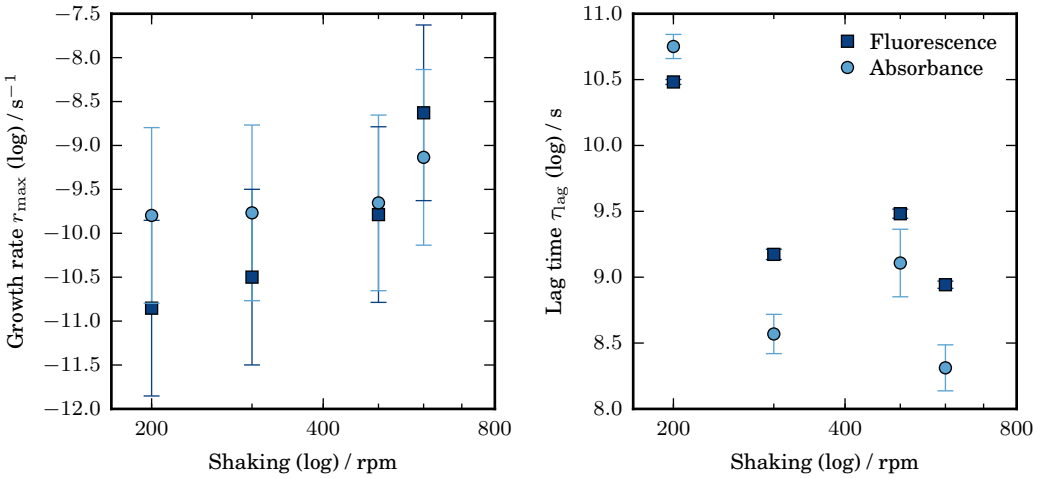

Figure 8.7: Maximum growth rate and associated lag time obtained from linear fits around the maximum growth rate for Thioflavin T fluorescence and absorbance at 600 nm measurements for 1 mg mL^{-1} α-synuclein 4, 50°C, pH 5, 150 mM NaCl with shaking by double orbital microplate shaking at various rates for 2.5 min in every 5 min cycle. StarWell microplates.

The effect of increasing agitation was investigated in StarWell microplates (Figures B.7 and B.8). At high shaking speeds the fluorescence intensity is found to drop off after reaching a maximum, thought to be due to the loss of material into well corners based on observations of the microplates at the end of the assay (the aggregated material is fluorescent due to bound ThT and precipitates, with large visible amounts accumulating in StarWell corners behind the protruding fins). Absorbance values were not affected in the same way but were very noisy and weak in comparison to those obtained for other aggregating proteins. Additionally, the initial absorbance is non-zero and the increase in absorbance occurs in most cases prior to the initial increase in fluorescence intensity, as is clear in the lag times in Figure 8.7. this may indicate the presence of an early non-ThT-binding species.

Increasing agitation was found to enhance aggregation, increasing growth rate and decreasing lag time (although this is within the standard deviation over this range of shaking speeds), as seen in Figure 8.7.

8.6 Effect of solution and environmental conditions in StarWell microplates

In contrast to previous literature results, increasing salt concentration was found to decrease aggregation propensity in StarWell microplates (Figure B.9). As salt concentration was increased from 150 to 500 mM the maximum fluorescence and absorbance were found to decrease (Figure B.10). Changes in growth rate with increasing salt were small, and within standard deviation, as shown in Figure 8.8. Lag time was found to increase with increasing salt up to 500mM by both absorbance and fluorescence. Above 500 mM the effect of increasing salt was diminished.

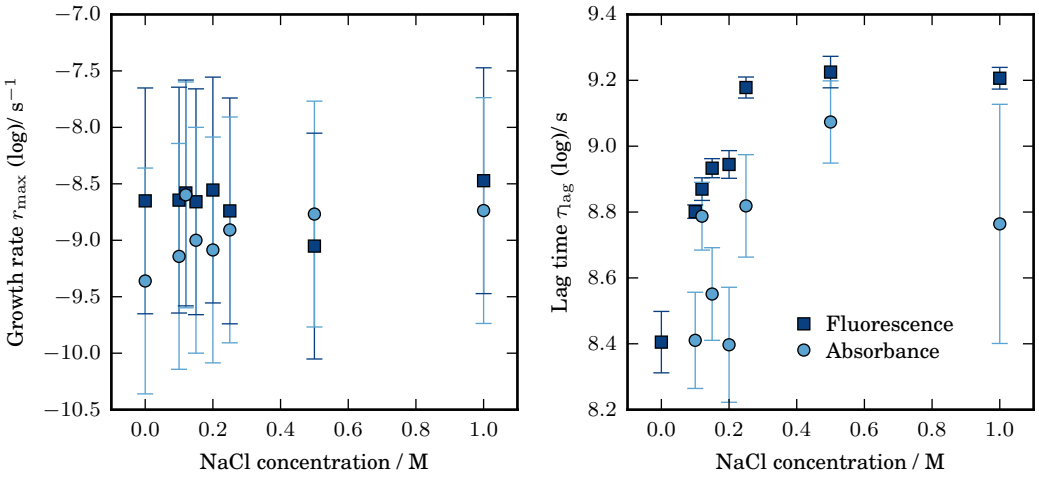

Figure 8.8: Maximum growth rate and associated lag time obtained from linear fits around the maximum growth rate for Thioflavin T fluorescence and absorbance at 600 nm measurements for 1 mg mL^{-1} α-synuclein 4, 50°C, pH 5, with shaking by double orbital microplate shaking at 600 rpm in the presence of various NaCl concentrations. StarWell microplates.

A similar result was obtained for α-syn 2 (purification in 50 mM ammonium acetate, followed by lyophilisation) where the lag time was found to increase from around 2.5 hours in ∼ 18 mM NaCl to around 15 hours in 120 mM NaCl (Figure 8.3). However, for both α-syn 2 and 4 the presence of 100-200 mM salt was found to improve reproducibility of growth curves.

The dramatic change in lag time upon increasing salt from ∼ 14 mM to 100 mM, with little to no change in growth rate, suggests that the effect of increasing salt is to inhibit the nucleation process. This is an unexpected result, and it is

possible that this is related to increased precipitation in the StarWell microplates due to accumulation of aggregated material behind the protruding StarWell fins. In addition, the variability in final fluorescence value was observed to increase with increasing salt, in combination with a decrease in the average obtained value. This may also suggest that an alternative aggregate species might be present. However, no evidence for such a species was observed by TEM. It is believed that the increased charge screening may have resulted in increased precipitation, and due to the microplate design this acted to remove aggregate-prone species from the solution rather than increase the measurable aggregate population.

All subsequent experiments were performed with a lower shaking rate, however, all experiments in StarWell plates are considered to have been affected by this behaviour, and were found to exhibit the reverse of the expected dependency on solution or environmental conditions. These included pH (Figures B.11 and B.12), where decreasing pH below the pI was found to result in an increased lag time with little change in growth rate, and protein concentration (Figure B.13) where growth rate was found to weakly decrease with increasing protein concentration, and lag times were found to increase with protein concentration above 100 µM, despite increases in maximum fluorescence with increasing protein concentration as would be expected (Figure B.14), as shown in Figure 8.9.

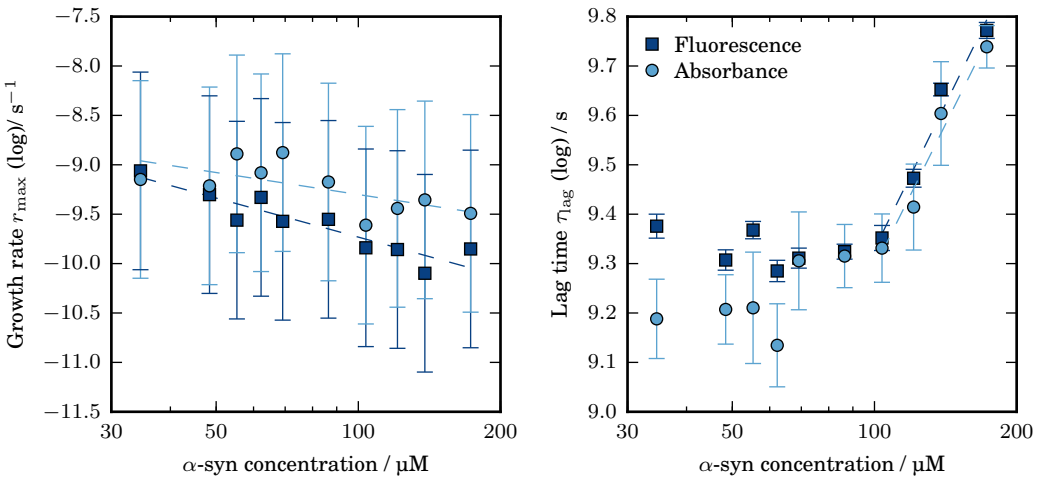

Figure 8.9: Maximum growth rate and associated lag time obtained from linear fits around the maximum growth rate for Thioflavin T fluorescence and absorbance at 600 nm measurements for various α-synuclein 4 concentrations at 50°C, pH 5, 150 mM NaCl with shaking by double orbital microplate shaking at 600 rpm. StarWell microplates.

Since this is thought to be a result of the microplate wells acting as an aggregate sink, and not predicted by any available growth models, these results cannot be used in combination with available growth models to gain insight into the dominant growth processes, but instead are used here for a brief curve-shape analysis.

The initial fluorescence growth was found to be best estimated by an exponential of the form $M(t) \sim \exp(k_1(t - \tau_1))$, in agreement with previous literature results and implying the dominance of secondary growth processes. The parameters obtained from the exponential fit are shown in Figure 8.10 (circles). The initial increase in absorbance was not investigated because of the non-zero initial value and because the absorbance readings were significantly more noisy and less reliable.

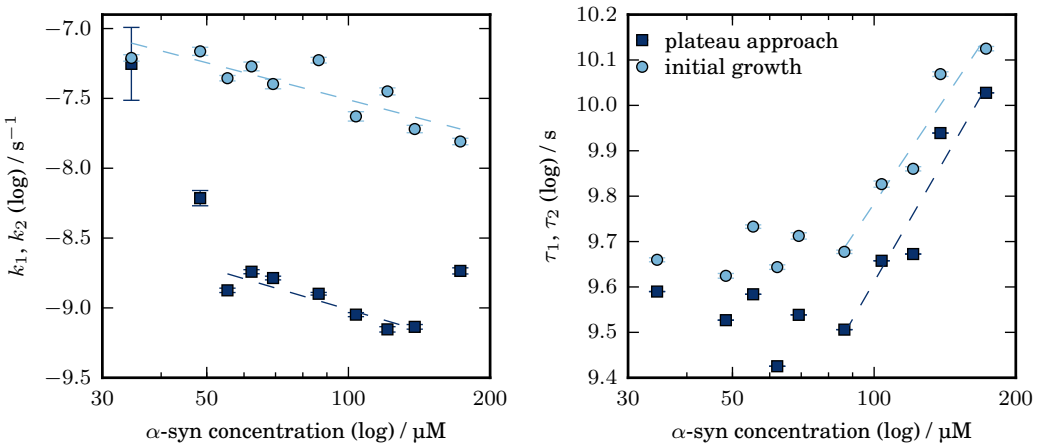

Figure 8.10: Fluorescence data. Apparent growth rates and associated characteristic times obtained from exponential fits to the initial period of growth and the final plateau approach for ThT fluorescence kinetics of α-synuclein (purification 4) concentrations at 50°C, pH 5, 150 mM NaCl with shaking by double orbital microplate shaking at 600 rpm. StarWell microplates.

The plateau approach was found to be roughly exponential, with approximately the form $M(t) \sim M(\infty) - \exp(-k_2(t - \tau_2))$. The parameters obtained from this exponential fit are shown in Figure 8.10. At 0.5 mg mL^{-1} the turn over to the plateau region is very sharp and fluorescence intensity then decreases. Above 1.5 mg mL^{-1} there is a period of slowly increasing fluorescence after the turn-over point rather than a plateau region, suggesting coagulation processes may become important. At concentrations between these points the plateau approach is found to be closer to exponential, clear from the inconsistent behaviour of the growth

rate parameter k_2 at the low and high concentration regions in Figure 8.10.

The apparent growth rates and characteristic times obtained from these fits agree with the growth rate and lag time behaviour obtained from the tangent to the maximum growth rate, and suggest that the process that results in the reversed concentration dependence is dominant throughout the fibrillar growth.

The fluorescence plateau approach was found to be much slower than the initial increase in fluorescence, clear from the separation of the apparent growth rates in Figure 8.10. As a result, the best fit to this data was obtained by the Gompertz function: a special case of the generalised logarithmic function with a slower approach to the right asymptote:

$$M(t) = \exp\left(-\tau_{\mathrm{m}} \mathrm{e}^{-kt}\right) \tag{8.1}$$

where $M(t)$ is the intensity of the curve, here assumed to be proportional to the mass of aggregate, τ_{m} is the characteristic time and k is the apparent growth rate.

A selection of fluorescence growth curves and the fits from the Gompertz function are shown in Figure 8.11. At low and high protein concentrations (0.7 mg mL^{-1} and below, 2 mg mL^{-1} and above) the Gompertz function provided a very good fit to the curve shape. However, at intermediate concentrations the plateau approach was found to be slower than the closest Gompertz curve.

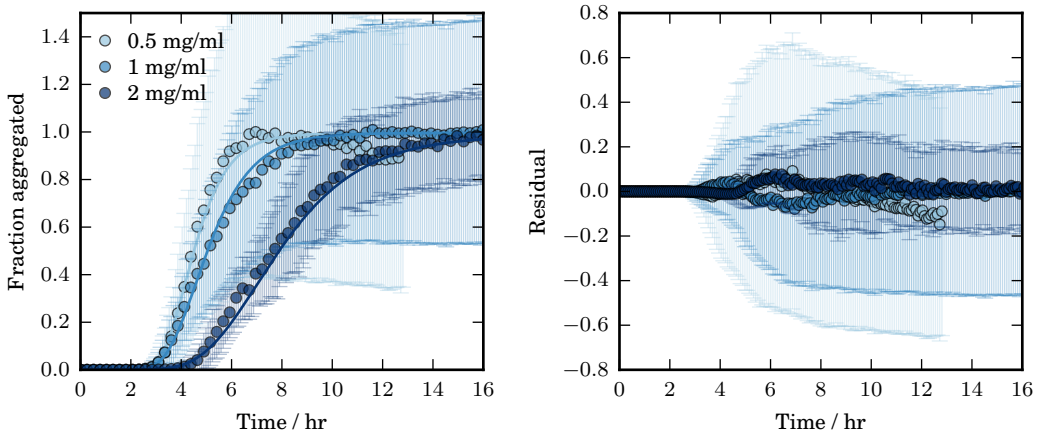

Figure 8.11: Normalised Thioflavin T fluorescence (circles) and corresponding fit to the Gompertz function (solid line in matching shade) for α-synuclein 4 concentrations at 50°C, pH 5, 150 mM NaCl with shaking by double orbital microplate shaking at 600 rpm. StarWell microplates.

The results obtained by absorbance at 600nm were considerably more noisy and the fits are less reliable (Figure B.15), however, the parameters obtained are also shown in Figure 8.12. Growth rate by fluorescence was found to decrease with increasing protein concentration, as previously observed. The characteristic time was also found to decrease with increasing protein concentration. The characteristic time obtained from fluorescence was found to have concentration order dependence of -0.6(2). The parameters obtained from the absorbance data are typically in agreement with those obtained from fluorescence, excluding those for 0.8-1 mg mL^{-1} (55-69 µM).

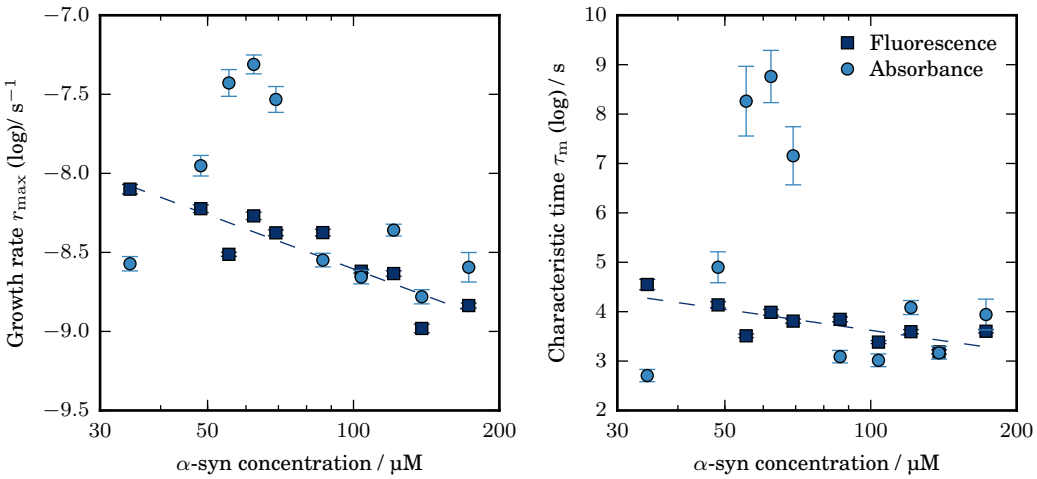

Figure 8.12: Growth rate k and characteristic time τ_m obtained from the closest Gompertz function to the growth curves of α-synuclein 4 concentrations at 50°C, pH 5, 150 mM NaCl with shaking by double orbital microplate shaking at 600 rpm. StarWell microplates.

Interestingly, the reversal in protein concentration dependence was not observed for α-syn 2 incubated in StarWell microplates with shaking at a lower speed (Figure B.16), despite sharing the reversed salt dependence. However, increased agitation was necessary to obtain reproducible growth curves with α-syn 4.

The parameters obtained from the tangent to the maximum growth rate for α-syn 2 incubated at 37°C, pH 5 in 120 mM NaCl with agitation, are shown in Figure 8.13. The growth rate was found to be approximately concentration independent from 0.2-1 mg mL^{-1} (14- - 69 µM), while the lag time was found to decrease with concentration order -0.27(6).

The initial increase in fluorescence was found to be best approximated by

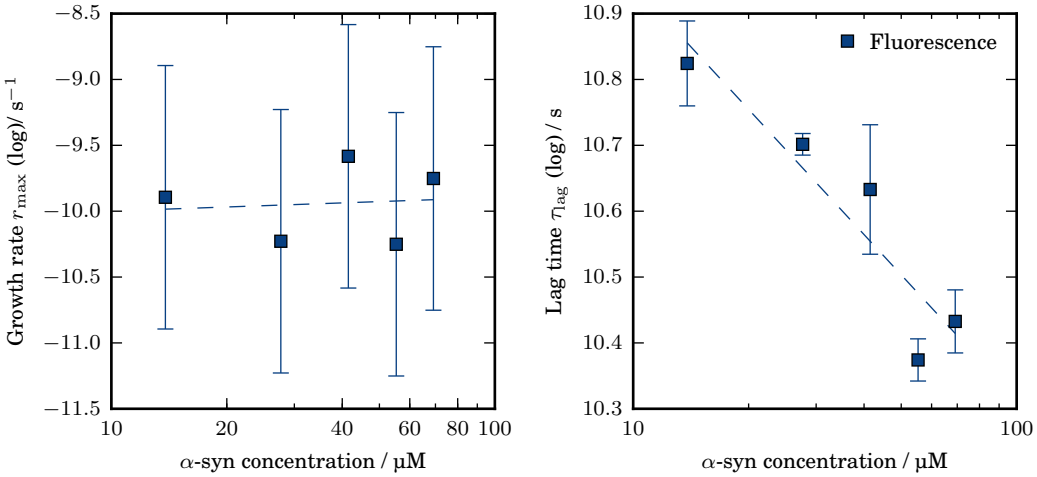

Figure 8.13: Maximum growth rate and associated lag time obtained the best tangent fit to the maximum growth rate for Thioflavin T fluorescence and absorbance at 600 nm measurements for various α-synuclein 2 concentrations at 37°C, pH 5, 120 mM NaCl with shaking by double orbital microplate shaking at 200 rpm. StarWell microplates.

the exponential $M(t) \sim \exp(k_1(t-\tau_1))$. At 0.8 mg mL^{-1} and above the plateau approach was found to be well approximated by the exponential $M(t) \sim M(\infty) - \exp(-k_2(t-\tau_2))$, while at low concentrations (less than 0.8 mg mL^{-1}) the growth curves were very noisy and discontinuous. The parameters obtained from these fits are shown in Figure 8.14.

The apparent growth rate of the initial increase in fluorescence was roughly concentration independent, while the characteristic time was found to decrease with increasing protein concentration at concentration order -0.22(6) (Figure 8.14). For 0.8-1 mg mL^{-1} α-syn the later region of growth was found to have an apparent growth rate decreasing with increasing protein concentration, perhaps suggesting that the growth is also affected by the same process as α-syn 4, but to a lesser degree. The characteristic time was also was found to decrease with increasing protein concentration, with concentration order -0.7(2).

The weak concentration dependence of the characteristic time and lag time is in agreement with previous results obtained for α-syn concentration dependence in the early stages of fibril growth, and was previously attributed to a heterogeneous nucleation mechanism [335]. A conformational conversion step during nucleation has also been proposed, and would be a concentration independent process [3, 321, 327]. However, unless the conformational conversion is very slow, it is unlikely that it would dominate at low α-syn concentrations, especially in the presence of

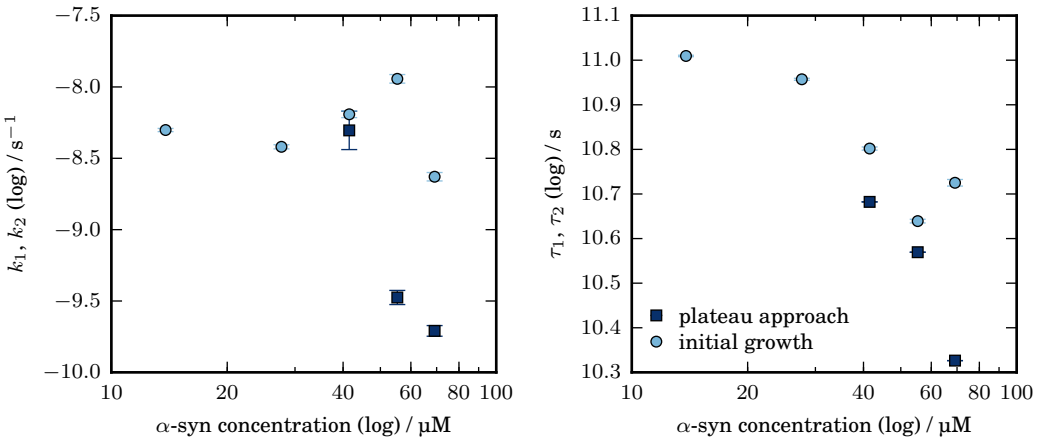

Figure 8.14: Apparent growth rates and associated characteristic times obtained from exponential fits to the initial period of growth and the final plateau approach for ThT fluorescence kinetics of α-synuclein 2 concentrations at 37°C, pH 5, 120 mM NaCl with shaking by double orbital microplate shaking at 200 rpm. StarWell microplates.

secondary growth processes.

The lag time obtained by absorbance was typically found to be shorter than the lag time obtained by fluorescence, suggesting the population of an aggregate species that does not significantly bind ThT at early times. This could be related to a population of a less-β-sheet rich oligomeric species, but the large inherent noise in these readings meant no further analysis was possible at this time.

Also consistent with previous observations [241, 315, 367], the initial growth was found to be exponential in form, and suggests the importance of secondary growth processes. This has been either attributed to fragmentation [300, 367], in particular under increased agitation in the presence of beads [300], or to a secondary nucleation process similar to branching at low pH [300]. It is not possible to determine the secondary growth mechanism that is most dominant from the results obtained here.

8.7 Sodium dodecyl sulphate (SDS)

In the presence of moderate SDS concentrations, α-synuclein aggregates into a curvilinear, worm-like fibrillar species that induces a less intense fluorescence response in ThT compared to fibrils formed in the absence of SDS [298], possibly as a result of their increased α-helical:β-sheet content [42, 233].

The aggregation of α-syn in the presence of membranes, and membrane-like species is thought to proceed along an alternative growth mechanism to fibril formation in the absence of these species, as discussed in Section 7.5. Nucleation is thought to occur in a heterogenous process at the water-lipid (or lipid-like, in this case the water-SDS) interface [42, 335]. As in the presence of lipid SUVs [335], the addition of SDS has been observed to enhance the nucleation process of α-syn [300], presumably through this alternative heterogenous nucleation process. Additionally, Giehm *et al.* [42] proposed that these filaments elongate as a bead-on-string structure, in which individual ellipsoidal SDS-α-syn complexes are bridged by strings of the protein and converted into β-sheet rich aggregates on the surface of SDS-protein micelles [42].

Furthermore, upon agitation worm-like fibrils of α-syn have been observed to convert into a more classical, straight fibril morphology with an increased β-sheet content that appeared to be a more thermodynamically stable species, with conversion from straight to curvilinear fibrils upon addition of SDS being a much slower process [42, 233].

In this section the aggregation of α-syn in the presence of SDS is investigated in more detail to provide insight into the aggregation mechanisms under these conditions.

8.7.1 Reproducibility in SDS assays

Since agitation induces a different aggregate morphology to the curvilinear filaments, and α-syn aggregation in the presence of SDS is found to be reproducible between sample replicates and repeat experiments without agitation, these experiments were performed in uncoated polystyrene Greiner 96-well, flat bottom microplates in quiescent conditions unless otherwise described.

As observed in the absence of SDS, the lag times, growth rates and maximum ThT fluorescence were dependent upon the α-syn purification. In all cases the shape of the growth curves was similar, and similar in shape to those previously obtained by Giehm *et al* [42]. However, the growth rate was found to vary noticeably between α-syn purifications, as shown in Figure 8.15.

Results were sensitive to solution conditions and buffer, as shown in Figure 8.16. How much of this difference can be attributed to change in pH is unclear. The initial solution pH in each case is adjusted to pH 7.4 before the

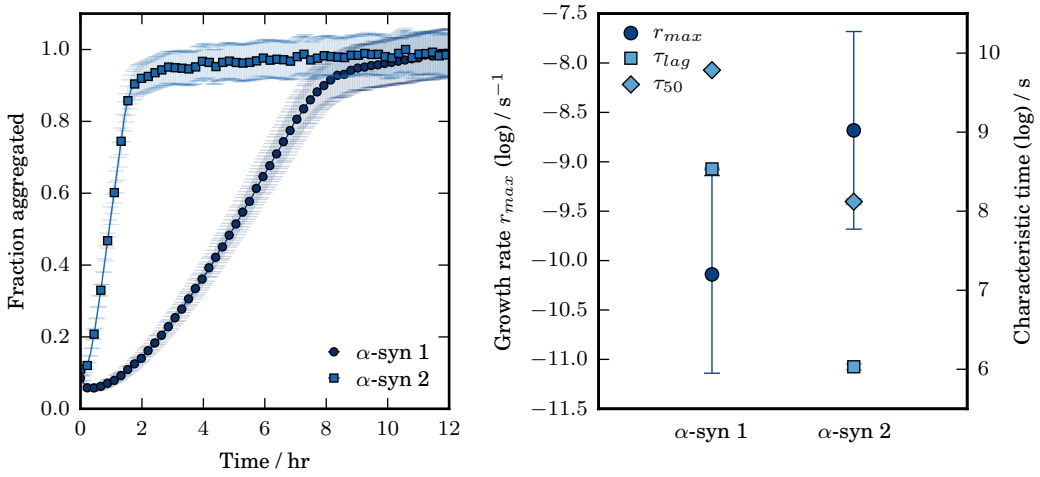

Figure 8.15: Normalised thioflavin T fluorescence (left) and the growth parameters obtained from the tangent to the maximum growth rate for 1 mg mL^{-1} α-syn purifications 1 (stock solution Tris-HCl) and 2 (lyophilised from ammonium acetate) in identical buffer conditions (∼ 3 mM Tris-HCl), incubated in 0.5 mM SDS at 37°C, pH 7.4, 120 mM NaCl.

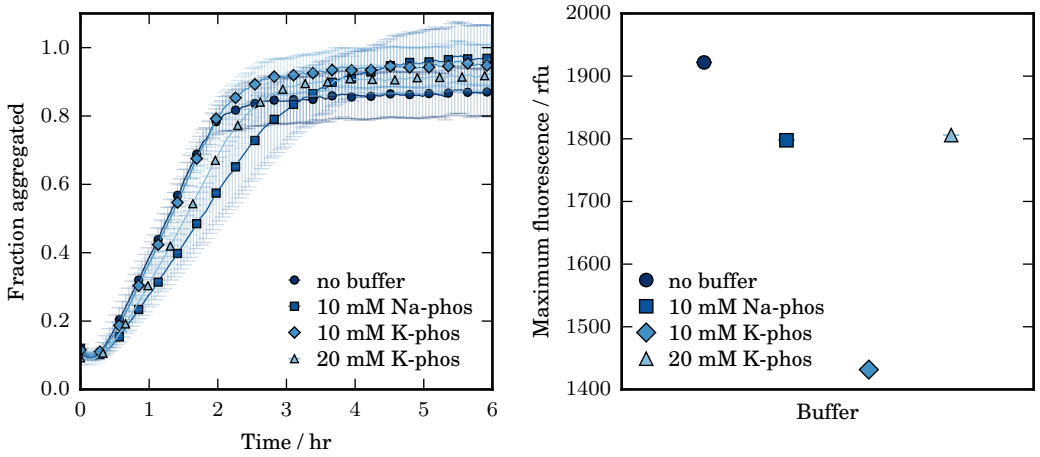

Figure 8.16: Normalised thioflavin T fluorescence (left) and the maximum fluorescence value obtained for 1 mg mL^{-1} α-syn 2 in the presence of different buffer solutions, incubated in 0.5 mM SDS at 37°C, pH 7.4, 120 mM NaCl.

addition of SDS, which is known to lower pH. It is assumed that where the SDS concentration is kept equal that the solution pH will be equivalent between samples. It is difficult to determine the pH of the samples in these experiments due to the rapid nature of the growth process. SDS was added immediately before microplates were placed into the reader, typically by means of a multichannel pipette. In solutions of 10 mM potassium phosphate buffer initially at pH 7.4

the final solution pH after aggregation was pH 6.7. In subsequent experiments, which were performed either in 20 mM potassium phosphate (for α-syn 2, since the final fluorescence value obtained was higher, as seen in Figure 8.16) or 5 mM phosphate buffer (α-syn 4), the final pH value was found to be in the range 6.7-7.

8.7.2 Effect of SDS concentration

Increasing SDS concentration up to around 0.5 mM SDS was found to enhance aggregation of 1 mg mL^{-1} α-syn 4 (Figure B.17). Increasing concentrations further, above around 0.75 mM were found to inhibit aggregation. Absorbance readings were typically much less reproducible (as seen by the error bars in Figure B.17 which represent the standard deviation).

The maximum fluorescence value and the growth parameters provide different measures of the optimum SDS concentration for inducing aggregation, as seen in Figures 8.17 and 8.18. The maximum fluorescence intensity was obtained for SDS concentrations in the range 0.75-1.0 mM SDS, while growth rate was found to increase up to around 0.4-0.5 mM SDS and to decrease above 0.5 mM, and lag time was found to increase above 0.75 mM SDS.

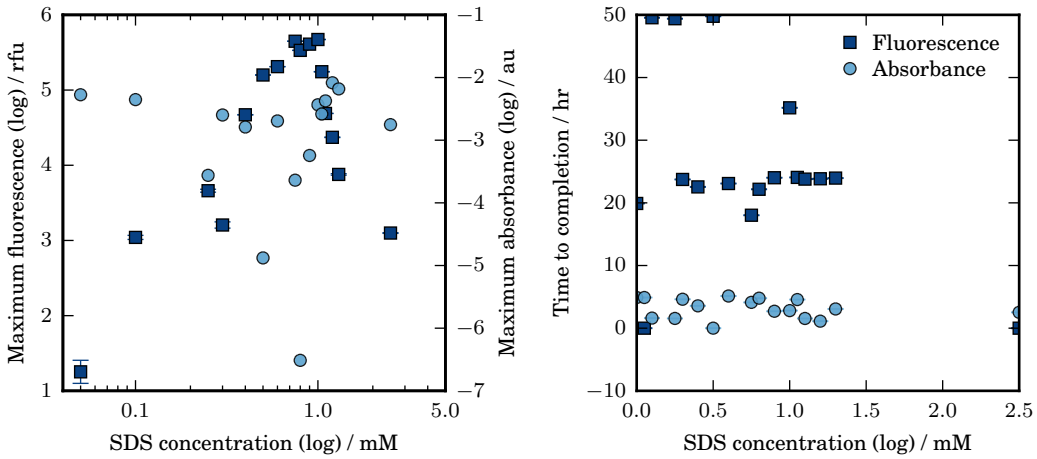

Figure 8.17: Left: Maximum Thioflavin T (ThT) fluorescence and absorbance at 600 nm obtained for 1 mg mL^{-1} α-syn 4 in various SDS concentrations at 50°C, pH 7.4, 120 mM NaCl. Right: The time taken to reach the maximum value.

The optimal range (0.5-0.75 mM) is in agreement with previous observations about α-syn aggregation [42, 338], and was proposed by Giehm *et al.* [42] to be related to the formation of mixed α-syn and SDS micelles where ∼ 12 SDS

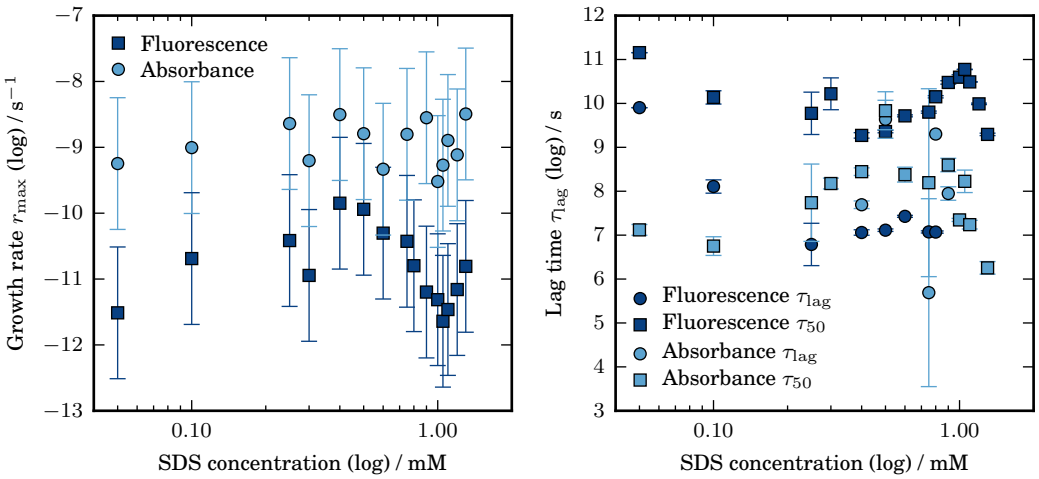

Figure 8.18: Maximum growth rate and associated characteristic time obtained (from tangent to linear region) from Thioflavin T fluorescence and simultaneous absorbance (600 nm) measurements for 1 mg mL^{-1} α-syn 4 in various SDS concentrations at 50°C, pH 7.4, 120 mM NaCl.

monomers bind to each α-syn monomer [42]. However, in the optimal range determined here (0.5-0.75 mM) the SDS:α-syn ratio varies from around 7:1 to 11:1.

The only notable change in absorbance behaviour was in lag time or time to 50% completion (τ_{50}), found to decrease steeply above 0.8 mM SDS, above the optimal SDS concentration, as seen in Figure 8.18. A similar change was observed in the fluorescence behaviour above 1 mM SDS, with a decrease in τ_{50} to approximately the lowest previous value and a corresponding increase in growth rate, although growth rate did not return to the maximum growth rate observed around 0.4-0.5 mM SDS. These results suggest a more complicated relation between the concentration of SDS and its affect on α-syn concentration than the optimal binding stoichometry previously proposed (where a clear minimum lag time coinciding with a maximum growth rate would be expected at the optimum concentration), which might be related to the ability of aggregates to form or elongate on the surface of micelles from a locally enhanced protein concentration as well as from micelle-bound α-syn. At higher SDS concentrations (2.5 mM SDS and above) no aggregation was observed over the experimental timescale.

To investigate the proposed 12:1 optimal ratio, SDS and protein concentration were varied under the condition that the ratio remained the same (Figure B.18). The maximum fluorescence value was found to be approximately linearly related

to the concentration of protein and SDS below 100 µM α-syn (Figure B.19). However, above this the concentration dependency begins to decrease with increasing protein concentration.

A small increase in growth rate and decrease in lag time was observed at the highest α-syn and SDS concentrations, but otherwise growth rate and characteristic times were roughly concentration independent within standard deviation, as seen in Figure 8.19.

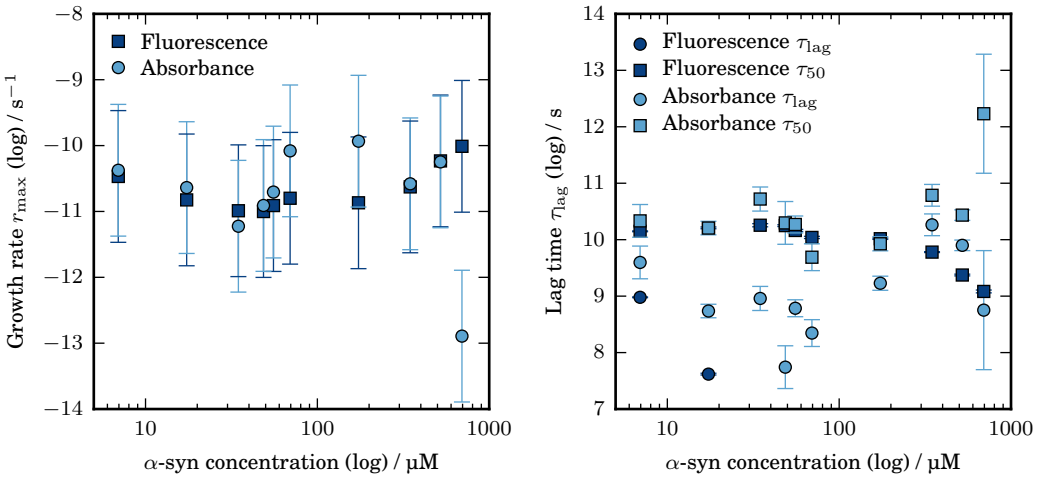

Figure 8.19: Maximum growth rate and associated characteristic time obtained (from tangent to linear region) from Thioflavin T fluorescence and simultaneous absorbance (600 nm) measurements for fixed α-syn 2 and SDS ratio (1:12) at 37°C, pH 7.4 (20 mM potassium phosphate buffer), 120 mM NaCl.

8.7.3 Effect of protein concentration and temperature

The effect of protein concentration was investigated at a range of temperatures for α-syn 4 and for the three different α-syn purifications (1,2 and 4) at constant SDS concentration. In all cases, increasing protein concentration was found to enhance aggregation, increasing the growth rate, decreasing lag time or τ_{50}, and increasing maximum ThT fluorescence.

The normalised growth curves obtained for increasing protein concentration at 40°C are shown in Figure 8.20. These results, along with the growth curves obtained at 30, 35, 45 and 50°C can also be found in Appendix B (Figures B.20, B.21, B.22, B.23 and B.24). As with the previous results at high temperature and low pH, absorbance readings were found to be considerably

erratic, and although they have been included, are much less reliable.

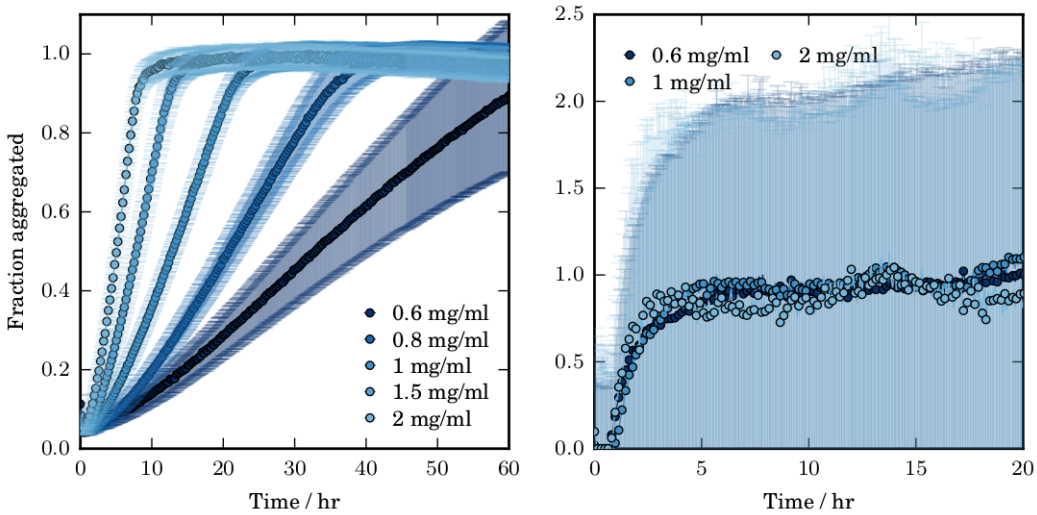

Figure 8.20: Thioflavin T fluorescence and simultaneous absorbance at 600 nm for α-syn 4 in 0.5 mM SDS at 40°C, 5 mM phosphate buffer, pH 7.4, 120 mM NaCl.

As temperature increases an increasingly large 'flick' was also observed at the beginning of the growth, where high initial fluorescence drops to a lower value before increasing again. Similar flicks were also observed in absorbance readings. Since the size of this feature is correlated with temperature, and microplates are not equilibrated before readings begin, this is thought to be a heating effect. Given the rapid nature of the aggregation, it is likely that aggregation begins immediately upon addition of SDS to the protein solution, and that heating promotes dissociation of some of these early species until the sample is equilibrated. This region of the fluorescence curve is therefore disregarded from further analysis.

The experimental method was designed to capture as much of the growth as possible. Allowing for a longer time period of incubation at room temperature in the presence of SDS before reading at a higher temperature resulted in a much larger initial fluorescence value and a minimum value at a higher fluorescence intensity. As a result, SDS was added immediately prior to addition of the plate to the reader by multichannel pipette.

At 30°C and 0.5 mM SDS (Figure B.20) aggregation proceeded slowly from a minimum fluorescence value at time zero. At no point was an extended lag phase observed. Fluorescence intensity was found either to increase from the

beginning of the experiment or not observed to increase over the time course of the experiment. Aggregation of 1 mg mL^{-1} (70 µM) α-syn 4 was not observed over the time course of this experiment (∼ 75 hours). At 35°C (Figure B.21) aggregation was found to proceed much more rapidly, as shown in Figure 8.21, with 1 mg mL^{-1} α-syn reaching a plateau region after around 30 hours and aggregation observed for concentrations of 0.5 mg mL^{-1} and above. Aggregation was further promoted by increasing temperature to 45°C but increasing temperature further was not found to enhance aggregation. In all cases fluorescence intensity was found to increase continuously from a minimum value or not at all (for example at low protein concentrations <1, <0.4 and <0.2 mg mL^{-1} at 30, 35 and 45°C respectively) over the experimental timescale (50-70 hours).

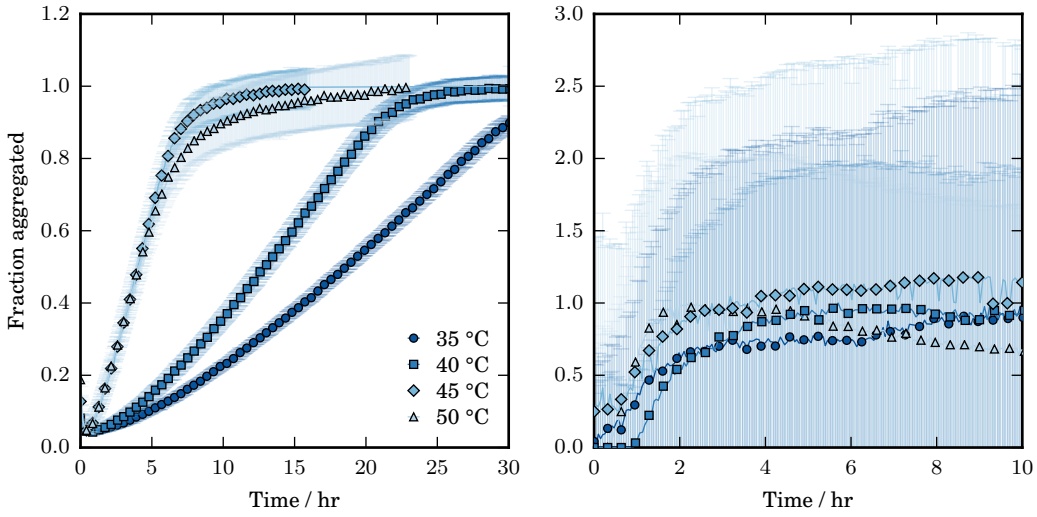

Figure 8.21: Thioflavin T fluorescence and simultaneous absorbance at 600 nm for 1 mg mL^{-1} α-syn 4 in 0.5 mM SDS at various temperatures, 5 mM phosphate buffer, pH 7.4, 120 mM NaCl.

Maximum ThT fluorescence was found to increase with increasing protein concentration at all temperatures, as shown in Figure 8.22. The relationship between the maximum fluorescence value and protein concentration is initially linear but is found to decrease with increasing protein concentration at each temperature. This is particularly obvious at the high protein concentrations investigated at 30°C. Increasing temperature was found to decrease the maximum fluorescence value obtained. ThT binding and intensity are not known to be affected by temperature in this range, and this may suggest a decrease in fibrillar mass, suggesting that the fibrillar species formed are not thermodynamically stable. This would be

consistent with the previous observation about transformation to a linear, high β-content species upon agitation but much slower reversion to worm-like fibrils [42].

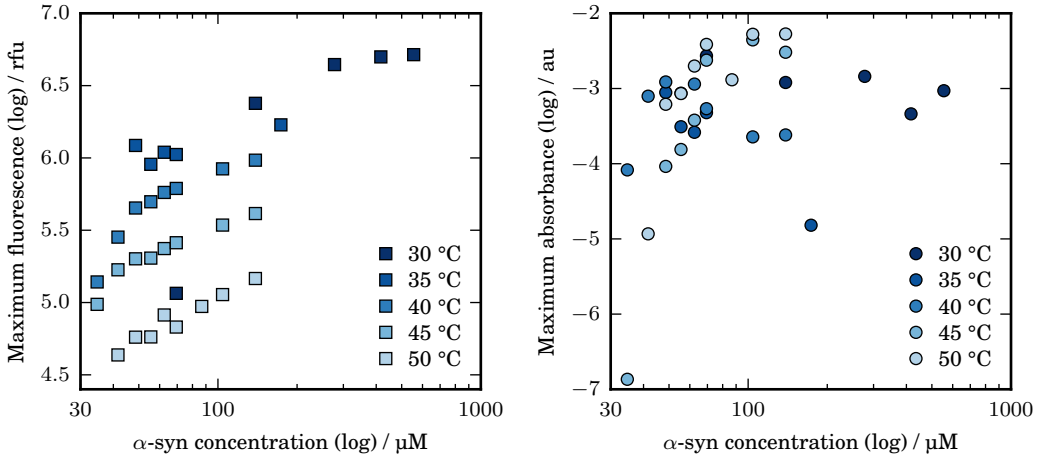

Figure 8.22: Maximum Thioflavin T (ThT) fluorescence (left) and absorbance at 600 nm (right) obtained for α-syn 4 in 0.5 mM SDS at various temperatures, 5 mM phosphate buffer, pH 7.4, 120 mM NaCl. Error bars representing standard deviation are smaller than data points for fluorescence, but have been deliberately removed for absorbance, the absorbance readings are not considered reliable.

The curve shape of the growth curves is not symmetrically sigmoidal and cannot be approximated by the generalised logistic function. It does not conform to the expected curve shapes of any current fibrillar growth model. The initial increase in fluorescence proceeds more slowly than the plateau approach following the inflection point, and the inflection point occurs at a later time than the system reaching 50% of its total fluorescence intensity. When compared to the closest generalised logistic function both the initial increase in fluorescence and the plateau approach deviate from the closest curve, with stronger deviation at the plateau approach.

Below 45°C the plateau approach is more rapid than the closest generalised logistic function, while at 45°C and above the plateau approach is much slower and exhibits an early turn-over point (for example at around 4 hours for 2 mg mL^{-1} at 45°C) followed by a slowly creeping increase in fluorescence to a final maximum value (reached at around 15 hours for 2 mg mL^{-1} at 45°C). The slow plateau approach is even more evident at 50°C, as seen in Figure 8.21.

The growth rates obtained from a tangent fit to the maximum growth rate are

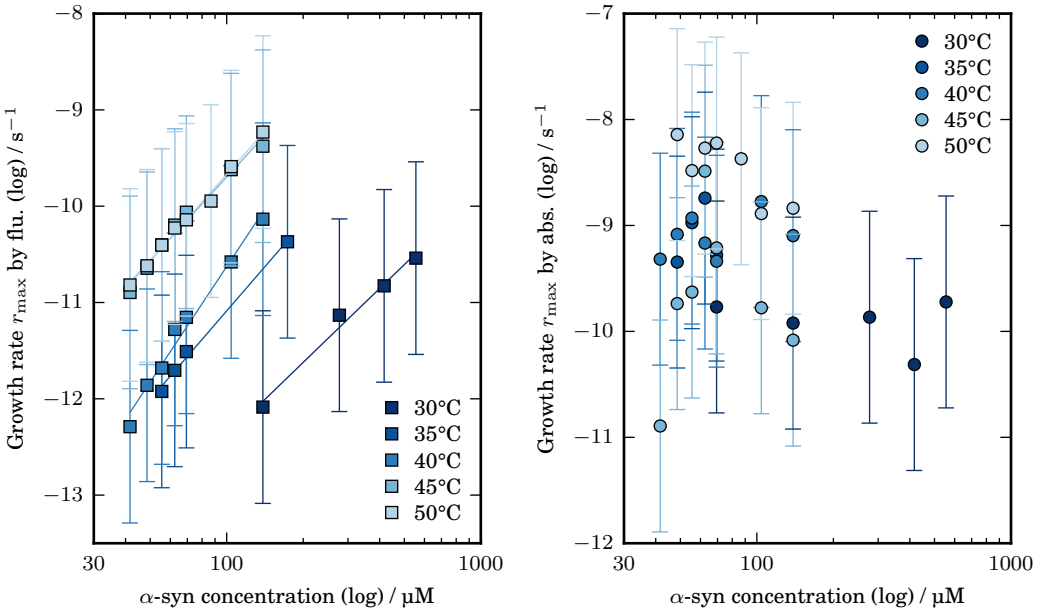

Figure 8.23: Maximum growth rate obtained (from tangent to linear region) from Thioflavin T fluorescence and simultaneous absorbance (600 nm) measurements for α-syn 4 in 0.5 mM SDS incubated at various temperatures, 5 mM phosphate buffer, pH 7.4, 120 mM NaCl.

shown in Figure 8.23. As previously noted, increase in temperature above 45°C was not found to promote aggregation, and the growth rate is approximately equal at 45 and 50°C at all protein concentrations investigated (0.5-2 mg mL^{-1}). At all temperatures the fluorescence growth rate was found to increase with increasing protein concentration. The concentration order dependence of the maximum growth rate, γ, was determined to be 1.1(1), 1.33(7), 1.7(1), 1.25(8) and 1.30(4) for temperatures 30, 35, 40, 45 and 50°C respectively. The uncertainty shown in Figure 8.23 is considered to be largely underestimated for the absorbance readings, and these are not considered reliable. However, the growth rates obtained from absorbance readings are consistently smaller than those obtained from fluorescence measurements, suggesting that the formation of small β-rich species that contribute to the fluorescence response is more rapid than the elongation of these species to the order of 600 nm, the wavelength of the absorbance measurement.

The lag time τ_{lag} estimated from the best fit tangent to the maximum growth rate is shown in Figure 8.24. In all cases the lag time was found to decrease with increasing protein concentration and to decrease with increasing temperature.

The concentration order dependence of τ_{lag} was determined to be -0.56(6),

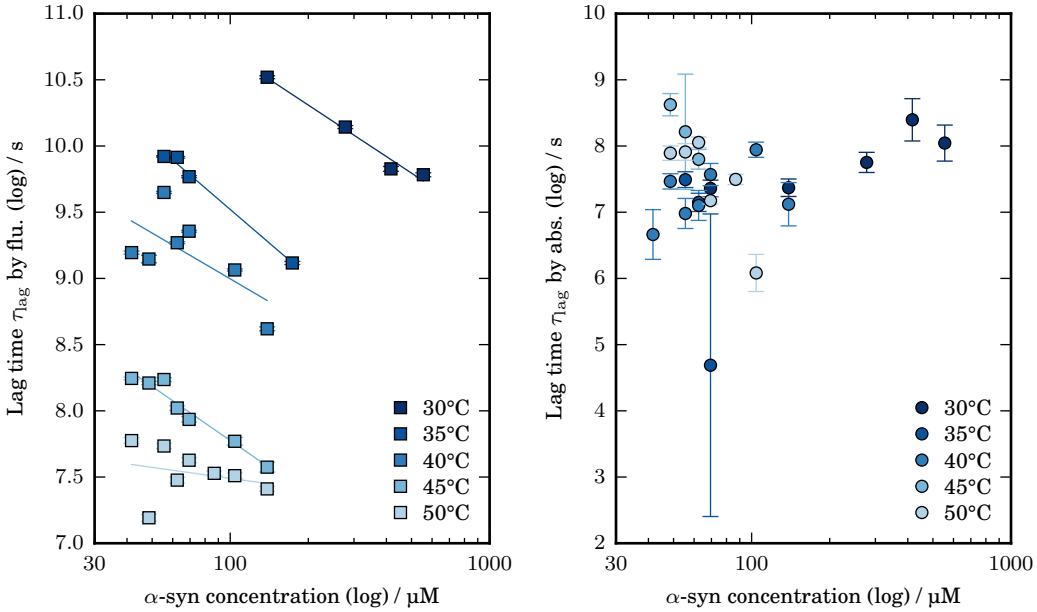

Figure 8.24: Lag time obtained (from the tangent to maximum growth rate) from Thioflavin T fluorescence (left) and simultaneous absorbance at 600 nm measurements (right) for α-syn 4 in 0.5 mM SDS incubated at various temperatures, 5 mM phosphate buffer, pH 7.4, 120 mM NaCl.

-0.73(5), -0.5(2), -0.59(6), -0.1(2) for temperatures 30, 35, 40, 45 and 50°C respectively. In most cases the characteristic times obtained from absorbance measurements were found to be shorter than those obtained by fluorescence, suggesting the population of a species with little to no binding affinity for ThT prior to the formation of β-rich species.

At lower temperatures (<45°C) up to 80% of the initial region of the growth curve was found to be well approximated by a simple polynomial of the form $M(t) \sim At^{k_p} + y_1$, where A is a constant, k_p is the apparent growth rate and y_1 is the initial intensity. A comparison of the curve shape in this region with both the closest polynomial and exponential functions is shown in Figure 8.25.

At all temperatures the majority of the growth curves conformed well to the polynomial approximation up to the inflection point, and the parameters obtained are shown in Figure 8.26. The constant A was not allowed to vary with protein concentration and k_p was found to be in the range 1.36-1.74 and to have weak concentration dependence of order 0.082(6), 0.116(8), 0.137(7), 0.124(9), 0.114(4) for temperatures 30, 35, 40, 45 and 50°C respectively.

Similarly weak results for the concentration dependence of k_p were obtained

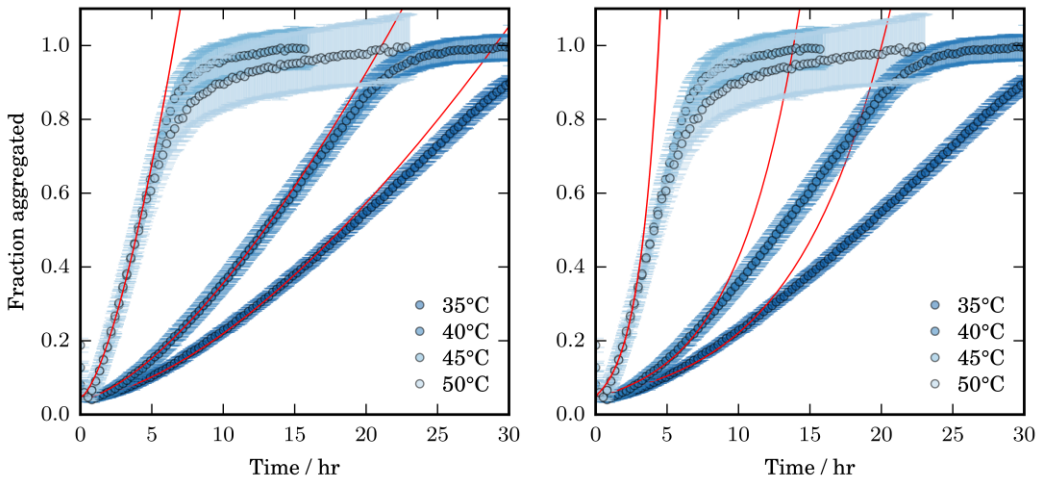

Figure 8.25: Fits to the initial increase in Thioflavin T fluorescence for 1 mg mL^{-1} α-syn 4 in 0.5 mM SDS incubated at various temperatures, 5 mM phosphate buffer, pH 7.4, 120 mM NaCl. Left: a polynomial fit ($M(t) = At^{k_P} + y_1$). Right: an exponential fit ($M(t) \sim \exp(k_1(t - \tau_1))$).

where A varied with protein concentration (Figure B.29) and were in the range 0.051(9)-0.30(3). In this case, the parameter A was found to increase with protein concentration below 40°C ($\gamma = 0.50(7), 1.2(3)$ for 30 and 35°C respectively) and to decrease with protein concentration at 40°C and above ($\gamma = -0.1(2), -1.5(2), -2.8(5)$ for 40, 45 and 50°C respectively).

The time to 50% completion, τ_{50}, was estimated from the polynomial fit and is shown in Figure 8.26. This parameter was found to decrease with increasing protein concentration and temperature up to 45°C, as observed for lag time in Figure 8.24. However, the concentration order dependence of τ_{50} was higher, at -0.91(7), -1.2(1), -1.45(8), -1.2(1) and -1.11(4) for temperatures 30, 35, 40, 45 and 50°C respectively, suggesting that different growth processes are dominant at early (where the polynomial fit applies) and later times (where the maximum growth rate is observed).

In most cases the last 30-40% of the growth curve (at and above the maximum growth rate) is found to be well approximated by a single exponential of the form $M(t) \sim M(\infty) - \exp(-k_2(t - \tau_2))$. However, as temperature or protein concentration increases the plateau approach begins to deviate from this shape. At high protein concentrations the plateau approach is initially rapid and exhibits a turn-over point at around 90% completion followed by a very slow continued creep upwards in fluorescence, as described previously. At higher temperatures

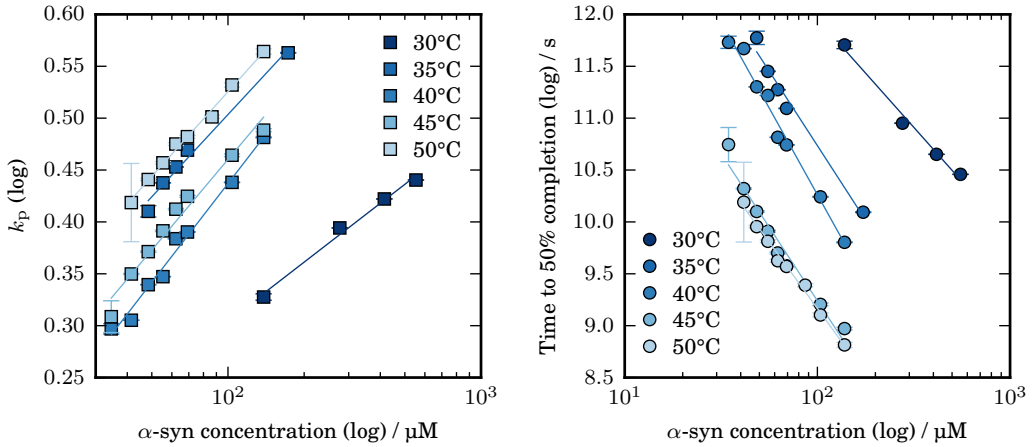

Figure 8.26: Growth parameters obtained from a polynomial fit ($M(t) = At^{k_P} + y_1$) to the initial increase in Thioflavin T fluorescence for α-syn 4 in 0.5 mM SDS incubated at various temperatures, 5 mM phosphate buffer, pH 7.4, 120 mM NaCl. The time to 50% completion is calculated from the curve of best fit.

the observation of this slow plateau approach region is observed for lower protein concentrations. For example, it is observed for 0.9 mg mL^{-1} and above at 50°C, 1.5 mg mL^{-1} and above at 45°C, 2 mg mL^{-1} (and presumably above) at 40°C and only observed at 8 mg mL^{-1} (and presumably above) at 30°C.

The parameters obtained from this fit are shown in Figure 8.27. The apparent growth rate in the plateau region, k_2, was found to have concentration order dependence 0.8(3), 1.04(5), 1.2(1), 0.74(4), 0.7(1) while the characteristic time τ_2 was found to have concentration order dependence -1.00(6), -1.28(6), -1.62(8), -1.3(1), -1.8(3) at temperature 30, 35, 40, 45 or 50°C respectively. The parameters were also correlated with $k_1 \sim \tau_1^{-x}$ and x in the range 0.9-1.0.

The purifications α-syn 1 (Tris-HCl buffered) and 2 (lyophilised from ammonium acetate) were found to exhibit similar protein concentration behaviour: diminishing dependence of maximum fluorescence as concentration increases (Figures B.25 and B.26 respectively), increasing growth rate and decreasing characteristic time. Similar to the results shown for α-syn 4, the growth rates for α-syn 1 and 2 were determined to have concentration order 1.30(8), 1.4(1), τ_{lag} concentration orders were determined to be -1.7(6), -1.14(5) and τ_{50} concentration order was found to be -1.16(5) and -1.3(1) respectively (Figures B.27 and B.28). Both experiments were performed at 37°C.

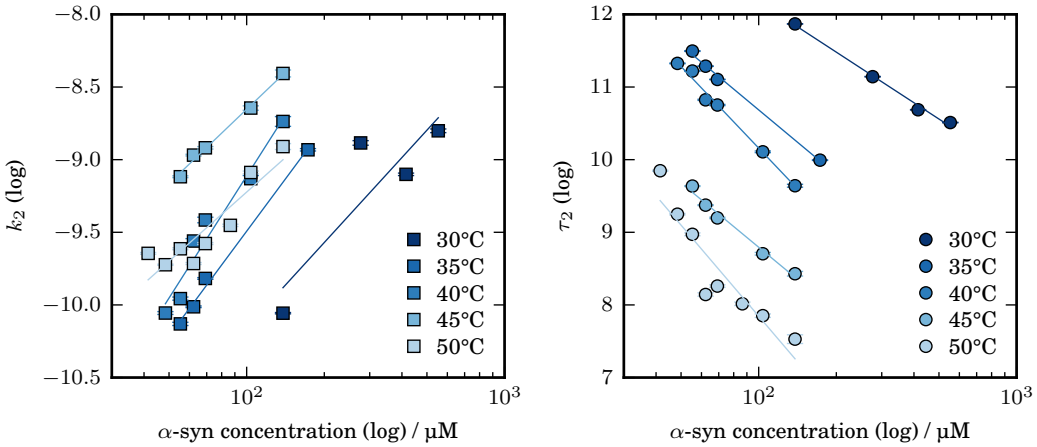

Figure 8.27: Growth parameters obtained from a single exponential fit ($M(t) \sim M(\infty) - \exp(-k_2(t-\tau_2))$) to the plateau approach of Thioflavin T fluorescence for α-syn 4 in 0.5 mM SDS incubated at various temperatures, 5 mM phosphate buffer, pH 7.4, 120 mM NaCl.

At all the temperatures investigated above, and for the different α-syn purifications, similarly shaped growth curves with similar concentration dependent trends were obtained. The growth curve shape obtained is unusual, having a slower initial growth period followed by a late inflection point and more rapid plateau approach (see Figure 8.26).

Unusually for protein fibrillation *in vitro*, where it is becoming more widely accepted that aggregation is typically dominated by secondary growth processes, the initial growth region was found to more closely represent a polynomial than an exponential increase. This is more reminiscent of traditional nucleation-dominated growth. The polynomial increase at early times was found to have weaker time order (t^x, x =1.3457(1)-1.758(5)) than any of the currently described homogeneous nucleation-like events for protein aggregation (all of which predict t^2 or above), and is thought to reflect a heterogenous nucleation process in or on the surface of SDS-α-syn micelle-like aggregates where the α-syn-bound SDS facilitates the formation of α-syn aggregates by inducing structural change.

This process is dependent upon both the protein and SDS concentration, and might be expected to exhibit Michaelis-Menten enzyme reaction-like kinetics [370]. It was observed that by keeping the ratio of these species constant the growth parameters became concentration independent (Section 8.7.2). However, the maximum growth rates shown in Figure 8.23 are estimated from the linear region of the growth curves and are found to have stronger protein concentration

dependence than expected in a Michaelis-Menten system [370] (estimated to be in the range 1.1-1.7).

In most cases the plateau approach was well estimated by a single exponential, and suggests that the aggregate species most likely elongate by monomer (or oligomer) addition. The maximum growth rate, associated with this region of growth, was also found to have concentration dependence consistent with elongation via monomer addition, with concentration dependence $k \propto m_{\mathrm{tot}}^{\gamma}$, γ =0.7(1)-1.2(1).

As temperature and protein concentration increased the plateau approach also began to exhibit a very slow upwards creep to a final fluorescence value, suggesting that coagulation may be a dominant growth process at later times under these conditions, potentially as the likelihood of end-to-end meeting increases with increasing mobility and concentration. This may also be related to the type of species formed at higher temperatures. As temperature increased the fluorescence maximum was found to decrease. Attempts to measure the mass of fibrils in this system were unreliable, and were unable to confirm whether or not this relates to a decrease in fibril mass fraction. However, no decrease was observed in absorbance with temperature, and this makes it more likely that the aggregate population has less affinity for ThT. If a larger population of smaller aggregate species is formed under these conditions it is more likely that coagulation processes would become more important as the monomer population is depleted, and earlier increases in absorbance relative to fluorescence provide some evidence for the existence of such a species in this system.

The temperature behaviour of the apparent growth rates obtained from the exponential fits to the initial increase in fluorescence and the plateau approach are shown in Figure 8.28. It is clear that the growth rates vary approximately linearly with temperature, and activation energies have been estimated from the Arrhenius equation. The estimated energies were not found to depend upon protein concentration in the range investigated and ranged from 38(10)-49(7) k_BT for the initial increase in fluorescence and 30(2)-36(5) k_BT for the plateau approach. These values are similar to those that have been reported for other aggregating protein systems [47, 48, 77, 201].

The different activation energies for the initial growth and plateau approach are consistent with different growth mechanisms being dominant in these regions,

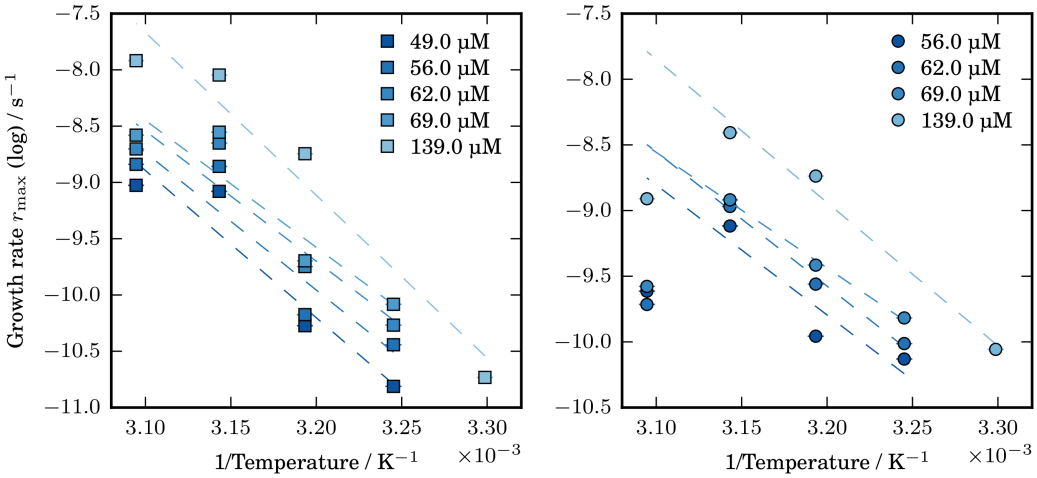

Figure 8.28: The temperature dependence of the initial growth rate (left) and plateau approach (right) (obtained from exponential fits) for α-syn 4 in 0.5 mM SDS incubated at various protein concentration and temperatures, 5 mM phosphate buffer, pH 7.4, 120 mM NaCl. Results at 50°C have been excluded from the fits to the plateau approach.

thought to be heterogenous nucleation and growth by monomer (or oligomer) addition respectively. The higher activation energy for the initial increase in fluorescence may be related to substantial conformational changes that occur in the formation of the initial β-rich species. If this is the case, the lower energy associated with the dominant processes at later times is consistent with elongation by subsequent joining of β-rich oligomers, as proposed by Giehm *et al.* [42], rather than monomer that presumably must undergo a similar structural transformation.

8.7.4 Effect of salt concentration

The effect of salt concentration on aggregation in the presence of 0.5 mM SDS was investigated at 50°C, and is shown in Figure 8.29. As well as the growth parameters, the shape of the growth curves was altered by increasing salt. In the absence of additional salt (at ∼ 14 mM NaCl) aggregation was still observed but was significantly slower, with a much lower final fluorescence value (data not shown). At 25 mM NaCl and above aggregation was dramatically enhanced.

As salt concentration increased the growth rate at early times was found to decrease and the plateau region was reached at increasingly later times, as seen in Figure 8.29. However, the maximum fluorescence was found to increase (Figure B.30), suggesting an increase in total aggregate mass.

Maximum fluorescence was observed to plateau between around 0.1-0.3 M NaCl (Figure B.30), and above this was found to increase further, coinciding with the considerably slower initial growth region as seen in Figure 8.29. Absorbance readings at 600 nm were less affected by changes in salt concentration and are less reliable, as previously observed.

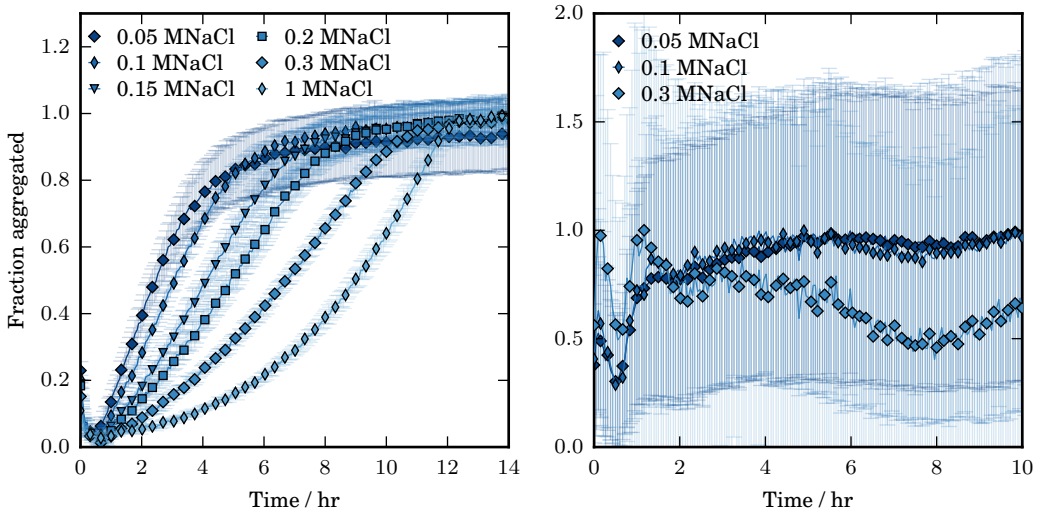

Figure 8.29: Thioflavin T fluorescence and simultaneous absorbance at 600 nm for 1 mg mL^{-1} α-syn 4 in 0.5 mM SDS at 50°C, pH 7.4, at various NaCl concentrations.

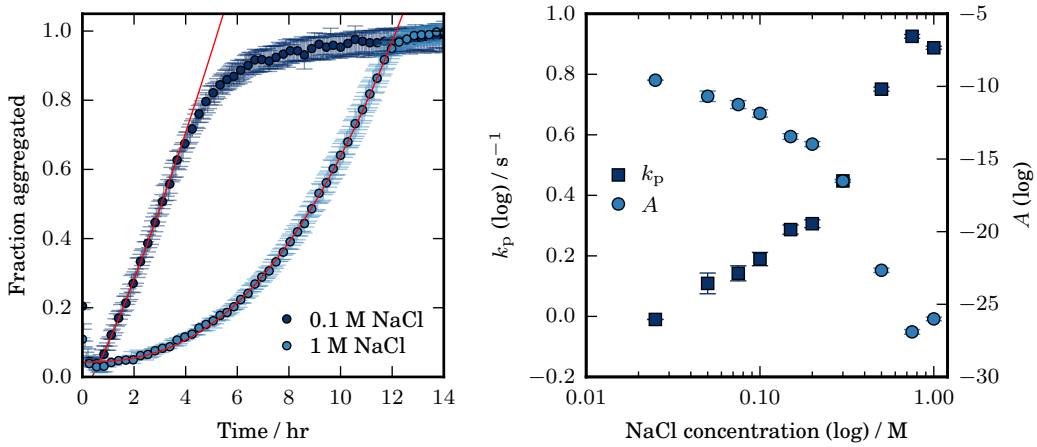

Figure 8.30: Growth parameters obtained from a polynomial fit ($M(t) = At^{k_p} + y_1$) to the initial increase in Thioflavin T fluorescence for α-syn 4 in 0.5 mM SDS incubated at various NaCl concentrations, 5 mM phosphate buffer, pH 7.4, 50°C.

The curve shape of the fluorescence growth was exponential-like at low salt, with a linear region of maximum growth rate at early times. This was

found to change towards the curve shape described in the previous section with increasing salt, where a slow polynomial increase in fluorescence is followed by an exponential-like plateau approach and a linear region of maximum growth rate at late times. The two extremes are highlighted in Figure 8.30.

As salt concentration increased the exponent of the polynomial increased from around 1 at very low salt concentrations to around 1.4 at 0.2 M NaCl. Above this it increases more rapidly with salt and finally appears to plateau at above 0.75 M NaCl at $\sim t^x$, x =2.4-2.5.

The plateau approach at all salt concentrations was well approximated by a single exponential function of the form $M(t) \sim M(\infty) - \exp(-k_2(t - \tau_2))$, indicating that elongation in this system is likely dominated by monomer (or oligomer) addition, irrespective of salt concentration.

At lower salt concentrations the majority of the growth curve conforms to the exponential approximation, and in the absence of salt the entire growth curve may have the form $M(t) \sim M(\infty) - \exp(-k_2(t - \tau_2))$. Such a curve shape suggests that elongation processes are dominant: either the system appears to be seeded where the creation of SDS-induced nucleus-like aggregates is very rapid and complete near the beginning of the growth; or all species are aggregation-competent under these conditions.

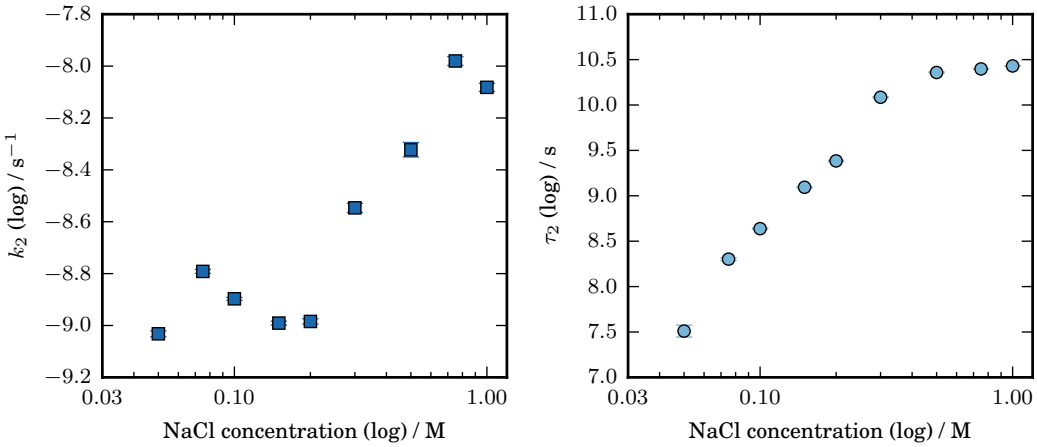

Figure 8.31: Growth parameters obtained from a single exponential fit ($M(t) \sim M(\infty) - \exp(-k_2(t - \tau_2))$) to the plateau approach of Thioflavin T fluorescence for α-syn 4 in 0.5 mM SDS incubated at various NaCl concentrations, 5 mM phosphate buffer, pH 7.4, 50°C.

The proportion of the growth curve estimated by the exponential function decreases with increasing salt and at 0.3 M NaCl and above this is reduced to

approximately the last 30% of the final intensity. The parameters obtained from the fits to the exponential function are shown in Figure 8.31.

It is clear in Figure 8.31 that the growth rate is initially concentration independent and then increases with increasing salt concentration above 0.2 M NaCl, appearing to plateau again at 0.75 M NaCl. In contrast, the characteristic time increases almost continuously with salt concentration and begins to slow in concentration dependence at high salt concentration (the plateau observed above $\sim$ 0.3 M is partly due to reducing the area of the curve that is included in the fit and does not give an exact estimate for a critical concentration of behavioural change).

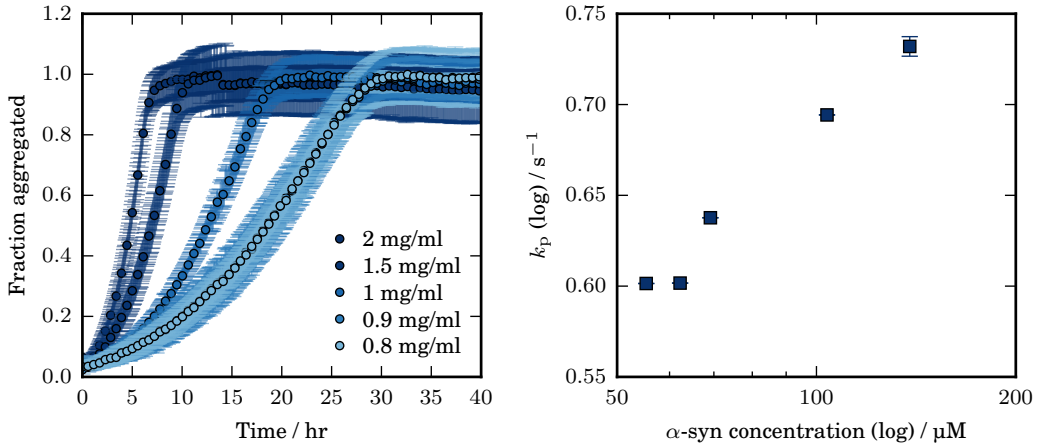

Figure 8.32: Left: Thioflavin T fluorescence measurements for various α-syn 4 concentrations in 0.5 mM SDS at 50°C, pH 7.4, 400 mM NaCl. Right: Growth parameters obtained from a polynomial fit ($M(t) = At^{k_p} + y_1$) to the initial increase in Thioflavin T fluorescence.

The concentration of salt associated with these changes in behaviour is similar to that observed in the absence of SDS (0.2-0.3M NaCl), suggesting a common charge-screening related transition. In the presence of SDS this acts to enhance the elongation rate, which may be related to a decreased intermolecular repulsion. However, increasing NaCl appears to have the opposite effect at early times, slowing the initial formation of SDS-induced aggregate species, decreasing the initial growth rate, and resulting in a polynomial curve.

In excess NaCl solutions, micelles of SDS have been found to become increasingly large and disordered [371], and the formation of larger micelles might result in decreased likelihood of α-syn aggregate formation in a similar way to increasing SDS concentration. Indeed, at low SDS concentrations curve

shapes were found to be approximately exponential and as SDS concentration was increased the early increase in fluorescence became increasingly slow and polynomial-like (Figure B.17).

To investigate the effect of salt concentration on the protein concentration behaviour, the effect of protein concentration was investigated at a higher salt concentration, 0.4 M NaCl, as shown in Figure 8.32. At 0.4 M NaCl the exponent of the polynomial was found to range from 1.8-2.0, higher than the time dependence observed at 0.12 M NaCl previously, and as expected given the salt dependence described above.

The maximum growth rate was found to plateau above around 100 µM α-syn (Figure B.31), and an approximation of the growth rate dependence on concentration (below 100 µM α-syn) gives a concentration order of 1.9(2), higher than the estimates at 0.12 M NaCl and indicating that increased salt results in increased polynomial order and increased protein concentration dependence at early times.

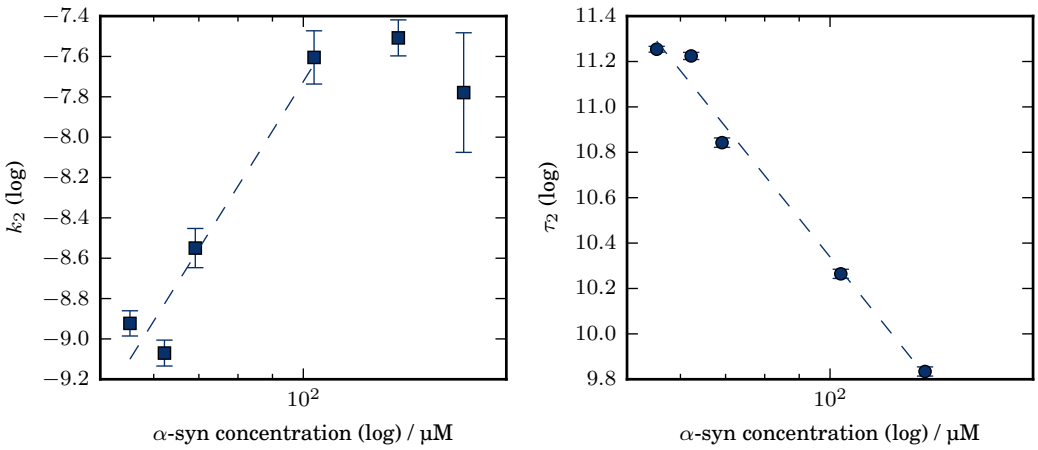

Figure 8.33: Growth parameters obtained from a single exponential fit ($M(t) \sim M(\infty) - \exp(-k_2(t - \tau_2))$) to the plateau approach of Thioflavin T fluorescence for α-syn 4 in 0.5 mM SDS, 50°C, 5 mM phosphate buffer, pH 7.4, 400 mM NaCl.

The plateau approach was found to have the form of a single exponential, and the characteristic time and apparent rate obtained from fitting to this region are shown in Figure 8.33. The characteristic time was found to have concentration order dependence -1.6(1) and the apparent rate to have order 2.3(5). These results suggest an increased protein concentration dependence persists to later times during the growth at higher salt, as expected given the salt concentration

dependence, and this is thought to be related to the heterogeneous nucleation event being increasingly rate limiting.

8.8 The formation of straight and worm-like fibrils in SDS

In a number of individual replicate samples a further increase in fluorescence intensity was observed after the increase in fluorescence associated with the formation of SDS-induced aggregates. In some cases this was observed following the plateau period associated with the SDS-induced aggregation and in some cases a much more rapid increase in fluorescence intensity was observed at early times and deviated from the typical shape of the SDS-associated growth curve, as shown in Figure 8.34.

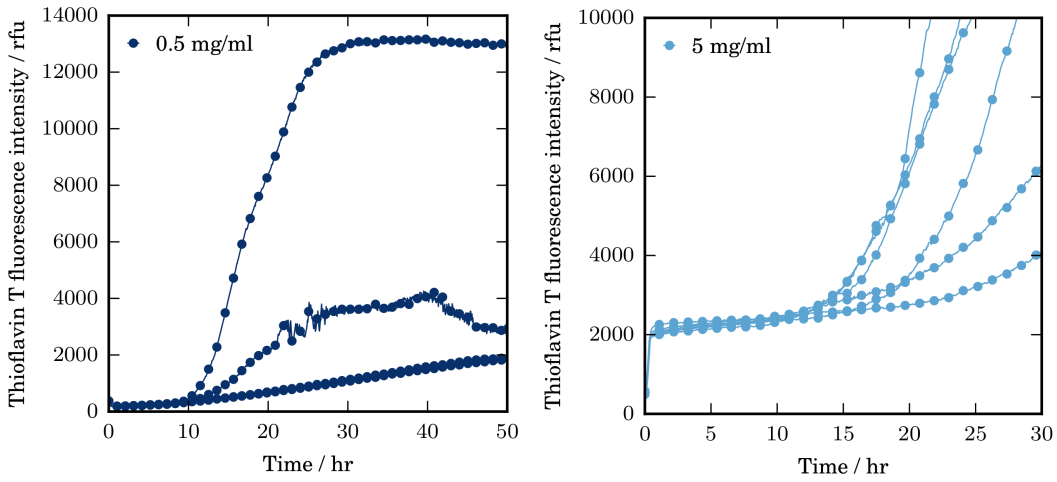

Figure 8.34: Thioflavin T fluorescence intensity obtained from individual sample replicates at the given α-syn concentration. Left: 0.5 mg mL^{-1} α-syn 1 incubated at 0.66 mM SDS, 37°C, 120 mM NaCl, pH 7.5. Right: α-syn 2 incubated at 0.5 mM SDS at 37°C, pH 7.4 (20 mM phosphate buffer), 120 mM NaCl.

As previously noted by Anunciado *et al.* [298], maximum fluorescence intensity associated with aggregation in the presence of SDS was much lower than for fibrils formed in the absence of SDS. Under similar growth conditions, the maximum fluorescence values obtained in the absence of SDS were typically of the order of 10,000 rfu, while those in the presence of SDS were of the order 100-1,000 rfu (although in both cases the exact values were dependent upon

the experimental conditions and the α-syn purification). To determine whether the increased fluorescence observed in some samples was due to the formation of straight fibrils similar to those observed in the absence of SDS, samples were taken for imaging by TEM from wells with unusually high fluorescence for comparison with those with fluorescence consistent with SDS-induced behaviour.

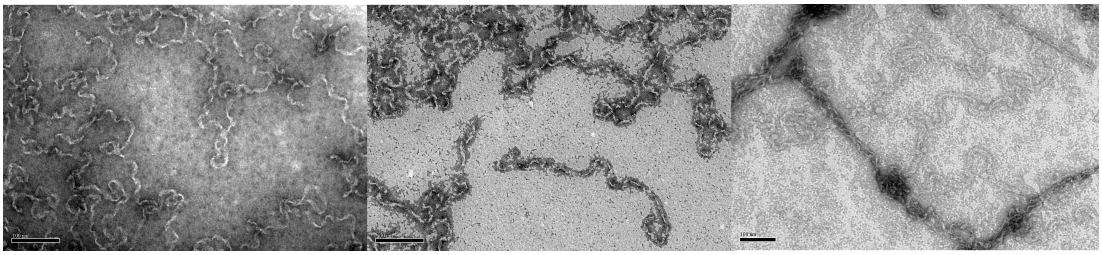

Figure 8.35: Transmission electron micrograph of negatively stained (uranyl acetate) fibrils from an incubation of 0.5 mg mL^{-1} α-syn 1 incubated at 0.66 mM SDS, 37°C, 120 mM NaCl, pH 7.5. Scale bars are 100 nm.

In the absence of unusual increases in fluorescence above the plateau region, only curvilinear or worm-like fibrils are observed, as shown in Figure 8.35. As well as worm-like fibrils a number of more linear structures were observed, but on closer inspection these appear to be worm-like ribbons that have become stretched by their association and tangles with other filaments, as seen in the right-most image in Figure 8.35. The curvilinear fibrils have a tape-like and twisted appearance. The width of these species was estimated to be 8(1) nm (from multiple measurements along at least 13 distinct filaments).

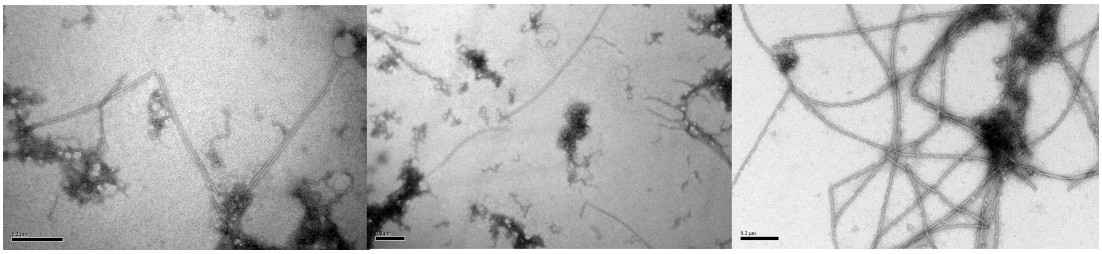

Figure 8.36: Transmission electron micrograph of negatively stained (uranyl acetate) fibrils from: *left and centre)* an incubation of 0.8 mg mL^{-1} α-syn 1 incubated at 0.9 mM SDS and *right)* 0.1 mg mL^{-1} α-syn 1 incubated at 0.33 mM SDS, both at 37°C, 120 mM NaCl, pH 7.5. Scale bars are 0.2 µm.

In samples exhibiting very high fluorescence straight fibrils were observed alongside the worm-like species, as shown in Figure 8.36. In contrast to the

curvilinear filaments, the straight fibrils do not have a tape-like appearance. They do appear to be twisted but the twists are not obvious and measurable in the images obtained, thus it was not possible to determine the periodicity. Individual filaments and wider fibrils that clearly consist of two laterally associated filaments were observed, individual filaments were estimated to have widths around 13(2) nm while the wider fibrils were found to have width of approximately 17(3) nm.

It was previously reported that on agitation a population of straight species was obtained from the worm-like SDS induced fibrils [42]. Samples that had reached the plateau period of growth in SDS under quiescent conditions were changed to a platereader shaking mode and readings were continued. In all cases, only very weak increases in fluorescence were observed over 24 hours of shaking. However, samples taken from the plate after shaking were found to contain increased numbers of straight filaments and bundles of straight filaments alongside the worm-like species, as shown in Figure 8.37. The widths of these fibrils were found to be $\sim$ 8(2) nm, more similar to the width of the worm-like species than the straight fibrils associated with higher ThT fluorescence. In addition, the straight fibrils obtained by agitation exhibited a more obvious twisted nature. Some of the observed filaments from this sample have the appearance of helical ribbons and the apparent width of these species (which does not take into consideration curvature) was found to be around 23(4) nm.

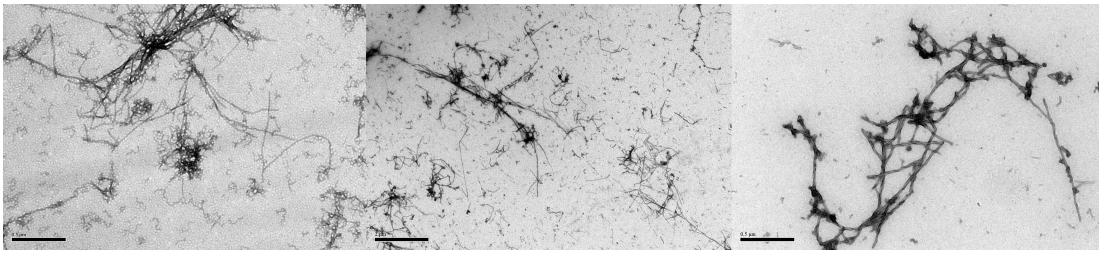

Figure 8.37: Transmission electron micrograph of negatively stained (uranyl acetate) fibrils from: *left)* an incubation of 0.8 mg mL^{-1} α-syn 1 incubated at 0.5 mM SDS and *centre and right)* 0.9 mg mL^{-1} α-syn 1 incubated at 0.5 mM SDS, both at 37°C, 120 mM NaCl, pH 7.5. Scale bars are 0.5 µm, 2 µm and 0.5 µm respectively.

A similar and stronger effect was observed by collecting fibrils formed in the absence of agitation by centrifugation, as shown in Figure 8.38. The fibril pellet was resuspended and diluted immediately prior to preparation for TEM on a copper grid, and was found to almost entirely consist of straight fibrils, with a

few small filaments with more curvilinear appearance attached in some places. The fibrils obtained from this sample were found to have widths around 9(1) nm, again more similar to those of the original worm-like fibrils, and the change in morphology may be similar to the stretching observed in Figure 8.35.

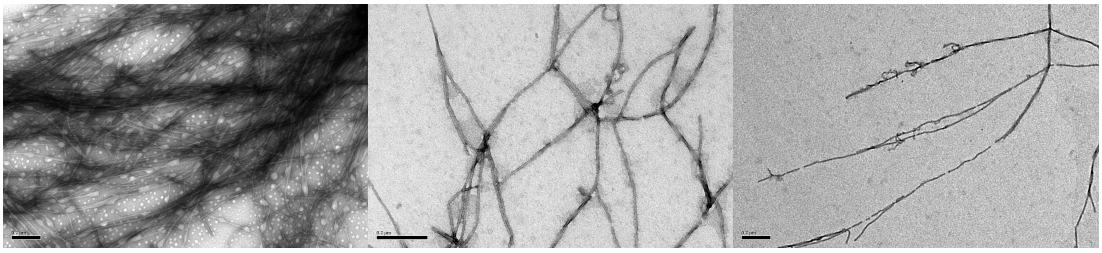

Figure 8.38: Transmission electron micrograph of negatively stained (uranyl acetate) fibrils collected by centrifugation from an incubation of 0.8 mg mL^{-1} α-syn 1 incubated at 0.5 mM SDS, 37°C, 120 mM NaCl, pH 7.5. Scale bars are 0.2 µm.

To investigate further, α-syn was incubated in SDS with agitation from the beginning of the experiment by microplate shaking. The sample replicates for two α-syn concentrations are shown in Figure 8.39. In all replicates (with shaking from the beginning of the experiment) a dramatic increase in fluorescence is observed beyond the values associated with SDS-induced aggregation, the growth curves for which are still observed at earlier times.

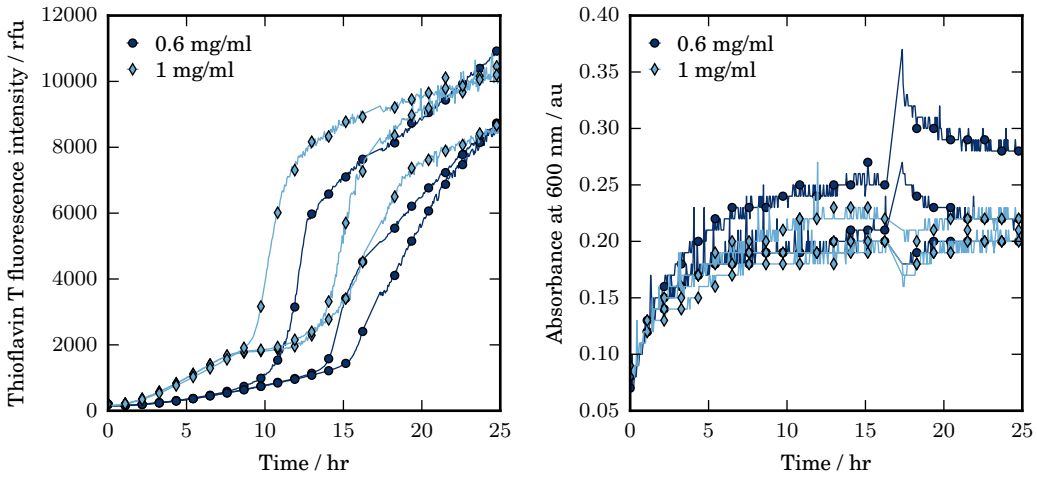

Figure 8.39: Thioflavin T fluorescence intensity (left) and simultaneous absorbance at 600 nm (right) obtained from individual sample replicates at the given α-syn 1 concentration incubated at 0.5 mM SDS at 37°C, pH 7.3, 120 mM NaCl.

In these samples a mix of straight filaments and worm-like fibrils were

observed, as shown in Figure 8.40. The samples were then stored at room temperature for a prolonged period of time ($\sim$ a month) before an aliquot was removed from the same sample to determine which species would persist over time. In the continued presence of 0.5 mM SDS a larger proportion of the 1 mg mL^{-1} α-syn sample was found to consist of worm-like filaments after $\sim$ a month. However, after around 2 months the majority of the sample appeared to consist of straight filaments. However, this was not the case for all concentrations, and may have varied between sample replicates. At 0.4 mg mL^{-1} only straight fibrils were observed after a month of incubation.

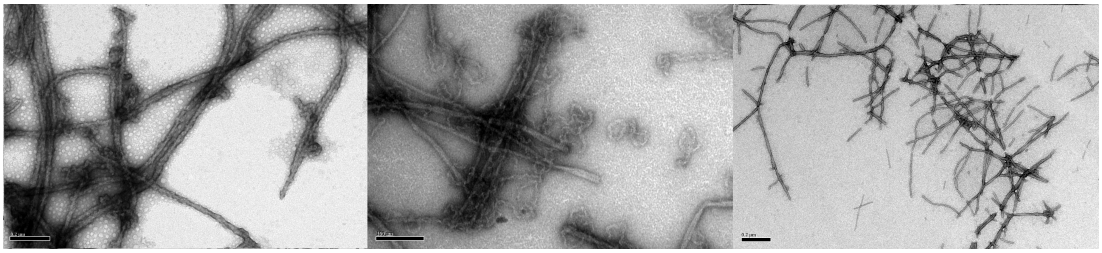

Figure 8.40: Transmission electron micrograph of negatively stained (uranyl acetate) fibrils of 1 mg mL^{-1} α-syn 1 incubated at 0.5 mM SDS at 37°C, pH 7.3, 120 mM NaCl. Sample diluted 10x immediately prior to grid preparation. *Left)* Aliquot from approximately 1 week following aggregation, scale bar 0.2 µm, *centre)* aliquot taken $\sim$ a month from aggregation, scale bar 100 nm, *right)* aliquot taken after 2 months, scale bar 0.2 µm.

The worm-like species exhibited the same width range previously observed. The straight fibrils exhibited some twisting but are considerably more rigid than the worm-like species, and in some cases rigid fibrils are clearly seen to consist of laterally associated and ribbon-like filaments. The average straight fibril width was found to be 30(5) nm, while individual fibrils ranged from $\sim$ 10-44 nm. Given the larger widths of the species obtained under these conditions compared to those in the absence of SDS it is possible that the straight fibrils that have matured by lateral association are the most thermodynamically stable species, and that the population of this species increases slowly over time, becoming the major species after long incubation times.

Chapter 9

Discussion: Fibril formation of α-synuclein

The aggregation of α-synuclein, an extensively studied intrinsically disordered protein (IDP) of pathological importance, has been investigated here under a range of solution and environmental conditions to determine how much can be inferred about the growth mechanisms that result in the formation of its different fibril polymorphs by growth curve analysis.

9.1 Reproducibility of growth kinetics

The difficulty in obtaining reproducible kinetic growth curves, and the sensitivity of α-syn aggregation to the environmental and solution conditions is well documented [43, 233]. The conditions required to produce reproducible growth curves were found to be equivalent to those discussed in the literature and included elevated temperature, pH values of around pH 5 and below ($\leq$ pI) and agitation by addition of glass beads or by using Nunc StarWell microplates.

The pH, temperature and agitation dependence of fibril formation were not investigated in great detail, but were found to be roughly consistent with previous reports [43, 233, 303, 310, 313–316]. Increasing temperature, increasing agitation and decreasing pH (to $\sim$ pI) were found to promote aggregation, in particular by reducing the lag phase.

In addition, increasing microplate hydrophobicity was found to enhance aggregation at high temperature and low pH. Changing from a hydrophilic (NBS

coated Corning microplates) to a hydrophobic surface (uncoated polystyrene Greiner microplates) more than halved the lag time prior to aggregation and notably decreased the variability between sample replicates. Many literature reports do not mention the microplate surface type used in platereader assays, and these results strongly indicate that the choice of equipment can have a large impact on the experimental results and may complicate comparisons between experiment types where the use of a different material is implicit.

The combination of conditions required to produce reproducible growth curves was found to vary between different α-syn stocks that followed different purification protocols or had different stock solutions, in particular α-syn concentration. This highlights the sensitivity of α-syn to solution, environmental and storage/treatment conditions, and suggests that literature reports about the behaviour of α-syn may be expected to vary. Performing size exclusion chromatography as a prerequisite to α-syn experiments, to ensure as close as possible a starting solution between replicate experiments, may be the most ideal methodology.

9.2 Aggregration in StarWell microplates

Introducing glass beads to increase agitation is common practice in α-syn aggregation assays. Nunc StarWell microplates were used in this investigation as an alternative means to increase agitation and hydrophobic surface area while both reducing the complication of introducing a third surface type and obtaining absorbance measurements.

However, in contrast to expected results [312–314], increasing ionic strength and increasing protein concentration were found to result in decreased aggregation propensity in StarWell microplates for the main α-syn purification investigated here. In particular, lag time was found to increase with increasing salt or protein concentration, suggesting that the process resulting in the formation of new aggregate species is most affected.

In agreement with previous literature results [241, 315, 367], initial growth was found to be exponential in form, indicating the importance of secondary growth processes. It was not possible to determine the nature of the secondary growth process, but given the sensitivity of α-syn aggregation to agitation, it

is likely that this is filament fragmentation. The reversal of expected salt and protein concentration dependence in StarWell plates is thought to be a result of increased precipitation and accumulation of aggregate behind StarWell fins acting as an aggregate sink and inhibiting this secondary growth process.

The weak concentration dependence of the characteristic time and lag time obtained are consistent with previous results obtained for α-syn in the early stages of fibril growth. This was previously attributed to a heterogeneous nucleation mechanism at the air-water interface [335]. A conformational conversion step during nucleation has also been proposed [3, 321, 327]. However, unless the conformational conversion is very slow, it is unlikely that it would dominate at low α-syn concentrations, especially in the presence of secondary growth processes.

The lag time obtained by absorbance was typically found to be shorter than the lag time obtained by fluorescence, suggesting the population of an aggregate species that does not significantly bind ThT at early times. This could be related to a population of a less-β-sheet rich oligomeric species, as previously observed in aggregating α-syn solutions [325, 326], but the large inherent noise in absorbance readings meant no further analysis was possible at this time.

Using Nunc StarWell microplates was shown to be an alternative method to produce reproducible growth curves during α-syn aggregation. However, the growth is thought to be affected by the microplate wells acting as an aggregate sink, and such a process has not been considered in any of the available growth models. Indeed, the growth curves obtained were found to exhibit a shape inconsistent with any current growth model. Additionally, absorbance measurements were very noisy, and little analysis was possible for these measurements. This is also thought to be a result of the loss of aggregate material from solution, and therefore Nunc StarWell microplates do not provide a significant advantage over the introduction of glass beads.

9.3 Formation of worm-like fibrils in SDS

The ability of α-syn to bind phospholipid membranes is well documented, and membrane binding is likely important for the protein's function [307, 331]. However, accelerated aggregation of α-syn is observed in the presence of moderate membrane [307, 321], detergent [334] and phospholipid vesicle [224, 298, 335]

concentrations and in the presence of supported phospholipid bilayers. Typically, detergents and fatty acids are micellar at these concentrations, since α-syn binding decreases the critical micelle concentration of these species [334].

Oligomeric or cluster-like multimers of α-syn formed either on the surface or in mixed micelles might directly transition into β-strand containing aggregates [304], resulting in membrane-induced heterogeneous aggregation that may be physiologically relevant in α-syn function or in the disease state [298, 298].

The behaviour of α-syn in the presence of the detergent sodium dodecyl sulphate (SDS) was investigated here as a case in which the aggregation behaviour appears to be similar to that in the presence of membranes and has been well studied in the literature. In addition, α-syn is known to aggregate into a curvilinear fibrillar polymorph in the presence of SDS [42], along what may be an alternative aggregation pathway to the formation of straight fibrils [300].

The fibrils obtained in the presence of SDS were flexible, worm-like filaments that induced a weaker fluorescence response than the rigid filaments formed at low pH and high temperature, consistent with previous reports [42, 233, 298].

The α-syn aggregation dependence on SDS concentration was consistent with previous literature observations [42, 311, 338]. Increasing SDS concentration was found to enhance aggregation up to an optimal concentration of 0.5 mM SDS by growth rate, or 0.75 mM SDS by maximum fluorescence and lag time. As SDS concentration increased further aggregation was inhibited, until no aggregation was observed at 2.5 mM and above. The optimum SDS concentration was at approximately 7-11 SDS per α-syn monomer, lower than the previously reported 12:1 optimum ratio. Additionally, a slight reversal in parameter behaviour from the expected decreases in growth rate and increases in lag time (or τ_{50}) as SDS concentration increased above 1 mM suggests a more complicated relationship between the concentrations of SDS and α-syn than the optimal binding stoichiometry previously proposed. This might be related to the ability of aggregates to form both on the surface of micelles from a locally enhanced protein concentration as well as in micelles from micelle-bound α-syn.

Increasing protein concentration was found to enhance aggregation, increasing the growth rate, decreasing lag time or τ_{50}, and increasing maximum ThT fluorescence. Increasing temperature was also found to increase growth rate (up to 45°C) and decrease lag time. However, maximum fluorescence values were

found to decrease with increasing temperature and this is thought to be related to a decrease in aggregate mass since the curvilinear filaments formed are not thought to be a thermodynamically stable species.

The shape of the growth curves obtained in the presence of SDS is unusual compared to those for most fibril forming species, and are consistent with those that have been previously obtained [42, 233]. No extended lag phase is observed prior to aggregation, initial growth is slow and approximately polynomial in form, followed by a late inflection point (occurring later than 50% completion), after which the plateau approach is more rapid and roughly exponential. However, at high temperature or protein concentration the plateau approach became increasingly slow, and suggestive of coagulation processes.

The polynomial increase at early times was found to have weaker time order (t^x, x =1.3457(1)-1.758(5)) than any of the currently described homogeneous nucleation-like events for protein aggregation (all of which predict t^2 or above), and is thought to reflect a heterogenous nucleation process in or on the surface of mixed SDS and α-syn micelle-like aggregates where the formation of α-syn aggregates is facilitated by structural changes induced by SDS-binding, as previously proposed [304]. In contrast to the growth of rigid fibrils, there was no evidence for rate-limiting secondary growth processes.

The plateau approach was well estimated by a single exponential, and the maximum growth rate, associated with the same region of growth, exhibited concentration dependence consistent with elongation by monomer (or oligomer) addition as a dominant growth mechanism at later times.

The different activation energies estimated from the temperature dependence of the growth rates for the initial growth and plateau approach were also consistent with different growth mechanisms being dominant in these regions, thought to be heterogenous nucleation and growth by monomer (or oligomer) addition respectively. The higher activation energy estimated for the initial increase in fluorescence is thought to be related to the formation of initial β-rich species in the heterogenous nucleation stage, while the lower energy associated with elongation at later times may suggest that elongation then occurs by oligomer addition, as proposed by Giehm *et al.* [42].

SDS induced aggregation was also found to be salt sensitive, exhibiting a similar critical concentration to behaviour observed in the absence of SDS,

suggesting a common charge-screening related transition. Increasing NaCl concentration was found to increase maximum fluorescence values, suggesting increases in total aggregate fraction, and to increase the maximum growth rate, but resulted in slower initial growth and increased time to 50% completion. Elongation therefore appears to be enhanced by an increase in intermolecular charge screening upon increasing salt, as has been previously proposed [312]. The heterogenous nucleation event thought to give rise to the polynomial behaviour at early times appears to be inhibited by increasing salt concentration, and appears to become increasingly rate limiting at high salt. Indeed, in excess NaCl solutions the micelles of SDS have been found to become increasingly large and disordered [371], and the formation of larger micelles might contribute to a decreased likelihood of α-syn aggregate formation in a similar way to increasing SDS concentration.

9.4 Distinct polymorphs

The curvilinear α-syn fibrils share common features with those of HEWL compared to their rigid counterparts formed at high temperature and low pH. In both cases the curvilinear filaments appear to be associated with growth by oligomer rather than monomer addition, and lower fluorescence enhancement of ThT that suggests these species may have less β-content.

When α-syn in the presence of SDS was subject to agitation from the beginning of the experiment, large increases in fluorescence were observed that were more reminiscent of increases in fluorescence intensity at high temperature and low pH. These were correlated with the observation of straight filaments by TEM. This is similar to the observations made for HEWL at high ionic strength with agitation, as described in Section 4.3. When mature SDS-induced curvilinear fibril samples were subject to agitation no large increases in fluorescence intensity were observed. Additionally, straight filaments observed following agitation of mature curvilinear species were found to have widths more similar to the original tape-like curvilinear species, suggesting that the curvilinear and straight filament species do not interconvert. It would appear therefore that, as for HEWL, these are two distinct species that both contribute to ThT fluorescence and under certain circumstances (in the presence of SDS and agitation) may compete for

monomer, further complicating growth curve analysis.

In addition, the growth kinetics of α-syn at high temperature and low pH, and in the presence of SDS, clearly highlight the need for incorporating alternative nucleation mechanisms into available fibril growth models. Given the potential importance of membrane induced aggregation *in vivo* [298, 298], the surface activity of many proteins [172, 216, 237], and the likelihood that nucleation in bulk *in vitro* experiments is heterogeneous [240] this has been a notably missing growth mechanism from descriptions of filament growth. Additionally, it is clear that complex nucleation processes may occur, with dependence on the concentration of interacting species as well as the aggregating protein, as in the case of α-syn in SDS. To my knowledge no growth model has yet incorporated a nucleation process aiming to account for such a situation in aggregate growth.

Chapter 10

Summary and conclusion

The ability of a protein to maintain its native, functional state is fundamental for biological activity. Misfolding and the accumulation of protein aggregates has been intimately linked with a large number of mammalian disorders. The study of amyloid-like fibril formation of proteins has been an ever expanding field since their implication in neurodegenerative disease, and one of the most common methods is the analysis of growth kinetics.

A complete description of fibril formation requires identification of the oligomeric species present and the pathway of association, including quantification of the kinetic rate constants, nucleus size and reaction orders that are of potential importance in pathology.

Fibril forming systems exhibit characteristic sigmoidal-like mass-of-aggregate growth profiles, and the range of possible growth mechanisms and their effect on growth characteristics have been well described. Many of the methods used to obtain kinetic data are relatively simple and inexpensive, such as turbidity, intrinsic and extrinsic fluorescence assays, and light scattering. Numerous growth models have been developed to describe the formation of linear protein aggregates, with the aim of determining the dominant, rate limiting growth mechanisms and important growth parameters. Combined with these growth models, kinetic growth curve analysis has been shown to be capable of delivering a substantial amount of information about the growth mechanisms of fibril forming systems.

Given the wealth of knowledge about growth mechanisms, the literature focus on finding analytical solutions to growth models in order to quantify important rate constants and the relatively simple and inexpensive techniques, the study

of fibrillar growth kinetics has become an increasingly large part of the analysis of fibril growth and is attracting more attention across scientific disciplines than ever before.

This research aims to demonstrate the level of information that can be obtained by growth curve analysis in the absence of, or as a prerequisite to performing computationally and/or time expensive fits to growth models.

Hen egg white lysozyme (HEWL) and α-synuclein, two extensively studied model systems for protein folding and misfolding were chosen for comparison. HEWL is a small globular protein, of importance in food science and due to its similarity to human lysozyme, the variants of which are implicated in hereditary systemic amyloidosis [244, 254, 256]. Alpha-synuclein is a small, intrinsically disordered protein associated with a range of neurodegenerative disorders, including Parkinson's disease and Dementia with Lewy bodies [289–293]. Both proteins are known to readily form fibrils *in vitro* at low pH and high temperature [113, 242–244, 247, 251–253, 258, 310, 312–314], high alcohol concentrations [4, 233, 254–261, 289, 321, 339], in the presence of denaturants or surfactants [42, 248–250, 311, 321], and to be sensitive to salt concentration [2, 89, 245–247, 258, 310, 312–314, 316].

Growth curve analysis has been shown here to be a very useful tool in the analysis of amyloid-like fibril growth, providing great insight into the growth mechanisms that control aggregation rate over the time course of fibrillar growth. In addition, a large amount of information about growth of HEWL and α-syn filaments has been obtained here using the simple, inexpensive, high-throughput, *in situ* and complementary techniques of turbidity and fluorescence measurement by platereader assay.

These results highlight the importance of using complementary techniques, without which important information about the coexistence and competition of distinct fibrillar pathways would not have been obtained. There are numerous alternative experimental methods that would also have been complementary, and each typically reports an individual parameter of the aggregating system, such as monomer concentration, mass-of-aggregate, average filament length, or end-point filament length distribution. Where possible many different techniques should be compared.

Mass-of-aggregate (or equivalently monomer depletion) data is likely to

be a minimum requirement to differentiate between different combinations of microscopic processes, and the conclusions drawn about growth by oligomer coalescence rather than monomer addition in the elongation of curvilinear filaments would not have been possible without the information obtained by imaging techniques such as TEM as implemented here.

In cases where growth conforms closely to the the behaviour associated with a well studied, dominant growth process, the growth mechanism can be reported with confidence. This was the case here for HEWL at high salt, high temperature and low pH, where growth curves were found to strongly conform to the predictions of the secondary process dominated model for fragmentation driven growth, and a reasonable fit to the analytical solution was obtained.

However, it is clear that where multiple growth processes contribute to the measurable growth kinetics the analysis of growth curves is non-trivial. The majority of the insights into the dominant growth mechanisms gained here were obtained using the wealth of knowledge about how such growth processes affect characteristic growth parameters rather than direct fitting to growth models.

The majority of the growth curves analysed here deviate from the analytical solutions to growth models that are obtained under limiting conditions, either as a result of the complexity of the fibrillar growth or because the growth processes have not yet been adequately described in models that include secondary growth mechanisms, in particular the heterogeneous nucleation and rate-limiting structural changes that have been shown here to be important for α-syn and HEWL aggregation.

Many systems also exhibit critical concentrations where the dominant growth processes change, and resemble a different analytical solution above and below the critical concentration. Analytical solutions are less likely to be found where changes in the dominant growth processes occur, especially if the comparative dominance of multiple growth processes changes gradually over time, or where two or more growth processes have similar contributions to the growth rate. The relative importance of fibril fragmentation and structural change as rate-limiting growth processes for HEWL aggregation is an obvious case for which an analytical solution may not be possible and growth curve analysis may provide insights that can feed into a computational modelling approach.

If growth processes change over time the typically reported parameters τ_{lag} and

r_{max} may also give misleading information, since these parameters may contain contributions from multiple dominant growth processes. This was very clear in analysis of parameters obtained for growth on either side of the inflection point for reduced HEWL, where the parameters r_{max} and the correspondingly derived τ_{lag} clearly gave a composite result of the behaviours at early and late times, highlighting the importance of analysing curve shape and considering changes that may happen to the rate-limiting growth mechanisms over time.

Alternatively, kinetic data may be complicated by the formation of different aggregate species formed along alternative and possibly competing aggregation pathways [1, 70, 75, 88]. In a number of aggregate systems non-fibrillar, amorphous-like aggregates have been observed alongside amyloid-like fibrils [53, 103, 227, 232–236]. These competing off-pathway species have recently been linked to a number of kinetic signatures including highly variable end-point signals and weak concentration dependence of the characteristic times [227, 232].

However, amorphous species are not considered to contribute to the mass-of-aggregate signal as obtained by ThT fluorescence measurements. Competing species that contribute to this signal may present a further challenge.

An increasing number of proteins and peptides have been shown to form curvilinear or worm-like fibrils [2, 40–97]. These species have typically been shown to exhibit many of the characteristics of amyloid fibrils and appear to be correlated with shorter or non-existent lag phases prior to aggregation, rate-limiting elongation processes rather than nucleation processes, elongation by oligomer coalescence rather than monomer addition, the ability to form closed loops and weaker ThT fluorescence enhancement that suggests a lower β-content. These curvilinear filaments may represent a common alternative and/or competing fibrillar growth pathway.

Straight, rigid filaments and curvilinear species have previously been observed in the aggregation of HEWL at high temperature and low pH, and were identified as distinct structural species formed along different growth pathways [1, 2, 88, 89]. The coexistence and competition for monomer between these species was confirmed here, and was most clear in the observation of multiple growth phases by *in situ* ThT fluorescence intensity and absorbance at 600nm. The coexistence, and presumably competition, of rigid and curvilinear filaments was also observed for α-synuclein in the presence of SDS under agitation.

Similar curvilinear fibrillar species were obtained under a range of solution conditions for HEWL, and appear to be formed along a common alternative growth pathway. In addition, the curvilinear species were found to be metastable, consistent with previous reports that rigid filaments are the thermodynamically stable aggregates [88]. Given this, it is likely that such species may be formed under a range of conditions for a wide range of proteins, and that they may compete for monomer at early times and affect growth kinetics, but be transient and hard to detect under conditions strongly favouring the growth of rigid filaments.

The analysis of growth kinetics has been shown here to be a powerful technique to enhance our understanding of the growth mechanisms driving amyloid-like fibril formation. However, this research also demonstrates the non-trivial nature of this pursuit, and highlights some of the key areas that need further attention in the development of fibrillar growth models. In addition, one can speculate that curvilinear filaments, given their shared characteristics and contrasts with rigid fibrils, represent a common alternative amyloid-like fibril pathway typified by particular kinetic signatures. The formation of a competing fibrillar species may be of particular importance to pathology, and presents further challenges to growth curve analysis.

A Appendix: HEWL

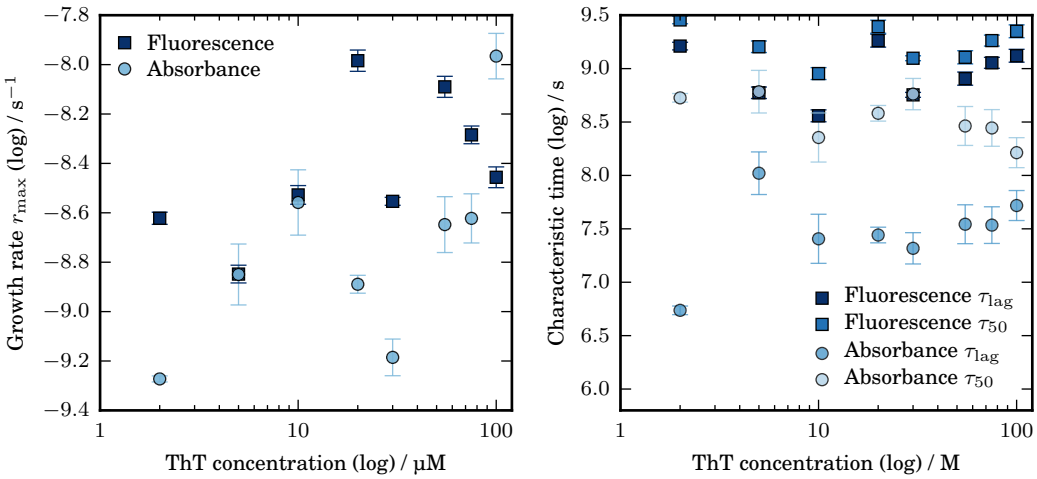

Figure A.1: Maximum growth rate and associated characteristic time obtained (from tangent to linear region) from Thioflavin T fluorescence and simultaneous absorbance (600 nm) measurements for 20 mg/ml HEWL at 65°C, pH 1.5, 200 mM NaCl under agitation (double orbital shaking at 700rpm for 2.5 min every 5 min) in the presence of various ThT concentrations.

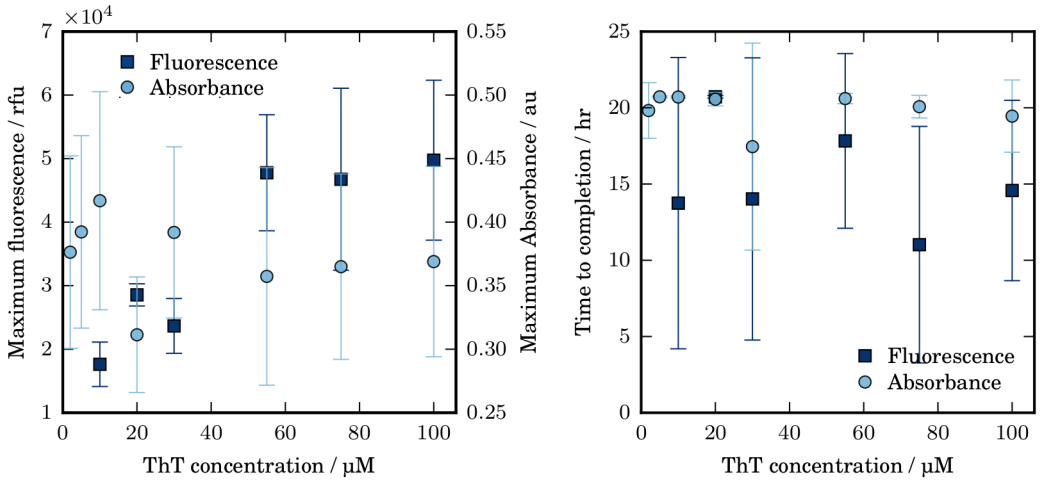

Figure A.2: Left: Maximum Thioflavin T (ThT) fluorescence and absorbance at 600 nm obtained for 20 mg/ml HEWL at 65°C, pH 1.5, 200 mM NaCl under agitation (double orbital shaking at 700rpm for 2.5 min every 5 min) in the presence of various ThT concentrations. Right: The time taken to reach the maximum value.

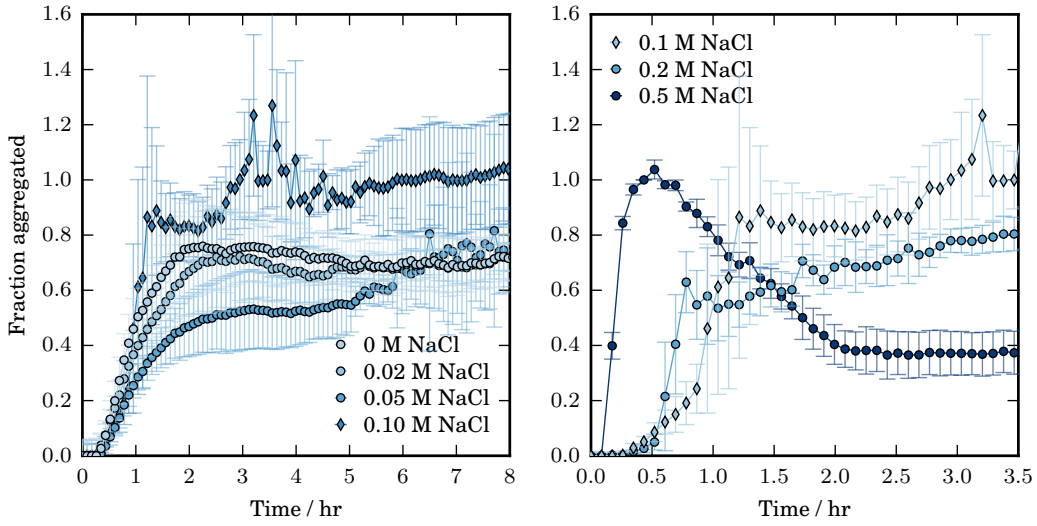

Figure A.3: Normalised absorbance at 600 nm over time for a range of salt concentrations for 10 mg/ml HEWL at 65°C, pH 1.6 (25 mM HCl), incubated with double orbital shaking at 700 rpm for 2.5 of each 5 minute cycle. The result at 0.1 M NaCl is shown in both graphs, highlighting the similarity of the slow initial growth at this concentration with the growth at lower concentration, and of the following rapid growth with the more rapid growth observed at higher concentrations of salt.

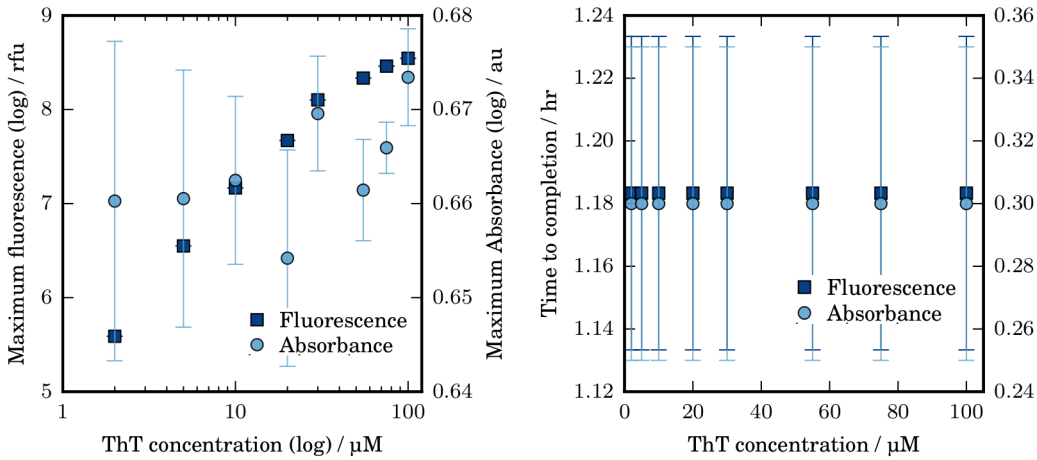

Figure A.4: The maximum Thioflavin T (ThT) fluorescence and absorbance at 600 nm obtained for 20 mg/ml HEWL at pH 2, 60°C in 1 M NaCl, at various ThT concentrations.

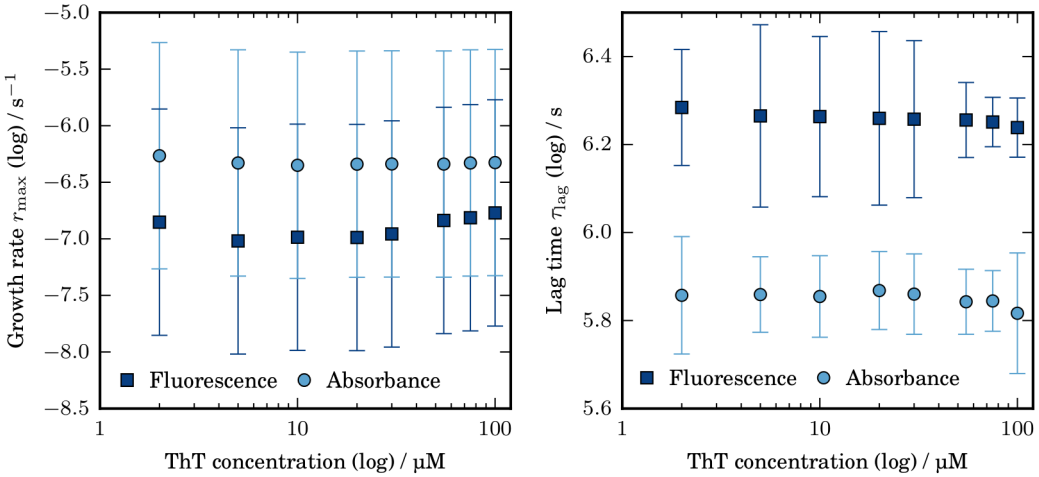

Figure A.5: The maximum growth rate and associated lag time obtained by Thioflavin T (ThT) fluorescence and absorbance at 600 nm for 20 mg/ml HEWL at pH 2, 60°C in 1 M NaCl, at various ThT concentrations. Data estimated from normalised growth curves.

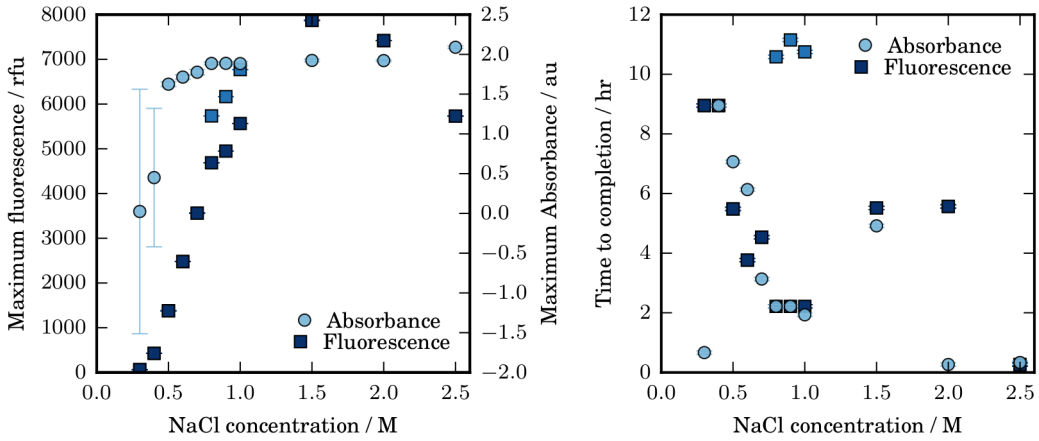

Figure A.6: Left: Maximum Thioflavin T fluorescence and absorbance at 600 nm obtained for 10 mg/ml HEWL incubated at pH 2, 60°C in the presence of increasing NaCl concentrations. Right: The time taken to reach these maximum values.

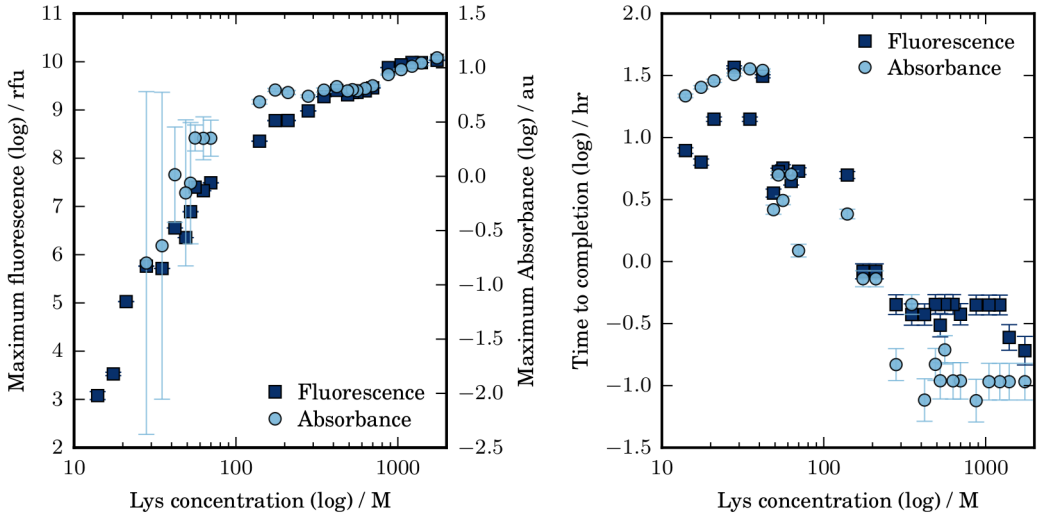

Figure A.7: Left: Maximum Thioflavin T fluorescence and absorbance at 600 nm (right) data for various concentrations of HEWL incubated at pH 2, 60°C in 1 M NaCl. Right: The time taken to reach this maximum value.

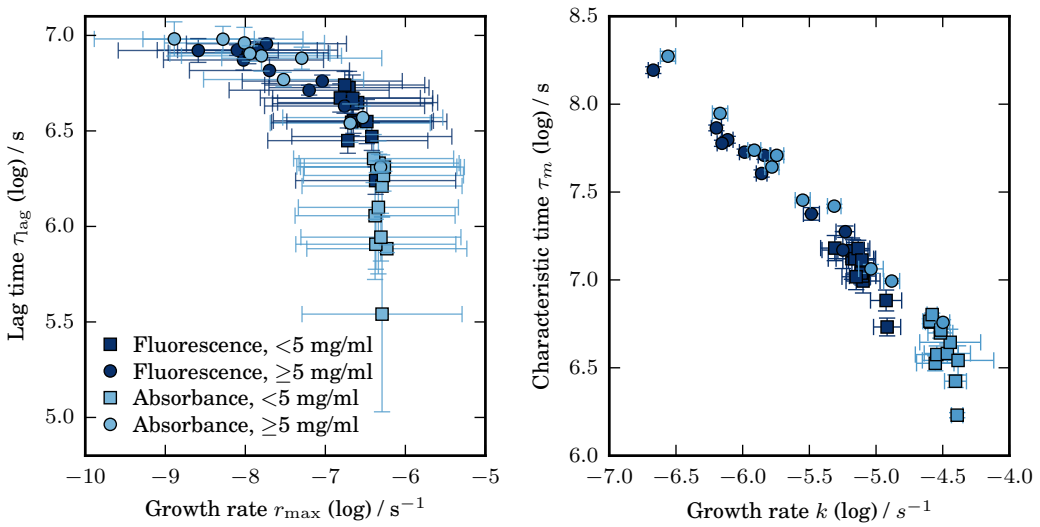

Figure A.8: Characteristic time versus apparent growth rate obtained by linearly fitting to the period of maximum growth (left) or fitting to the generalised logistic function (right) for various HEWL concentrations incubated at pH 2, 1 M NaCl, 60°C.

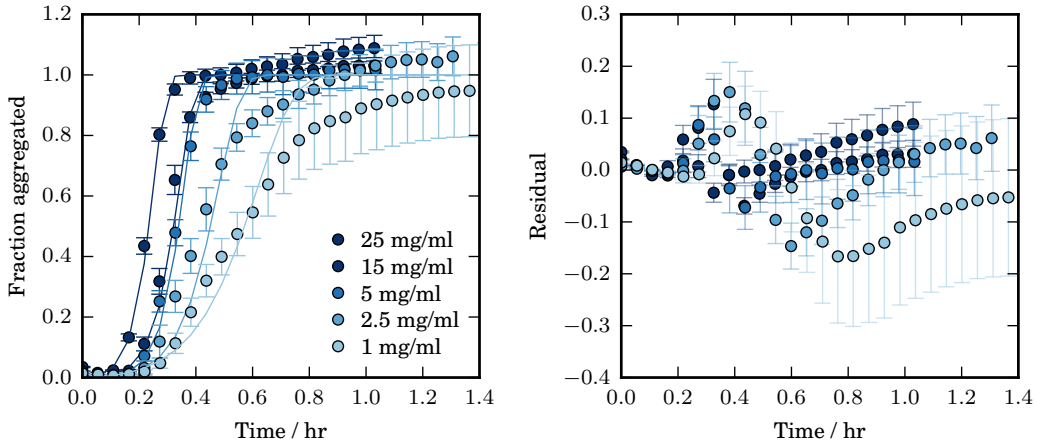

Figure A.9: Normalised Thioflavin T fluorescence (circles) and corresponding fit to the simplest SDP model (solid line in matching shade) for various concentrations of HEWL incubated at pH 2, 60°C in 1 M NaCl.

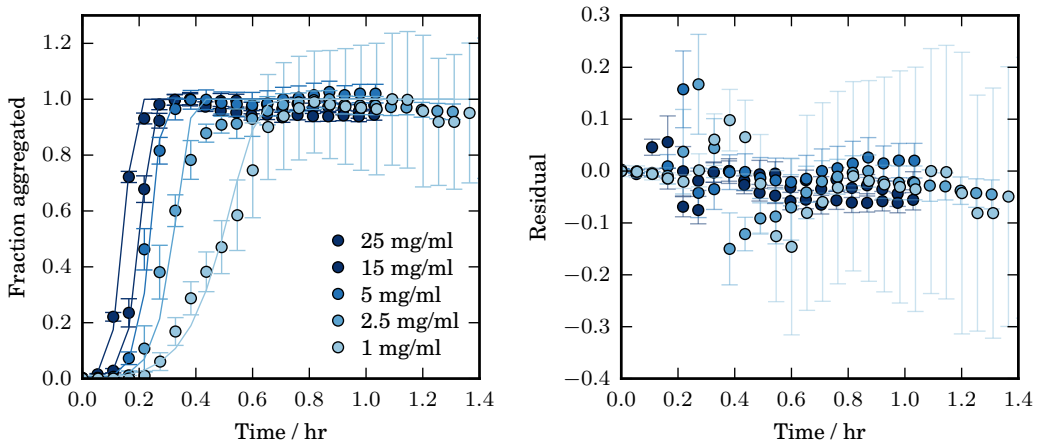

Figure A.10: Normalised absorbance at 600 nm (circles) and corresponding fit to the simplest SDP model (solid line in matching shade) for various concentrations of HEWL incubated at pH 2, 60°C in 1 M NaCl.

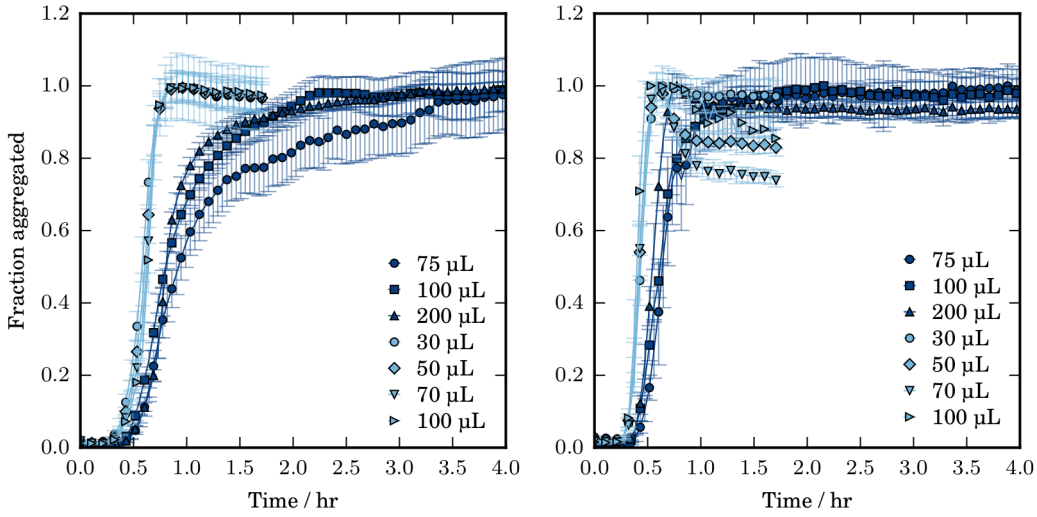

Figure A.11: (Left) Thioflavin T fluorescence and (right) absorbance at 600 nm obtained during the aggregation of 5 mg/ml HEWL at pH 2, 1M NaCl, 60°C at various sample volumes in either a 384-well (pale blue) or 96-well (dark blue) Corning NBS coated microplate.

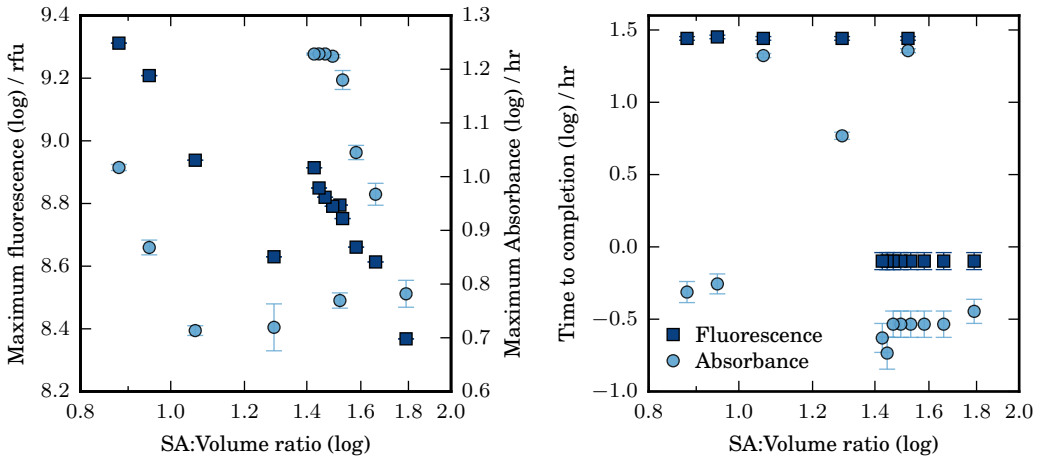

Figure A.12: Left: maximum Thioflavin T fluorescence and absorbance at 600 nm obtained during the aggregation of 5 mg/ml HEWL at pH 2, 1M NaCl, 60°C at various sample volumes in either a 384-well (pale blue) or 96-well (dark blue) Corning NBS coated microplate. Right: the time taken to reach the maximum value. Surface area to volume ratios were calculated using average well geometries.

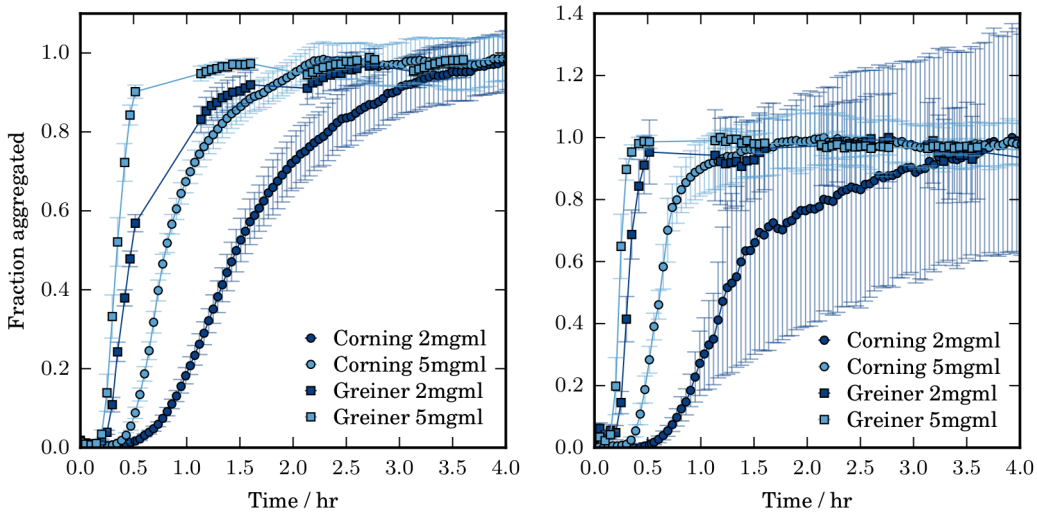

Figure A.13: (Left) Thioflavin T fluorescence and (right) absorbance at 600 nm obtained during the aggregation of 2 and 5 mg/ml HEWL at pH 2, 1M NaCl, 60°C in either a Corning NBS coated microplate or an uncoated Greiner microplate. The missing section of data in the Greiner results was due to a pause in microplate reading.

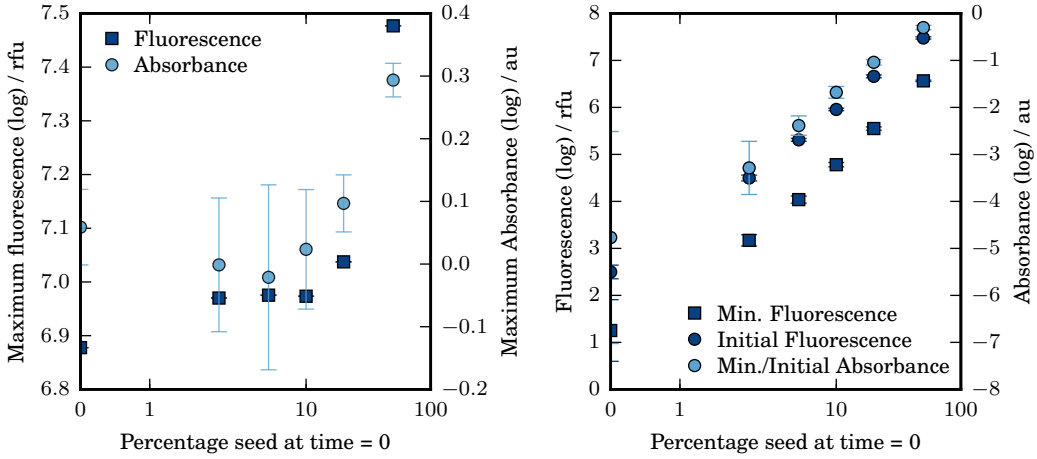

Figure A.14: Maximum (left), minimum and initial (right) thioflavin T fluorescence and absorbance at 600 nm obtained for samples of 2 mg/ml total concentration (including seed) HEWL incubated at 1 M NaCl, 60°C, pH 2 in the presence of various seed concentrations. Preformed seeds produced under the same aggregation conditions.

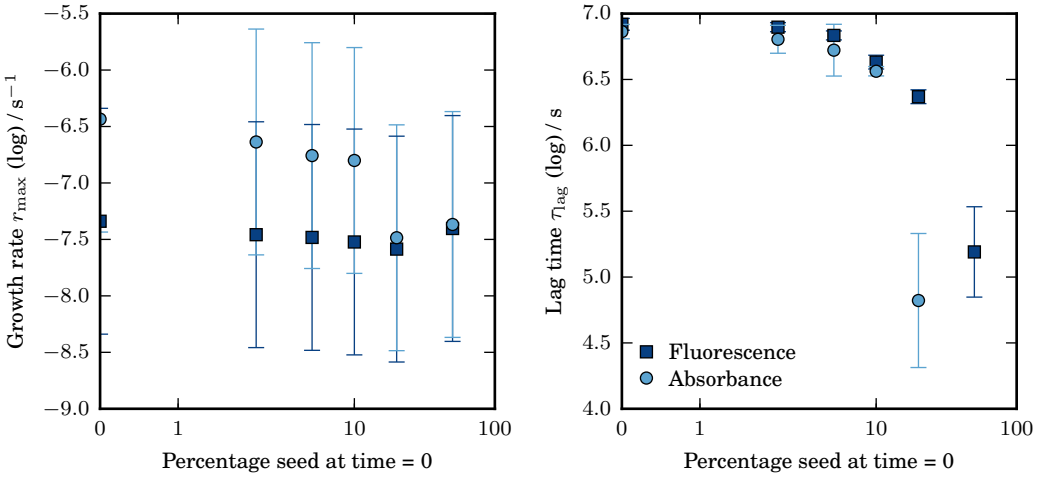

Figure A.15: Maximum growth rate and associated lag time obtained from the best fit tangent to the maximum growth rate for thioflavin T fluorescence and absorbance at 600 nm for samples of 2 mg/ml total concentration (including seed) HEWL incubated at 1M NaCl, 60 °C, pH 2 in the presence of various seed concentrations. Preformed seeds produced under the same aggregation conditions.

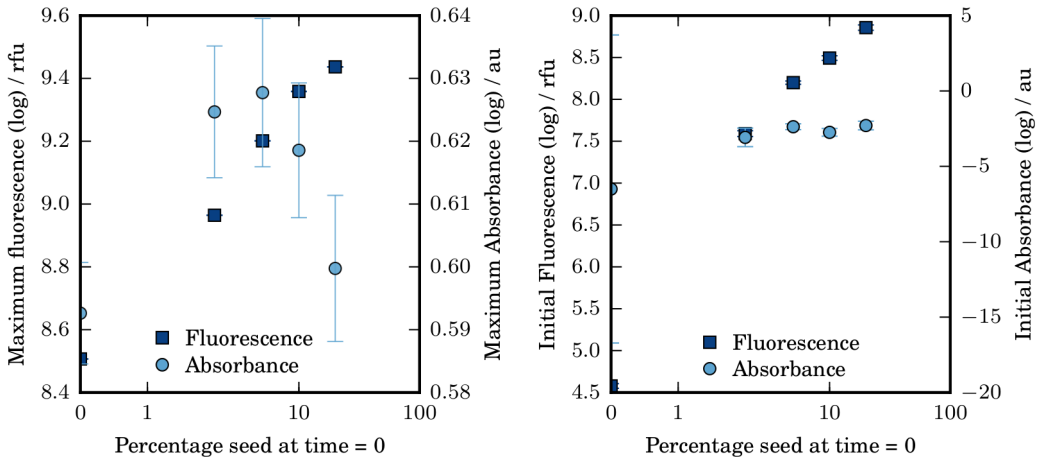

Figure A.16: Maximum (left), minimum and initial (right) thioflavin T fluorescence and absorbance at 600 nm obtained for samples of 10 mg/ml total concentration (including seed) HEWL incubated at 1 M NaCl, 60°C, pH 2 in the presence of various seed concentrations. Preformed seeds produced at pH 1.5, 65°C, 200 mM NaCl with agitation by Eppendorf Thermomixer shaking at 700 rpm for 20 hours.

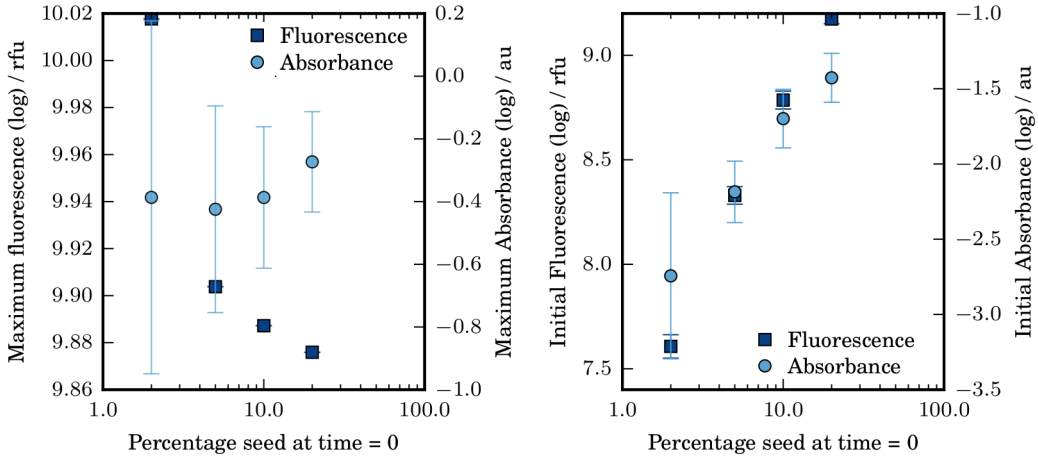

Figure A.17: Maximum (left), minimum and initial (right) thioflavin T fluorescence and absorbance at 600 nm obtained for samples of 10 mg/ml total concentration (including seed) HEWL incubated at 200 mM NaCl, 60°C, pH 2 in the presence of various seed concentrations. Preformed seeds produced at pH 1.5, 65°C, 200 mM NaCl with agitation by Eppendorf Thermomixer shaking at 700 rpm for 20 hours.

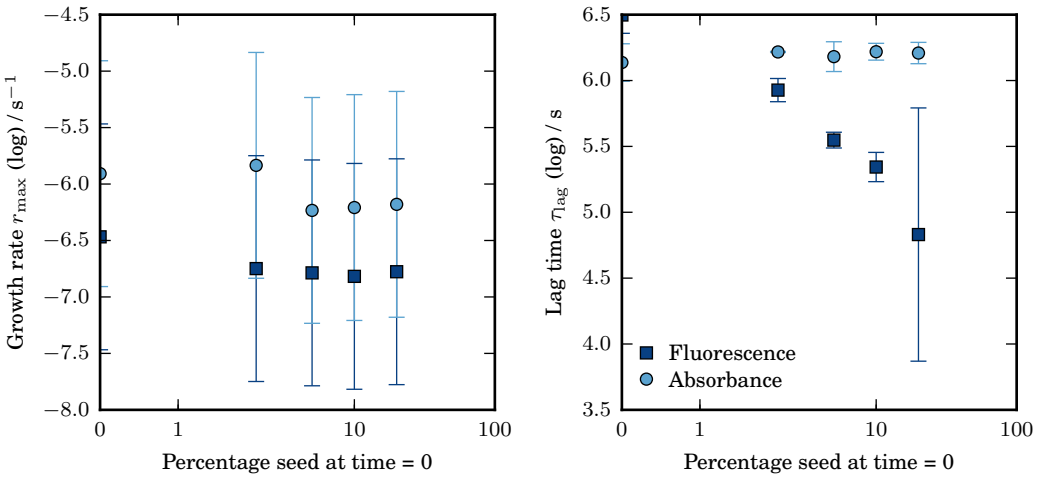

Figure A.18: Maximum growth rate and associated lag time obtained from the best fit tangent to the maximum growth rate for thioflavin T fluorescence and absorbance at 600 nm for samples of 10 mg/ml total concentration (including seed) HEWL incubated at 1 M NaCl, 60 °C, pH 2 in the presence of various seed concentrations. Preformed seeds produced at pH 1.5, 65°C, 200 mM NaCl with agitation by Eppendorf Thermomixer shaking at 700 rpm for 20 hours.

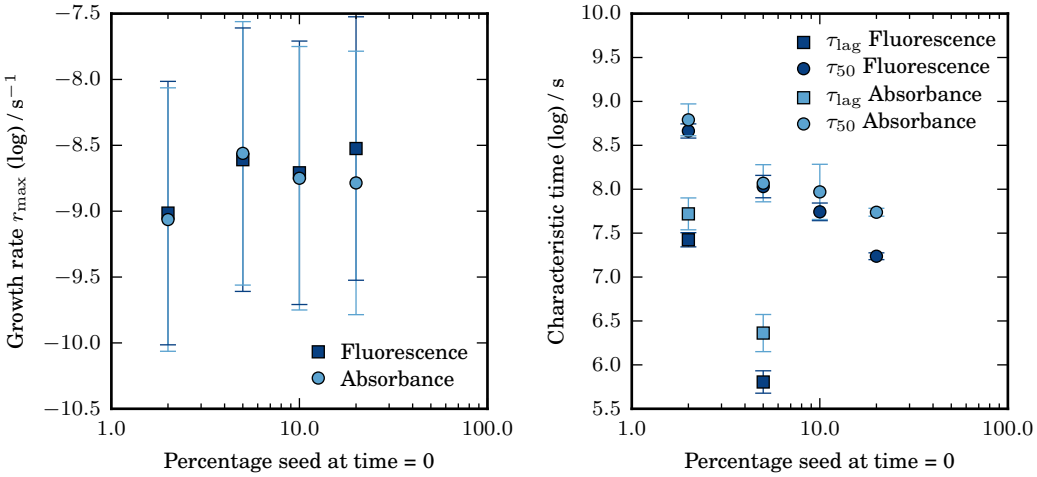

Figure A.19: Maximum growth rate and associated lag time obtained from the best fit tangent to the maximum growth rate for thioflavin T fluorescence and absorbance at 600 nm for samples of 10 mg/ml total concentration (including seed) HEWL incubated at 200 mM NaCl, 60 °C, pH 2 in the presence of various seed concentrations. Preformed seeds produced at pH 1.5, 65°C, 200 mM NaCl with agitation by Eppendorf Thermomixer shaking at 700 rpm for 20 hours.

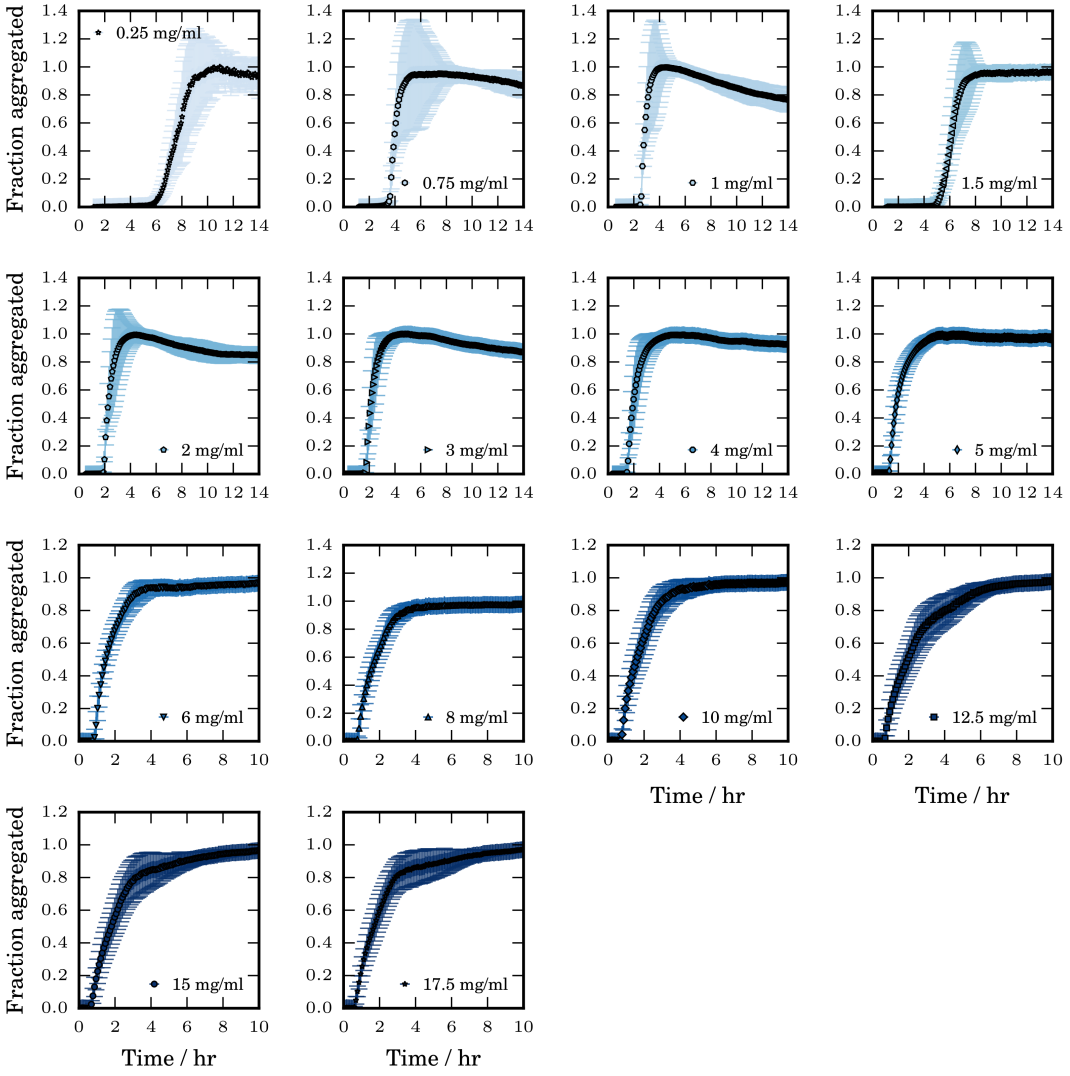

Figure A.20: Average fluorescence aggregation kinetics for HEWL at 65°C, pH 1.5, 200 mM NaCl under agitation (double orbital shaking at 700rpm for 2.5 min every 5 min) at various HEWL concentrations. Data are normalised to the maximum value for each concentration. Error bars are standard deviation. X-axis error bars are not shown.

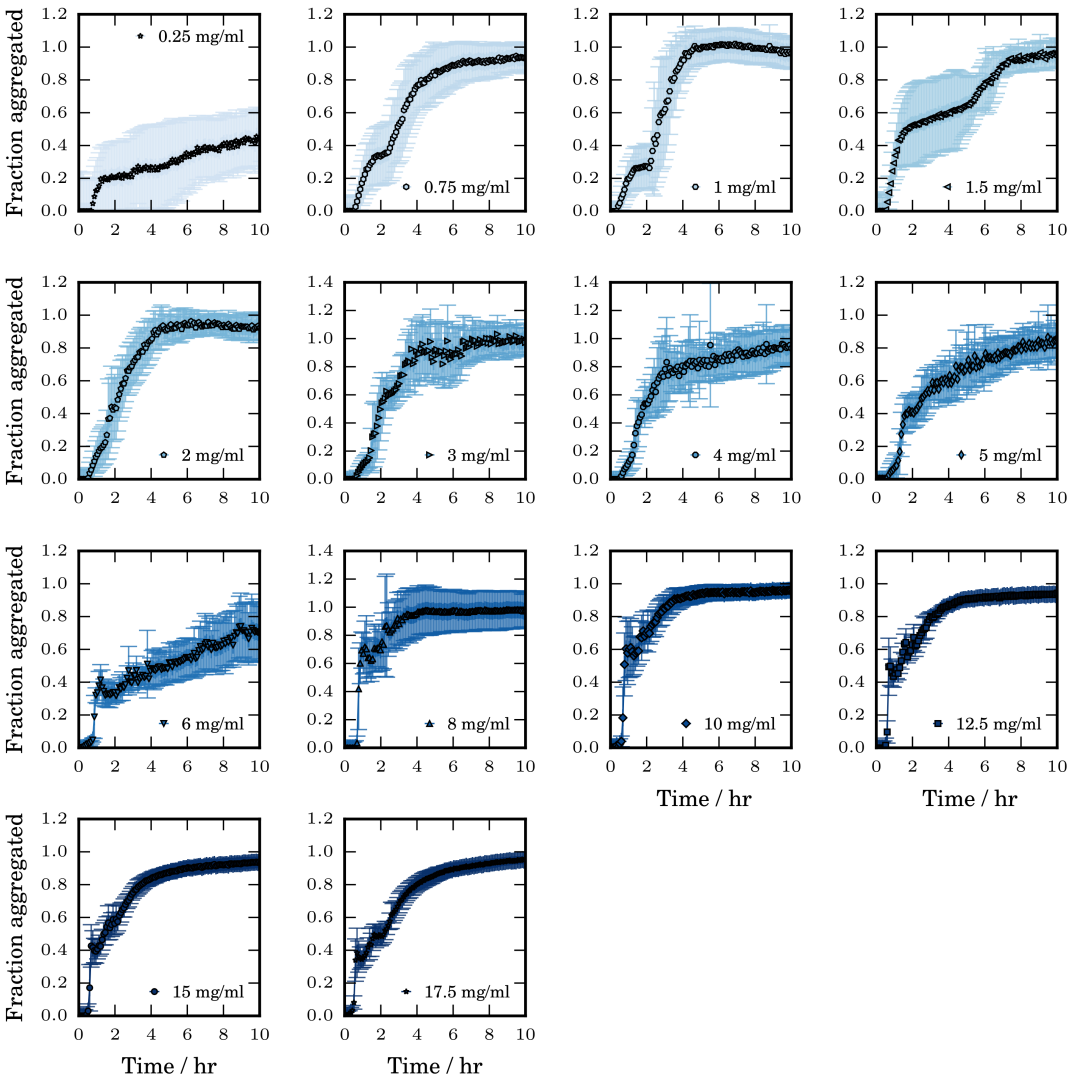

Figure A.21: Average absorbance aggregation kinetics for HEWL at 65°C, pH 1.5, 200 mM NaCl under agitation (double orbital shaking at 700rpm for 2.5 min every 5 min) at various HEWL concentrations. Data are normalised to the maximum absorbance value for each concentration. Error bars are standard deviation.

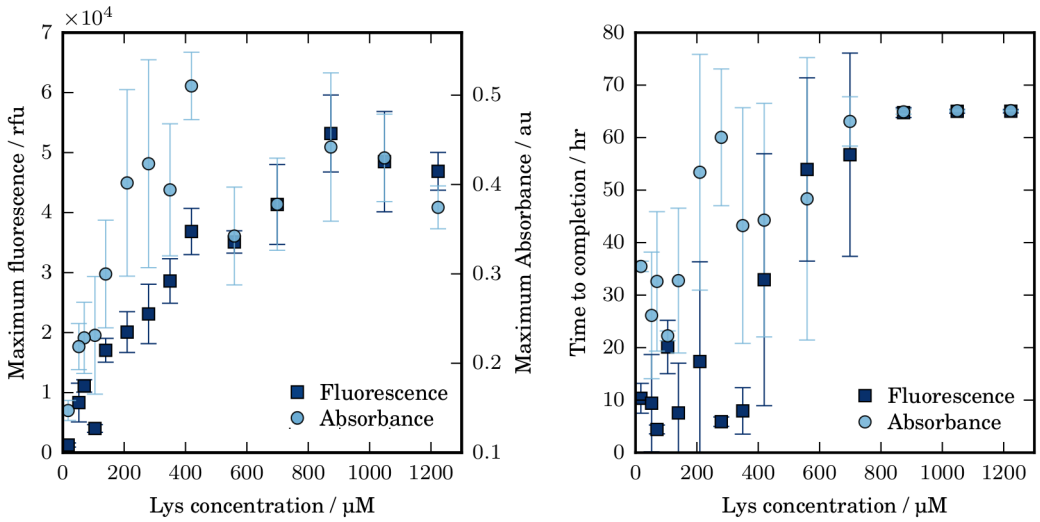

Figure A.22: Left: The maximum values of ThT fluorescence and absorbance at 600nm obtained for various concentrations of HEWL incubated at 65°C, pH 1.6, 200 mM NaCl. Right: The time taken for the kinetic growth to reach the maximum fluorescence or absorbance value.

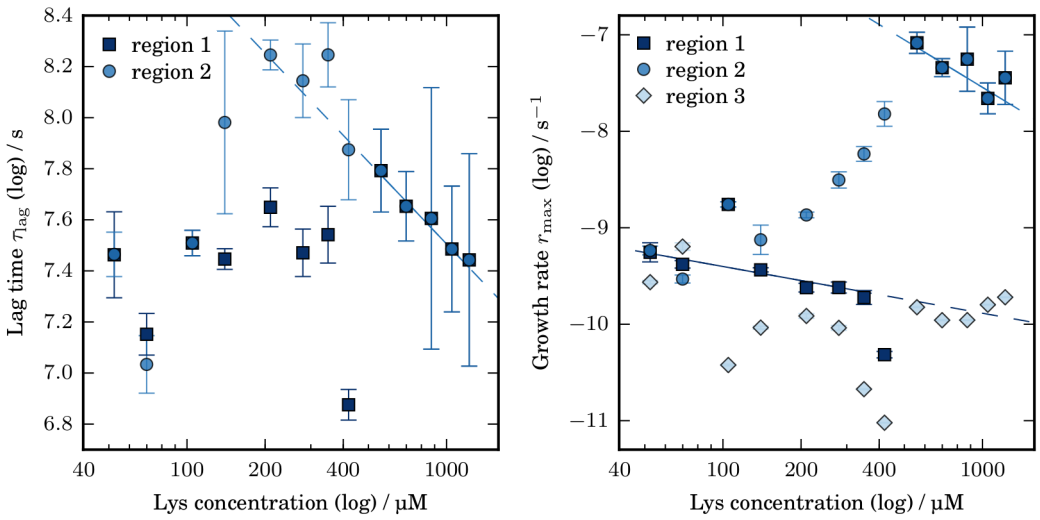

Figure A.23: Absorbance data. Maximum growth rates and associated lag times obtained from linearly fitting about the maximum growth rate of observed absorbance regions for various concentrations of HEWL, pH 1.5, 65°C, 200 mM NaCl with agitation (double orbital shaking at 700rpm). At high concentrations (8 mg/ml, 560 µM, and above) for region 2 ($\tau_{lag} \propto m_{\mathrm{tot}}^{\gamma}$) gives an exponent -0.46(5). In region 1 an exponent of -0.5(3) is obtained for the concentration dependence of the growth rate below 6 mg/ml (420 µM). At 8 mg/ml (560 µM) and above the exponent of the linear fit is -0.7(2). However, the apparent growth rates are coupled to the intensity and do not necessarily represent the real growth rates.

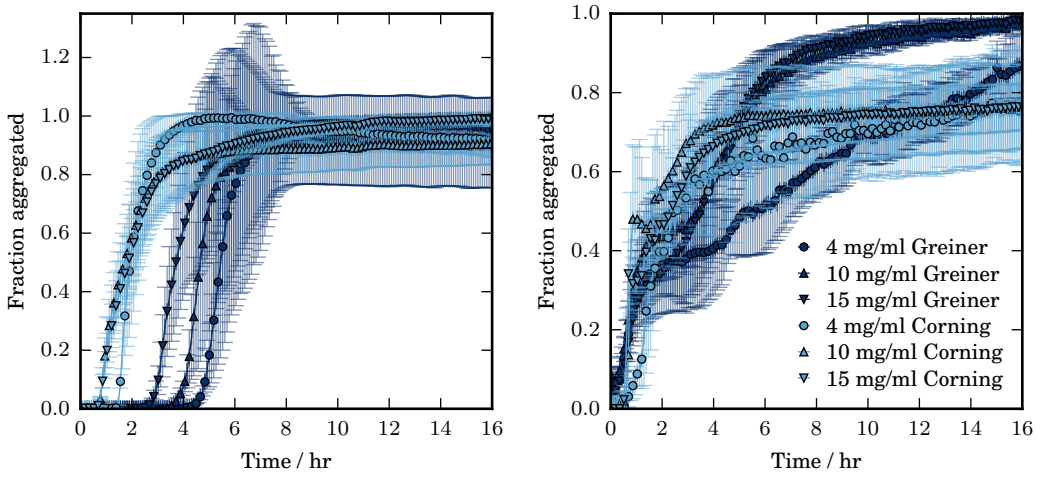

Figure A.24: Thioflavin T fluorescence and simultaneous absorbance at 600 nm for various HEWL concentrations incubated at pH 1.5, 65°C, 200 mM NaCl with agitation (double orbital shaking at 700rpm) in Corning NBS coated or Greiner uncoated microplates.

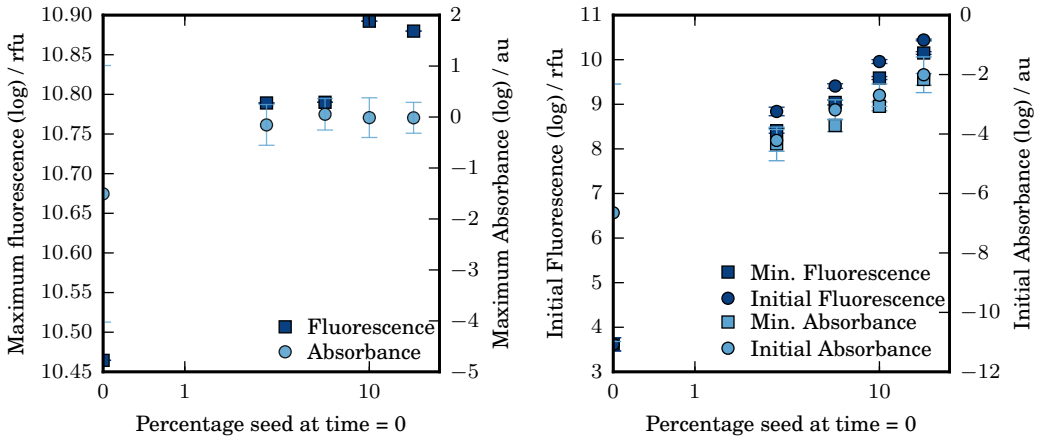

Figure A.25: Maximum (left) and minimum (right) ThT fluorescence and absorbance at 600 nm obtained for 10 mg/ml HEWL incubated at 65°C, pH 1.5, 200mM NaCl with agitation by double orbital platereader shaking at 700 rpm with various concentrations of added seed. Seeds formed by incubation in the same solution conditions with agitation by Thermomixer shaking at 700rpm at 65°C for 20 hours.

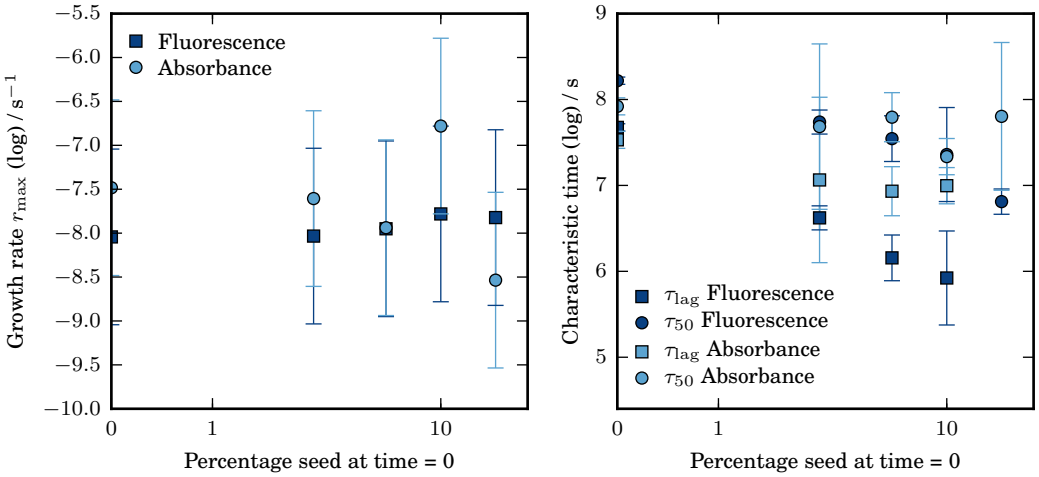

Figure A.26: Growth rate and associated lag times obtained from the best fit tangent to the maximum growth rate for 10 mg/ml HEWL incubated at 65°C, pH 1.5, 200mM NaCl with agitation by double orbital platereader shaking at 700 rpm with various concentrations of added seed. Seeds formed by incubation in the same solution conditions with agitation by Thermomixer shaking at 700rpm at 65°C for 20 hours.

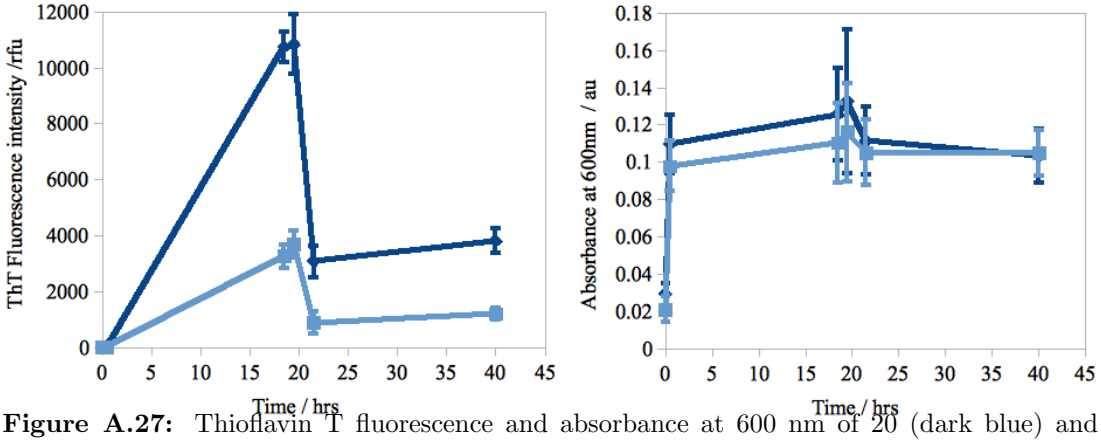

Figure A.27: Thioflavin T fluorescence and absorbance at 600 nm of 20 (dark blue) and 10 (light blue) mg/ml HEWL incubated at pH 2, 90°C with agitation by Eppendorf shaking. Readings performed by platereader assay of aliquots removed from the incubated Eppendorf at various time points.

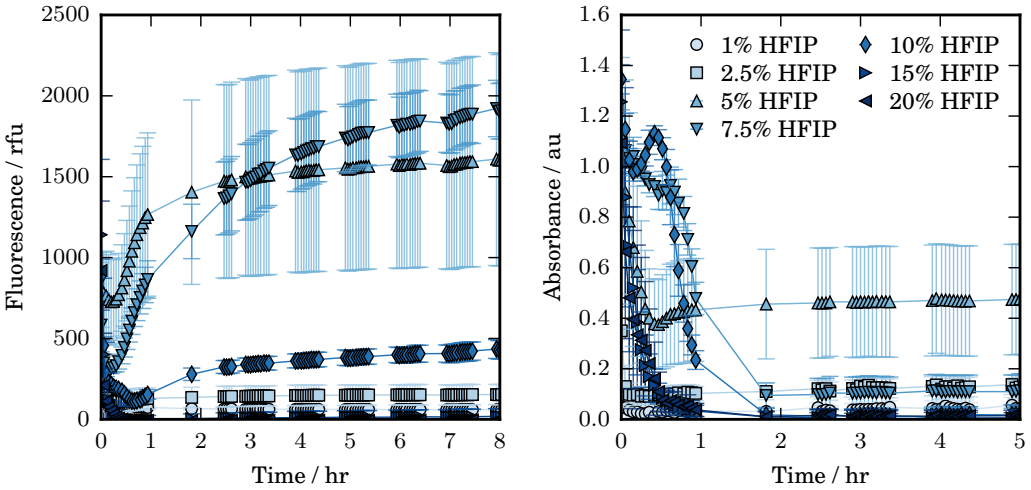

Figure A.28: Thioflavin T fluorescence and absorbance at 600 nm obtained during the aggregation of 10 mg/ml HEWL in the presence of various HFIP concentrations at 35°C, pH 7.4 (20 mM potassium phosphate buffer) under quiescent conditons.

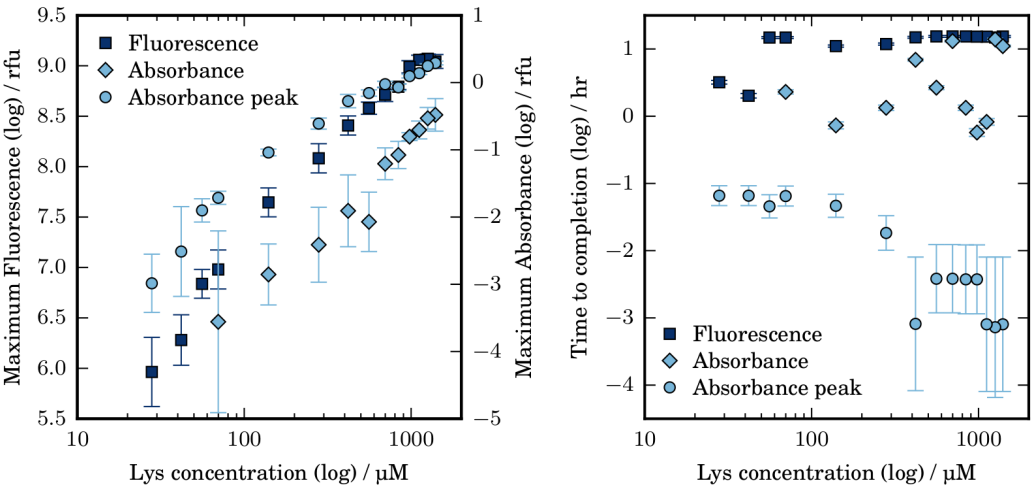

Figure A.29: Maximum Thioflavin T fluorescence and absorbance at 600 nm obtained for various HEWL concentrations aggregated in the presence of 5%HFIP at 35C, pH 7.4 (20 mM potassium phosphate buffer) in quiescent conditions. Experiment performed in 96 well, flat bottomed, Corning NBS coated microplates.

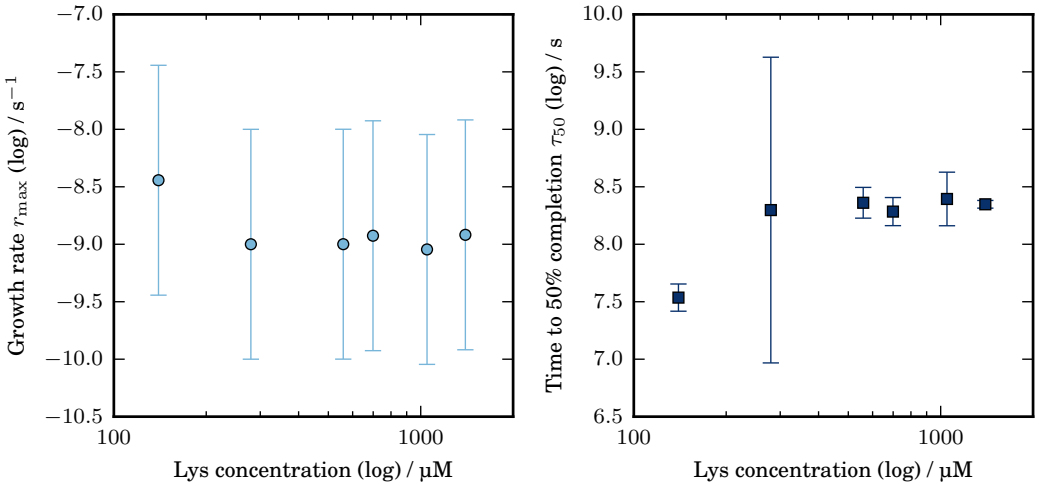

Figure A.30: Growth rate and associated lag time and time to 50% completion obtained from the best fit tangent about the maximum growth rate for aggregation followed by Thioflavin T fluorescence for HEWL incubated at 5%HFIP, 35C, pH 7.4 (20 mM potassium phosphate buffer) in quiescent conditions. 96 well, flat bottomed, uncoated Greiner microplates.

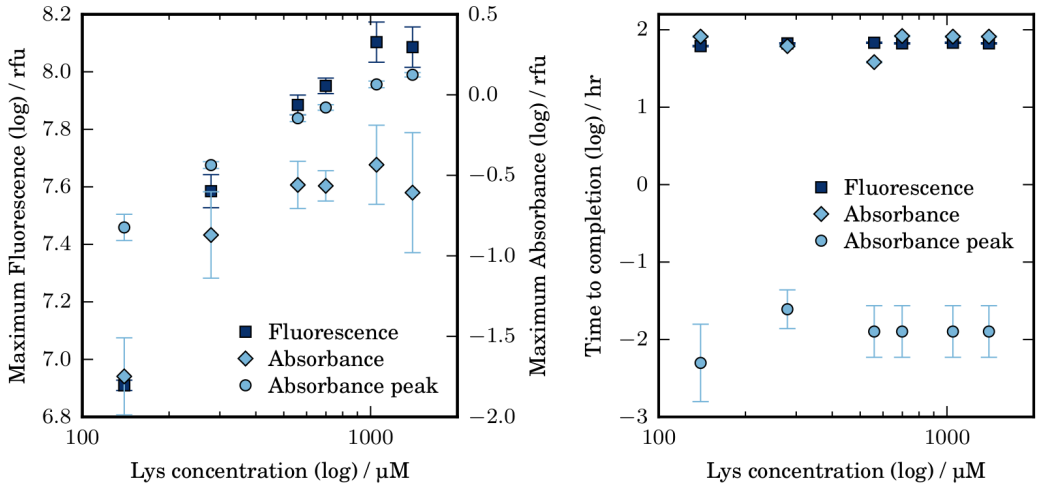

Figure A.31: Maximum Thioflavin T fluorescence and absorbance at 600 nm obtained for various HEWL concentrations aggregated in the presence of 5%HFIP at 35C, pH 7.4 (20 mM potassium phosphate buffer) in quiescent conditions. Experiment performed in 96 well, flat bottomed, uncoated Greiner microplates.

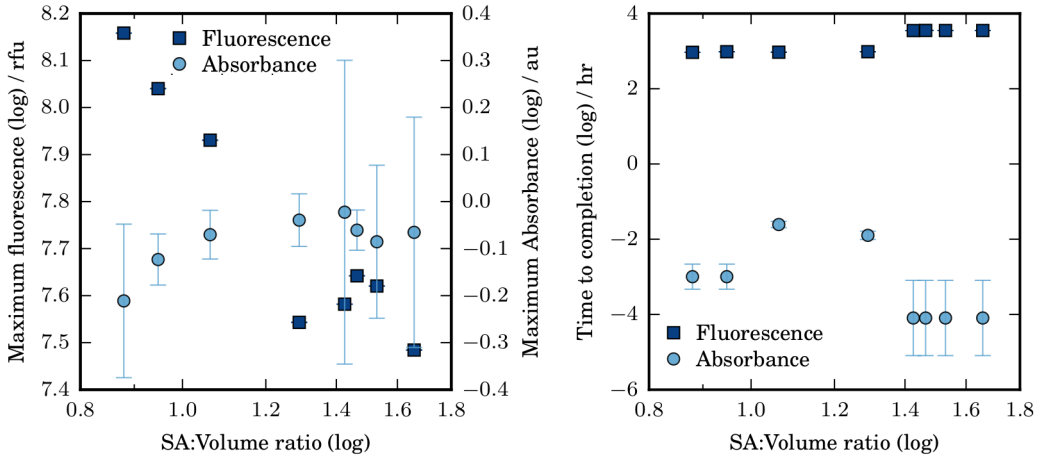

Figure A.32: Maximum thioflavin T fluorescence and absorbance at 600 nm (after the dip) obtained during the aggregation of various volumes of 5 mg/ml HEWL in the presence of 5%HFIP at 35C, pH 7.4 (20 mM potassium phosphate buffer) in quiescent conditions. Corning NBS coated microplate.

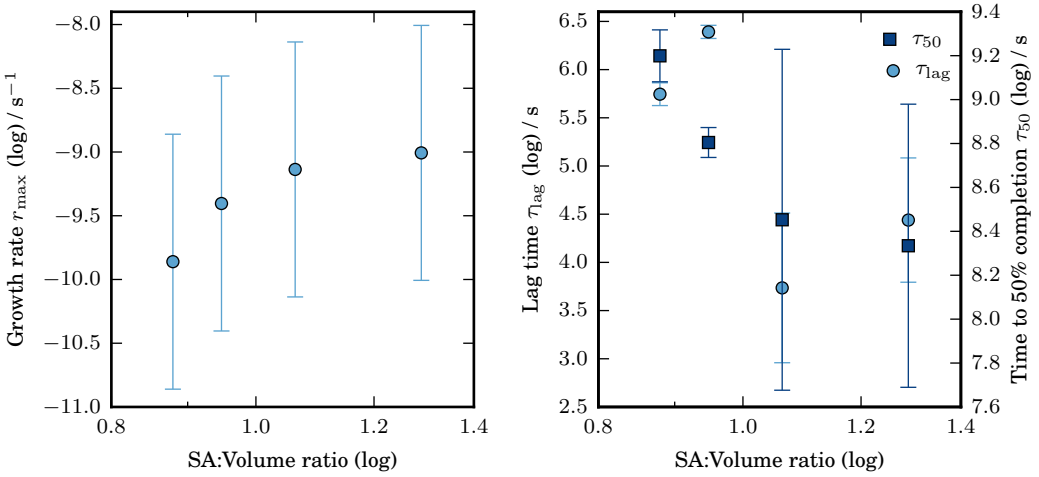

Figure A.33: Growth rate and associated lag time and time to 50% completion obtained from the best fit tangent about the maximum growth rate for aggregation of 5mg/ml HEWL incubated at 5%HFIP, 35C, pH 7.4 (20 mM potassium phosphate buffer) in quiescent conditions at various volumes in either 96 well or 384 well, flat bottomed, uncoated polystyrene Greiner microplates.

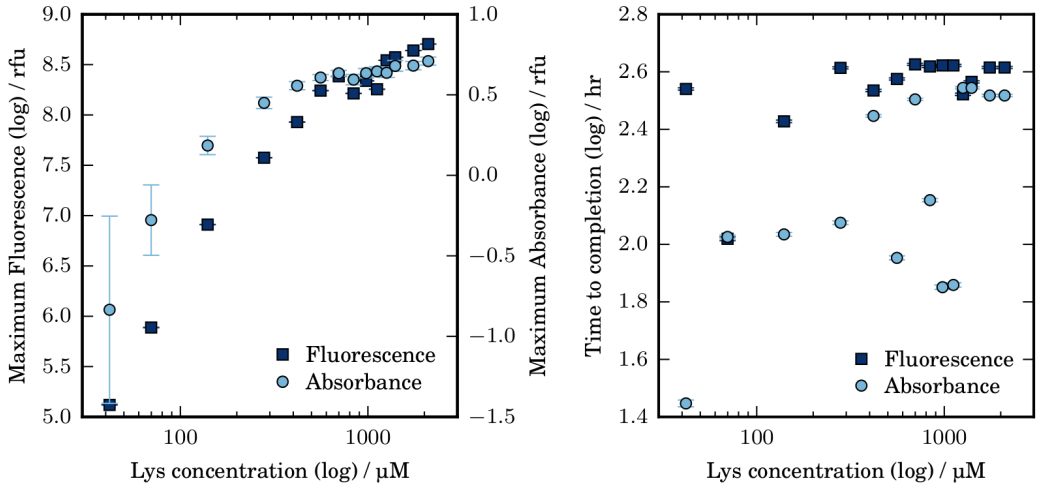

Figure A.34: Maximum thioflavin T fluorescence and absorbance at 600 nm obtained for various HEWL concentrations incubated at 30°C, pH 7.4 (20 mM potassium phosphate buffer), in the presence of 20 mM DTT.

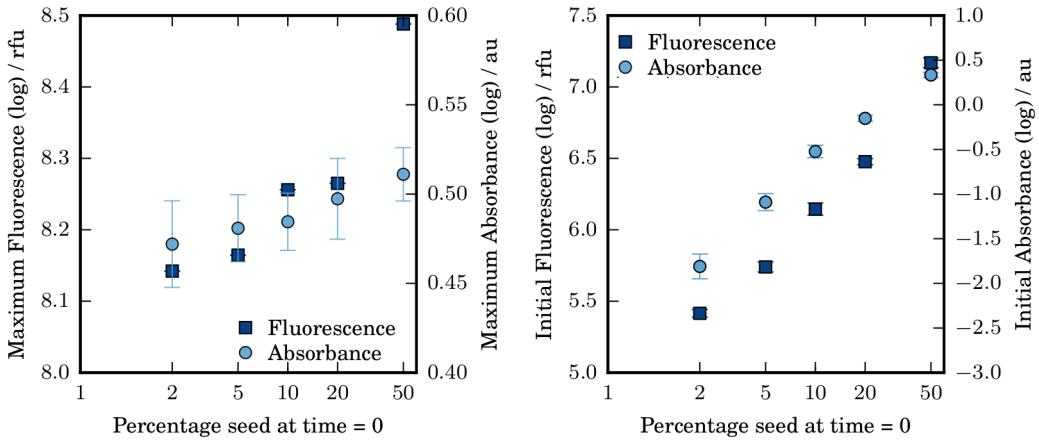

Figure A.35: Maximum (left) and initial (right) thioflavin T fluorescence and absorbance at 600 nm obtained for the aggregation of 10 mg/ml HEWL incubated at 20 mM DTT, pH 7.4 (20 mM potassium phosphate buffer), 35°C with various concentrations of preformed seed. Seed formed under the same conditions.

B Appendix: α-synuclein

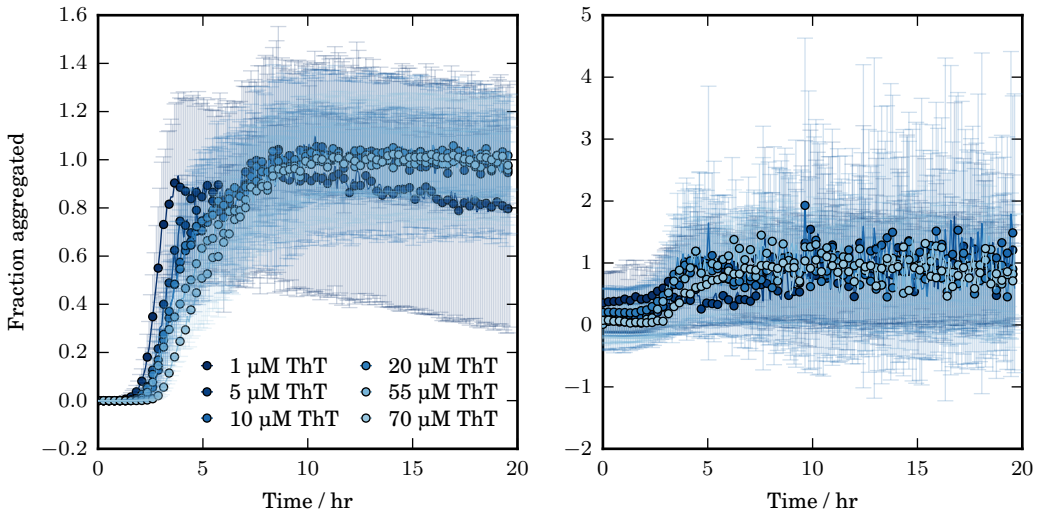

Figure B.1: Thioflavin T fluorescence and simultaneous absorbance (600 nm) measurements for 1 mg/ml α-syn 4 at 50°C, pH 5, 150 mM NaCl under agitation (double orbital shaking at 500rpm for 2.5 min every 5 min) in the presence of various ThT concentrations.

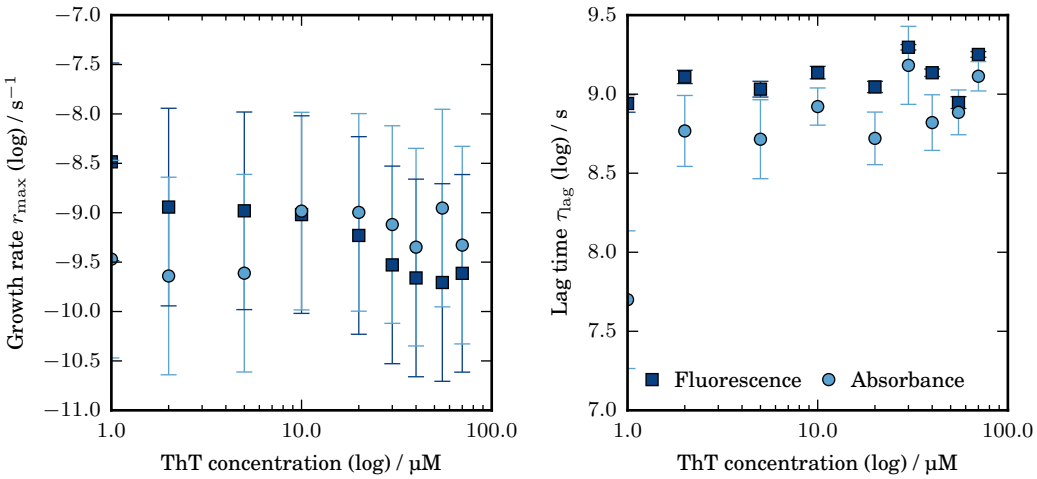

Figure B.2: Maximum growth rate and associated lag time obtained (from tangent to linear region) from Thioflavin T fluorescence and simultaneous absorbance (600 nm) measurements for 1 mg/ml α-syn 4 at 50°C, pH 5, 150 mM NaCl under agitation (double orbital shaking at 500rpm for 2.5 min every 5 min) in the presence of various ThT concentrations.

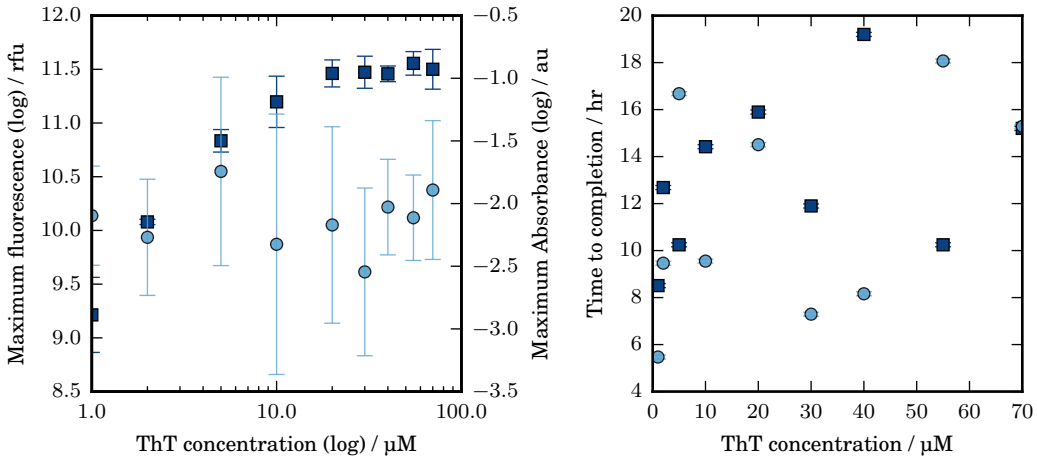

Figure B.3: Left: Maximum Thioflavin T (ThT) fluorescence and absorbance at 600 nm obtained for 1 mg/ml α-syn 4 at 50°C, pH 5, 150 mM NaCl under agitation (double orbital shaking at 500rpm for 2.5 min every 5 min) in the presence of various ThT concentrations. Right: The time taken to reach the maximum value.

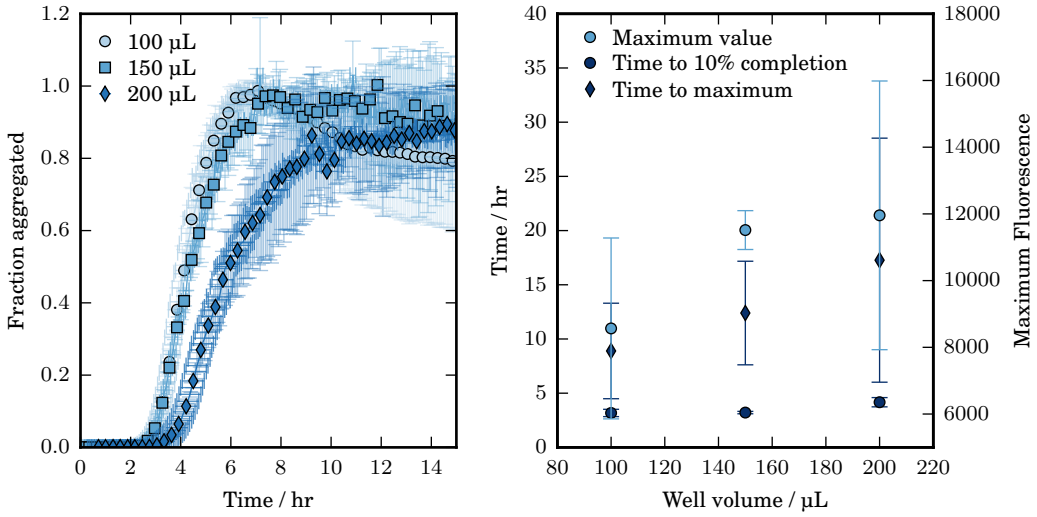

Figure B.4: Left: Thioflavin T fluorescence and simultaneous absorbance at 600 nm for 1 mg/ml α-syn 4 at 50°C, pH 5, 150 mM NaCl under agitation (double orbital shaking at 600rpm for 2.5 min every 5 min) at different well volumes in StarWell microplates. Right: The time taken to reach the maximum value, 10% completion and the maximum fluorescence value.

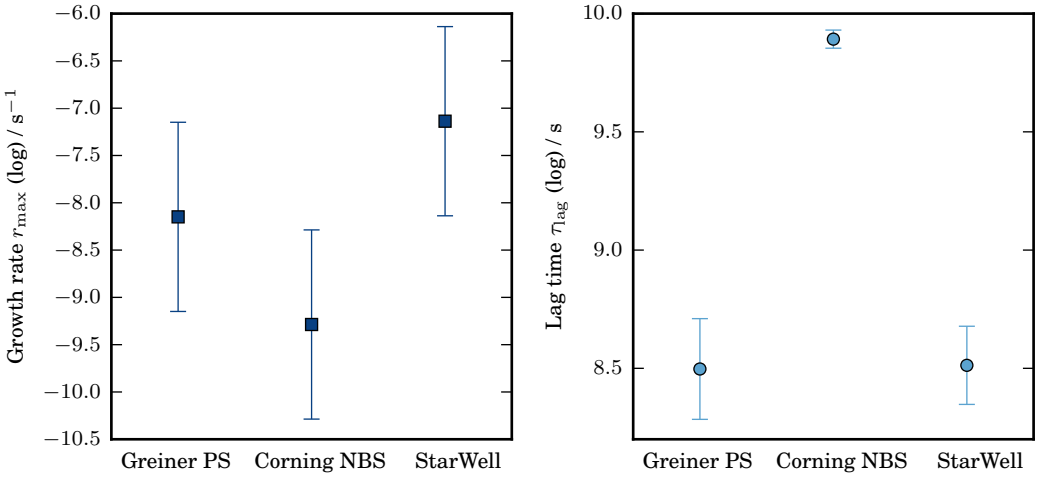

Figure B.5: Maximum growth rate and associated lag time obtained (from tangent to linear region) from Thioflavin T fluorescence and simultaneous absorbance (600 nm) measurements for 1 mg/ml α-syn 4 at 60°C, pH 3.5, 150 mM NaCl, double orbital shaking at 600rpm for 5 min every 6 min).

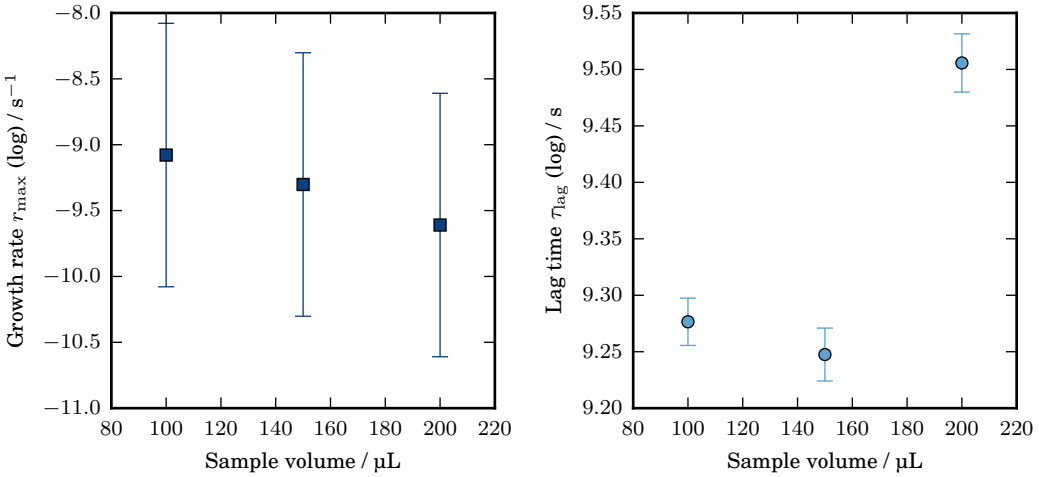

Figure B.6: Maximum growth rate and associated lag time obtained (from tangent to linear region) from Thioflavin T fluorescence and simultaneous absorbance (600 nm) measurements for 1 mg/ml α-syn 4 at 50°C, pH 5, 150 mM NaCl, double orbital shaking at 600rpm for 2.5 min every 5 min, at different well volumes in StarWell microplates.

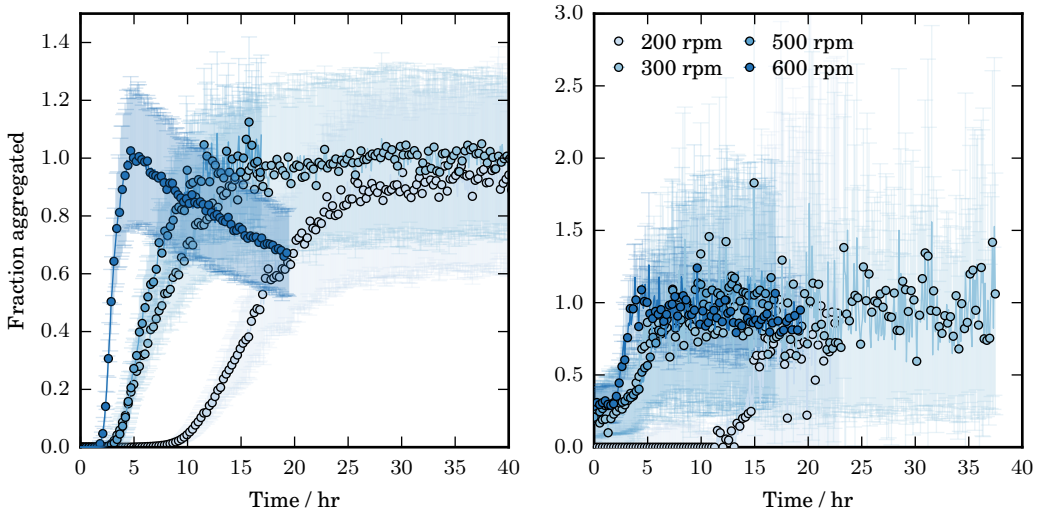

Figure B.7: Normalised Thioflavin T fluorescence (left) and simultaneous absorbance at 600 nm (right) data for 1 mg/ml α-synuclein 4, 50°C, pH 5, 150 mM NaCl with shaking by double orbital microplate shaking at various rates for 2.5 min in every 5 min cycle. StarWell microplates.

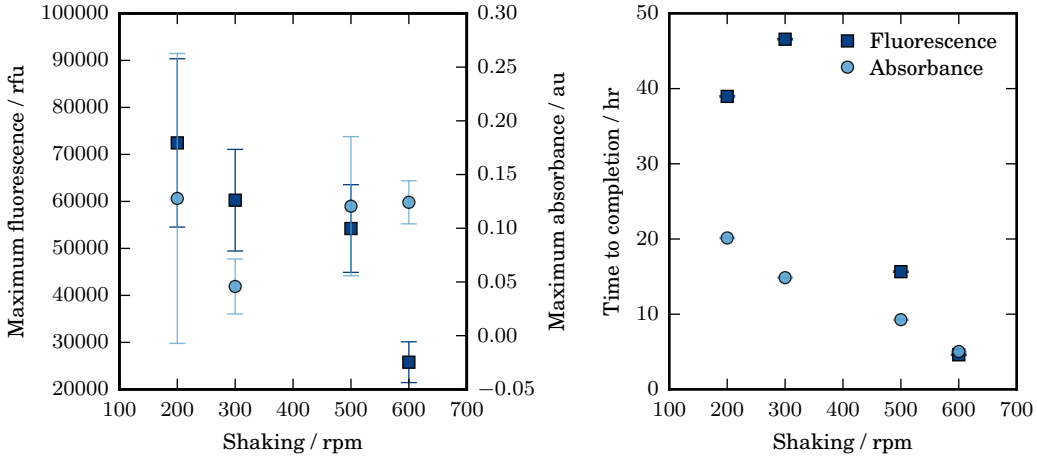

Figure B.8: Maximum Thioflavin T fluorescence, absorbance at 600 nm and the time taken to reach the maximum value for 1 mg/ml α-synuclein 4, 50°C, pH 5, 150 mM NaCl with shaking by double orbital microplate shaking at various rates for 2.5 min in every 5 min cycle. StarWell microplates.

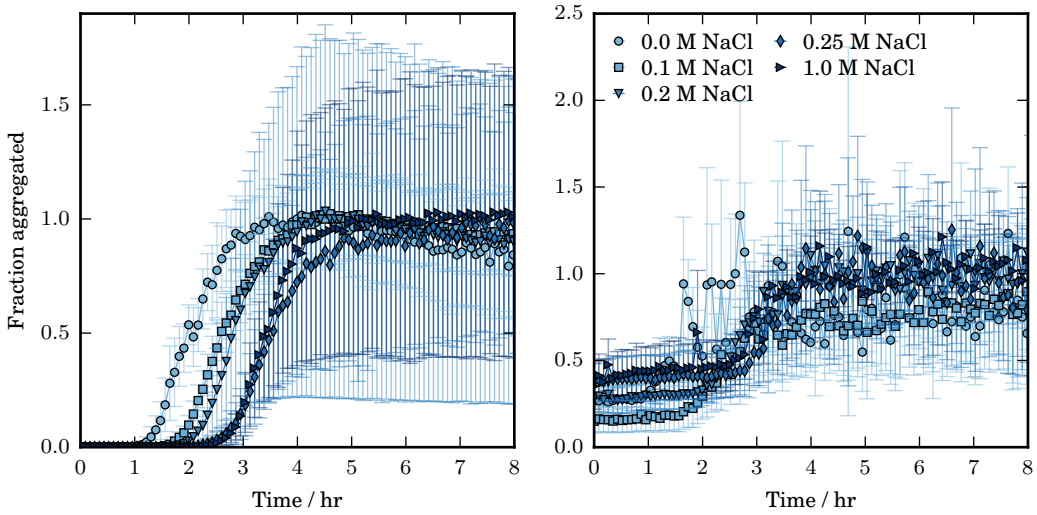

Figure B.9: Normalised Thioflavin T fluorescence (left) and simultaneous absorbance at 600 nm (right) data for 1 mg/ml α-synuclein (purification 4), 50°C, pH 5, with shaking by double orbital microplate shaking at 600rpm in the presence of various NaCl concentrations. The 0.0 M NaCl sample contains 0.014 M NaCl. StarWell microplates.

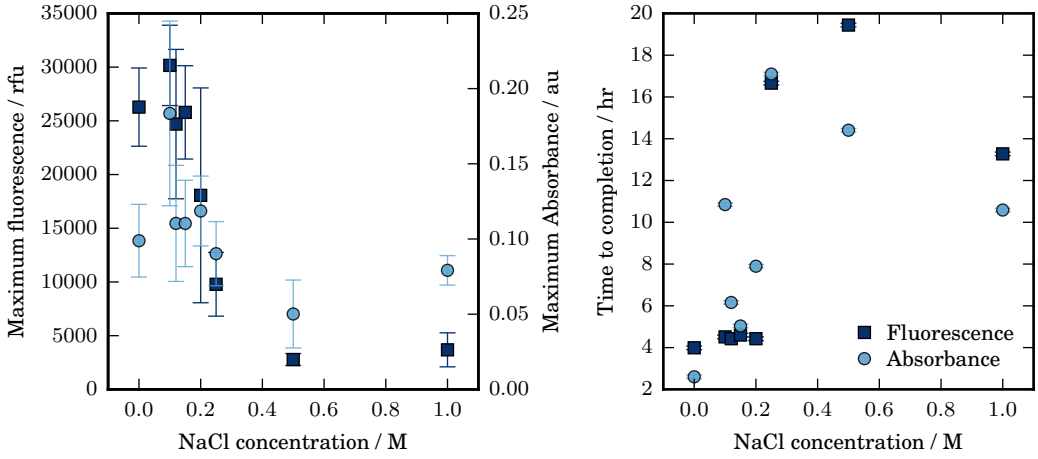

Figure B.10: Maximum Thioflavin T fluorescence, absorbance at 600 nm and the time taken to reach the maximum value for 1 mg/ml α-synuclein 4, 50°C, pH 5, with shaking by double orbital microplate shaking at 600rpm in the presence of various NaCl concentrations. StarWell microplates.

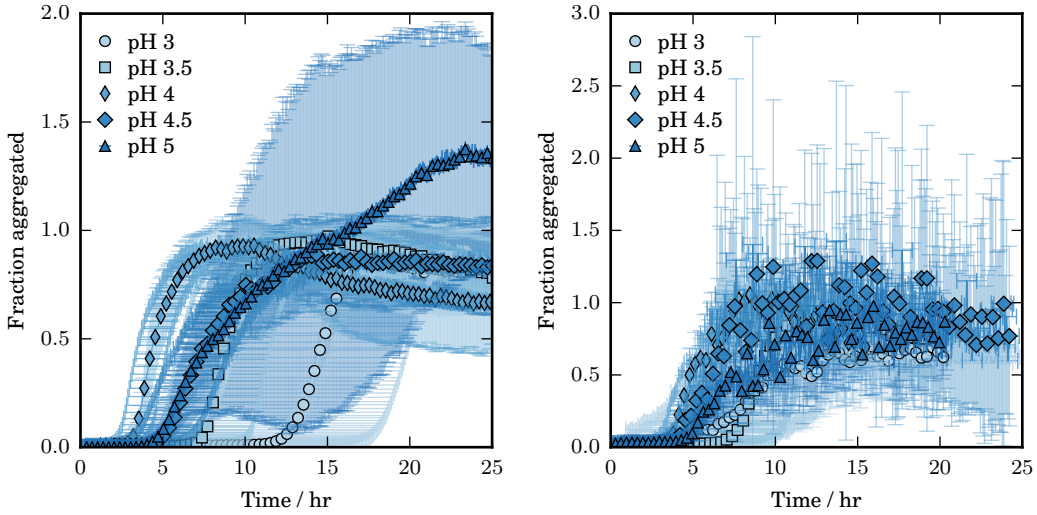

Figure B.11: Thioflavin T fluorescence and simultaneous absorbance at 600 nm for 1 mg/ml α-syn 4 at 37°C, 150 mM NaCl under agitation (medium shaking in Biotek platereader for 2.5 min every 5 min) at various solution pH, altered by addition of HCl. The shaking conditions in the Biotek platereader were not sufficient to produce reproducible growth curves, as evident in the x-axis uncertainty. StarWell microplates.

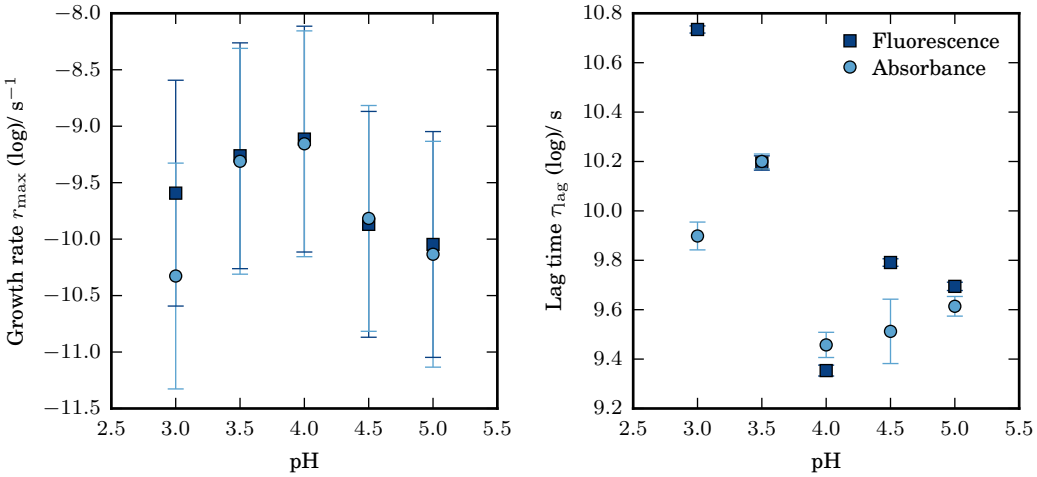

Figure B.12: Maximum growth rate and associated characteristic time obtained (from tangent to linear region) from Thioflavin T fluorescence and simultaneous absorbance at 600 nm for 1 mg/ml α-syn 4 at 37°C, 150 mM NaCl under agitation (medium shaking in Biotek platereader for 2.5 min every 5 min) at various solution pH, altered by addition of HCl. StarWell microplates.

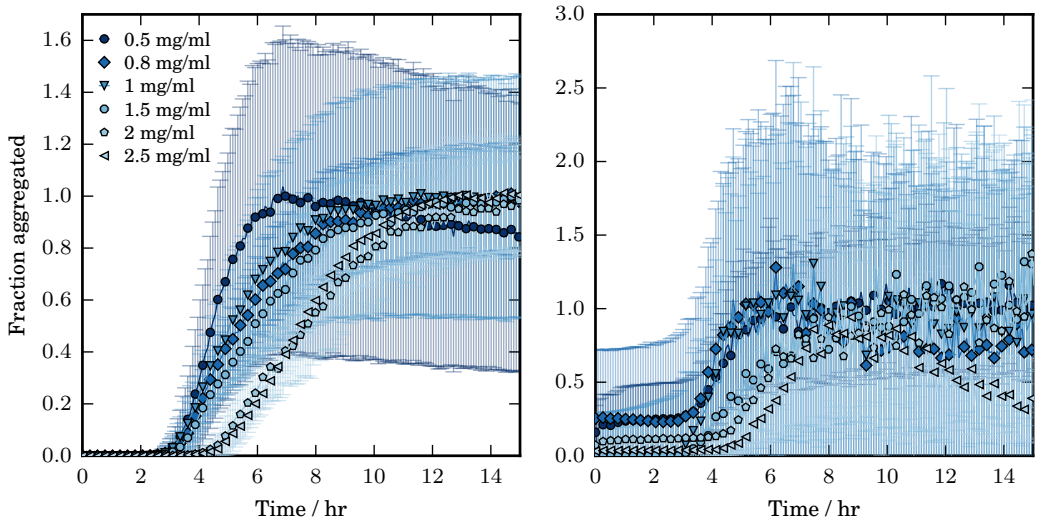

Figure B.13: Normalised Thioflavin T fluorescence (left) and simultaneous absorbance at 600 nm (right) data for various α-synuclein 4 concentrations at 50°C, pH 5, 150 mM NaCl with shaking by double orbital microplate shaking at 600rpm. StarWell microplates.

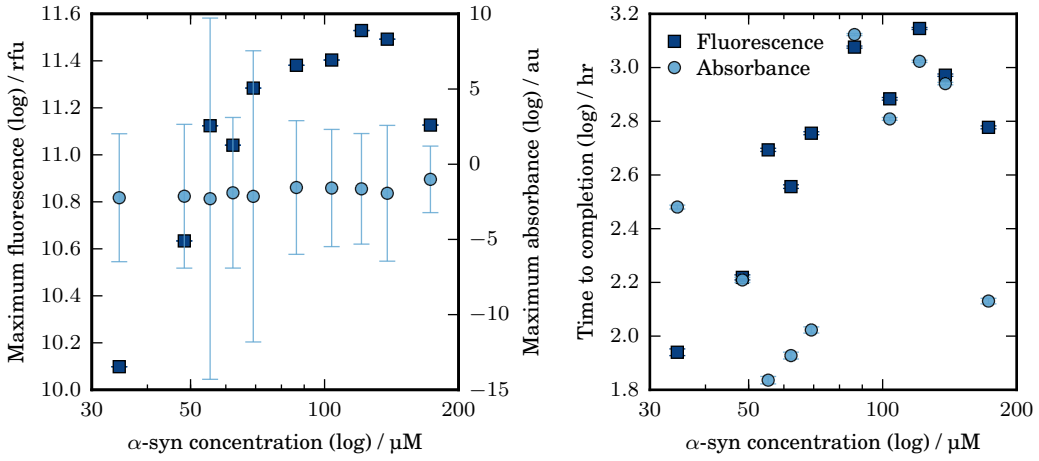

Figure B.14: Maximum Thioflavin T fluorescence, absorbance at 600 nm and the time taken to reach the maximum value for various α-synuclein 4 concentrations at 50°C, pH 5, 150 mM NaCl with shaking by double orbital microplate shaking at 600rpm. StarWell microplates.

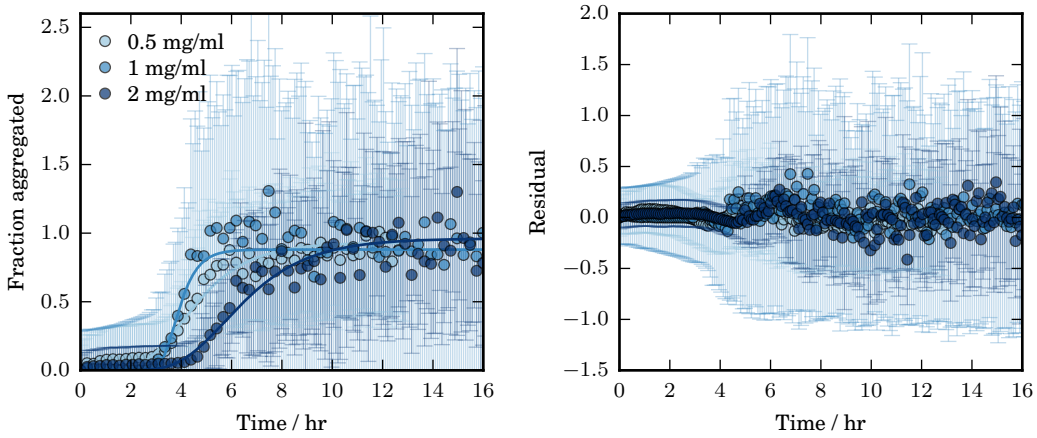

Figure B.15: Normalised absorbance at 600 nm (circles) and corresponding fit to the Gompertz function (solid line in matching shade) for various concentrations ofα-synuclein 4 at 50°C, pH 5, 150 mM NaCl with shaking by double orbital microplate shaking at 600rpm. StarWell microplates.

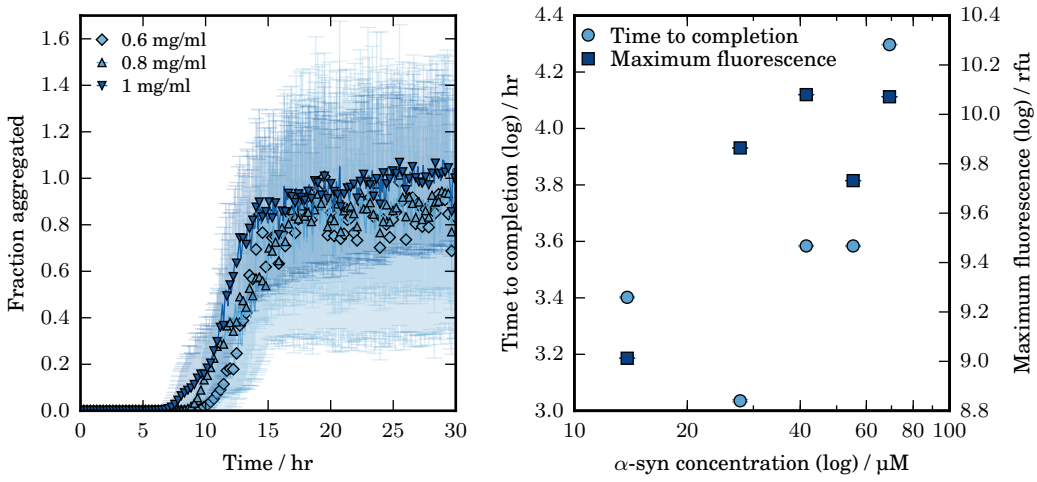

Figure B.16: Normalised Thioflavin T fluorescence (left) and the maximum ThT fluorescence value and time to reach maximum fluorescence (right) data for various α-synuclein 2 concentrations at 37°C, pH 5, 120 mM NaCl with shaking by double orbital microplate shaking at 200rpm. StarWell microplates.

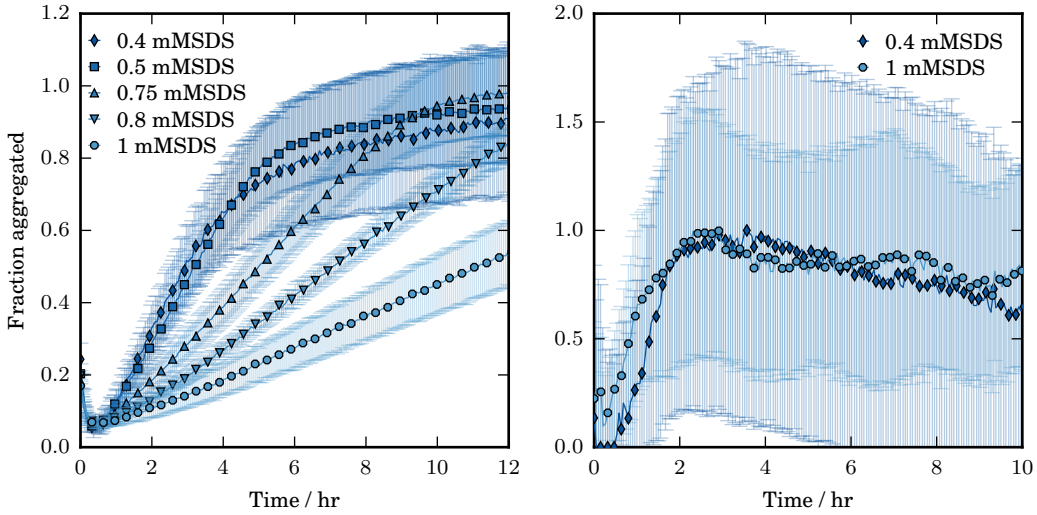

Figure B.17: Thioflavin T fluorescence and simultaneous absorbance at 600 nm for 1 mg/ml α-syn in various SDS concentrations at 50°C, pH 7.4, 120 mM NaCl.

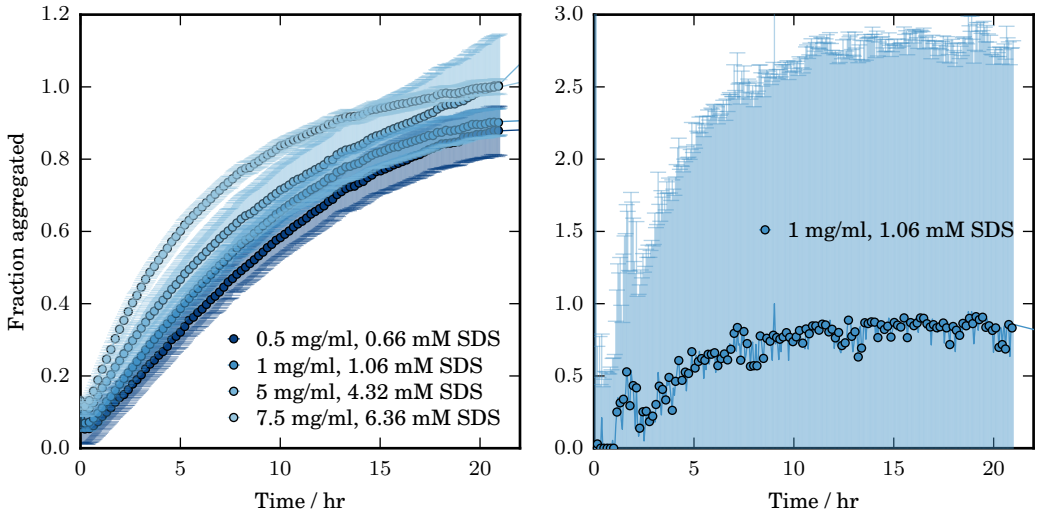

Figure B.18: Thioflavin T fluorescence and simultaneous absorbance at 600 nm for various α-syn 2 and SDS concentrations at 37°C, pH 7.4 (20 mM potassium phosphate buffer), 120 mM NaCl.

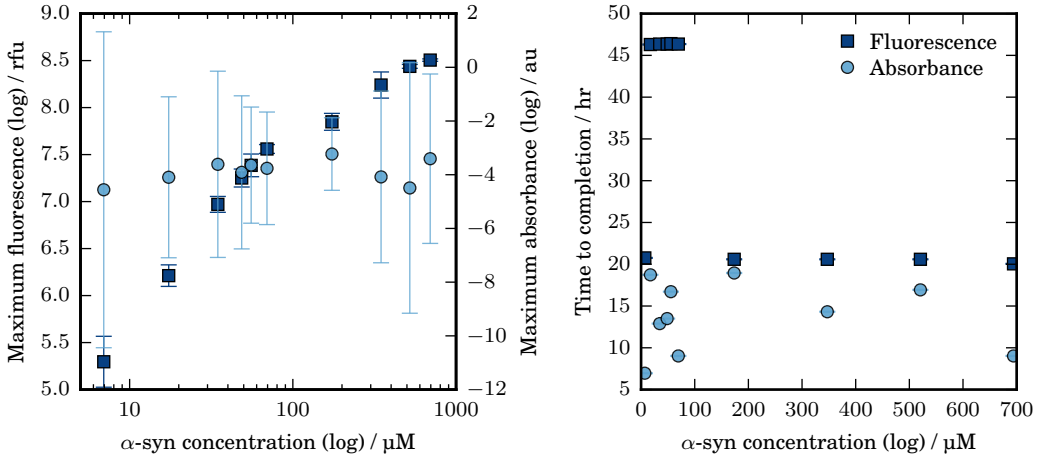

Figure B.19: Left: Maximum Thioflavin T (ThT) fluorescence and absorbance at 600 nm obtained for various α-syn 2 and SDS concentrations at 37°C, pH 7.4 (20 mM potassium phosphate buffer), 120 mM NaCl. Right: The time taken to reach the maximum value.

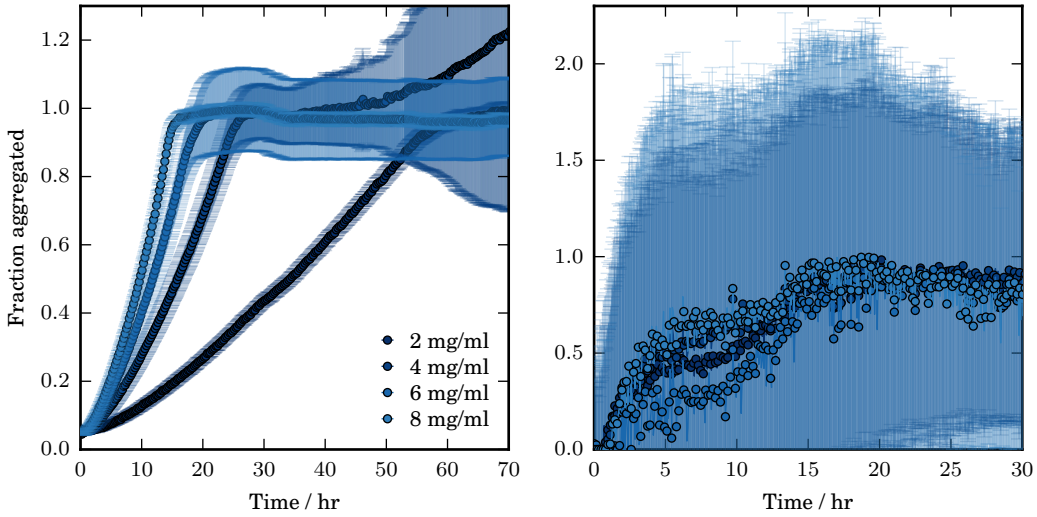

Figure B.20: Thioflavin T fluorescence and simultaneous absorbance at 600 nm for various α-syn 4 concentrations in 0.5 mM SDS at 30°C, pH 7.4, 120 mM NaCl.

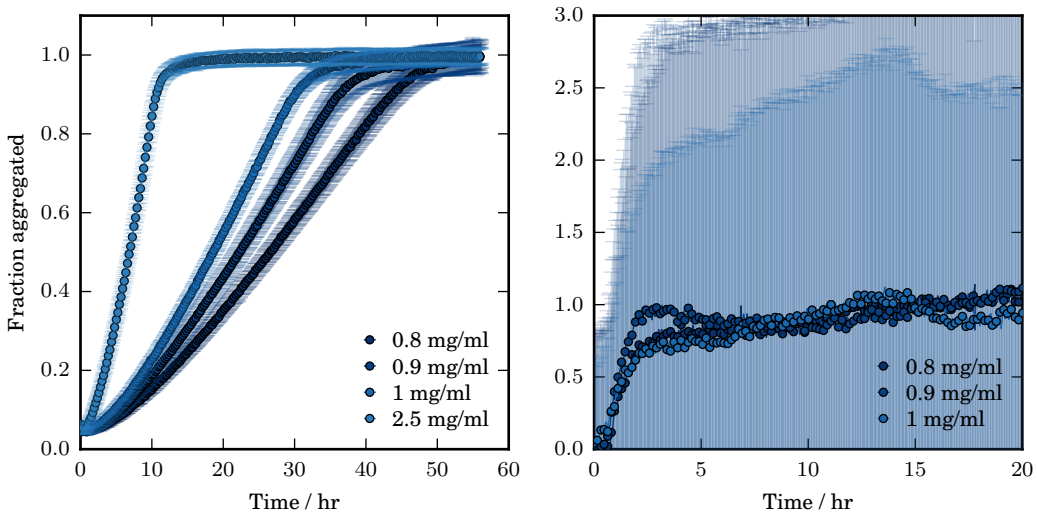

Figure B.21: Thioflavin T fluorescence and simultaneous absorbance at 600 nm for various α-syn 4 concentrations in 0.5 mM SDS at 35°C, pH 7.4, 120 mM NaCl.

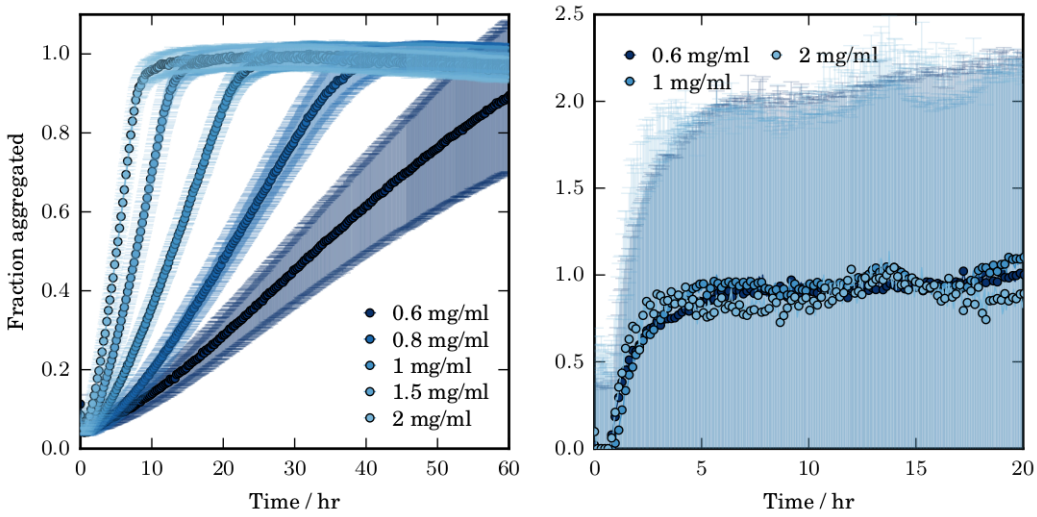

Figure B.22: Thioflavin T fluorescence and simultaneous absorbance at 600 nm for various α-syn 4 concentrations in 0.5 mM SDS at 40°C, pH 7.4, 120 mM NaCl.

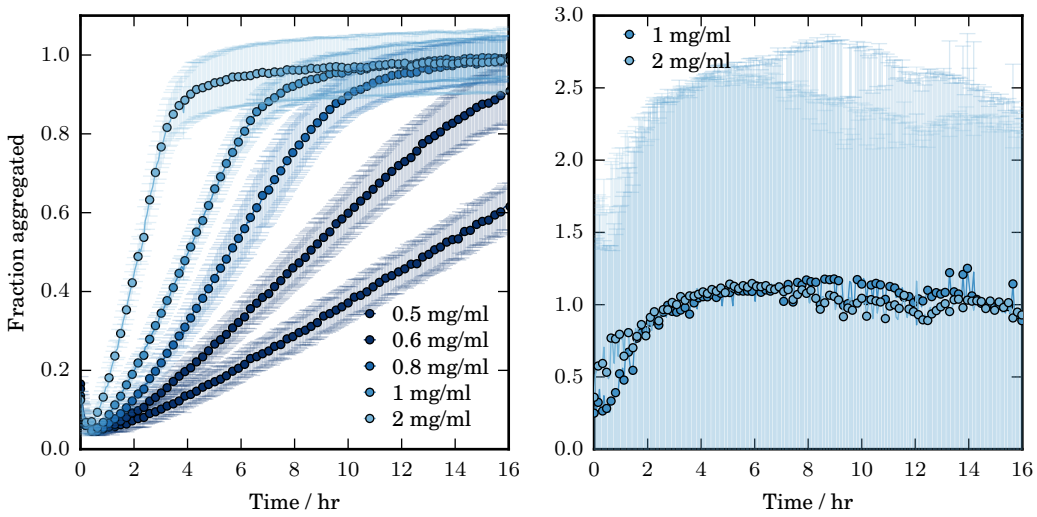

Figure B.23: Thioflavin T fluorescence and simultaneous absorbance at 600 nm for various α-syn 4 concentrations in 0.5 mM SDS at 45°C, pH 7.4, 120 mM NaCl.

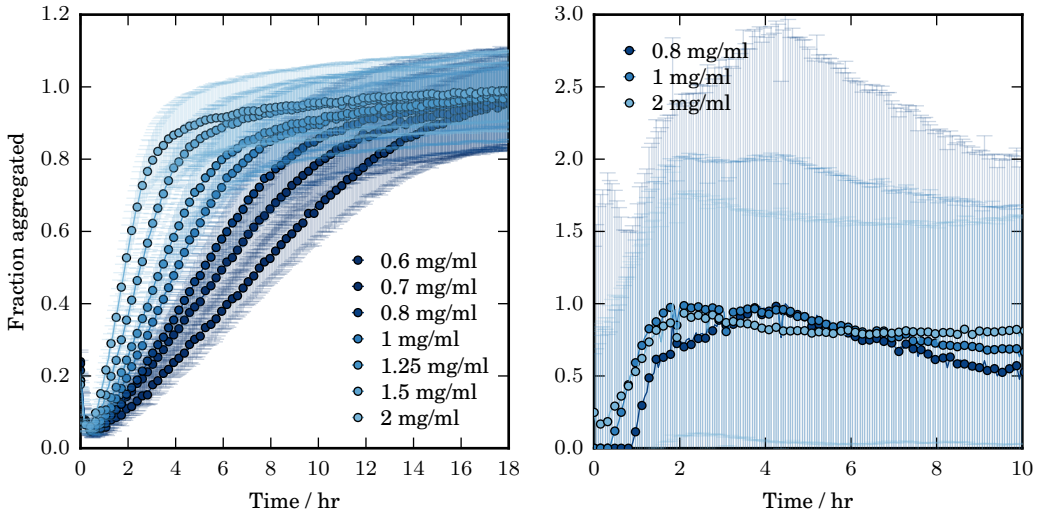

Figure B.24: Thioflavin T fluorescence and simultaneous absorbance at 600 nm for various α-syn 4 concentrations in 0.5 mM SDS at 50°C, pH 7.4, 120 mM NaCl.

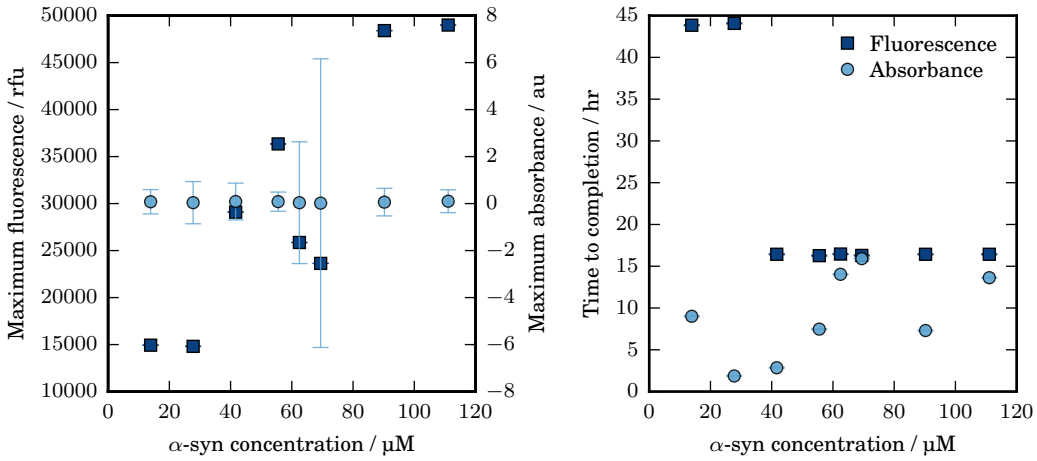

Figure B.25: Left: Maximum Thioflavin T (ThT) fluorescence and absorbance at 600 nm obtained for α-syn 1 in 0.5 mM SDS at 37°C, pH 7.4 (20 mM potassium phosphate buffer), 120 mM NaCl. Right: The time taken to reach the maximum value.

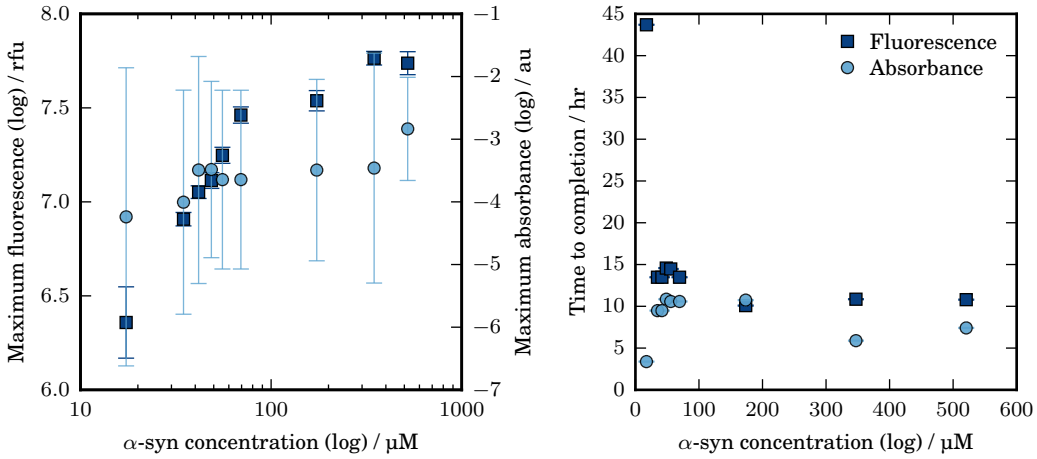

Figure B.26: Left: Maximum Thioflavin T (ThT) fluorescence and absorbance at 600 nm obtained for α-syn 2 in 0.5 mM SDS at 37°C, pH 7.4 (20 mM potassium phosphate buffer), 120 mM NaCl. Right: The time taken to reach the maximum value.

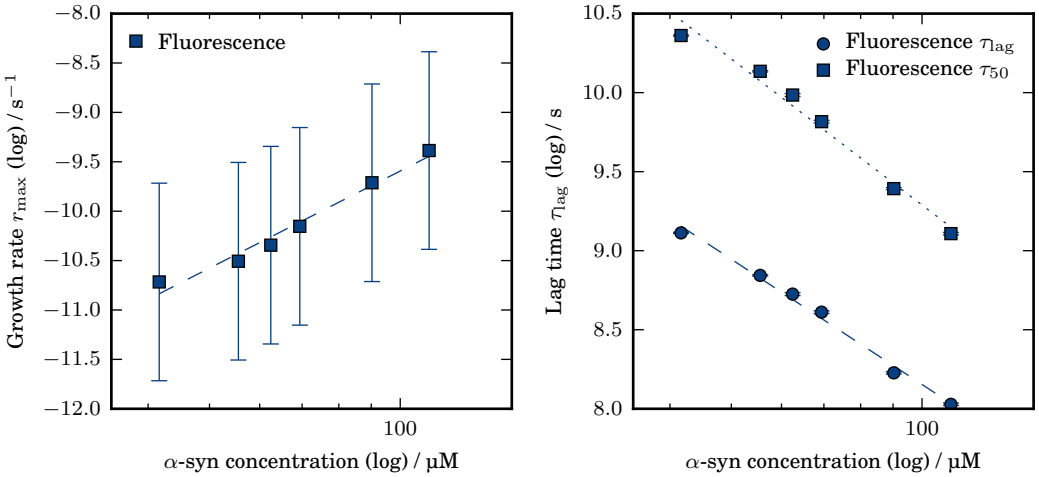

Figure B.27: Maximum growth rate and associated characteristic times obtained (from tangent to linear region) from Thioflavin T fluorescence and simultaneous absorbance (600 nm) measurements for α-syn 1 in 0.5 mM SDS at 37°C, pH 7.4 (20 mM potassium phosphate buffer), 120 mM NaCl.

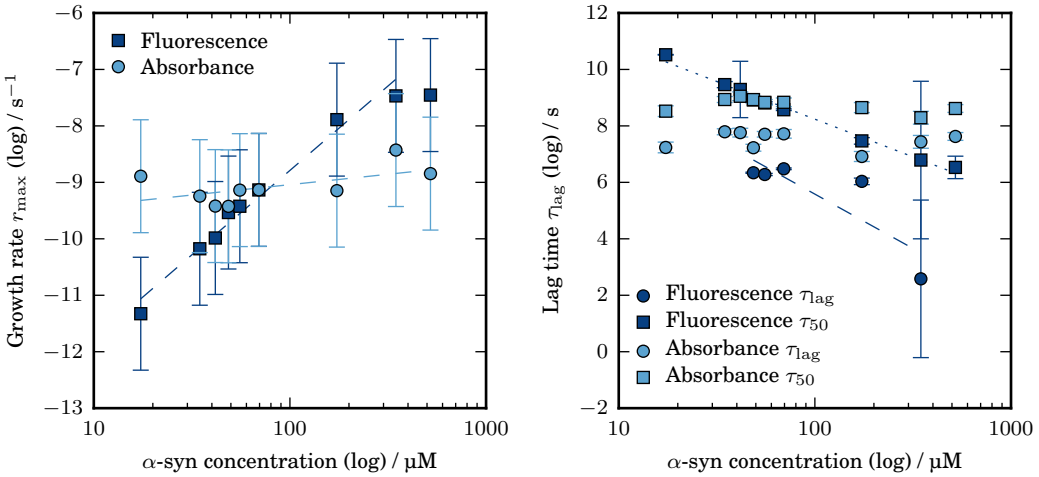

Figure B.28: Maximum growth rate and associated characteristic time obtained (from tangent to linear region) from Thioflavin T fluorescence and simultaneous absorbance (600 nm) measurements for α-syn 2 in 0.5 mM SDS at 37°C, pH 7.4 (20 mM potassium phosphate buffer), 120 mM NaCl.

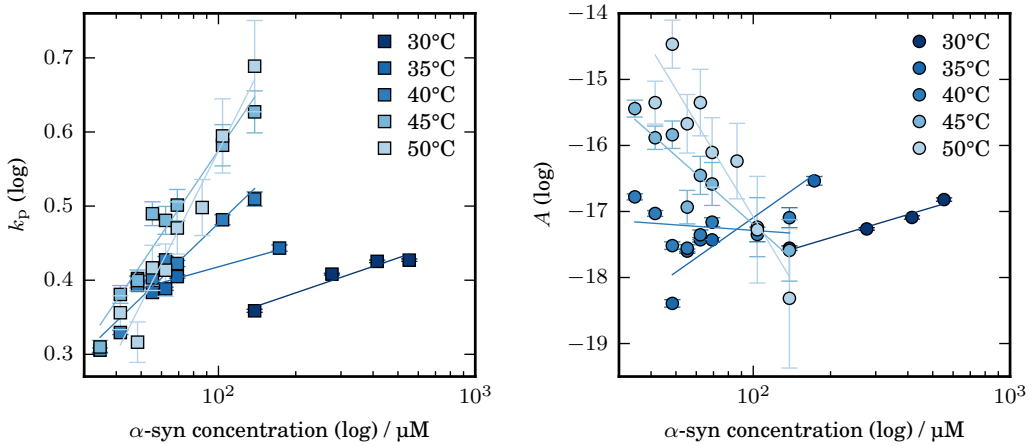

Figure B.29: Growth parameters obtained from a polynomial fit ($M(t) = At^{k_p} + y_1$) to the initial increase in Thioflavin T fluorescence for α-syn 4 in 0.5 mM SDS incubated at various temperatures, 5 mM phosphate buffer, pH 7.4, 120 mM NaCl.

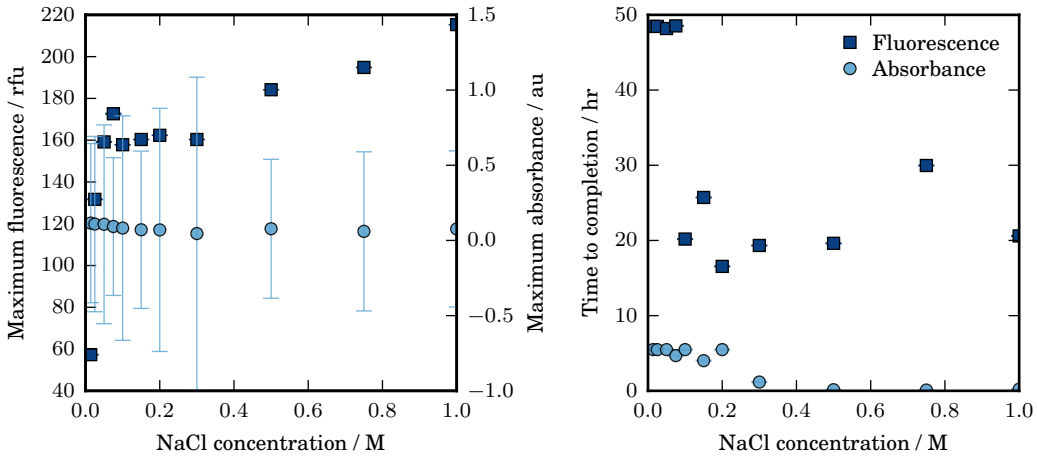

Figure B.30: Left: Maximum Thioflavin T (ThT) fluorescence and absorbance at 600 nm obtained for 1 mg/ml α-syn 4 in 0.5 mM SDS at 50°C, pH 7.4, 400 mM NaCl. Right: The time taken to reach the maximum value.

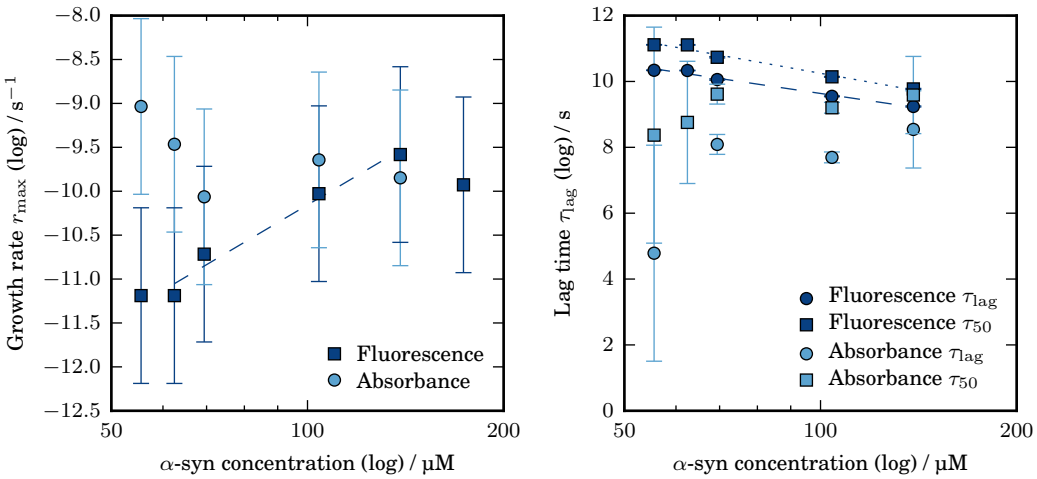

Figure B.31: Maximum growth rate and associated characteristic times obtained (from tangent to linear region) from Thioflavin T fluorescence and simultaneous absorbance (600 nm) measurements for α-syn in 0.5 mM SDS at 50°C, pH 7.4, 400 mM NaCl.

Bibliography

[1] Miti T, Mulaj M, Schmit J D and Muschol M 2015 *Biomacromolecules* **16** 326–35

[2] Hill S E, Robinson J, Matthews G and Muschol M 2009 *Biophys. J.* **96** 3781–90

[3] Tosatto L, Horrocks M H, Dear A J, Knowles T P J, Dalla Serra M, Cremades N, Dobson C M and Klenerman D 2015 *Sci. Rep.* **5** 16696

[4] Anderson V L, Ramlall T F, Rospigliosi C C, Webb W W and Eliezer D 2010 *Proc. Natl. Acad. Sci. U. S. A.* **107** 18850–5

[5] Walsh D M and Selkoe D J 2007 *J. Neurochem.* **101** 1172–84

[6] Dauer W and Przedborski S 2003 *Neuron* **39** 889–909

[7] DiFiglia M, Sapp E, Chase K O, Davies S W, Bates G P, Vonsattel J P and Aronin N 1997 *Science* **277** 1990–3

[8] Rhoades E, Agarwal J and Gafni a 2000 *Biochim. Biophys. Acta* **1476** 230–8

[9] Prusiner S B 1991 *Science* **252** 1515–22

[10] Roberts C J 2003 *J. Phys. Chem. B* **107** 1194–1207

[11] Morozova-Roche L and Malisauskas M 2007 *Curr. Med. Chem.* **14** 1221–30

[12] van der Linden E and Venema P 2007 *Curr. Opin. Colloid Interface Sci.* **12** 158–165

[13] Chi E Y, Krishnan S, Randolph T W and Carpenter J F 2003 *Pharm. Res.* **20** 1325–36

[14] Maury C P J 2009 *J. Intern. Med.* **265** 329–34

[15] Morris K and Serpell L 2010 *Chem. Soc. Rev.* **39** 3445–53

[16] McGlinchey R P, Shewmaker F, McPhie P, Monterroso B, Thurber K and Wickner R B 2009 *Proc. Natl. Acad. Sci. U. S. A.* **106** 13731–6

[17] Majumdar A, Cesario W C, White-Grindley E, Jiang H, Ren F, Khan M R, Li L, Choi E M L, Kannan K, Guo F, Unruh J, Slaughter B and Si K 2012 *Cell* **148** 515–29

[18] Channon K J, Devlin G L and MacPhee C E 2009 *J. Am. Chem. Soc.* **131** 12520–1

[19] Gras S L, Tickler A K, Squires A M, Devlin G L, Horton M a, Dobson C M and MacPhee C E 2008 *Biomaterials* **29** 1553–62

[20] Serpell L C, Sunde M and Blake C C 1997 *Cell. Mol. Life Sci.* **53** 871–87

[21] Sunde M, Serpell L C, Bartlam M, Fraser P E, Pepys M B and Blake C C 1997 *J. Mol. Biol.* **273** 729–39

[22] Baldwin A J, Knowles T P J, Tartaglia G G, Fitzpatrick A W, Devlin G L, Shammas S L, Waudby C a, Mossuto M F, Meehan S, Gras S L, Christodoulou J, Anthony-Cahill S J, Barker P D, Vendruscolo M and Dobson C M 2011 *J. Am. Chem. Soc.* **133** 14160–3

[23] Chiti F, Webster P, Taddei N, Clark a, Stefani M, Ramponi G and Dobson C M 1999 *Proc. Natl. Acad. Sci. U. S. A.* **96** 3590–4

[24] Dobson C M and Karplus M 1999 *Curr. Opin. Struct. Biol.* **9** 92–101

[25] Shammas S L, Knowles T P J, Baldwin A J, Macphee C E, Welland M E, Dobson C M and Devlin G L 2011 *Biophys. J.* **100** 2783–91

[26] Ferreira S T, Vieira M N N and De Felice F G 2007 *IUBMB Life* **59** 332–45

[27] Xue W F, Hellewell A L, Gosal W S, Homans S W, Hewitt E W and Radford S E 2009 *J. Biol. Chem.* **284** 34272–82

[28] Chiti F and Dobson C M 2006 *Annu. Rev. Biochem.* **75** 333–66

[29] Glabe C G and Kayed R 2006 *Neurology* **66** S74–8

[30] Hall D and Edskes H 2004 *J. Mol. Biol.* **336** 775–786

[31] Lesné S, Koh M T, Kotilinek L, Kayed R, Glabe C G, Yang A, Gallagher M and Ashe K H 2006 *Nature* **440** 352–7

[32] Kayed R, Head E, Thompson J L, McIntire T M, Milton S C, Cotman C W and Glabe C G 2003 *Science* **300** 486–9

[33] Campioni S, Mannini B, Zampagni M, Pensalfini A, Parrini C, Evangelisti E, Relini A, Stefani M, Dobson C M, Cecchi C and Chiti F 2010 *Nat. Chem. Biol.* **6** 140–7

[34] Kodali R and Wetzel R 2007 *Curr. Opin. Struct. Biol.* **17** 48–57

[35] Makin O S and Serpell L C 2005 *FEBS J.* **272** 5950–61

[36] Perutz M F, Finch J T, Berriman J and Lesk A 2002 *Proc. Natl. Acad. Sci. U. S. A.* **99** 5591–5595

[37] Monsellier E and Chiti F 2007 *EMBO Rep.* **8** 737–42

[38] Harper J D and Lansbury P T 1997 *Annu. Rev. Biochem.* **66** 385–407

[39] Westermark G T, Johnson K H and Westermark P 1999 *Staining Methods for identification of amyloid in tissue* (*Methods in Enzymology* vol 309) (Academic Press) ISBN 978-0-12-182210-1

[40] aJ Modler, Gast K, Lutsch G and Damaschun G 2003 *J. Mol. Biol.* **325** 135–148

[41] Damaschun G, Damaschun H, Fabian H, Gast K, Kröber R, Wieske M and Zirwer D 2000 *Proteins* **39** 204–11

[42] Giehm L, Oliveira C L P, Christiansen G, Pedersen J S and Otzen D E 2010 *J. Mol. Biol.* **401** 115–33

[43] Giehm L and Otzen D E 2010 *Anal. Biochem.* **400** 270–81

[44] Thorn D C, Ecroyd H, Sunde M, Poon S and Carver J a 2008 *Biochemistry* **47** 3926–36

[45] Ecroyd H and Carver J a 2009 *Cell. Mol. Life Sci.* **66** 62–81

[46] Juárez J, Taboada P and Mosquera V 2009 *Biophys. J.* **96** 2353–70

[47] Stirpe A, Pantusa M, Rizzuti B, Sportelli L, Bartucci R and Guzzi R 2011 *Int. J. Biol. Macromol.* **49** 337–42

[48] Arya S, Kumari A, Dalal V, Bhattacharya M and Mukhopadhyay S 2015 *Phys. Chem. Chem. Phys.* **17** 22862–22871

[49] Hurshman A R, White J T, Powers E T and Kelly J W 2004 *Biochemistry* **43** 7365–81

[50] Yamaguchi T, Yagi H, Goto Y, Matsuzaki K and Hoshino M 2010 *Biochemistry* **49** 7100–7

[51] Rangachari V, Moore B D, Reed D K, Sonoda L K, Bridges A W, Conboy E, Hartigan D and Rosenberry T L 2007 *Biochemistry* **46** 12451–62

[52] O'Nuallain B, Freir D B, Nicoll A J, Risse E, Ferguson N, Herron C E, Collinge J and Walsh D M 2010 *J. Neurosci.* **30** 14411–9

[53] Nichols M R, Moss M a, Reed D K, Cratic-McDaniel S, Hoh J H and Rosenberry T L 2005 *J. Biol. Chem.* **280** 2471–80

[54] Paranjape G S, Gouwens L K, Osborn D C and Nichols M R 2012 *ACS Chem. Neurosci.* **3** 302–11

[55] Scheidt H a, Morgado I, Rothemund S, Huster D and Fändrich M 2011 *Angew. Chem. Int. Ed. Engl.* **50** 2837–40

[56] Kumar S, Mohanty S K and Udgaonkar J B 2007 *J. Mol. Biol.* **367** 1186–204

[57] Kumar S and Udgaonkar J B 2009 *J. Mol. Biol.* **385** 1266–76

[58] Kumar S and Udgaonkar J B 2009 *Biochemistry* **48** 6441–9

[59] Gast K, Modler a J, Damaschun H, Krber R, Lutsch G, Zirwer D, Golbik R and Damaschun G 2003 *Eur. Biophys. J.* **32** 710–723

[60] Sekhar A and Udgaonkar J B 2011 *Biochemistry* **50** 805–19

[61] Holm N K, Jespersen S K, Thomassen L V, Wolff T Y, Sehgal P, Thomsen L a, Christiansen G, Andersen C B, Knudsen A D and Otzen D E 2007 *Biochim. Biophys. Acta* **1774** 1128–38

[62] Gosal W S, Morten I J, Hewitt E W, Smith D A, Thomson N H and Radford S E 2005 *J. Mol. Biol.* **351** 850–64

[63] Smith A M, Jahn T R, Ashcroft A E and Radford S E 2006 *J. Mol. Biol.* **364** 9–19

[64] Smith D P, Woods L a, Radford S E and Ashcroft A E 2011 *Biophys. J.* **101** 1238–47

[65] Ahn M, Kang S, Koo H J, Lee J H, Lee Y S and Paik S R 2010 *Biotechnol. Prog.* **26** 1759–64

[66] McParland V J, Kad N M, Kalverda A P, Brown A, Kirwin-Jones P, Hunter M G, Sunde M and Radford S E 2000 *Biochemistry* **39** 8735–8746

[67] Myers S L, Thomson N H, Radford S E and Ashcroft A E 2006 *Rapid Commun. Mass Spectrom.* **20** 1628–36

[68] Liu C, Sawaya M R and Eisenberg D 2011 *Nat. Struct. Mol. Biol.* **18** 49–55

[69] Adamcik J and Mezzenga R 2012 *Macromolecules* **45** 1137–1150

[70] Gosal W S, Clark A H and Ross-Murphy S B 2004 *Biomacromolecules* **5** 2408–19

[71] Chatani E, Lee Y H, Yagi H, Yoshimura Y, Naiki H and Goto Y 2009 *Proc. Natl. Acad. Sci. U. S. A.* **106** 11119–24

[72] Jones O G, Handschin S, Adamcik J, Harnau L, Bolisetty S and Mezzenga R 2011 *Biomacromolecules* **12** 3056–65

[73] Jordens S, Adamcik J, Amar-Yuli I and Mezzenga R 2011 *Biomacromolecules* **12** 187–93

[74] Loveday S M, Wang X L, Rao M A, Anema S G and Singh H 2011 *J. Agric. Food Chem.* **59** 8467–74

[75] Loveday S, Wang X, Rao M, Anema S, Creamer L and Singh H 2010 *Int. Dairy J.* **20** 571–579

[76] VandenAkker C C, Engel M F M, Velikov K P, Bonn M and Koenderink G H 2011 *J. Am. Chem. Soc.* **133** 18030–3

[77] Jain S and Udgaonkar J B 2008 *J. Mol. Biol.* **382** 1228–41

[78] Singh J, Sabareesan a T, Mathew M K and Udgaonkar J B 2012 *J. Mol. Biol.* **423** 217–31

[79] Jain S and Udgaonkar J B 2010 *Biochemistry* **49** 7615–24

[80] Jain S and Udgaonkar J B 2011 *Biochemistry* **50** 1153–61

[81] Teoh C L, Yagi H, Griffin M D W, Goto Y and Howlett G J 2011 *J. Biochem.* **149** 67–74

[82] Binger K J, Pham C L L, Wilson L M, Bailey M F, Lawrence L J, Schuck P and Howlett G J 2008 *J. Mol. Biol.* **376** 1116–29

[83] Hatters D M, MacPhee C E, Lawrence L J, Sawyer W H and Howlett G J 2000 *Biochemistry* **39** 8276–83

[84] Hatters D M, MacRaild C A, Daniels R, Gosal W S, Thomson N H, Jones J A, Davis J J, MacPhee C E, Dobson C M and Howlett G J 2003 *Biophys. J.* **85** 3979–90

[85] Yang S, Griffin M D W, Binger K J, Schuck P and Howlett G J 2012 *J. Mol. Biol.* **421** 364–77

[86] Griffin M D W, Mok M L Y, Wilson L M, Pham C L L, Waddington L J, Perugini M a and Howlett G J 2008 *J. Mol. Biol.* **375** 240–56

[87] MacRaild C a, Stewart C R, Mok Y F, Gunzburg M J, Perugini M a, Lawrence L J, Tirtaatmadja V, Cooper-White J J and Howlett G J 2004 *J. Biol. Chem.* **279** 21038–45

[88] Foley J, Hill S E, Miti T, Mulaj M, Ciesla M, Robeel R, Persichilli C, Raynes R, Westerheide S and Muschol M 2013 *J. Chem. Phys.* **139** 121901

[89] Hill S E, Miti T, Richmond T and Muschol M 2011 *PLoS One* **6** e18171

[90] Kalapothakis J, Morris R, Szavits-Nossan J, Eden K, Covill S, Tabor S, Gillam J, Barran P, Allen R and MacPhee C 2015 *Biophys. J.* **108** 2300–2311

[91] Lara C, Gourdin-Bertin S, Adamcik J, Bolisetty S and Mezzenga R 2012 *Biomacromolecules* **13** 4213–21

[92] Aggeli A, Nyrkova I A, Bell M, Harding R, Carrick L, McLeish T C, Semenov A N and Boden N 2001 *Proc. Natl. Acad. Sci. U. S. A.* **98** 11857–11862

[93] Relini A, Torrassa S, Ferrando R, Rolandi R, Campioni S, Chiti F and Gliozzi A 2010 *Biophys. J.* **98** 1277–84

[94] Ruzafa D, Morel B, Varela L, Azuaga A I and Conejero-Lara F 2012 *PLoS One* **7** e49690

[95] Wang J M, Yang X Q, Yin S W, Yuan D B, Xia N and Qi J R 2011 *J. Agric. Food Chem.* **59** 11270–7

[96] Zhang Y H, Tang C H, Wen Q B, Yang X Q, Li L and Deng W L 2010 *Food Hydrocoll.* **24** 266–274

[97] Bhosale S V, Kalyankar M B, Bhosale S V, Patil S G, Lalander C H, Langford S J and Nalage S V 2011 *Supramol. Chem.* **23** 263–268

[98] Loveday S M, Rao M a, Creamer L K and Singh H 2009 *J. Food Sci.* **74** R47–55

[99] Hiramatsu H, Lu M, Matsuo K, Gekko K, Goto Y and Kitagawa T 2010 *Biochemistry* **49** 742–51

[100] Teoh C L, Bekard I B, Asimakis P, Griffin M D W, Ryan T M, Dunstan D E and Howlett G J 2011 *Biochemistry* **50** 4046–57

[101] Yagi H, Ban T, Morigaki K, Naiki H and Goto Y 2007 *Biochemistry* **46** 15009–17

[102] Teoh C L, Pham C L L, Todorova N, Hung A, Lincoln C N, Lees E, Lam Y H, Binger K J, Thomson N H, Radford S E, Smith T a, Müller S a, Engel A, Griffin M D W, Yarovsky I, Gooley P R and Howlett G J 2011 *J. Mol. Biol.* **405** 1246–66

[103] Adachi M, So M, Sakurai K, Kardos J and Goto Y 2015 *J. Biol. Chem.* **290** 18134–18145

[104] DuBay K F, Pawar A P, Chiti F, Zurdo J, Dobson C M and Vendruscolo M 2004 *J. Mol. Biol.* **341** 1317–26

[105] Jansen R, Dzwolak W and Winter R 2005 *Biophys. J.* **88** 1344–53

[106] Lashuel H a, Labrenz S R, Woo L, Serpell L C and Kelly J W 2000 *J. Am. Chem. Soc.* **122** 5262–77

[107] VandenAkker C C, Engel M F M, Velikov K P, Bonn M and Koenderink G H 2011 *J. Am. Chem. Soc.* **133** 18030–3

[108] Anderson M, Bocharova O V, Makarava N, Breydo L, Salnikov V V and Baskakov I V 2006 *J. Mol. Biol.* **358** 580–596

[109] Meehan S, Knowles T P J, Baldwin A J, Smith J F, Squires A M, Clements P, Treweek T M, Ecroyd H, Tartaglia G G, Vendruscolo M, Macphee C E, Dobson C M and Carver J a 2007 *J. Mol. Biol.* **372** 470–84

[110] González J M, Vélez M, Jiménez M, Alfonso C, Schuck P, Mingorance J, Vicente M, Minton A P and Rivas G 2005 *Proc. Natl. Acad. Sci. U. S. A.* **102** 1895–900

[111] Conway K A, Lee S J, Rochet J C, Ding T T, Williamson R E and Lansbury P T 2000 *Proc. Natl. Acad. Sci.* **97** 571–576

[112] Wetzel R 1996 *Cell* **86** 699–702

[113] Uversky V N 2001 *J. Biol. Chem.* **276** 43495–43498

[114] Uversky V N and Fink A L 2004 *Biochim. Biophys. Acta* **1698** 131–53

[115] Dusa A, Kaylor J, Edridge S, Bodner N, Hong D p and Fink A L 2006 *Biochemistry* **45** 2752–60

[116] Morris A M, Watzky M a and Finke R G 2009 *Biochim. Biophys. Acta* **1794** 375–97

[117] Sanchez-Ruiz J M 2010 *Biophys. Chem.* **148** 1–15

[118] Nielsen L, Khurana R, Coats a, Frokjaer S, Brange J, Vyas S, Uversky V N and Fink a L 2001 *Biochemistry* **40** 6036–46

[119] Munishkina L a and Fink A L 2007 *Biochim. Biophys. Acta* **1768** 1862–85

[120] Kamihira M, Naito a, Tuzi S, Nosaka a Y and Saitô H 2000 *Protein Sci.* **9** 867–77

[121] Moniatte M, van der Goot F, Buckley J, Pattus F and van Dorsselaer A 1996 *FEBS Lett.* **384** 269–272

[122] Bleiholder C, Dupuis N F, Wyttenbach T and Bowers M T 2011 *Nat. Chem.* **3** 172–7

[123] Beveridge R, Chappuis Q, Macphee C and Barran P 2013 *Analyst* **138** 32–42

[124] Lomakin A, Teplow D B, Kirschner D A and Benedek G B 1997 *Proc. Natl. Acad. Sci. U. S. A.* **94** 7942–7

[125] Lomakin A, Benedek G and Teplow D 1999 *Methods Enzymol.* **309**

[126] Knowles T P J, Shu W, Devlin G L, Meehan S, Auer S, Dobson C M and Welland M E 2007 *Proc. Natl. Acad. Sci. U. S. A.* **104** 10016–21

[127] Buell A K, Blundell J R, Dobson C M, Welland M E, Terentjev E M and Knowles T P J 2010 *Phys. Rev. Lett.* **104** 228101

[128] Milhiet P E, Yamamoto D, Berthoumieu O, Dosset P, Le Grimellec C, Verdier J M, Marchal S and Ando T 2010 *PLoS One* **5** e13240

[129] Andersen C B, Yagi H, Manno M, Martorana V, Ban T, Christiansen G, Otzen D E, Goto Y and Rischel C 2009 *Biophys. J.* **96** 1529–36

[130] Ferkinghoff-Borg J, Fonslet J, Andersen C B, Krishna S, Pigolotti S, Yagi H, Goto Y, Otzen D and Jensen M H 2010 *Phys. Rev. E* **82** 010901

[131] Yagi H, Abe Y, Takayanagi N and Goto Y 2014 *Biochim. Biophys. Acta* **1844** 1881–8

[132] Li Y and Roberts C J 2009 *J. Phys. Chem. B* **113** 7020–32

[133] Oosawa F, Asakura S, Hotta K, Imai N and Ooi T 1959 *Journal of Polymer Science* **37** 323–36

[134] Oosawa F and Kasai M 1962 *J. Mol. Biol.* **4** 10–21

[135] Oosawa F and Asakura S 1975 *Thermodynamics of the polymerization of protein* (Academic Press) ISBN 9780125270502

[136] Auer S and Kashchiev D 2010 *Proteins* **78** 2412–6

[137] Watzky M a, Morris A M, Ross E D and Finke R G 2008 *Biochemistry* **47** 10790–800

[138] Cohen S I a, Vendruscolo M, Welland M E, Dobson C M, Terentjev E M and Knowles T P J 2011 *J. Chem. Phys.* **135** 065105

[139] Gebauer D and Cölfen H 2011 *Nano Today* **6** 564–584

[140] Roberts C J 2007 *Biotechnol. Bioeng.* **98** 927–38

[141] Powers E T and Powers D L 2006 *Biophys. J.* **91** 122–32

[142] Cohen S I a, Vendruscolo M, Dobson C M and Knowles T P J 2011 *Int. J. Mol. Sci.* **12** 5844–52

[143] Flyvbjerg H, Jobs E and Leibler S 1996 *Proc. Natl. Acad. Sci. U. S. A.* **93** 5975–9

[144] Knowles T P J, Waudby C A, Devlin G L, Cohen S I A, Aguzzi A, Vendruscolo M, Terentjev E M, Welland M E and Dobson C M 2009 *Science* **326** 1533–7

[145] Ferrone F 1999 *Analysis of Protein aggregation* (*Methods in Enzymology* vol 309) (Academic Press) ISBN 978-0-12-182210-1

[146] Kodaka M 2004 *Biophys. Chem.* **109** 325–32

[147] Oosawa F 1970 *J. Theor. Biol.* **27** 69–86

[148] Cohen S I a, Vendruscolo M, Dobson C M and Knowles T P J 2011 *J. Chem. Phys.* **135** 065107

[149] Kunes K, Cox D and Singh R 2005 *Phys. Rev. E* **72** 051915

[150] Collins S R, Douglass A, Vale R D and Weissman J S 2004 *PLoS Biol.* **2** e321

[151] Wegner A and Engel J 1975 *Biophys. Chem.* **3** 215–25

[152] Lomakin A, Chung D S, Benedek G B, Kirschner D A and Teplow D B 1996 *Proc. Natl. Acad. Sci. U. S. A.* **93** 1125–9

[153] Padrick S B and Miranker A D 2002 *Biochemistry* **41** 4694–703

[154] Skerget K, Vilfan A, Pompe-Novak M, Turk V, Waltho J P, Turk D and Zerovnik E 2009 *Proteins* **74** 425–36

[155] Pallitto M M and Murphy R M 2001 *Biophys. J.* **81** 1805–22

[156] Powers E T and Powers D L 2008 *Biophys. J.* **94** 379–91

[157] Frieden C and Goddette D W 1983 *Biochemistry* **22** 5836–43

[158] Ferrone F a, Hofrichter J, Sunshine H R and Eaton W a 1980 *Biophys. J.* **32** 361–80

[159] Bishop M and Ferrone F 1984 *Biophys. J.* **46** 631–644

[160] Sluzky V, Tamada J a, Klibanov a M and Langer R 1991 *Proc. Natl. Acad. Sci. U. S. A.* **88** 9377–81

[161] Lee C C, Nayak A, Sethuraman A, Belfort G and McRae G J 2007 *Biophys. J.* **92** 3448–58

[162] Goldstein R and Stryer L 1986 *Biophys. J.* **50** 583–599

[163] Arnaudov L N and de Vries R 2007 *J. Chem. Phys.* **126** 145106

[164] Arosio P, Beeg M, Nicoud L and Morbidelli M 2012 *Chem. Eng. Sci.* **78** 21–32

[165] Hofrichter J, Ross P D and Eaton W a 1974 *Proc. Natl. Acad. Sci. U. S. A.* **71** 4864–8

[166] Kelly J W 2000 *Nat. Struct. Biol.* **7** 824–6

[167] Librizzi F and Rischel C 2005 *Protein Sci.* **14** 3129–34

[168] Firestone M P and de Levie R 1983 *J. Theor. Biol.* **104** 535–52

[169] Serio T R 2000 *Science (80-.).* **289** 1317–1321

[170] Gillam J E and MacPhee C E 2013 *J. Phys. Condens. Matter* **25** 373101

[171] Xue W F, Homans S W and Radford S E 2008 *Proc. Natl. Acad. Sci. U. S. A.* **105** 8926–31

[172] Ruschak A M and Miranker A D 2007 *Proc. Natl. Acad. Sci. U. S. A.* **104** 12341–6

[173] Manno M, Craparo E F, Martorana V, Bulone D and San Biagio P L 2006 *Biophys. J.* **90** 4585–91

[174] Manno M, Mauro M, Craparo E F, Podestà A, Bulone D, Carrotta R, Martorana V, Tiana G and San Biagio P L 2007 *J. Mol. Biol.* **366** 258–74

[175] Zhu L, Zhang X J, Wang L Y, Zhou J M and Perrett S 2003 *J. Mol. Biol.* **328** 235–254

[176] Foderà V, Librizzi F, Groenning M, van de Weert M and Leone M 2008 *J. Phys. Chem. B* **112** 3853–8

[177] Morris R J, Eden K, Yarwood R, Jourdain L, Allen R J and Macphee C E 2013 *Nat. Commun.* **4** 1891

[178] Fändrich M 2007 *J. Mol. Biol.* **365** 1266–70

[179] Meinhardt J, Tartaglia G G, Pawar A, Christopeit T, Hortschansky P, Schroeckh V, Dobson C M, Vendruscolo M and Fändrich M 2007 *Protein Sci.* **16** 1214–22

[180] Christopeit T, Hortschansky P, Schroeckh V, Gührs K, Zandomeneghi G and Fändrich M 2005 *Protein Sci.* **14** 2125–31

[181] Hall D and Edskes H 2009 *Biophys. Chem.* **145** 17–28

[182] Taylor B M, Sarver R W, Fici G, Poorman R a, Lutzke B S, Molinari A, Kawabe T, Kappenman K, Buhl A E and Epps D E 2003 *J. Protein Chem.* **22** 31–40

[183] Knowles T P J and Buehler M J 2011 *Nat. Nanotechnol.* **6** 469–79

[184] Wegner A 1982 *Nature* **296** 266–267

[185] Ramachandran G and Udgaonkar J B 2012 *J. Mol. Biol.* **421** 296–314

[186] Hong L and Yong W A 2013 *Biophys. J.* **104** 533–40

[187] Baskakov I V 2007 *FEBS J.* **274** 3756–65

[188] Cohen S I a, Vendruscolo M, Dobson C M and Knowles T P J 2011 *J. Chem. Phys.* **135** 065106

[189] Binger K J, Griffin M D W and Howlett G J 2008 *Biochemistry* **47** 10208–17

[190] Pöschel T, Brilliantov N V and Frömmel C 2003 *Biophys. J.* **85** 3460–74

[191] Medkour T, Ferrone F, Galactéros F and Hannaert P 2008 *Acta Biotheor.* **56** 103–22

[192] Cohen S I a, Vendruscolo M, Dobson C M and Knowles T P J 2012 *J. Mol. Biol.* **421** 160–71

[193] Hong Y, Meng L, Chen S, Leung C W T, Da L T, Faisal M, Silva D A, Liu J, Lam J W Y, Huang X and Tang B Z 2012 *J. Am. Chem. Soc.* **134** 1680–9

[194] Ganapol B D 2012 *Transp. Theory Stat. Phys.* **41** 153–174

[195] Cerdà-Costa N, Esteras-Chopo a, Avilés F X, Serrano L and Villegas V 2007 *J. Mol. Biol.* **366** 1351–63

[196] Auer S, Ricchiuto P and Kashchiev D 2012 *J. Mol. Biol.* **422** 723–30

[197] Sorci M, Grassucci R a, Hahn I, Frank J and Belfort G 2009 *Proteins* **77** 62–73

[198] Pease L F, Sorci M, Guha S, Tsai D H, Zachariah M R, Tarlov M J and Belfort G 2010 *Biophys. J.* **99** 3979–85

[199] Li D w, Han L and Huo S 2007 *J. Phys. Chem. B* **111** 5425–33

[200] Hingant E, Fontes P, eresa Alvarez-Martinez M T, Arnaud J D, Liautard J P and Pujo-Menjouet L 2014 *PLoS Comput. Biol.* **10** e1003735

[201] Arosio P, Rima S, Lattuada M and Morbidelli M 2012 *J. Phys. Chem. B* **116** 7066–75

[202] Hill T 1983 *Biophys. J.* **44** 285–288

[203] Lorenzen N, Cohen S I a, Nielsen S B, Herling T W, Christiansen G, Dobson C M, Knowles T P J and Otzen D 2012 *Biophys. J.* **102** 2167–75

[204] Ryan T M, Teoh C L, Griffin M D W, Bailey M F, Schuck P and Howlett G J 2010 *J. Mol. Biol.* **399** 731–40

[205] Ryan T M, Griffin M D W, Teoh C L, Ooi J and Howlett G J 2011 *J. Mol. Biol.* **406** 416–29

[206] Faria T Q, Almeida Z L, Cruz P F, Jesus C S H, Castanheira P and Brito R M M 2015 *Phys. Chem. Chem. Phys.* **17** 7255–63

[207] Eisenberg H 1971 *Acc. Chem. Res.* **4** 379–385

[208] Adams E T and Lewis M S 1968 *Biochem.* **7** 1044–53

[209] Holde K E V and Rossetti G P 1967 *Biochem.* **6** 2189–94

[210] Morris A M, Watzky M a, Agar J N and Finke R G 2008 *Biochemistry* **47** 2413–27

[211] Thusius D 1975 *J. Mol. Biol.* **94** 367–83

[212] Thusius D, Dessen P and Jallon J M 1975 *J. Mol. Biol.* **92** 413–32

[213] Carulla N, Caddy G L, Hall D R, Zurdo J, Gairí M, Feliz M, Giralt E, Robinson C V and Dobson C M 2005 *Nature* **436** 554–8

[214] Carnall J M a, Waudby C a, Belenguer A M, Stuart M C a, Peyralans J J P and Otto S 2010 *Science* **327** 1502–6

[215] Aizenstein H J, Nebes R D, Saxton J a, Price J C, Mathis C a, Tsopelas N D, Ziolko S K, James J a, Snitz B E, Houck P R, Bi W, Cohen A D, Lopresti B J, DeKosky S T, Halligan E M and Klunk W E 2008 *Arch. Neurol.* **65** 1509–17

[216] Morinaga A, Hasegawa K, Nomura R, Ookoshi T, Ozawa D, Goto Y, Yamada M and Naiki H 2010 *Biochim. Biophys. Acta* **1804** 986–95

[217] Cino E a, Karttunen M and Choy W Y 2012 *PLoS One* **7** e49876

[218] Zhou Z, Fan J B, Zhu H L, Shewmaker F, Yan X, Chen X, Chen J, Xiao G F, Guo L and Liang Y 2009 *J. Biol. Chem.* **284** 30148–58

[219] Magno A, Caflisch A and Pellarin R 2010 *J. Phys. Chem. Lett.* **1** 3027–3032

[220] Munishkina L a, Ahmad A, Fink A L and Uversky V N 2008 *Biochemistry* **47** 8993–9006

[221] White D a, Buell A K, Dobson C M, Welland M E and Knowles T P J 2009 *FEBS Lett.* **583** 2587–92

[222] Ma Q, Fan J B, Zhou Z, Zhou B R, Meng S R, Hu J Y, Chen J and Liang Y 2012 *PLoS One* **7** e36288

[223] Martins I C, Kuperstein I, Wilkinson H, Maes E, Vanbrabant M, Jonckheere W, Van Gelder P, Hartmann D, D'Hooge R, De Strooper B, Schymkowitz J and Rousseau F 2008 *EMBO J.* **27** 224–33

[224] Comellas G, Lemkau L R, Zhou D H, George J M and Rienstra C M 2012 *J. Am. Chem. Soc.* **134** 5090–9

[225] Wang S S S, Liu K N and Han T C 2010 *Biochim. Biophys. Acta* **1802** 519–30

[226] Murphy R M 2007 *Biochim. Biophys. Acta* **1768** 1923–34

[227] Crespo R, Villar-Alvarez E, Taboada P, Rocha F a, Damas A M and Martins P M 2015 *J. Biol. Chem.* **291** jbc.M115.699348

[228] Hall D, Kardos J, Edskes H, Carver J a and Goto Y 2015 *FEBS Lett.* **589** 672–679

[229] Muta H, Lee Y H, Kardos J, Lin Y, Yagi H and Goto Y 2014 *J. Biol. Chem.* **289** 18228–18238

[230] Ciryam P, Kundra R, Morimoto R I, Dobson C M and Vendruscolo M 2015 *Trends Pharmacol. Sci.* **36** 72–77

[231] Eden K, Morris R, Gillam J, MacPhee C and Allen R 2015 *Biophys. J.* **108** 632–643

[232] Van Der Zwaag D, Pieters P A, Korevaar P A, Markvoort A J, Spiering A J H, De Greef T F A and Meijer E W 2015 *J. Am. Chem. Soc.* **137** 12677–12688

[233] Giehm L, Lorenzen N and Otzen D E 2011 *Methods* **53** 295–305

[234] Yoshimura Y, Lin Y, Yagi H, Lee Y h, Kitayama H, Sakurai K, So M, Ogi H, Naiki H and Goto Y 2012 *Proc. Natl. Acad. Sci. U. S. A.* **109** 14446–51

[235] Souillac P O, Uversky V N and Fink A L 2003 *Biochemistry* **42** 8094–104

[236] Borgia M B, Nickson A a, Clarke J and Hounslow M J 2013 *J. Am. Chem. Soc.* **135** 6456–64

[237] Jean L, Lee C F, Lee C, Shaw M and Vaux D J 2010 *FASEB J.* **24** 309–17

[238] Linse S, Cabaleiro-Lago C, Xue W F, Lynch I, Lindman S, Thulin E, Radford S E and Dawson K a 2007 *Proc. Natl. Acad. Sci. U. S. A.* **104** 8691–6

[239] Linse S and Lund M 2014

[240] Sear R P 2007 *J. Phys. Condens. Matter* **19** 033101

[241] Wood S J, Wypych J, Steavenson S, Louis J C, Citron M and Biere A L 1999 *J. Biol. Chem.* **274** 19509–12

[242] Krebs M R H, Morozova-Roche L a, Daniel K, Robinson C V and Dobson C M 2004 *Protein Sci.* **13** 1933–1938

[243] Xu M, Ermolenkov V V, He W, Uversky V N, Fredriksen L and Lednev I K 2005 *Biopolymers* **79** 58–61

[244] Arnaudov L N and de Vries R 2005 *Biophys. J.* **88** 515–26

[245] Zhang Y and Cremer P S 2009 *Proc. Natl. Acad. Sci. U. S. A.* **106** 15249–53

[246] Raccosta S, Martorana V and Manno M 2012 *J. Phys. Chem. B* **116** 12078–87

[247] Sasahara K, Yagi H, Naiki H and Goto Y 2007 *J. Mol. Biol.* **372** 981–91

[248] Moosavi-Movahedi a a, Pirzadeh P, Hashemnia S, Ahmadian S, Hemmateenejad B, Amani M, Saboury a a, Ahmad F, Shamsipur M, Hakimelahi G H, Tsai F Y, Alijanvand H H and Yousefi R 2007 *Colloids Surf. B. Biointerfaces* **60** 55–61

[249] Hung Y T, Lin M S, Chen W Y and Wang S S S 2010 *Colloids Surf. B. Biointerfaces* **81** 141–51

[250] Jain N, Bhattacharya M and Mukhopadhyay S 2011 *J. Fluoresc.* **21** 615–25

[251] Mishra R, Sörgjerd K, Nyström S, Nordigården A, Yu Y C and Hammarström P 2007 *J. Mol. Biol.* **366** 1029–44

[252] Frare E, Polverino De Laureto P, Zurdo J, Dobson C M and Fontana A 2004 *J. Mol. Biol.* **340** 1153–65

[253] Lara C, Adamcik J, Jordens S and Mezzenga R 2011 *Biomacromolecules* **12** 1868–75

[254] Goda S, Takano K, Yamagata Y, Nagata R, Akutsu H, Maki S, Namba K and Yutani K 2000 *Protein Sci.* **9** 369–75

[255] Tanaka S, Oda Y, Ataka M, Onuma K, Fujiwara S and Yonezawa Y 2001 *Biopolymers* **59** 370–9

[256] Yonezawa Y, Tanaka S, Kubota T, Wakabayashi K, Yutani K and Fujiwara S 2002 *J. Mol. Biol.* **323** 237–251

[257] Fujiwara S, Matsumoto F and Yonezawa Y 2003 *J. Mol. Biol.* **331** 21–28

[258] Trexler A J and Nilsson M R 2007 *Curr. Protein Pept. Sci.* **8** 537–57

[259] D'Amico M, Raccosta S, Cannas M, Martorana V and Manno M 2011 *J. Phys. Chem. B* **115** 4078–87

[260] Holley M, Eginton C, Schaefer D and Brown L R 2008 *Biochem. Biophys. Res. Commun.* **373** 164–8

[261] Sassi P, Giugliarelli A, Paolantoni M, Morresi A and Onori G 2011 *Biophys. Chem.* **158** 46–53

[262] Moraitakis G and Goodfellow J M 2003 *Biophys. J.* **84** 2149–58

[263] Dumoulin M, Kumita J R and Dobson C M 2006 *Acc. Chem. Res.* **39** 603–10

[264] Vernaglia B a, Huang J and Clark E D 2004 *Biomacromolecules* **5** 1362–70

[265] Blake C C, Koenig D F, Mair G a, North a C, Phillips D C and Sarma V R 1965 *Nature* **206** 757–761

[266] Squires A M, Devlin G L, Gras S L, Tickler A K, MacPhee C E and Dobson C M 2006 *J. Am. Chem. Soc.* **128** 11738–9

[267] Babu K R and Bhakuni V 1997 *Eur. J. Biochem.* **245** 781–9

[268] Buell A K, Dhulesia A, Mossuto M F, Cremades N, Kumita J R, Dumoulin M, Welland M E, Knowles T P J, Salvatella X and Dobson C M 2011 *J. Am. Chem. Soc.* **133** 7737–43

[269] Lin Y, Lee Y H, Yoshimura Y, Yagi H and Goto Y 2014 *Langmuir* **30** 1845–1854

[270] Cao A 2004 *Protein Sci.* **13** 319–324

[271] Green R J, Su T J, Joy H and Lu J R 2000 *Langmuir* **16** 5797–5805

[272] Yan H, Frielinghaus H, Nykanen a, Ruokolainen J, Saiani a and Miller a F 2008 *Soft Matter* **4** 1313

[273] Kumar S, Ravi V K and Swaminathan R 2008 *Biochem. J.* **415** 275–88

[274] Morshedi D, Ebrahim-Habibi A, Moosavi-Movahedi A A and Nemat-Gorgani M 2010 *Biochim. Biophys. Acta* **1804** 714–22

[275] Colombié S, Gaunand A, Rinaudo M and Lindet B 2000 *Biotechnol. Lett.* **22** 277–283

[276] Humblet-Hua N P, Sagis L M C and van der Linden E 2008 *J. Agric. Food Chem.* **56** 11875–82

[277] Colombié S, Gaunand a and Lindet B 2001 *Enzyme Microb. Technol.* **28** 820–826

[278] Kim D T, Blanch H W and Radke C J 2002 *Langmuir* **18** 5841–5850

[279] Lara C, Handschin S and Mezzenga R 2013 *Nanoscale* **5** 7197–201

[280] Kurouski D, Lu X, Popova L, Wan W, Shanmugasundaram M, Stubbs G, Dukor R K, Lednev I K and Nafie L A 2014 *J. Am. Chem. Soc.* **136** 2302–12

[281] Yagi N, Ohta N and Matsuo T 2009 *Int. J. Biol. Macromol.* **45** 86–90

[282] Mossuto M F, Dhulesia A, Devlin G, Frare E, Kumita J R, de Laureto P P, Dumoulin M, Fontana A, Dobson C M and Salvatella X 2010 *J. Mol. Biol.* **402** 783–96

[283] Knowles T P J, White D a, Abate A R, Agresti J J, Cohen S I a, Sperling R a, De Genst E J, Dobson C M and Weitz D a 2011 *Proc. Natl. Acad. Sci. U. S. A.* **108** 14746–51

[284] Tomizawa H, Yamada H and Imoto T 1994 *Biochemistry* **33** 13032–13037

[285] Orpiszewski J and Benson M D 1999 *J. Mol. Biol.* **289** 413–28

[286] Phillips A S, Gomes A F, Kalapothakis J M D, Gillam J E, Gasparavicius J, Gozzo F C, Kunath T, MacPhee C and Barran P E 2015 *Analyst* **140** 3070–3081

[287] Cheng F, Vivacqua G and Yu S 2011 *J. Chem. Neuroanat.* **42** 242–8

[288] Auluck P K, Caraveo G and Lindquist S 2010 *Annu. Rev. Cell Dev. Biol.* **26** 211–33

[289] Roberts H and Brown D 2015 *Biomolecules* **5** 282–305

[290] Uversky V N 2008 *Curr. Protein Pept. Sci.* **9** 507–40

[291] Spillantini M G, Crowther R A, Jakes R, Hasegawa M and Goedert M 1998 *Proc. Natl. Acad. Sci. U. S. A.* **95** 6469–73

[292] Goedert M 2001 *Nat. Rev. Neurosci.* **2** 492–501

[293] Eriksen J L, Dawson T M, Dickson D W and Petrucelli L 2003 *Neuron* **40** 453–6

[294] Dehay B, Bourdenx M, Gorry P, Przedborski S, Vila M, Hunot S, Singleton A, Olanow C W, Merchant K M, Bezard E, Petsko G A and Meissner W G 2015 *Lancet Neurol.* **14** 855–866

[295] Devine M J, Gwinn K, Singleton A and Hardy J 2011 *Mov. Disord.* **26** 2160–8

[296] Lesage S, Anheim M, Letournel F, Bousset L, Honoré A, Rozas N, Pieri L, Madiona K, Dürr A, Melki R, Verny C and Brice A 2013 *Ann. Neurol.* **73** 459–471

[297] Krüger R, Müller T and Riess O 2000 *J. Neural Transm.* **107** 31–40

[298] Anunciado D, Rai D K, Qian S, Urban V and O'Neill H 2015 *Biochim. Biophys. Acta - Proteins Proteomics* **1854** 1881–1889

[299] Curtain C C, Kirby N M, Mertens H D T, Barnham K J, Knott R B, Masters C L, Cappai R, Rekas A, Kenche V B and Ryan T 2015 *Mol. Biosyst.* **11** 190–6

[300] Buell A K, Galvagnion C, Gaspar R, Sparr E, Vendruscolo M, Knowles T P J, Linse S and Dobson C M 2014 *Proc. Natl. Acad. Sci.* **111** 7671–7676

[301] Fauvet B, Mbefo M K, Fares M B, Desobry C, Michael S, Ardah M T, Tsika E, Coune P, Prudent M, Lion N, Eliezer D, Moore D J, Schneider B, Aebischer P, El-Agnaf O M, Masliah E and Lashuel H a 2012 *J. Biol. Chem.* **287** 15345–15364

[302] Solanki A, Neupane K and Woodside M T 2014 *Phys. Rev. Lett.* **112** 158103

[303] Nam M K, Han J H, Jang J Y, Yun S E, Kim G Y, Kang S and Rhim H 2015 *Biochim. Biophys. Acta - Gen. Subj.* **1850** 2497–2505

[304] Burre J, Sharma M and Sudhof T C 2015 *J. Neurosci.* **35** 5221–5232

[305] Pratt M, Abeywardana T and Marotta N 2015 *Biomolecules* **5** 1210–1227

[306] Zarbiv Y, Simhi-Haham D, Israeli E, Elhadi S A, Grigoletto J and Sharon R 2014 *Neurobiol. Dis.* **70** 90–98

[307] Ysselstein D, Joshi M, Mishra V, Griggs A M, Asiago J M, McCabe G P, Stanciu L A, Post C B and Rochet J C 2015 *Neurobiol. Dis.* **79** 150–163

[308] Mirecka E a, Shaykhalishahi H, Gauhar A, Akgül S, Lecher J, Willbold D, Stoldt M, Hoyer W, Akgül , Lecher J, Willbold D, Stoldt M and Hoyer W 2014 *Angew. Chem. Int. Ed. Engl.* **53** 1–5

[309] Shaykhalishahi H, Gauhar A, Wördehoff M M, Grüning C S R, Klein A N, Bannach O, Stoldt M, Willbold D, Härd T and Hoyer W 2015 *Angew. Chemie Int. Ed.* n/a–n/a

[310] Uversky V N 2001 *J. Biol. Chem.* **276** 10737–10744

[311] Basak S, Prasad G V R K, Varkey J and Chattopadhyay K 2015

[312] Trexler A J and Rhoades E 2010 *Biophys. J.* **99** 3048–55

[313] Uversky V and Eliezer D 2009 *Curr. Protein Pept. Sci.* **10** 483–499

[314] Hoyer W, Antony T, Cherny D, Heim G, Jovin T M and Subramaniam V 2002 *J. Mol. Biol.* **322** 383–393

[315] Fink A L 2006 *Acc. Chem. Res.* **39** 628–34

[316] Narkiewicz J, Giachin G and Legname G 2014 *Prion* **8** 1–14

[317] Uversky V N, M Cooper E, Bower K S, Li J and Fink A L 2002 *FEBS Lett.* **515** 99–103

[318] Scarlata S and Golebiewska U 2014 *J. Bioenerg. Biomembr.* **46** 93–98

[319] Zijlstra N, Claessens M M a E, Blum C and Subramaniam V 2014 *Biophys. J.* **106** 440–446

[320] Gallea J I and Celej M S 2014 *J. Biol. Chem.* **289** 26733–26742

[321] Ghosh D, Singh P K, Sahay S, Jha N N, Jacob R S, Sen S, Kumar A, Riek R and Maji S K 2015 *Sci. Rep.* **5** 9228

[322] Illes-Toth E, Ramos M, Cappai R, Dalton C and Smith D 2015 *Biochem. J.* **468** 485–493

[323] Paslawski W, Andreasen M, Nielsen S B, Lorenzen N, Thomsen K, Kaspersen J D, Pedersen J S and Otzen D E 2014 *Biochemistry* **53** 6252–63

[324] Paslawski W, Mysling S, Thomsen K, Jørgensen T J D and Otzen D E 2014 *Angew. Chem. Int. Ed. Engl.* **53** 7560–3

[325] Celej M S, Sarroukh R, Goormaghtigh E, Fidelio G D, Ruysschaert J M and Raussens V 2012 *Biochem. J.* **443** 719–26

[326] Chen S W, Drakulic S, Deas E, Ouberai M, Aprile F A, Arranz R, Ness S, Roodveldt C, Guilliams T, De-Genst E J, Klenerman D, Wood N W, Knowles T P, Alfonso C, Rivas G, Abramov A Y, Valpuesta J M, Dobson C M and Cremades N 2015 *Proc. Natl. Acad. Sci.* **112** E1994–E2003

[327] Horrocks M H, Tosatto L, Dear A J, Garcia G A, Iljina M, Cremades N, Dalla Serra M, Knowles T P J, Dobson C M and Klenerman D 2015 *Anal. Chem.* **87** 8818–8826

[328] Hinault M P, Cuendet A F H, Mattoo R U H, Mensi M, Dietler G, Lashuel H a and Goloubinoff P 2010 *J. Biol. Chem.* **285** 38173–82

[329] Zou Y, Li Y, Hao W, Hu X and Ma G 2013 *J. Phys. Chem. B* **117** 4003–13

[330] Campioni S, Carret G, Jordens S, Nicoud L, Mezzenga R and Riek R 2014 *J. Am. Chem. Soc.* **136** 2866–2875

[331] Burré J, Sharma M and Südhof T C 2014 *Proc. Natl. Acad. Sci.* **111** E4274–E4283

[332] Fusco G, De Simone A, Gopinath T, Vostrikov V, Vendruscolo M, Dobson C M and Veglia G 2014 *Nat. Commun.* **5** 1–8

[333] Lee S J C, Lee J W, Choi T S, Jin K S, Lee S, Ban C and Kim H I 2014 *Anal. Chem.* **86** 1909–1916

[334] Necula M, Chirita C N and Kuret J 2003 *J. Biol. Chem.* **278** 46674–80

[335] Galvagnion C, Buell A K, Meisl G, Michaels T C T, Vendruscolo M, Knowles T P J and Dobson C M 2015 *Nat. Chem. Biol.* **11** 229–234

[336] Zhu M and Fink A L 2003 *J. Biol. Chem.* **278** 16873–7

[337] Tian J, Sethi A, Anunciado D, Vu D M and Gnanakaran S 2012 *J. Phys. Chem. B* **116** 4417–24

[338] Ahmad M F, Ramakrishna T, Raman B and Rao C M 2006 *J. Mol. Biol.* **364** 1061–72

[339] Munishkina L a, Phelan C, Uversky V N and Fink A L 2003 *Biochemistry* **42** 2720–30

[340] Brown D R 2010 *IUBMB Life* **62** 334–9

[341] Bisaglia M, Tessari I, Mammi S and Bubacco L 2009 *Neuromolecular Med.* **11** 239–51

[342] Berrocal R, Vasquez V, Krs S R, Gadad B S and Ks R 2014 *Mol. Neurobiol.* 1417–1431

[343] Uversky V N 2001 *J. Biol. Chem.* **276** 44284–44296

[344] Brown D R 2009 *Biochem. Biophys. Res. Commun.* **380** 377–81

[345] Levitan K, Chereau D, Cohen S I a, Knowles T P J, Dobson C M, Fink A L, Anderson J P, Goldstein J M and Millhauser G L 2011 *J. Mol. Biol.* **411** 329–33

[346] Xiang W, Menges S, Schlachetzki J C, Meixner H, Hoffmann A C, Schlötzer-Schrehardt U, Becker C M, Winkler J and Klucken J 2015 *Mol. Neurodegener.* **10** 1–16

[347] Kim Y M, Jang W H, Quezado M M, Oh Y, Chung K C, Junn E and Mouradian M M 2011 *J. Neurol. Sci.* **307** 157–61

[348] Beyer K 2006 *Acta Neuropathol.* **112** 237–51

[349] Oueslati A, Paleologou K E, Schneider B L, Aebischer P and Lashuel H a 2012 *J. Neurosci.* **32** 1536–44

[350] Krumova P, Meulmeester E, Garrido M, Tirard M, Hsiao H H, Bossis G, Urlaub H, Zweckstetter M, Kügler S, Melchior F, Bähr M and Weishaupt J H 2011 *J. Cell Biol.* **194** 49–60

[351] Stefanovic A N D, Lindhoud S, Semerdzhiev S A, Claessens M M A E and Subramaniam V 2015 *Biochemistry* **54** 3142–3150

[352] Lázaro D F, Rodrigues E F, Langohr R, Shahpasandzadeh H, Ribeiro T, Guerreiro P, Gerhardt E, Kröhnert K, Klucken J, Pereira M D, Popova B, Kruse N, Mollenhauer B, Rizzoli S O, Braus G H, Danzer K M and Outeiro T F 2014 *PLoS Genet.* **10** e1004741

[353] Nielsen S B, Macchi F, Raccosta S, Langkilde A E, Giehm L, Kyrsting A, Svane A S P, Manno M, Christiansen G, Nielsen N C, Oddershede L, Vestergaard B and Otzen D E 2013 *PLoS One* **8** e67713

[354] Lv Z, Krasnoslobodtsev A V, Zhang Y, Ysselstein D, Rochet J C, Blanchard S C and Lyubchenko Y L 2015 *Biophys. J.* **108** 2038–2047

[355] Nors Perdersen M, Foderà V, Horvath I, van Maarschalkerweerd A, Nørgaard Toft K, Weise C, Almqvist F, Wolf-Watz M, Wittung-Stafshede P and Vestergaard B 2015 *Sci. Rep.* **5** 10422

[356] Gath J, Bousset L, Habenstein B, Melki R, Meier B H and Böckmann A 2014 *Biomol. NMR Assign.* **8** 395–404

[357] Sidhu A, Segers-Nolten I and Subramaniam V 2014 *Biochim. Biophys. Acta* **1844** 2127–2134

[358] Heise H, Hoyer W, Becker S, Andronesi O C, Riedel D and Baldus M 2005 *Proc. Natl. Acad. Sci.* **102** 15871–15876

[359] Gath J, Habenstein B, Bousset L, Melki R, Meier B H and Böckmann A 2012 *Biomol. NMR Assign.* **6** 51–55

[360] Heise H, Celej M S, Becker S, Riedel D, Pelah A, Kumar A, Jovin T M and Baldus M 2008 *J. Mol. Biol.* **380** 444–50

[361] Sahu K K, Woodside M T and Tuszynski J A 2015 *Biochimie* **116** 133–140

[362] Rodriguez J A, Ivanova M I, Sawaya M R, Cascio D, Reyes F E, Shi D, Sangwan S, Guenther E L, Johnson L M, Zhang M, Jiang L, Arbing M A, Nannenga B L, Hattne J, Whitelegge J, Brewster A S, Messerschmidt M, Boutet S, Sauter N K, Gonen T and Eisenberg D S 2015 *Nature* **advance on** 486–490

[363] Eugene C, Laghaei R and Mousseau N 2014 *J. Chem. Phys.* **141** 135103

[364] Atsmon-Raz Y and Miller Y 2015 *J. Phys. Chem. B* 150722124221003

[365] Vilar M, Chou H T, Luhrs T, Maji S K, Riek-Loher D, Verel R, Manning G, Stahlberg H and Riek R 2008 *Proc. Natl. Acad. Sci.* **105** 8637–8642

[366] Comellas G, Lemkau L R, Nieuwkoop A J, Kloepper K D, Ladror D T, Ebisu R, Woods W S, Lipton A S, George J M and Rienstra C M 2011 *J. Mol. Biol.* **411** 881–895

[367] Shvadchak V V, Claessens M M a E and Subramaniam V 2015 *J. Phys. Chem. B* **119** 1912–1918

[368] Morris A M and Finke R G 2009 *Biophys. Chem.* **140** 9–15

[369] Wördehoff M M, Bannach O, Shaykhalishahi H, Kulawik A, Schiefer S, Willbold D, Hoyer W and Birkmann E 2015 *J. Mol. Biol.* **427** 1428–1435

[370] Berg J M, Tymoczko J L and Stryer L 2002 *Biochemistry, 5th edition* (W. H. Freeman and Company) ISBN 0-7167-3051-0

[371] Sammalkorpi M, Karttunen M and Haataja M 2009 *J. Phys. Chem. B* **113** 5863–5870

Publications

J E Gillam and C E MacPhee. Modelling amyloid fibril formation kinetics. *Journal of Physics: Condensed Matter*, 2013.